PolyPublie
Polytechnique Montréal

POLYTECHNIQUE MONTRÉAL
UNIVERSITÉ D'INGÉNIERIE

Titre: Title:	A model study of the effect of gap junction resistance on the frequency entrainment of a pair of cardiac cells
Auteur: Author:	Rabih Jamaleddine
Date:	1996
Type:	Mémoire ou thèse / Dissertation or Thesis
Référence: Citation:	Jamaleddine, R. (1996). A model study of the effect of gap junction resistance on the frequency entrainment of a pair of cardiac cells [Thèse de doctorat, École Polytechnique de Montréal]. PolyPublie. https://publications.polymtl.ca/31204/

Document en libre accès dans PolyPublie
Open Access document in PolyPublie

URL de PolyPublie: PolyPublie URL:	https://publications.polymtl.ca/31204/
Directeurs de recherche: Advisors:	Fernand A. Roberge, & Robert Vinet
Programme: Program:	Non spécifié

Ce fichier a été téléchargé à partir de PolyPublie, le dépôt institutionnel de Polytechnique Montréal
This file has been downloaded from PolyPublie, the institutional repository of Polytechnique Montréal

https://publications.polymtl.ca

UNIVERSITÉ DE MONTRÉAL

A MODEL STUDY OF THE EFFECT OF GAP JUNCTION RESISTANCE ON THE FREQUENCY ENTRAINMENT OF A PAIR OF CARDIAC CELLS.

RABIH JAMALEDDINE

INSTITUT DE GÉNIE BIOMEDICAL

ÉCOLE POLYTECHNIQUE DE MONTRÉAL

THÈSE PRÉSENTÉE EN VUE DE L'OBTENTION

DU DIPLÔME DE PHILOSOPHIAE DOCTOR (Ph.D.)

(GÉNIE BIOMÉDICAL)

AVRIL 1996

© Rabih Jamaleddine, 1996.

National Library
of Canada

Acquisitions and
Bibliographic Services Branch

395 Wellington Street
Ottawa, Ontario
K1A 0N4

Bibliothèque nationale
du Canada

Direction des acquisitions et
des services bibliographiques

395, rue Wellington
Ottawa (Ontario)
K1A 0N4

Your file *Votre référence*

Our file *Notre référence*

The author has granted an irrevocable non-exclusive licence allowing the National Library of Canada to reproduce, loan, distribute or sell copies of his/her thesis by any means and in any form or format, making this thesis available to interested persons.

L'auteur a accordé une licence irrévocable et non exclusive permettant à la Bibliothèque nationale du Canada de reproduire, prêter, distribuer ou vendre des copies de sa thèse de quelque manière et sous quelque forme que ce soit pour mettre des exemplaires de cette thèse à la disposition des personnes intéressées.

The author retains ownership of the copyright in his/her thesis. Neither the thesis nor substantial extracts from it may be printed or otherwise reproduced without his/her permission.

L'auteur conserve la propriété du droit d'auteur qui protège sa thèse. Ni la thèse ni des extraits substantiels de celle-ci ne doivent être imprimés ou autrement reproduits sans son autorisation.

ISBN 0-612-17808-0

Canada

Nom Rabih JAMALEDDINE

Dissertation Abstracts International est organisé en catégories de sujets. Veuillez s.v.p. choisir le sujet qui décrit le mieux votre thèse et inscrivez le code numérique approprié dans l'espace réservé ci-dessous.

Ingénierie Biomédicale

SUJET

0	5	4	1

CODE DE SUJET

U·M·I

Catégories par sujets

HUMANITÉS ET SCIENCES SOCIALES

COMMUNICATIONS ET LES ARTS
Architecture 0729
Beaux-arts 0357
Bibliothéconomie 0399
Cinéma 0900
Communication verbale 0459
Communications 0708
Danse 0378
Histoire de l'art 0377
Journalisme 0391
Musique 0413
Sciences de l'information 0723
Théâtre 0465

ÉDUCATION
Généralités 515
Administration 0514
Art 0273
Collèges communautaires 0275
Commerce 0688
Économie domestique 0278
Éducation permanente 0516
Éducation préscolaire 0518
Éducation sanitaire 0680
Enseignement agricole 0517
Enseignement bilingue et multiculturel 0282
Enseignement industriel 0521
Enseignement primaire. 0524
Enseignement professionnel 0747
Enseignement religieux 0527
Enseignement secondaire 0533
Enseignement spécial 0529
Enseignement supérieur 0745
Évaluation 0288
Finances 0277
Formation des enseignants 0530
Histoire de l'éducation 0520
Langues et littérature 0279
Lecture 0535
Mathématiques 0280
Musique 0522
Orientation et consultation 0519
Philosophie de l'éducation 0998
Physique 0523
Programmes d'études et enseignement 0727
Psychologie 0525
Sciences 0714
Sciences sociales 0534
Sociologie de l'éducation 0340
Technologie 0710

LANGUE, LITTÉRATURE ET LINGUISTIQUE
Langues
- Généralités 0679
- Anciennes 0289
- Linguistique 0290
- Modernes 0291

Littérature
- Généralités 0401
- Anciennes 0294
- Comparée 0295
- Médiévale 0297
- Moderne 0298
- Africaine 0316
- Américaine 0591
- Anglaise 0593
- Asiatique 0305
- Canadienne (Anglaise) 0352
- Canadienne (Française) 0355
- Germanique 0311
- Latino-américaine 0312
- Moyen-orientale 0315
- Romane 0313
- Slave et est-européenne 0314

PHILOSOPHIE, RELIGION ET THÉOLOGIE
Philosophie 0422
Religion
- Généralités 0318
- Clergé 0319
- Études bibliques 0321
- Histoire des religions 0320
- Philosophie de la religion 0322

Théologie 0469

SCIENCES SOCIALES
Anthropologie
- Archéologie 0324
- Culturelle 0326
- Physique 0327

Droit 0398
Économie
- Généralités 0501
- Commerce-Affaires 0505
- Économie agricole 0503
- Économie du travail 0510
- Finances 0508
- Histoire 0509
- Théorie 0511

Études américaines 0323
Études canadiennes 0385
Études féministes 0453
Folklore 0358
Géographie 0366
Gérontologie 0351
Gestion des affaires
- Généralités 0310
- Administration 0454
- Banques 0770
- Comptabilité 0272
- Marketing 0338

Histoire
- Histoire générale 0578
- Ancienne 0579
- Médiévale 0581
- Moderne 0582
- Histoire des noirs 0328
- Africaine 0331
- Canadienne 0334
- États-Unis 0337
- Européenne 0335
- Moyen-orientale 0333
- Latino-américaine 0336
- Asie, Australie et Océanie 0332

Histoire des sciences 0585
Loisirs 0814
Planification urbaine et régionale 0999
Science politique
- Généralités 0615
- Administration publique 0617
- Droit et relations internationales 0616

Sociologie
- Généralités 0626
- Aide et bien-être social 0630
- Criminologie et établissements pénitentiaires 0627
- Démographie 0938
- Études de l' individu et de la famille 0628
- Études des relations interethniques et des relations raciales 0631
- Structure et développement social 0700
- Théorie et méthodes. 0344
- Travail et relations industrielles 0629

Transports 0709
Travail social 0452

SCIENCES ET INGÉNIERIE

SCIENCES BIOLOGIQUES
Agriculture
- Généralités 0473
- Agronomie. 0285
- Alimentation et technologie alimentaire 0359
- Culture 0479
- Élevage et alimentation 0475
- Exploitation des pâturages 0777
- Pathologie animale 0476
- Pathologie végétale 0480
- Physiologie végétale 0817
- Sylviculture et faune 0478
- Technologie du bois 0746

Biologie
- Généralités 0306
- Anatomie 0287
- Biologie (Statistiques) 0308
- Biologie moléculaire 0307
- Botanique 0309
- Cellule 0379
- Écologie 0329
- Entomologie 0353
- Génétique 0369
- Limnologie 0793
- Microbiologie 0410
- Neurologie 0317
- Océanographie 0416
- Physiologie 0433
- Radiation 0821
- Science vétérinaire 0778
- Zoologie 0472

Biophysique
- Généralités 0786
- Medicale 0760

SCIENCES DE LA TERRE
Biogéochimie 0425
Géochimie 0996
Géodésie 0370
Géographie physique 0368
Géologie 0372
Géophysique 0373
Hydrologie 0388
Minéralogie 0411
Océanographie physique 0415
Paléobotanique 0345
Paléoécologie 0426
Paléontologie 0418
Paléozoologie 0985
Palynologie 0427

SCIENCES DE LA SANTÉ ET DE L'ENVIRONNEMENT
Économie domestique 0386
Sciences de l'environnement 0768
Sciences de la santé
- Généralités 0566
- Administration des hôpitaux 0769
- Alimentation et nutrition 0570
- Audiologie 0300
- Chimiothérapie 0992
- Dentisterie 0567
- Développement humain 0758
- Enseignement 0350
- Immunologie 0982
- Loisirs 0575
- Médecine du travail et thérapie 0354
- Médecine et chirurgie 0564
- Obstétrique et gynécologie 0380
- Ophtalmologie 0381
- Orthophonie 0460
- Pathologie 0571
- Pharmacie 0572
- Pharmacologie 0419
- Physiothérapie 0382
- Radiologie 0574
- Santé mentale 0347
- Santé publique 0573
- Soins infirmiers 0569
- Toxicologie 0383

SCIENCES PHYSIQUES
Sciences Pures
Chimie
- Généralités 0485
- Biochimie 487
- Chimie agricole 0749
- Chimie analytique 0486
- Chimie minérale 0488
- Chimie nucléaire 0738
- Chimie organique 0490
- Chimie pharmaceutique 0491
- Physique 0494
- PolymÇres 0495
- Radiation 0754

Mathématiques 0405
Physique
- Généralités 0605
- Acoustique 0986
- Astronomie et astrophysique 0606
- Électronique et électricité 0607
- Fluides et plasma 0759
- Météorologie 0608
- Optique 0752
- Particules (Physique nucléaire) 0798
- Physique atomique 0748
- Physique de l'état solide 0611
- Physique moléculaire 0609
- Physique nucléaire 0610
- Radiation 0756

Statistiques 0463

Sciences Appliqués Et Technologie
Informatique 0984
Ingénierie
- Généralités 0537
- Agricole 0539
- Automobile 0540
- Biomédicale 0541
- Chaleur et thermodynamique 0348
- Conditionnement (Emballage) 0549
- Génie aérospatial 0538
- Génie chimique 0542
- Génie civil 0543
- Génie électronique et électrique 0544
- Génie industriel 0546
- Génie mécanique 0548
- Génie nucléaire 0552
- Ingénierie des systèmes 0790
- Mécanique navale 0547
- Métallurgie 0743
- Science des matériaux 0794
- Technique du pétrole 0765
- Technique minière 0551
- Techniques sanitaires et municipales 0554
- Technologie hydraulique 0545

Mécanique appliquée 0346
Géotechnologie 0428
Matières plastiques (Technologie) 0795
Recherche opérationnelle 0796
Textiles et tissus (Technologie) 0794

PSYCHOLOGIE
Généralités 0621
Personnalité 0625
Psychobiologie 0349
Psychologie clinique 0622
Psychologie du comportement 0384
Psychologie du développement 0620
Psychologie expérimentale 0623
Psychologie industrielle 0624
Psychologie physiologique 0989
Psychologie sociale 0451
Psychométrie 0632

Name _____

Dissertation Abstracts International is arranged by broad, general subject categories. Please select the one subject which most nearly describes the content of your dissertation. Enter the corresponding four-digit code in the spaces provided.

SUBJECT TERM

SUBJECT CODE

U·M·I

Subject Categories

THE HUMANITIES AND SOCIAL SCIENCES

COMMUNICATIONS AND THE ARTS
Architecture 0729
Art History 0377
Cinema 0900
Dance 0378
Fine Arts 0357
Information Science 0723
Journalism 0391
Library Science 0399
Mass Communications 0708
Music 0413
Speech Communication 0459
Theater 0465

EDUCATION
General 0515
Administration 0514
Adult and Continuing 0516
Agricultural 0517
Art 0273
Bilingual and Multicultural 0282
Business 0688
Community College 0275
Curriculum and Instruction 0727
Early Childhood 0518
Elementary 0524
Finance 0277
Guidance and Counseling 0519
Health 0680
Higher 0745
History of 0520
Home Economics 0278
Industrial 0521
Language and Literature 0279
Mathematics 0280
Music 0522
Philosophy of 0998
Physical 0523
Psychology 0525
Reading 0535
Religious 0527
Sciences 0714
Secondary 0533
Social Sciences 0534
Sociology of 0340
Special 0529
Teacher Training 0530
Technology 0710
Tests and Measurements 0288
Vocational 0747

LANGUAGE, LITERATURE AND LINGUISTICS
Language
- General 0679
- Ancient 0289
- Linguistics 0290
- Modern 0291

Literature
- General 0401
- Classical 0294
- Comparative 0295
- Medieval 0297
- Modern 0298
- African 0316
- American 0591
- Asian 0305
- Canadian (English) 0352
- Canadian (French) 0355
- English 0593
- Germanic 0311
- Latin American 0312
- Middle Eastern 0315
- Romance 0313
- Slavic and East European 0314

PHILOSOPHY, RELIGION AND THEOLOGY
Philosophy 0422
Religion
- General 0318
- Biblical Studies 0321
- Clergy 0319
- History of 0320
- Philosophy of 0322

Theology 0469

SOCIAL SCIENCES
American Studies 0323
Anthropology
- Archaeology 0324
- Cultural 0326
- Physical 0327

Business Administration
- General 0310
- Accounting 0272
- Banking 0770
- Management 0454
- Marketing 0338

Canadian Studies 0385
Economics
- General 0501
- Agricultural 0503
- Commerce-Business 0505
- Finance 0508
- History 0509
- Labor 0510
- Theory 0511

Folklore 0358
Geography 0366
Gerontology 0351
History
- General 0578
- Ancient 0579
- Medieval 0581
- Modern 0582
- Black 0328
- African 0331
- Asia, Australia and Oceania 0332
- Canadian 0334
- European 0335
- Latin American 0336
- Middle Eastern 0333
- United States 0337

History of Science 0585
Law 0398
Political Science
- General 0615
- International Law and Relations 0616
- Public Administration 0617

Recreation 0814
Social Work 0452
Sociology
- General 0626
- Criminology and Penology ... 0627
- Demography 0938
- Ethnic and Racial Studies 0631
- Individual and Family Studies 0628
- Industrial and Labor Relations 0629
- Public and Social Welfare 0630
- Social Structure and Development 0700
- Theory and Methods 0344

Transportation 0709
Urban and Regional Planning 0999
Women's Studies 0453

THE SCIENCES AND ENGINEERING

BIOLOGICAL SCIENCES
Agriculture
- General 0473
- Agronomy 0285
- Animal Culture and Nutrition 0475
- Animal Pathology 0476
- Food Science and Technology 0359
- Forestry and Wildlife 0478
- Plant Culture 0479
- Plant Pathology 0480
- Plant Physiology 0817
- Range Management 0777
- Wood Technology 0746

Biology
- General 0306
- Anatomy 0287
- Biostatistics 0308
- Botany 0309
- Cell 0379
- Ecology 0329
- Entomology 0353
- Genetics 0369
- Limnology 0793
- Microbiology 0410
- Molecular 0307
- Neuroscience 0317
- Oceanography 0416
- Physiology 0433
- Radiation 0821
- Veterinary Science 0778
- Zoology 0472

Biophysics
- General 0786
- Medical 0760

EARTH SCIENCES
Biogeochemistry 0425
Geochemistry 0996
Geodesy 0370
Geology 0372
Geophysics 0373
Hydrology 0388
Mineralogy 0411
Paleobotany 0345
Paleoecology 0426
Paleontology 0418
Paleozoology 0985
Palynology 0427
Physical Geography 0368
Physical Oceanography 0415

HEALTH AND ENVIRONMENTAL SCIENCES
Environmental Sciences 0768
Health Sciences
- General 0566
- Audiology 0300
- Chemotherapy 0992
- Dentistry 0567
- Education 0350
- Hospital Management 0769
- Human Development 0758
- Immunology 0982
- Medicine and Surgery 0564
- Mental Health 0347
- Nursing 0569
- Nutrition 0570
- Obstetrics and Gynecology .. 0380
- Occupational Health and Therapy 0354
- Ophthalmology 0381
- Pathology 0571
- Pharmacology 0419
- Pharmacy 0572
- Physical Therapy 0382
- Public Health 0573
- Radiology 0574
- Recreation 0575
- Speech Pathology 0460
- Toxicology 0383

Home Economics 0386

PHYSICAL SCIENCES
Pure Sciences
Chemistry
- General 0485
- Agricultural 0749
- Analytical 0486
- Biochemistry 0487
- Inorganic 0488
- Nuclear 0738
- Organic 0490
- Pharmaceutical 0491
- Physical 0494
- Polymer 0495
- Radiation 0754

Mathematics 0405
Physics
- General 0605
- Acoustics 0986
- Astronomy and Astrophysics 0606
- Atmospheric Science 0608
- Atomic 0748
- Electronics and Electricity 0607
- Elementary Particles and High Energy 0798
- Fluid and Plasma 0759
- Molecular 0609
- Nuclear 0610
- Optics 0752
- Radiation 0756
- Solid State 0611

Statistics 0463

Applied Sciences
Applied Mechanics 0346
Computer Science 0984

Engineering
- General 0537
- Aerospace 0538
- Agricultural 0539
- Automotive 0540
- Biomedical 0541
- Chemical 0542
- Civil 0543
- Electronics and Electrical 0544
- Heat and Thermodynamics ... 0348
- Hydraulic 0545
- Industrial 0546
- Marine 0547
- Materials Science 0794
- Mechanical 0548
- Metallurgy 0743
- Mining 0551
- Nuclear 0552
- Packaging 0549
- Petroleum 0765
- Sanitary and Municipal 0554
- System Science 0790

Geotechnology 0428
Operations Research 0796
Plastics Technology 0795
Textile Technology 0994

PSYCHOLOGY
General 0621
Behavioral 0384
Clinical 0622
Developmental 0620
Experimental 0623
Industrial 0624
Personality 0625
Physiological 0989
Psychobiology 0349
Psychometrics 0632
Social 0451

UNIVERSITÉ DE MONTRÉAL

ÉCOLE POLYTECHNIQUE DE MONTRÉAL

Cette thèse intitulée:

A MODEL STUDY OF THE EFFECT OF GAP JUNCTION RESISTANCE ON THE FREQUENCY ENTRAINMENT OF A PAIR OF CARDIAC CELLS.

présentée par: JAMALEDDINE Rabih

en vue de l'obtention du diplôme de: Philosophiae Doctor

a été dûment acceptée par le jury d'examen constitué de:

M. SAVARD Pierre, Ph.D., président

M. ROBERGE Fernand A., Ph.D., membre et directeur de recherche

M. VINET Alain,Ph.D., membre et co-directeur de recherche

M. LONGTIN André, Ph.D., membre externe

M. LEON Joshua L., Ph.D., membre

To Mona, Rand, and Omar

ACKNOWLEDGMENT

First of all, I would like to thank the two most supportive people for helping me out in this project: Dr. Fernand Roberge and Dr. Alain Vinet. Dr. Roberge's passion and valuable remarks, and Dr. Vinet's enormous enthusiasm and helpful explanations in the area of nonlinear dynamics, made this work rewarding and challenging.

I would also like to thank Dr. Joshua Leon for his great help and Dr. Robert Leblanc for his support and kindness.

Many credits to: André Bleau for his technical support which enabled me to produce the colour illustrations and to Jean-François Lefevre for his willingness to reload my backup files almost weekly.

A big credit to Kathleen Lennon for her assistance and to Angèle Elias for making the administration jungle a pacific ocean.

Many thanks to: Nicolas Friedman for making his Mac a great help and for being a good friend (and a great soccer player!), Mohamed Argoubi, Maryse Thivierge, Ali Awada, and Zouheir Kaouk for sharing with me their thoughts and their friendship.

Finally, this thesis would have never been completed if not for the great support of my wife, Mona, whose presence, love and comprehension gave me that energy that never stopped.

SOMMAIRE

Cette étude décrit l'utilisation d'un modèle d'une paire de cellules musculaires (myocytes) cardiaques couplées pour investiguer le rôle de la résistance intercellulaire (résistance de jonction) au cours de l'entraînement de fréquence. Chacune des cellules a la forme d'un petit cylindre de membrane excitable (10 μm de diamètre et 100 μm de longueur), avec une résistance infinie à chaque bout. La membrane cellulaire comprend une capacitance (1 $\mu F/cm^2$) en parallèle avec des conductances ioniques de type Hodgkin-Huxley pour les ions Na, K et Ca. La concentration intracellulaire des ions calcium ($[Ca]_{in}$) augmente en fonction du courant calcium transmembranaire au début du potentiel d'action et retourne à son niveau de base à la fin de la phase de repolarisation. Ce modèle de membrane a fait l'objet de plusieurs études par de nombreux chercheurs et est connu sous le nom de modèle Beeler-Reuter modifié (MBR).

On suppose que chaque cellule a un potentiel membranaire uniforme. Les deux myocytes sont couplés par une résistance, de sorte que la différence de potentiel entre les deux cellules génère un courant de couplage Ig. Nous avons étudié deux conditions: une avec une résistance de couplage fixe (R), et une avec une résistance de couplage variable (Rj) contrôlée par la $[Ca]_{in}$ de chaque myocyte. Le système a été stimulé en appliquant une pulsation rectangulaire de courant transmembranaire à la première cellule (C1). La deuxième cellule (C2) est alors stimulée par le courant de couplage généré par la montée du potentiel d'action de C1. Les réponses de C1 et C2 ont été enregistrées suite à l'application de trains de stimuli ayant un cycle de base (BCL) fixe choisi entre 100 et 1000 ms. La résolution numérique du système d'équations différentielles nonlinéaires ordinaires a été effectuée à l'aide d'une méthode d'intégration hybride décrite dans la littérature.

Dans un premier temps, nous avons examiné le comportement d'un myocyte

isolé (potentiel membranaire spatialement uniforme) dans le but d'établir les caractéristiques dynamiques du modèle MBR utilisé dans la présente étude. La durée du potentiel d'action (APD) est le temps écoulé entre le début du stimulus et l'instant (T_{-50}) où la phase de repolarisation passe par -50 mV. L'intervalle diastolique (DIA) est l'intervalle de temps entre T_{-50} et le stimulus suivant. Il est utile d'utiliser DIA comme variable indépendante (en fixant DIA = 0 à T_{-50}) pour décrire les changements d'excitabilité qui suivent la période réfractaire absolue (ARP), définissant ainsi la fonction Thr(DIA). On utilise aussi la fonction APD(DIA) pour décrire la caractéristique de restitution des APDs. Dans le présent modèle MBR on a ARP = APD + 14 ms.

Nos résultats de simulation avec le myocyte isolé ont permis de confirmer toutes les observations publiées antérieurement par d'autres chercheurs. Si on applique un stimulus test (S2, de durée T_{stim2} et d'intensité I_{stim2}) dans la foulée d'un potentiel d'action conditionnant (produit par S1, avec T_{stim1} et I_{stim1}), on a alors une stimulation prématurée avec un intervalle de couplage (S1-S2) ou, de façon équivalente, avec DIA = (S1 - S2 - T_{-50}). En dépit du fait que l'ARP et l'APD diminuent progressivement avec un BCL (ou intervalle (S1-S1)) de plus en plus court, la fonction Thr(DIA) reste pratiquement inchangée, ce qui indique une absence d'effet de mémoire. Si T_{stim1} et I_{stim1} sont assez faibles, ils ont un effet minime sur Thr(DIA) et APD(DIA). D'autre part, Thr(DIA) est très sensible à la valeur de T_{stim2} alors que APD(DIA) et la dispersion des APDs dépendent fortement de I_{stim2} et T_{stim2} lorsque leurs amplitudes sont passablement grandes.

Au cours de l'entraînement de fréquence du myocyte MBR isolé (les paramètres sont alors T_{stim}, I_{stim} et BCL), il y a doublage de période pour des faibles et moyennes valeurs de I_{stim} lorsque T_{stim} est courte, et pour des valeurs moyennes de I_{stim} lorsque T_{stim} est plus longue. Un modèle itératif simple nous a permis de montrer que le doublage de période se produit lorsque dAPD/dDIA > 1. L'addition de périodes est observée pour de faibles et de grandes amplitudes de I_{stim} avec de grandes

valeurs de T_{stim}, ceci à cause de la réduction importante de la dispersion des APDs qui élimine la région de dAPD/dDIA > 1. La cascade de bifurcations 1:1→ 2:2→ 1:1→ 1:0, ou 1:1→ l:0, ne peut être prédite par le modèle itératif simple vu que Thr(DIA) et APD(DIA) ne reflètent pas les phénomènes de base associés aux réponses bloquées. Une observation inédite de la présente étude est l'obtention d'un entraînement 1:1 ou 1:0, en présence de valeurs élevées de I_{stim} qui produisent de nombreuses réponses bloquées, dû au fait qu'il se produit un reset de la réponse et une interruption de la cascade de bifurcations au-delà de la période 2.

Dans la paire de myocytes avec résistance de couplage fixe (système à couplage-R) stimulée sous conditions constantes, les réponses d'entraînement varient avec R. Si R est faible, les deux cellules se comportent comme une seule unité et leurs réponses d'entraînement sont semblables à celle d'une cellule isolée. Lorsque R est augmentée, l'amplitude de Ig diminue et la fréquence d'activité répétitive de C2 est abaissée. L'absence d'un potentiel d'action dans C2 produit un court APD_1 dans C1, diminuant ainsi la dispersion des valeurs d'APD_1 et modifiant la forme de la courbe $APD_1(DIA_1)$. Dans ces conditions, un taux rapide de stimulation produit une fréquence de décharge de C1 qui est plus régulière que celle d'une cellule isolée, de sorte que le rythme 1:1 peut être maintenu pour des BCLs beaucoup plus courts. Pour une valeur donnée de R, le comportement du système à couplage-R peut être expliqué par les courbes APD(DIA) de C1 et C2.

La résistance de jonction Rj fut modélisée au moyen d'un mécanisme de portes sensibles à $[Ca]_{in}$, avec un paramètre Rb représentant la résistance maximum de la résistance de jonction lorsque tous les canaux sont complètement ouverts. L'entraînement de fréquence de la paire de cellules (système à couplage-Rj), à un BCL donné, produit une augmentation graduelle de Rj. La valeur transitoire finale de Rj augmente avec la fréquence de stimulation. Une fois les transitoires de C1, C2 et Rj terminées, lesquelles dépendent du choix de BCL et de Rb, le système atteint un état final stable ou oscillant.

Globalement, pour des valuers données de BCL et de Rb, les réponses d'entraînement de fréquence du système à couplage-Rj peuvent être interprétées en comparaison avec le comportement du système à couplage-R pour le même BCL. Dans ce dernier système, un BCL donné correspond à une série de valeurs de R qui définissent les transitions entre les zones adjacentes d'entraînement de fréquence (numéro de période et rapport d'activation). En changeant les valeurs de Rb et de BCL, les réponses sont inchangées en autant que la transitoire maximum de Rj reste à l'intérieur de l'une des zones d'entraînement de fréquence définie dans le système à couplage-R. Autrement, lorsque la transitoire maximum de Rj traverse un lieu donné de transition entre deux zones d'entraînement de fréquence, le découplage partiel des deux cellules entraîne un court APD ou une réponse bloquée dans C2, ce qui résulte en une diminution de Rj et un couplage accentué. Cet effect de feedback négatif mène à un passage oscillant de Rj à travers le lieu de transition entre deux zones voisines, produisant alors des rythmes de C1 et C2 qui sont une combinaison de ceux des zones adjacentes impliquées. Par exemple, si la limite d'un rythme de période 1 est Rj_1, et que celle d'un rythme de période 2 est Rj_2, avec $Rj_2 > Rj_1$, des conditions qui amènent la transitoire maximum de Rj profondément dans la zone de période 2 produiront des oscillations de Rj dans le voisinage du lieu de transition entre les zones de période 1 et de période 2, avec des réponses de C1 et C2 constituées par un mélange de rythmes de période 1 et période 2. Lorsque la transitoire maximum de Rj est proche de Rj_1, la composante dominante du rythme est de période 1 tandis qu'elle de période 2 si la transitoire maximum de Rj et proche de Rj_2.

Nos résultats avec le système à couplage-R sont exactement semblables aux observations expérimentales faites sur une paire de myocytes cardiaques couplés par un circuit RC. Vu que la cellule stimulée peut maintenir une décharge répétitive soutenue qui n'est pas affectée par l'activité de la cellule couplée dans le système à couplage-Rj, le mécanisme de feedback négatif contrôlant les changements de Rj assure un couplage intercellulaire plus serré sur un grand intervalle de fréquences de stimulation.

ABSTRACT

The present study uses a model of a pair of coupled cardiac myocytes to describe the role played by the intercellular (gap junction) resistance during frequency entrainment. Each myocyte is represented as a small cylinder of excitable membrane (10 μm in diameter and 100 μm in length) with an infinite resistance at each end. The cell membrane consists of a capacitance (1 μF/cm2) in parallel with Hodgkin-Huxley type ionic conductances for Na, K, and Ca ions. The intracellular calcium concentration ($[Ca]_{in}$) increases as a function of the calcium membrane current at the beginning of the action potential and returns to its resting level at the end of the repolarization phase. This membrane model has been extensively studied by a number of investigators and is known as the modified Beeler-Reuter (MBR) model.

We assume that each cell has a uniform membrane potential. The two myocytes are coupled through a resistance, such that the potential difference between the two cells generates a coupling current (Ig). We studied two conditions: one with a fixed coupling resistance (R), and one with a variable coupling resistance (Rj) controlled by the $[Ca]_{in}$ of each myocyte. The two-cell system was paced by applying a rectangular pulse of transmembrane current to the first cell (C1). The second cell (C2) was then stimulated by the coupling current generated by the action potential upstroke of C1. The responses of C1 and C2 were recorded as the basic cycle length (BCL) of the stimulus train was set a different fixed values between 100 and 1000 ms. Numerical solutions were obtained by integrating the set of nonlinear ordinary differential equations using an hybrid integration scheme described in the literature.

As a first step, we examined the behavior of a the isolated myocyte (space-clamped membrane) in order to document the dynamic characteristics of the MBR model used in the present study. The action potential duration (APD) is defined as the time elapsed between the stimulus onset and the time (T_{-50}) at which the repolarization phase reaches -50 mV. The diastolic interval (DIA) is the time between T_{-50} and the next stimulus. We found it convenient to use DIA as the independent variable (setting DIA = 0 at T_{-50}) to describe the excitability changes following the absolutlely refractory period (ARP), thus defining a Thr(DIA) function. We also use APD(DIA) to describe the APD restitution characteristics of the membrane. In the present MBR model, we have ARP = APD + 14 ms.

Our simulation results with the space-clamped MBR model have reproduced previously published observations. The application of a test stimulus (S2, with duration T_{stim2} and strength I_{stim2}) in the wake of a conditioning action potential (produced by S1, with T_{stim1} and I_{stim1}) corresponds to premature stimulation at a coupling interval (S1-S2) or, equivalently, at DIA = (S1 - S2 - T_{-50}). Although the ARP and APD decrease progressively with shorter and shorter (S1-S1) intervals (or BCLs), the Thr(DIA) function remains practically invariant and indicates the absence of a threshold memory effect. If T_{stim1} and I_{stim1} are low enough, they have minimal effects on Thr(DIA) and APD(DIA). On the other hand, Thr(DIA) is highly sensitive to T_{stim2}, while APD(DIA) and the dispersion of APD values are strongly dependent on I_{stim2} and T_{stim2} when these parameters are faily large.

During pacing of the space-clamped MBR model (parameters are T_{stim}, I_{stim} and BCL), period doubling frequency entrainment occurs at low and medium I_{stim} when T_{stim} is short, and at medium I_{stim} when T_{stim} is longer. A simple iterative difference equation showed that period doubling occurs when dAPD/dDIA > 1. Period adding

exists at both low and high I_{stim} for large T_{stim}, due to the important reduction of the APD dispersion which eliminates the region of dAPD/dDIA > 1. The 1:1→2:2→1:1 →1:0 or 1:1→1:0 bifurcation cascades observed with the MBR model are not predicted by the iterative difference equation since the Thr(DIA) and APD(DIA) functions do not reflect the basic underlying phenomena associated with blocked responses. A new observation of the present study is the role of blocked responses at very large I_{stim} values, which caused a resetting of the response pattern and an interruption of the bifurcation cascade after period 2, such that the system then moved to 1:1 or 1:0 entrainment.

In the two-cell system with a fixed resistance (R-coupled system) and constant stimulation parameters, the entrainment responses varied with R. At low R, both cells behaved like a single unit and their entrainment responses were similar to those of the isolated cell. Once R was increased, the amplitude of Ig decreased and the firing rate of C2 diminished. The absence of an action potential in C2 caused a shorter APD_1 in C1, thus decreasing the dispersion of APD_1 values and modifying the shape of $APD_1(DIA_1)$. As a result, the rate of firing of C1 became more regular than that of the isolated cell at high pacing rates and 1:1 frequency entrainment could be maintained for very low BCLs. For a given R value, the behavior of the R-coupled system can be explained by the APD(DIA) curves of C1 and C2.

The variable gap junction resistance (Rj) was modeled by means of a gating mechanism sensitive to $[Ca]_{in}$, with parameter Rb representing the maximum resistance of the gap junction when all gated channels are fully opened. Frequency entrainment of the two-cell system (Rj-coupled system) at a given BCL produced a gradual increase in Rj, with higher Rj values as the pacing frequency was increased. Following transient C1 and C2 responses and a concomitant transient Rj increase, determined by the particular BCL and Rb values, the system reached either a stable

or oscillatory steady state.

Globally, for a given BCL and Rb, the response patterns of the Rj-coupled system can be understood by comparison with the behavior of the R-coupled system for the same BCL. In the R-coupled system, a given BCL corresponds to a series of R values defining the transitions between adjacent zones of frequency entrainment (period numbers or activation ratios). When Rb and BCL were changed, the same response pattern persisted as long as the maximum transient increase in Rj remained within one of the frequency entrainment zones defined in the R-coupled system. Otherwise, when the transient Rj increase traversed a given transition locus, the partial decoupling of the two cells yielded short APDs or blocked responses in C2, and thus a concomitant decrease in Rj and increased coupling. This negative feedback effect leads to an oscillatory Rj crossing of the transition locus, with C1 and C2 rhythms exhibiting a mix of patterns drawn from the two adjacent zones of frequency entrainment. For example, if the limit of period 1 rhythm is at Rj_1, and that of period 2 is Rj_2, where $Rj_2 > Rj_1$, a set of conditions which brings the maximum Rj transient deep into the period 2 zone will give rise to Rj oscillations in the vicinity of the transition locus between period 1 and period 2 zones, with C1 and C2 responses representing a mix of period 1 and period 2 rhythms. When the maximum Rj transient is close to Rj_1, the dominant pattern is of period 1 whereas it is of period 2 when the maximum Rj transient is close to Rj_2.

Our results with the R-coupled system are similar to experimental observations on a pair of cardiac myocytes coupled through a fixed RC circuit. Since sustained repetitive firing of the stimulated cell may remain unaffected by the activity of the follower cell in the Rj-coupled system, the negative feedback mechanism of Rj changes ensures a tighter intercellular coupling over a wide range of stimulation rates.

CONDENSÉ EN FRANCAIS

Il est généralement admis que la réentrée est le principal mécanisme sous-jacent aux arythmies cardiaques graves comme la tachycardie ventriculaire et la fibrillation. La réentrée constitue une perturbation électrophysiologique selon laquelle un front d'activation, constitué par la montée rapide et simultanée du potentiel d'action d'un grand nombre de cellules cardiaques, réussit à se propager à travers le tissu myocardique en suivant un circuit en boucle fermée. Un tel circuit peut entourer un obstacle anatomique comme l'orifice d'un grand vaisseau ou un ilot de tissu infarci. Alternativement il peut comporter un foyer central inexcitable définit par le parcours même du centre de rotation du front d'activation à chaque instant, donnant lieu à une réentrée dite fonctionnelle.

Le substrat myocardique dans lequel se produit la réentrée peut être considéré comme un réseau de cellules individuelles (aussi appelées myocytes), chacune ayant la forme d'un petit cylindre d'environ 12 à 20 μm de diamètre et d'environ 100μ de longueur. Les myocytes adjacents sont physiquement et électriquement reliés par des canaux ioniques spécialisés définissant des "gap junctions" (ou nexus) . La résistance électrique (R_j) de ces jonctions est déterminée par divers facteurs qui sont contrôlés indirectement par le taux de répétition des potentiels d'action des cellules adjacentes couplées, notamment par la concentration intracellulaire d'ions calcium et d'ions hydrogène. Par exemple, lorsque le taux d'activité répétitive est élevé, comme c'est le cas au cours de la réentré, la concentration intracellulaire d'ions calcium ($[Ca]_{in}$)

augmente et entraîne une augmentation de R_j. Des valeurs plus élevées de R_j causent un découplage intercellulaire et ralentissent la propagation. En particulier une réentrée plus lente correspond à un taux plus faible d'activité répétitive, ce qui entraîne une baisse de $[Ca]_{in}$ et une diminution de R_j, menant alors à un couplage électrique intercellulaire plus fort. Il existe donc une rétroaction négative liant l'activité répétitive des cellules et la résistance de couplage R_j. Ce mécanisme est susceptible de modifier de façon importante les caractéristiques dynamiques de la réentrée.

Le but du présent travail est d'étudier ce mécanisme à l'aide d'un modèle d'une paire de cellules cardiaques couplées par une résistance intercellulaire R_j, en soumettant la paire de cellules à une stimulation répétitive à différentes fréquences. Les deux cellules sont identiques et ont un potentiel transmembranaire uniforme. Elles sont couplées de façon à ce que la différence de potentiel entre les deux cellules génère un courant de couplage Ig. Nous avons étudié deux conditions: une avec une résistance de couplage fixe (R), et une avec une résistance de couplage variable (R_j) contrôlée par la $[Ca]_{in}$ de chaque myocyte. Le système a été stimulé en appliquant une pulsation rectangulaire de courant transmembranaire à la première cellule (C1). La deuxième cellule (C2) est alors stimulée par le courant de couplage généré par la montée du potentiel d'action de C1. Les réponses de C1 et C2 ont été enregistrées suite à l'application de trains de stimuli ayant un cycle de base (BCL) fixe choisi entre 100 et 1000 ms. Les résultats servent à préciser l'influence de la résistance de couplage sur les différents scénarios d'entraînement de fréquence du système.

1. Méthodes

Chaque cellule est modélisée par un petit cylindre de membrane excitable (10 μm de diamètre et 100 μm de longueur). La membrane cellulaire comprend une capacitance (1 $\mu F/cm^2$) en parallèle avec des conductances ioniques de type Hodgkin-Huxley pour les ions sodium, potassium et calcium. La valeur de ($[Ca]_{in}$) augmente en fonction du courant calcium transmembranaire au début du potentiel d'action et retourne à son niveau de base à la fin de la phase de repolarisation. Ce modèle de membrane a fait l'objet de plusieurs études par de nombreux chercheurs et est connu sous le nom de modèle Beeler-Reuter modifié (MBR).

La présente version du modèle MBR n'inclut pas l'inactivation lente du courant sodium (variable de porte j comportant une constante de temps d'environ 100 ms). Sous conditions nominales, le modèle a un seul état d'équilibre qui est globalement stable. Il possède aussi une propriété de pseudo-seuil correspondant à une entrée brusque et massive du courant sodium (I_{Na}) dans la cellule, lequel définit alors la montée initiale du potentiel d'action. Lorsque le seuil est atteint, le pic de I_{Na} est supérieur à tous les autres courants par au moins deux ordres de grandeur. On peut donc se servir de l'amplitude du pic de courant ionique total comme indicateur du phénomène de seuil et de l'existence d'une réponse active. On a choisit un critère de 10% de l'amplitude maximale obtenue en stimulant à partir du potentiel de repos, pour une durée de 0.55 ms. Si ce critère n'est pas rencontré, la réponse est dite passive ou bloquée.

Dans un premier temps, nous avons examiné le comportement d'un myocyte isolé (potentiel membranaire spatialement uniforme) dans le but d'établir les caractéristiques dynamiques du modèle MBR utilisé dans la présente étude. La durée du potentiel d'action (APD) est défini comme le temps écoulé entre le début du stimulus et l'instant (T_{-50}) ou la phase de repolarisation passe par -50 mV. L'intervalle diastolique (DIA) est l'intervalle de temps entre T_{-50} et le stimulus suivant. Il est utile d'utiliser DIA comme variable indépendante (en fixant DIA = 0 à T_{-50}) pour décrire les changements d'excitabilité qui suivent la période réfractaire absolue (ARP), définissant ainsi la fonction Thr(DIA). On utilise aussi la fonction APD(DIA) pour décrire la caractéristique de restitution des APDs. Dans le présent modèle MBR on a établi que ARP = APD + 14 ms.

La résistance de jonction variable R_j fut modélisée au moyen d'un mécanisme de portes sensibles à $[Ca]_{in}$, avec un paramètre R_b représentant la résistance maximum de la résistance de jonction lorsque tous les canaux intercellulaires sont complètement ouverts. L'entraînement de fréquence de la paire de cellules, à un BCL donné, produit une augmentation graduelle de R_j. La valeur transitoire finale de R_j augmente avec la fréquence de stimulation. Une fois les transitoires de C1, C2 et R_j terminées, lesquelles dépendent du choix du BCL et de R_b, le système atteint un état final stable ou oscillant.

Un train régulier d'impulsions rectangulaires (durée d'une milliseconde et amplitude de 1.25 fois l'amplitude seuil) fut appliqué à C1, avec un taux de répétition suffisamment lent pour avoir une réponse active de C1 à chaque impulsion. Sauf

pour le système à couplage variable (système-R_j), on s'intéresse seulement au réponses stables du système (répétition périodique d'un regroupement de réponses consécutives) et le système est toujours ramené à son état de repos au début de l'application d'un BCL donné. On définit le rapport d'activation (AR) par deux nombres, m:n, où m est le nombre de stimuli dans le regroupement périodique de réponses consécutives et n le nombre de réponses actives incluses dans le regroupement. Le rang de la période (P) correspond au nombre m de stimuli qui définissent le regroupement de réponses.

Les courants membranaires furent intégrés numériquement à l'aide d'une méthode hybride décrite dans la littérature, avec un pas de temps fixe de 10 μs. Les programmes furent écrits en langage C et exécutés sur une station IRIS 4/25.

2. Myocyte isolé

Nous avons d'abord vérifié une propriété importante du modèle MBR, soit l'invariance relative de son seuil d'excitabilité suite à un potentiel d'action conditionnant (absence de mémoire de seuil). Si on applique un stimulus test (S2, de durée T_{stim2} et d'intensité I_{stim2}) dans la foulée d'un potentiel d'action conditionnant (produit par S1, avec T_{stim1} et I_{stim1}), on a alors une stimulation prématurée avec un intervalle de couplage (S1-S2) ou, de façon équivalente, avec DIA = (S1 - S2 - T_{-50}). Cette procédure nous a permis de constater que l'amplitude du courant de seuil au repos (I_{thR}) et la forme des courbes Thr(DIA) étaient très sensibles à T_{stim2}. On a

trouvé également que la fonction Thr(DIA) est affectée par les paramètres de la stimulation conditionnante, soit le BCL (ou l'intervalle S1-S1), T_{stim1} et I_{stim1}. L'effet le plus marqué fut la translation des courbes Thr(DIA), donnant ainsi lieu à différentes valeurs de l'ARP. L'APD et l'ARP sont diminuées avec un pacing rapide (court BCL) et de fortes valeurs de T_{stim1} et I_{stim1}. La translation de Thr(DIA) est éliminée en prenant DIA comme variable temporelle indépendante au lieu de S1-S2.

La courbe de restitution, APD(DIA), et la dispersion des valeurs d'APD sont essentiellement indépendantes des paramètres de stimulation si I_{stim2} ne dépasse pas trop l'intensité seuil et si T_{stim2} est assez courte. Une augmentation de T_{stim2} raccourcit l'APD lorsque DIA est court ou moyen. Toutefois, le facteur le plus puissant pour modifier APD(DIA) est l'amplitude I_{stim2} du stimulus. Les changements les plus importants sont obtenus lorsque les deux quantités T_{stim2} et I_{stim2} sont augmentées en même temps.

Lors de l'entrainement du modèle MBR, l'amplitude et la durée du stimulus (T_{stim} et I_{stim}) ont une forte influence sur le comportement du système. Dans ce travail, l'intérêt principal porte sur les transitions entre les rythmes 1:1, 2:2, 2:1 et 1:0. Ces rythmes correspondent à des zones bien définies sur les diagrammes de bifurcation, c'est-à-dire les cartes présentant le BCL en regard de l'intensité du stimulus ou de la résistance de couplage intercellulaire. Les transitions entre ces zones, ou bifurcations, sont des caractéristiques de première importance.

Dans l'étude du modèle de cellule isolée, nous avons choisi de garder T_{stim} fixe

(1 ms) et d'étudier l'effet des variations de I_{stim}. Dans ces conditions, le diagramme de bifurcation montre qu'un entraînement 1:1 est possible si le BCL est plus grand que 262 ms. Trois types de bifurcation ont été identifiés, le premier et le deuxième types sont, respectivement, le doublage et l'addition du rang de la période, tandis que le troisième est la cascade 1:1→2:2→2:1→1:0. Il y a doublage de période pour des faibles et moyennes valeurs de I_{stim} lorsque T_{stim} est courte, et pour des valeurs moyennes de I_{stim} lorsque T_{stim} est plus longue. En utilisant un modèle itératif simple, nous avons montré que la transition entre l'addition et le doublage du rang de la période correspond au point où la pente de la courbe APD(DIA) dépasse l'unité. L'addition de périodes est observée pour de faibles et de grandes amplitudes de I_{stim} avec de grandes valeurs de T_{stim}, ceci à cause de la réduction importante de la dispersion des APDs qui élimine la région où la pente de APD(DIA) est plus grande que l'unité. La cascade de bifurcations 1:1→2:2→2:1→1:0, ou 1:1→1:0, ne peut être prédite par le modèle itératif simple vu que Thr(DIA) et APD(DIA) ne reflètent pas l'occurrence de réponses bloquées. Une observation inédite de la présente étude est l'obtention d'un entraînement 1:1 ou 1:0, en présence de valeurs élevées de I_{stim} qui produisent de nombreuses réponses bloquées, dû au fait qu'il se produit un reset de la réponse et une interruption de la cascade de bifurcations au-delà de la période de rang 2.

3. Paire de myocytes couplées par une résistance fixe

Dans la paire de myocytes avec résistance de couplage fixe (système à

couplage-R) stimulée sous conditions constantes, les réponses d'entraînement varient avec R. Si R est faible, le diagramme de bifurcation montre que les deux cellules se comportent comme une seule unité, et leurs réponses d'entraînement sont semblables à celle d'une cellule isolée, soit un rythme 1:1 pour un BCL plus grand que 262 ms. Les courbes APD(DIA) sont alors identiques pour les deux cellules. Lorsque R est augmentée, l'amplitude de Ig diminue et la fréquence d'activité répétitive de C2 est abaissée. L'absence d'un potentiel d'action dans C2 produit un gradient de potentiel élevé qui sert à augmenter la valeur du courant Ig sortant de C1. Ce courant sortant a le même effet qu'un courant membranaire repolarisant (e.g., un courant potassium) et cause un retour rapide du potentiel transmembranaire vers sa valeur de repos. Le résultat est donc un fort raccourcissement de la durée du potentiel d'action (APD_1) de C1. Dans ces conditions, il est impossible d'obtenir des valeurs élevées d'APD même si le pacing est lent et il y a donc réduction de la dispersion des valeurs d'APD_1, et modification de la forme de la courbe $APD_1(DIA_1)$.

Pour cette raison un taux rapide de stimulation produit une fréquence de décharge de C1 qui est plus régulière que celle d'une cellule isolée, de sorte que le rythme 1:1 peut être maintenu pour des BCLs aussi courts que 100 ms. Pour une valeur donnée de R, le comportement du système à couplage-R peut être expliqué par les courbes APD(DIA) de C1 et C2. Cependant, dans le cas de la cellule C2, l'augmentation de R est sensiblement equivalente à une augmentation de la durée du stimulus et à une diminution de son amplitude. On a pu alors vérifier que C2 se comportait alors comme une cellule isolée, soit un scénario de doublage du rang de la période, d'addition du rang de la période et, finalement, de réponses passives.

4. Paire de myocytes couplées par une résistance variable

Dans le modèle à résistance variable, R_j est contrôlée caractérisé par une variable dynamique ayant une longue constante de temps (variant entre 18 et 35 secondes) et une très haute sensibilité à pCa_{in} (inverse du logarithme de $[Ca]_{in}$). Au cours du potentiel d'action, le changement important de $[Ca]_{in}$ (environ un ordre de grandeur, ce qui correspond à une variation de pCa_{in} entre 7.1 et 6.2) produit un changement appréciable de R_j en dépit de la longue constante de temps. Cette variations de R_j persiste pendant environ 100 ms au-delà de la fin du potentiel d'action, ce qui permet une augmentation cumulative de R_j au cours du rythme 1:1 d'activité répétitive de C1 et C2. Lorsque le rythme 1:1 cesse, pCa_{in} diminue rapidement à une valeur déterminée par le paramètre R_b (voir Méthodes).

Globalement, pour des valeurs données de BCL et de R_b, les réponses d'entraînement de fréquence du système à couplage- R_j peuvent être interprétées en comparaison avec le comportement du système à couplage-R pour le même BCL. Par exemple, pour un BCL de 500 ms, le système à couplage-R passe de la période de rang 1 à celle de rang 2 pour $R > 425$ MΩ. Un phénomène semblable se produit dans le système à couplage-R_j, et il y a un intervalle de valeurs du paramètre R_b pour lequel la réponse à l'état stable du système est un mélange de périodes de rang 1 et de rang 2, avec une oscillation de R_j. En augmentant R_b, la réponse périodique stable s'approche davantage de la période de rang 2, jusqu'à ce qu'elle soit purement de rang 2 lorsque R_b est assez élevée. Subséquemment, si R_b est augmentée davantage,

la réponse du système s'approche de la transition entre des périodes de rang 2 et de rang 3.

Lorsque le pacing est plus rapide dans le système à couplage-R, par exemple pour BCL = 300 ms et R = 362 MΩ, C1 montre une transition entre un AR de 1:1 et un AR de 2:2 tandis que C2 montre une transition entre 1:1 et 2:1. Une situation comparable se retrouve dans le système à couplage-R_j lorsque R_b = 1000 KΩ, sous la forme d'une oscillation lente de R_j entre 320 et 372 MΩ. On observe alors des variations oscillantes de APD_1 et APD_2, représentant un mélange de rythmes 1:1 et 2:2, le premier correspondant à de faibles valeurs de R_j et le second à des valeurs élevées. Ici encore une augmentation de R_b déplace la dynamique du système vers la période de rang 2 où, éventuellement, on retrouve du 2:2 dans C1 et du 2:1 dans C2.

Dans l'ensemble, pour le système à couplage-R_j, des valeurs données de BCL et de R_b définissent un couplage qui place la dynamique du système dans des conditions qui s'apparentent à celles observées dans le système à couplage-R. La différence majeure est que R_j varie continuellement en fonction de l'activité répétitive de C1 et de C2, de sorte que des transitions entre différents types de rythmes peuvent être observées. En changeant les valeurs de R_b et de BCL, les réponses sont inchangées en autant que la transitoire maximum de R_j reste à l'intérieur de l'une des zones d'entraînement de fréquence définie dans le système à couplage-R. Autrement, lorsque la transitoire maximum de R_j traverse une bifurcation entre deux zones d'entraînement de fréquence, le découplage partiel des deux cellules produit une

réponse bloquée dans C2 et un court APD dans C1, ce qui résulte en une diminution de R_j et un couplage accentué.

Cet effect de feedback négatif mène à un passage oscillant de R_j à travers la bifurcation entre deux zones voisines, produisant alors des rythmes de C1 et C2 qui sont une combinaison de ceux des zones adjacentes impliquées. Par exemple, si la limite d'un rythme de période de rang 1 est R_{j1}, et que celle d'un rythme de période de rang 2 est R_{j2}, avec $R_{j2} > R_{j1}$, des conditions qui amènent la transitoire maximum de R_j profondément dans la zone de période de rang 2 produiront des oscillations de R_j dans le voisinage du lieu de transition entre les zones de périodes de rang 1 et de rang 2, avec des réponses de C1 et C2 constituées par un mélange de périodes de rangs 1 et 2. Lorsque la transitoire maximum de R_j est proche de R_{j1}, la composante dominante du rythme est de rang 1 tandis qu'elle est de rang 2 si la transitoire maximum de R_j et proche de R_{j2}.

Nos résultats avec le système à couplage-R sont semblables aux observations expérimentales faites sur une paire de myocytes cardiaques couplés par un circuit RC. Vu que la cellule stimulée peut maintenir une décharge répétitive soutenue qui n'est pas affectée par l'activité de la cellule couplée dans le système à couplage-R_j, le mécanisme de feedback négatif contrôlant les changements de R_j assure un couplage intercellulaire plus serré sur un grand intervalle de fréquences de stimulation.

TABLE OF CONTENTS

LIST OF TABLES

LIST OF FIGURES

PARTIAL LIST OF SYMBOLS AND ABREVIATIONS

A: Cell membrane area (4.19×10^{-5} cm^2).

APD: Action potential duration (ms) measured from dV_{max}/dt to V_{-50}. APD_1 and APD_2 refer to C1 and C2, respectively.

APD_0: Action potential duration for the stable 1:1 rhythm in the space-clamped membrane.

APD_c: Action potential duration for dAPD/dDIA = 1.

AR: Activation ratio (number of stimuli vs number of different active responses during constant pacing).

ARP: Absolutely refractory periode (ms) which is measured from the S1 stimulus onset to the onset of the large amplitude S2 that fails to trigger an action potential.

BCL: Basic cycle length of stimulation (ms).

BCL_T: The basic cycle length at which the period number changes from 1 to 2.

C: Cell capacitance (1 $\mu F/cm^2$).

C1: Cell one of the cell pair.

C2: Cell two of the cell pair.

$[Ca]_{in}$: Intracellular calcium concentration (μM).

DIA: Diastolic interval (ms). DIA_1 and DIA_2 refer to C1 and C2, respectively.

DIA_0: Diastolic interval for the stable 1:1 rhtythm in the space-clamped membrane.

DIA_c: Diastolic interval for dAPD/dDIA = 1.

I.D.: Irregular dynamics.

I_{ion}: Membrane ionic current ($\mu A/cm^2$).

I_k: Total potassium outward membrane current ($\mu A/cm^2$).

I_{k1}: Outward time-independent potassium membrane current ($\mu A/cm^2$).

I_{Na}: Fast sodium inward membrane current ($\mu A/cm^2$).

Ig: Coupling current ($\mu A/cm^2$).

I_p: Peak ionic current ($\mu A/cm^2$). We use Ip_1 for C1 and Ip_2 for C2 . ΔIp is a change in I_p

I_{thR} : Threshold current for stimulation from the resting state ($\mu A/cm^2$) in the space-clamped membrane..

I_{thr} : Threshold current for stimulation away from the resting state ($\mu A/cm^2$) in the space-clamped membrane.

I_{thRC1} : Resting threshold current of C1 as R is changed in the two-cell system.

I_{si}: Secondary inward membrane current ($\mu A/cm^2$).

I_{stim}: Pulse stimulus amplitude ($\mu A/cm^2$). We have I_{stim1} for stimulus S1 and I_{stim2} for stimulus S2. ΔI_{stim} is a change in I_{stim}.

I_x: Outward time-dependent potassium membrane current ($\mu A/cm^2$).

Lat: Latency of the action potential upstroke (ms).

P: Period number or number of stimuli.

pCa_{in}: $-Log[Ca]_{in}$.

r: Calcium-dependent gating variable controlling the gap junction resistance (Rj), with steady state characteristic r_∞ and time constant τ_r. We use r_1 for C1 and r_2 for C2.

R: Fixed gap junction resistance (Ω).

Rj: Calcium-dependent gap junction resistance (Ω).

Rb: Minimum resistance of all the connexons attached to two coupled cells (KΩ).

(S1-S1): Interval between two successive S1 stimuli (ms).

(S1-S2): Interval between a conditioning stimulus S1 and a test stimulus S2 (ms).

TR: Time to repolarization, i.e., from stimulus onset to T_{-50}. ΔTR is a change in TR

T_{stim}: Pulse stimulus duration (ms). We have T_{stim1} for stimulus S1 and T_{stim2} for stimulus S2. ΔT_{stim} is a change in T_{stim}.

T_{-50} : Time of -50 mV repolarization of the action potential measured from the stimulus onset.

Thr(DIA): Threshold function defining the required threshold current at a given DIA, and normalized with respect to the resting threshold.

V: Membrane potential (mV). We use V_1 for C1 and V_2 for C2.

V_{max}: Maximum membrane potential shift during the upstroke (mV).

V_{min}: Minimum membrane potential prior to or following the action potential (mV).

V_{-50}: Membrane potential at -50 mV repolarization of the action potential.

y: Gating variables of MBR model (m, h, d, f, x).

$y_{i\infty}(V)$: Steady state values of gating variables (m_∞, h_∞, d_∞, f_∞, x_∞).

τ_i(ms): Time contants of gating variables (τ_m, τ_h, τ_d, τ_f, τ_x)

CHAPTER I

INTRODUCTION

A normal, coordinated, and effective ventricular contraction is initiated and controlled by the propagated cell-to-cell spread of electrical excitation through the myocardial substratum. If, for some reason, the normal excitation sequence is disrupted, the effectiveness of cardiac contraction is substantially reduced. The various types of disruptions of the normal excitation and repolarization patterns during propagation through the myocardium are known under the generic term of cardiac arrhythmias. There are several types of cardiac arrhythmias ranging from the relatively benign supraventricular flutter to life-threatening arrhythmias such as ventricular tachycardia and fibrillation.

The most accepted hypothesis for the initiation and maintenance of tachycardia and fibrillation is through reentry (Wit et al., 1978; Allessie et al., 1977; Bernstein et al., 1990; Davidenko et al., 1992). Reentry is an electrophysiological disorder in which an activation front continuously finds a closed propagation pathway through the myocardium. The pathway might form around an anatomical obstacle, such as the orifice of a major vessel (Frame et al., 1986; Bernstein et al., 1990) or an island of infarcted tissue (de Bakker et al., 1988). It might also form around functionally refractory, but

otherwise normal, regions of myocardium (Allessie et al., 1973, 1976, 1977; Frazier et al., 1989; Davidenko et al., 1992).

As a first approximation, the myocardial substratum may be viewed as a network of parallel interconnected individual rod-shaped myocytes having an average diameter of 12-20 μm and a length of about 100 μm (Sjöstrand et al., 1954). The myocytes are physically (Sommer et al., 1985) and electrically (Dewey et al., 1964) interconnected through low resistance channels called nexuses or gap junctions (Peracchia, 1990). Despite their often postulated "low resistance", these junctions still present resistive hindrances to intercellular currents (relative to intracellular currents), and thus create discontinuities in the transmission of excitation from cell to cell (Spach et al., 1981). When the myocytes are abutted end-to-end to form elongated cardiac fibres, two consecutive cells are generally linked by only a small number of gap junctions which offer a low resistance to current flow and propagation can be considered reasonably continuous (Spach et al., 1983). On the other hand, in the direction normal to the long cell axis, two neighbouring fibres are much more loosely coupled via a number of gap junctions which give rise to a substantially larger equivalent junctional resistance that makes transverse propagation essentially discontinuous (Spach, 1983).

During anisotropic propagation in cardiac muscle, unidirectional block of a premature action potential may very well arise in the longitudinal direction while transverse propagation may be more secure (Spach et al., 1990; Keener, 1988). The

occurrence of unidirectional block is considered to be the main event leading to reentry and therefore to different types of tachyarrhythmias (Spach et al., 1982). In addition, since the gap junction resistance is known to vary substantially during repetitive activity through changes in factors such as the intracellular calcium concentration ($[Ca]_{in}$) and the intracellular pH (De Mello, 1982), it constitutes a potent mechanism to modulate the continuation or termination of the reentry. The distribution of gap junction resistances throughout the myocardial substratum is clearly a key determinant of cardiac propagation and the properties of gap junctions may enhance or inhibit the occurrence of severe cardiac arrhythmias.

The central problem addressed in the present model study is the role of the gap junction resistance in the coupling of two cardiac myocytes during regular pacing applied to one of the cells. We consider the following three cases in increasing order of complexity: 1) regular pacing of an isolated myocyte, 2) regular pacing of a pair of cells coupled through a fixed resistance, and 3) regular pacing of a two-cell system in which the junctional resistance varies with the rate of repetitive firing of both cells through changes in their intracellular calcium concentration. It is anticipated that a better understanding of the dynamic behaviour of a pair of myocytes under reasonably realistic physiological conditions will offer useful insights for the prevention and clinical management of some cardiac arrhythmias.

1.1 Membrane Models

In the late 1970s, two models of the electrical activity of cardiac cells were formulated based on the formalism introduced by Hodgkin and Huxley (1952). McAllister et al. (1975) developed a model of the cardiac Purkinje fibre action potential. Subsequently, Beeler and Reuter (1977) published a model of the electrical activity of the mammalian ventricular myocyte (referred to as the BR model in the present work). The BR model was based on experimental data that were available at the time from voltage-clamp studies, and were drawn from various preparations so that an "average" action potential was in fact reconstructed. These data were subject to limitations in available voltage-clamp techniques and their application to multicellular preparations of cardiac muscle (Ebihara & Johnson, 1980). In addition, the concentrations of ions in the extracellular clefts of the multicellular preparations were unknown.

With the development of single-cell and single-channel recording techniques in the 1980s, the limitation of voltage-clamp measurements were overcome and the intracellular and extracellular ionic environments could be controlled. A major limitation of the BR model involved the Na current kinetics which were shown to be too slow in the light of experimental data obtained in single cells. This led Ebihara and Johnson (1980) to propose a new formulation, and Drouhard and Roberge (1987) to modify the sodium current formulation of the BR model to constitute the present version of the MBR

model used in many subsequent studies (Vinet et al., 1990, 1994).

The data from single-channel recordings provide a basis for a quantitative description of channel kinetics and membrane ionic currents. In 1985, DiFrancesco and Noble (1985) developed a model of the Purkinje fibre action potential based on available single-cell and single-channel data, which included also a representation of intracellular sodium and calcium concentration changes. This model was subsequently extensively revised by Nordin (1993).

Rasmusson et al. (1990) developed a model of cardiac atrial activity based on data from the bullfrog atrium. Lemieux et al. (1990) added a biochemical model of active Na-K transport to the MBR model and studied the effects of ionic concentration changes on the action potential; they also subsequently described a new non-inactivating delayed rectifier potassium current to replace that of the BR model (Lemieux et al., 1994). Luo and Rudy (1991) proposed another version of the BR model (called LR model, phase-1) which incorporated a new potassium current that activates at plateau potentials and the possibility of changing the extracellular potassium concentration. A phase-2 LR model was subsequently proposed (Luo and Rudy, 1994), which incorporated a number of extensions to include a new formulation of the sarcolemmal calcium current, a sodium-calcium exchanger, and a mechanism of calcium-induce-calcium-release for the sarcoplasmic reticulum combined with the regulation of the intracellular calcium concentration.

Although there is considerable interest in the new comprehensive cardiac membrane phase 2-LR model (Luo and Rudy, 1994), its high complexity makes it poorly suited for the type of study undertaken in the present thesis. Since we consider the behaviour of a single cell and that of a system of two coupled cells subjected to a wide range of pacing frequencies, we need to have a thorough understanding of the dynamic properties of the membrane model to identify clearly the new dynamical features that could be introduced by the variations of the gap junction resistance. This understanding is not yet fully documented for all the main aspects of the dynamic behaviour of the phase-2 LR model and its use in the present study would have been premature.

On the other hand, although the MBR model does not include many of the membrane conductance components and intracellular features influencing the shape of the action potential discovered in recent years, it does incorporate the three widely recognized scales of channel gating times constants: a short time constant for the action potential upstroke, a medium one for the plateau phase, and a long one for the repolarization phase. In addition, the dynamic properties of the MBR model have been extensively studied in terms of its stability characteristics and oscillatory behaviour (Chay et al., 1985; Vinet, 1988; Vinet and Roberge, 1990), including the expression of its activation and repolarization processes by simplified dynamic equivalents (Vinet and Roberge, 1994) and their representation by means of iterative difference equation equivalents (Chialvo et al., 1990; Lewis et al., 1990).

Part of the work described in the present thesis (Chapters II, III and IV) is a refinement and an extension of previous studies on the bifurcation structure of the space-clamped MBR model (Vinet et al., 1990). This confirmation and extension of previous results appeared important and also allowed us to undertake the study of the system of two coupled cells on a firmer basis.

1.2 Properties of Cardiac Gap Junctions

A cardiac gap junction consists of an aggregate of channels that span the plasma membranes of adjacent cells and link their cytoplasmic compartments together. The component channels of the gap junction are formed from pairs of connexons aligned with one another so as to bridge the narrow gap between adjacent cell membranes. Each connexon consists of six subunits, and each subunit is formed from a separate protein molecule (Zimmer et al., 1987; Milks et al., 1988; Unwin et al., 1980; Sosinsky et al., 1988). These subunits are assembled in a quasi-hexagonal array (Figure 1.2.1) which constitutes a cytoplasmic channel permeable to various ions and molecules of up to 1 KDa (Lowenstein, 1981; Peracchia, 1981; Ramon et al., 1987; Rook et al., 1988).

The gap junction exhibits electrical properties and functions based on the direct exchange of ions and various molecules between adjoining cells. A primary function of the gap junction is the electrical coupling of myocytes (cardiac muscle cell), enabling the

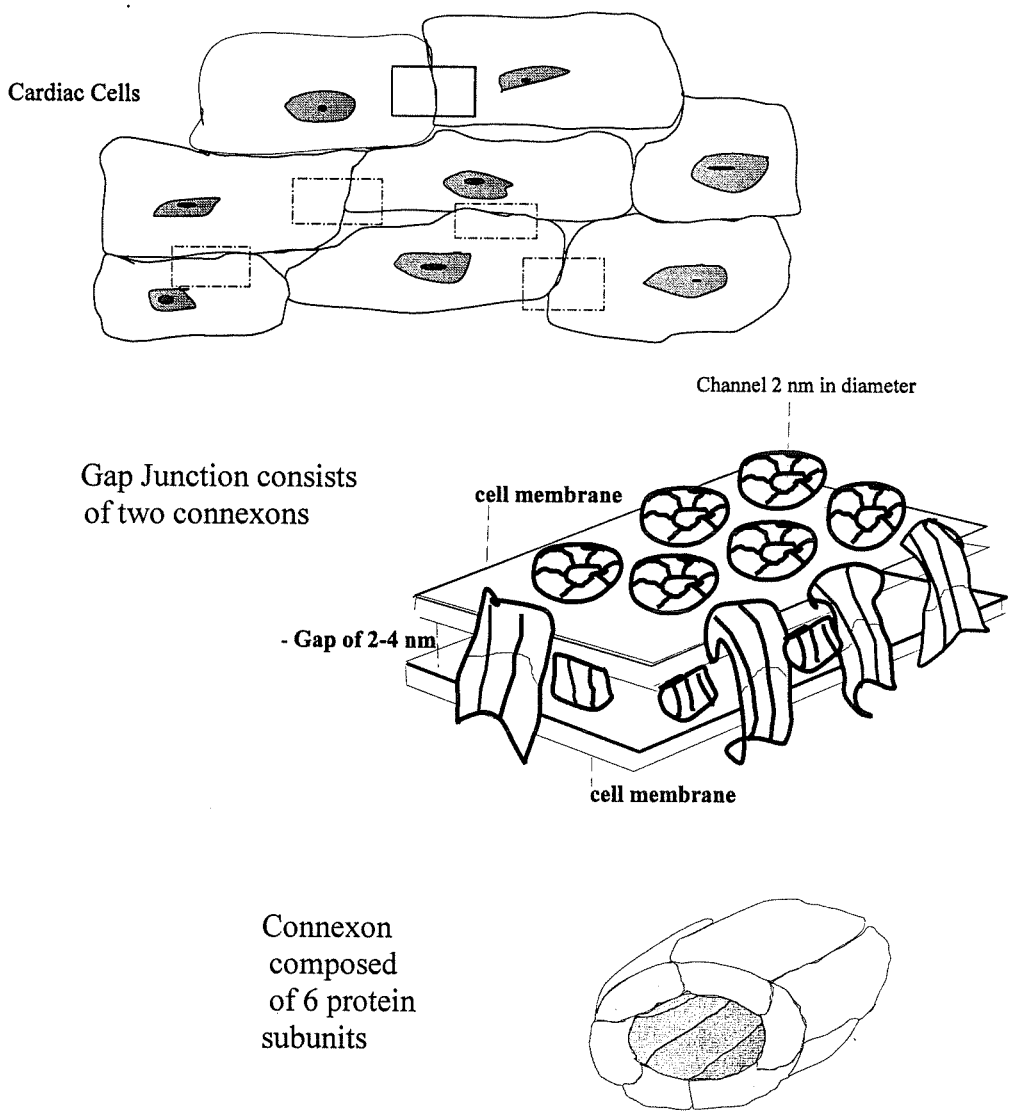

Figure 1.2.1: Structural characteristics of the cardiac gap junction. Cell assembly (at the top) with rectangles drawn around particular gap junctions. Diagram of part of a gap junction (middle) showing two opposing membrane patches and several bridging channels. Each channel is made of two abutted connexons of the type shown at bottom.

integrated operation of neighbouring cells and propagation of the action potential throughout the myocardium. Hence the gap junction provides a resistive pathway for local current flow between adjacent cells and thus permits the spread of electrical activity over the entire excitable tissue.

During pathological conditions leading to cell injury, the healthy cell seals itself from its injured neighbours by increasing the electrical resistance of its gap junctions. This phenomenon is called the "healing over" process and the resulting electrical isolation prevents the deterioration of myocytes that are coupled to cells that have died (De Mello, 1982). In normal tissue, gap junctions should have a low resistance to facilitate the spread of electrical activity. For example, the electrical signals produced by the SA node reach the AV node by propagation through the atrial myocardium and subsequently access the ventricular myocardium via the Purkinje fibre system. Therefore, if gap junctions in a given region of the heart do not provide low-resistance pathways, there will be conduction and repolarization disturbances that may lead to arrhythmias (Joyner et al., 1984; 1986). The question of central interest in the present work is the mechanism by which the gap junction resistance is altered during activity.

Many drugs and ions affect the resistance of the gap junction. Experimental studies that focused on the electrical characteristics of the gap junction channel, in different excitable tissues, reported the following observations. An increase in intracellular hydrogen ions increases the resistance of the gap junction channel in

amphibian embryonic cells (Turin et al., 1977, 1980), in *Chironomus* salivary gland cells (Rose et al., 1978), in embryonic cells from *Fundulus heteroclitus* (Spray et al., 1982), in adult dog ventricular epicardium (Hoyt et al., 1990), in the adult rat myocyte (White et al., 1990), and in ventricular cells of guinea pig hearts (Noma et al., 1987). Moreover, a parallel increase in junctional resistance and intracellular calcium concentration has been reported first by Lowenstein (1966) in perforated salivary gland cells and confirmed by the work of Rose et al. (1976) and (1978). Similar observations were made in cardiac Purkinje fibres of the sheep heart (Dahl et al., 1980), in embryonic killifish (Spray et al., 1982), in ventricular cells of guinea pig hearts (Kameyama, 1983; Noma et al., 1987), and in adult ventricular rat hearts (Metzger et al., 1985; Maurer et al., 1987, White et al., 1990).

Although there are several cases in which electrical coupling has been shown to be influenced by transmembrane potential changes, the gap junction resistance of adult mammalian heart is believed to be voltage independent. Voltage-dependent gap junctions have been shown to be present in crayfish nerve (Jaslove et al., 1986; Giaum et al., 1983; Margiotta et al., 1983). Moreover, the gating of the gap junction channel, in amphibian blastomeres, has been shown to exhibit marked voltage dependence (Harris et al., 1981; Bennett et al., 1984). This voltage dependence was seen also in neonatal rat heart's cells (Rook et al., 1988) and in the embryonic cardiac tissue of many species (Margiotta et al., 1983; Spray et al., 1985; White et al., 1982). This potential dependence was not shown to be present in adult ventricular tissue of these species.

Various drugs affect directly or indirectly the resistance of the gap junction. Volatile anaesthetics such as halothane and ethrane have great influence on the gap junction resistance. Increasing the concentration of such agents decouples cardiac cells isolated from neonatal rat hearts within 20 minutes (Burt et al., 1989). In another experiment, the resistance of the gap junction between pairs of neonatal rat heart cells was rapidly and reversibly increased by oleic acid in a time-dependent manner (Burt et al., 1991). Many studies showed that heptanol and octanol increase the cardiac gap junction resistance (Joyner et al., 1985; Hauswirth, 1968; Terrar et al., 1988). On the other hand, Verapamil has been used to prevent the increase in gap junction resistance during pacing of ischemic tissue (Hiramatsu et al., 1989). However, the mechanism by which these drugs affect the gap junction resistance is not yet well established.

These characteristic changes of the gap junction resistance suggest the following questions. Is the gap junction resistance constant and steady during the spread of membrane depolarization, despite a tenfold increase in $[Ca^{2+}]_{in}$? Does the rate of repetitive activity change the gap junction resistance, given that low stimulation frequency produces long diastolic intervals and rapid pacing yields small diastolic intervals or missed beats? To be able to answer such questions, one should have first a good quantitative representation of the variation of the gap junction resistance during electrical activation. An important goal of this thesis is to describe a model for the calcium dependence of the gap junction resistance of cardiac cells.

1.3 An Overview of the Thesis

The membrane dynamical properties of the MBR model are well established (Vinet et al., 1990, 1994; Chay et al., 1990; Lewis and Guevara, 1990) and it constitutes a very useful tool to investigate the behavior of a system of two coupled myocytes. This system was studied in the presence of a fixed junctional resistance in order to better understand how the first stimulated cell influences the second one during repetitive activity. There is considerable interest also in a more physiological representation of the junctional resistance when its rate-dependent features can be taken into account during frequency entrainment.

Because of the complexity of the system of coupled cells, we have chosen to begin with a careful description of the effects of the pulse stimulus parameters on the behavior of the MBR model. Chapter II presents a formal description of the model, with additional details provided in Appendix A, and focuses on the way the threshold behavior is affected by the conditioning and test stimuli and by the rate of regular pacing. Chapter III follows in the same vein and addresses the transformation of the action potential duration as a function of the same parameters. Chapter IV provides a detailed description of the repetitive response of the MBR model to regular pacing, particularly in terms of bifurcation maps based on the strength of the driving stimulus as the bifurcation parameter.

We introduce the system of two coupled myocytes in Chapter V and describe its behavior when the first cell is entrained at various fixed rates with different values of the constant coupling resistance. The major points of interest are the loading of the first cell by the second, the modulation of the coupling current intensity by the coupling resistance, and the wide variations in the firing latency of each cell.

Chapter VI describes a new model of the cardiac gap junction resistance. The central feature of this model is the dependence on the intracellular calcium concentration of each cell. As a result, the gap junction resistance becomes a function of the rate of firing of both cells.

This new model of the gap junction resistance is incorporated into the two cell system and the behavior of the resulting assembly is studied in Chapter VII. Since the gap junction resistance increases with the firing rate of both cells, it acts as a negative feedback mechanism to limit the maximum firing rate of the two cell assembly. There are complex interactions between the driven cell (directly stimulated) and the follower cell (stimulated by the coupling current) and they are compared to the results of Chapter V obtained with a constant junctional resistance.

Chapter VIII summarizes the main results of the study and presents a general discussion of the major points.

CHAPTER II

THRESHOLD PROPERTIES OF THE MEMBRANE MODEL

2.1 The Model

We used a modified version of the Beeler-Reuter model (BR) with the formulation of the sodium current introduced by Drouhard and Roberge (1987), which we call the MBR model. It is a seven-dimensional Hodgkin-Huxley (H-H) type formulation that includes the membrane potential (V), 5 gating variables (y_i = m, h, d, f, x) and a representation of intracellular calcium concentration changes ($[Ca]_{in}$). The equations are:

$$C\frac{dV}{dt} = -I_{ion}(V, [Ca]_{in}, y_i, i=1,5) + I_{stim}(t) \qquad (2.1)$$

$$\frac{dy_i}{dt} = \frac{1}{\tau_i(V)}(y_i - y_{i\infty}(V)) \quad , \quad i=1,5 \qquad (2.2)$$

$$I_{ion} = I_{Na}(V, m, h) + I_{si}(V, d, f, [Ca]_{in}) + I_k(V, x) + I_{Nac}(V) \quad (2.3)$$

$$\frac{d[Ca]_{in}}{dt} = -7.5\times10^{-8} I_{si} - 0.07(10^{-7} - [Ca]_{in}) \quad (2.4)$$

where C is the membrane capacitance (1 $\mu F/cm^{-2}$), I_{ion} is the total ionic current that includes two inward currents, I_{Na} and I_{si}, and the potassium outward current I_k comprising a delayed rectifier I_x and a time-independent component I_{k1}. I_{stim} is a rectangular current pulse stimulus. The voltage-dependent steady-state characteristic ($y_{i\infty}(V)$) and time constant ($\tau_i(V)$) of gating variables y_i are depicted in Fig. 2.1.1. The equation describing $[Ca]_{in}$ changes in the original BR model was modified to give more moderate changes in $[Ca]_{in}$ during the course of a normal action potential. $[Ca]_{in}$ at rest is around 0.1-0.2 μM in cardiac myocytes of various species, and may reach a maximum of 1.0-1.2 μM during the plateau of the action potential (Noma et al., 1987; Weingart et al., 1987; Noble et al., 1986). In the standard BR model, the maximum $[Ca]_{in}$ reached during the plateau is substantially larger. Here, by reducing the first constant of Eq. 2.4 by 75%, we have diminished peak $[Ca]_{in}$ by 25% to about 5 μM.

Expressions for the ionic currents are:

$$\begin{aligned} I_{Na} &= \overline{g_{Na}}\, m^3\, h\, (V-E_{Na}) \\ I_{si} &= \overline{g_{si}}\, d\, f\, (V-E_{si}) \\ I_k &= I_x(V)\, x + I_{kl}(V) \end{aligned} \quad (2.5)$$

where $\overline{g}_{Na}$ is the maximum sodium conductance (15 $\mu S/cm^2$), E_{Na} is the reversal potential

(60 mV) and $\bar{g}_{si}$ is the maximum slow inward current conductance (0.09 μS /cm^2). E_{si}= -82.3 mV - 13.0287 ln($[Ca]_{in}$) is the reversal potential for I_{si}. Expressions for $I_x(V)$ and $I_{k1}(V)$ can be found in Appendix A.

Note that τ_h and τ_d are of comparable magnitude and more than 100 times larger than τ_m (Fig.2.1.B), while τ_f and τ_x are approximately 10 times larger than τ_h or τ_d. The presence of three well separated ranges of time constants (τ_m for the upstroke, τ_h and τ_d for the plateau, and τ_f and τ_x for the repolarization phase) defines the main dynamic characteristics of the MBR model. It has an intermediate level of complexity, between the simple two-time scales formulation of the Fitzhugh-Nagumo model (1962) and the more involved formulations incorporating ionic pumps and exchangers, as well as different processes of internal ionic concentration regulation (Noble et al., 1986; Lemieux et al., 1990; Luo et al., 1994; Nordin, 1993).

The model also includes a sodium background current:

$$I_{Nac} = \overline{g_{Nac}} \, (V - E_{Na}) \qquad (2.6)$$

with $\bar{g}_{Nac}$ = 0.003 μS /cm^2.

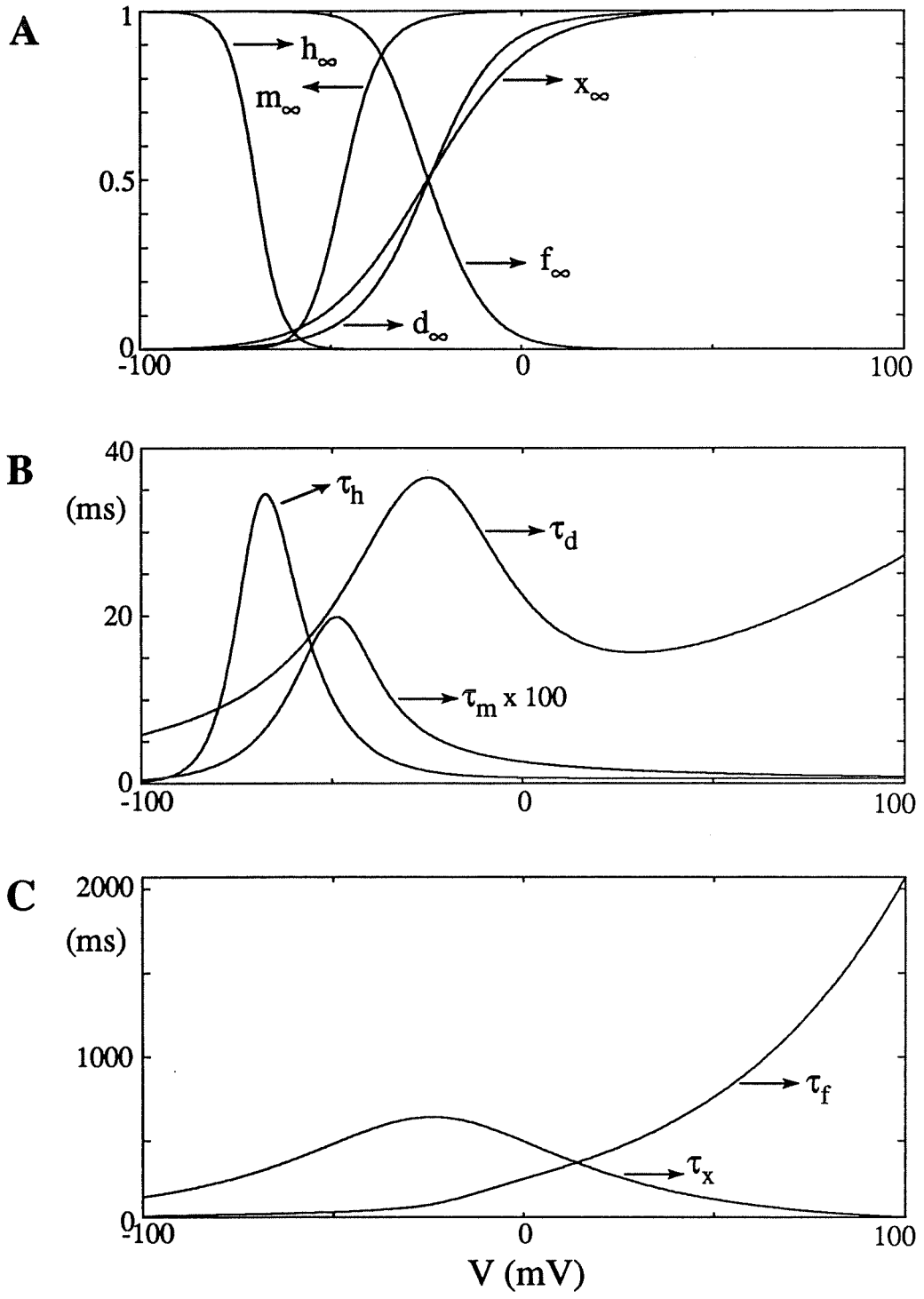

Figure 2.1.1: Gating variables of the MBR model. A) Steady-state characteristics: m_∞, h_∞, d_∞, f_∞, x_∞. B) and C) Corresponding time constants.

2.2 The Calculation Method

The set of nonlinear ordinary differential equations (Eqs 2.1, 2.2, 2.3, 2.4 and 2.5) was solved numerically. Peak $\tau_m(V)$ is in the range of 0.2 ms while peak $\tau_x(V)$ is greater than 600 ms. Moreover, $\tau_f(V)$ increases monotonically with V to reach 1000 ms at 80 mV. In such a stiff system of differential equations, the standard numerical integration methods require small time steps to converge, leading to extremely long calculation times (Victorri et al., 1985).

We used an hybrid integration method described by Moore and Ramon (1974) and Drouhard et al. (1982a), which was shown to converge by Victorri (1982) . The method is based on the approximation that $y_{i\infty}(V)$ and $\tau_i(V)$ may be considered constant during a time increment Δt if the variation of V is kept small. With this approximation, Eq. 2.2 may be solved analytically as:

$$y_i(t+\Delta t) = y_{i\infty}(V(t)) - (y_{i\infty}(V(t)) - y_i(t)) e^{\left(-\frac{\Delta t}{\tau_i(V(t))}\right)} \qquad (2.7)$$

Then, Eq. 2.1 was solved as:

$$V(t+\Delta t) = V(t) + \frac{\Delta t}{C}(I_{stim} - I_{ion})$$

$$I_{ion} = \frac{I_{ion}(V(t),[Ca]_{in}(t),y_i(V(t))) + I_{ion}(V(t), [Ca]_{in}(t), y_i(V(t+\Delta t)))}{2} \quad (2.8)$$

and Eq. 2.4 as:

$$[Ca]_{in}(t+\Delta t) = \Delta t\ (-7.5\times10^{-8} I_{si} - 0.07(10^{-7} - [Ca]_{in}(t)) + [Ca]_{in}(t)) \quad (2.9)$$

For the solution to converge, the method requires that the variations of V and $[Ca]_{in}$ remain small at each time step. For the single isolated membrane patch, we used time steps between 0.001 and 0.512 ms. When V variations were within 0.4 to 1 mV, and $[Ca]_{in}$ changes did not exceed 4%, the time step was accepted. When V or $[Ca]_{in}$ variations were larger, Δt was halved and computation was restarted. When ΔV was below 0.4 mV and $\Delta[Ca]_{in}$ less than 1%, Δt for the following time step was doubled. To precisely get a fixed BCL or T_{stim}, Δt was always adjusted to get the onset and termination of the stimulation at the prescribed times with a precision greater than 10^{-8} ms, even if Δt was required to be more than 10^{-3} ms.

2.3 Threshold Properties at Rest

With the parameters given above, the model has a resting point P_r corresponding to V_r= -84.75 mV, $y_{ir} = y_{i\infty}(V_r)$, and $[Ca]_{inr}$ = 1.5823 μM as determined by numerical simulation. Linearization has been used to show that P_r is locally stable (Chay et al.,1985; Vinet et al.,

1990). Since the system was always observed to return to P_r after a wide range of perturbations, we assume that it is the only stable state of the system. Clearly, then, such a continuous excitable system cannot have a real threshold behaviour, with a separatrix dividing the basins of attraction corresponding to distinct stable points (Fitzhugh, 1955; Guckenheimer and Holmes, 1988). At the end of any stimulation, the system will follow a continuous trajectory which converges asymptotically toward the resting point. Moreover, any continuous change of the stimulation amplitude or duration (I_{stim} and T_{stim}) would result in a continuous variation of the state at the end of stimulation, to yield a family of continuous trajectories ending at P_r.

However, for T_{stim} fixed and continuous variation of I_{stim}, we observed a sharp transition in the time course of repolarization, as with other versions of the MBR model (Vinet et al., 1990; 1994). For low I_{stim}, the peak inward current (I_p) always remained below 1 $\mu A/cm^2$. Then, within a small range of I_{stim}, I_p jumps to a few hundred $\mu A/cm^2$ (see Fig. 2.3.1). The sharp change in I_p is associated with a change in the form of the response, from a short graded response to a fully developed action potential with a much longer time course. This feature was quantified by computing the time to repolarisation (TR), defined as the time elapsed from the onset of the stimulation to the -80 mV down-crossing during repolarization. TR reacts like I_p to an increased I_{stim}, varying abruptly from a few milliseconds for electrotonic responses to a few hundreds of milliseconds for action potentials (Fig. 2.3.1). In the example shown in figure 2.3.2, using T_{stim} = 5 ms and changing I_{stim} by $\pm 10^{-6}$ $\mu A/cm^2$, I_p varies from a minimum of 0.133 $\mu A/cm^2$ (not shown) to a maximum of 230 $\mu A/cm^2$, with

an intermediate value of 61 $\mu A/cm^2$. This surge of membrane current is caused by the activation of I_{Na} (Fig. 2.3.3). Hence, the abrupt rise in I_p or TR could be used to define threshold and the threshold current could be taken as the I_{stim} value for which ($\Delta I_p/\Delta I_{stim}$) or ($\Delta TR/\Delta I_{stim}$) reached a maximum (Vinet et al., 1994). Since the phenomenon is not strictly "all or none", but rather a steep continuous transition, it corresponds to a quasi-threshold property (FitzHugh, 1955). Since our goal was to obtain the shape of the threshold function, we simplified the calculations by searching for the minimum stimulus intensity which induced a net surge of inward membrane current for more than 0.55 ms (as in Vinet et al., 1990). The search was done by stepping I_{stim} back and forth, until the criterion was satisfied with a precision of 0.01 $\mu A/cm^2$.

Fig. 2.3.4 shows the threshold current at rest (I_{thR}) for T_{stim} variations between 0.5 to 50 ms in steps of 0.5 ms. I_{thR} decreases monotonically with T_{stim}. The sharpest decline occurs during the first 15 ms, with I_{thR} falling from 61.3 $\mu A/cm^2$ at T_{stim}= 0 .5 ms to 3.5 $\mu A/cm^2$ at T_{stim}= 15 ms. The subsequent decrease is much slower, reaching 2.3 $\mu A/cm^2$ at 50 ms. The I_{thR} vs T_{stim} curve was fitted with a double-exponential function, leading to a minimum asymptotic value (i.e. $T_{stim} \rightarrow \infty$) of = 2.1$\mu A/cm_2$.

This result reflects the fact that I_{thR} cannot go to zero while T_{stim} is increased because there must be some residual value of gating variable h for which m begins to open. Since m_∞(V) has a substantial value in the range of voltage where h_∞ (V) is already closed (Fig. 2.1), there is a limit to the time spent below threshold beyond which h will be closed and no

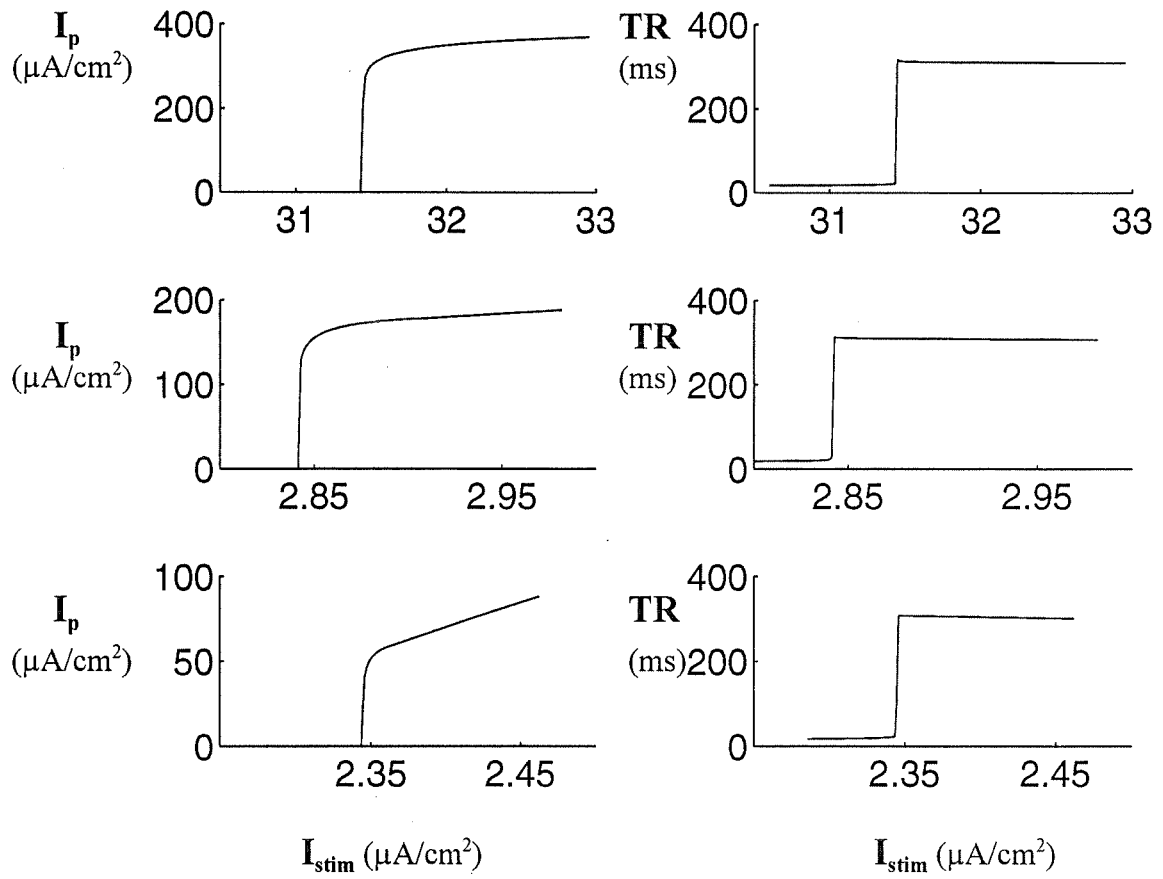

Figure 2.3.1: Variation of I_p (left columm) and TR (right columm)for T_{stim}= 1 ms (upper panels), T_{stim} = 25 ms (middle panels), and T_{stim} = 50 ms (lower panels).

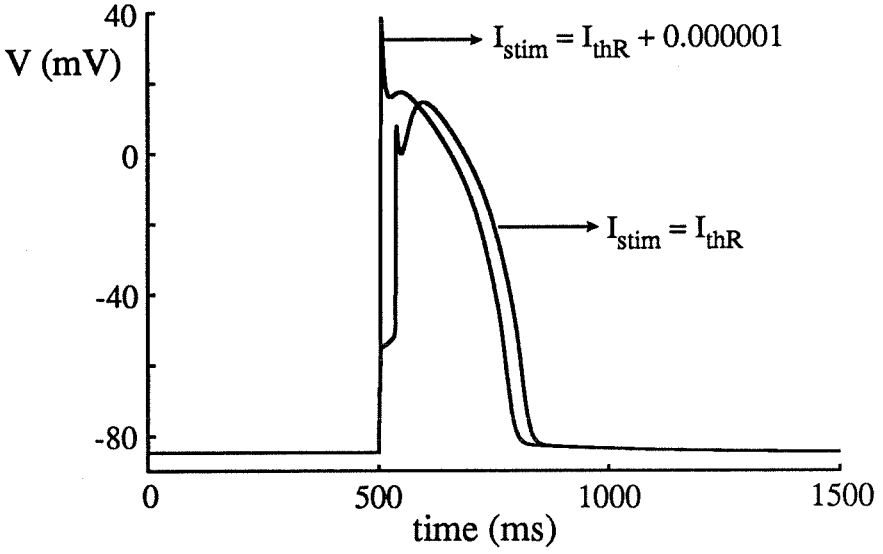

Figure 2.3.2: Membrane potential responses from the resting state, when T_{stim} = 5 ms, I_{stim} = 7.4502602, and I_{stim} = 7.4502612 μA/cm^2. A small variation of I_{stim} leads to major differences in the responses.

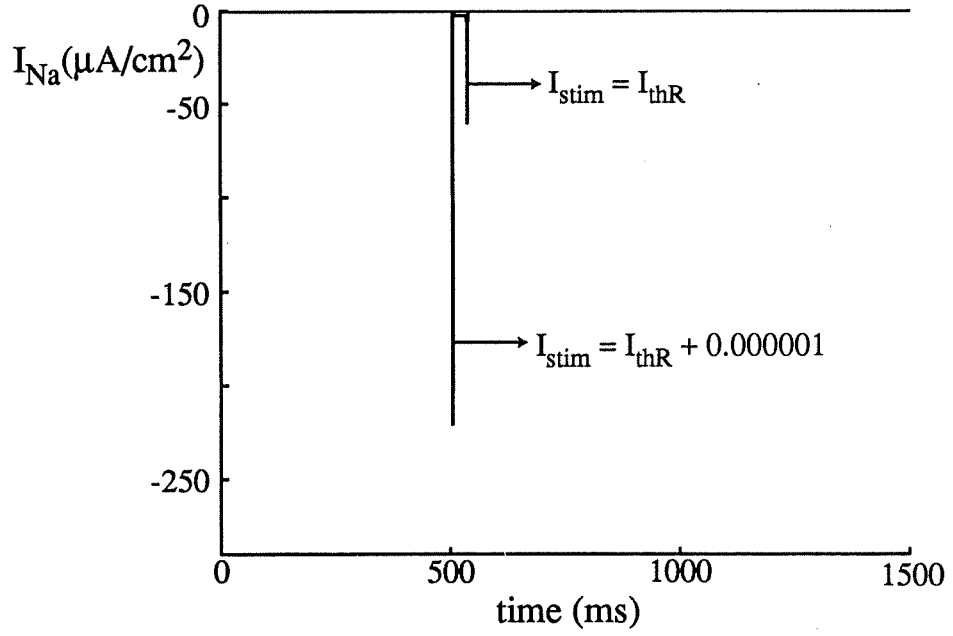

Figure 2.3.3: Sodium current responses from the resting state for T_{stim} = 5 ms, I_{stim} = 7.4502602, and I_{stim} = 7.4502612 μA/cm^2. A small variation of I_{stim} leads to major difference in I_{Na}.

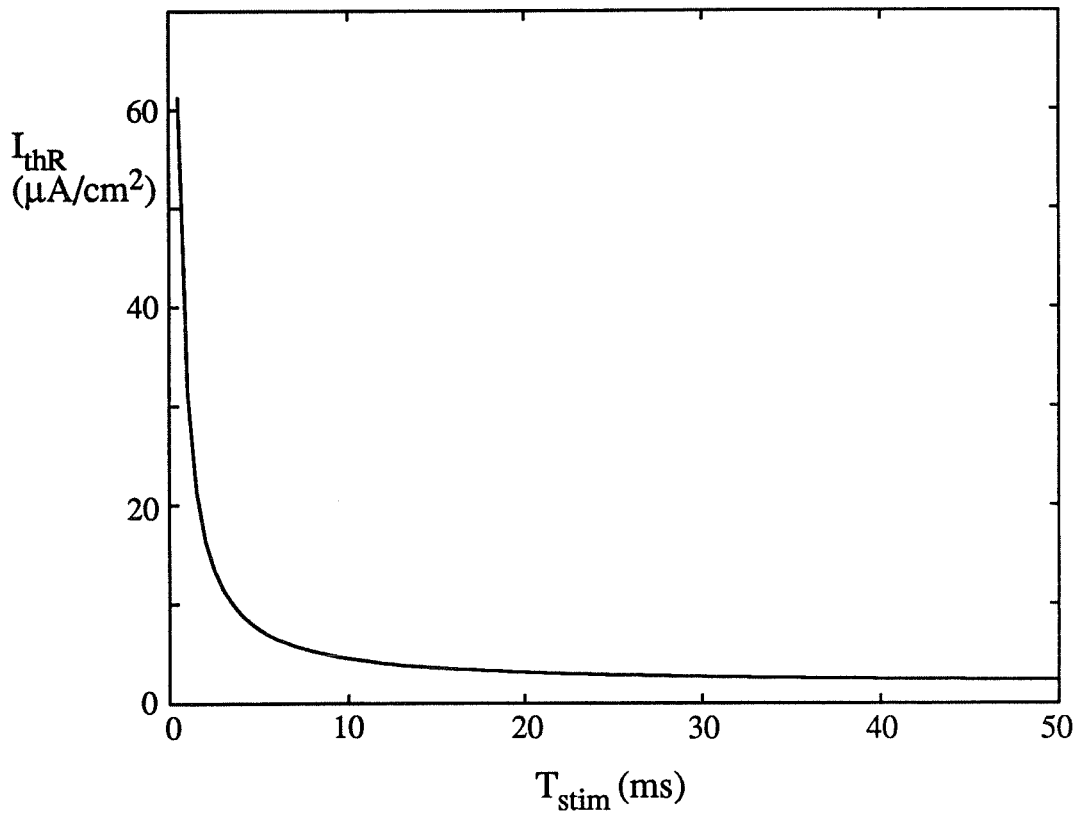

Figure 2.3.4: Changes of I_{thR} ($\mu A/cm^2$) vs T_{stim}.

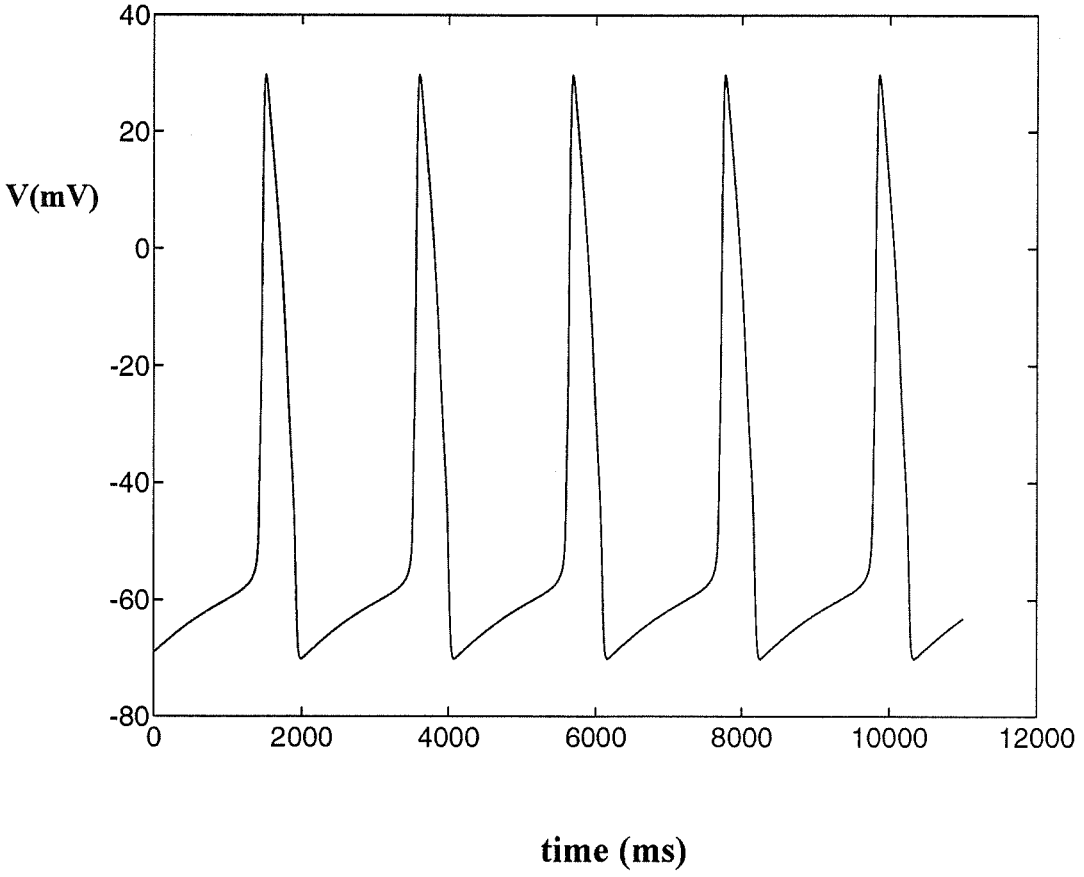

Figure 2.3.5: The automaticity of the system when $T_{stim} = \infty$ and $I_{stim} = 2.01\ \mu A/cm^2$. The frequency is = 0.538 Hz.

surge of I_{Na} will be possible. In fact, for very long T_{stim}, the I_{thR} values should be close to the value of the bias current for which the system becomes automatic. We found by simulation that the system was automatic with a frequency of 0.538 Hz for a bias current of 2.01 $\mu A/cm^2$ (Fig. 2.3.5), which is close to the asymptotic value of the I_{thR} vs T_{stim} curve (2.1 $\mu A/cm^2$, Fig. 2.3.4).

2.4 Excitability Recovery

In addition to its dependence on T_{stim}, the threshold current is also a function of the state of the system at the onset of stimulation. An exhaustive exploration of the whole space of initial conditions is obviously impossible. Since our ultimate goal is to study the entrainment characteristics of the model, we have chosen to restrict our exploration to a subset of initial conditions representative of those occurring at the onset of stimulation during regular pacing.

We followed a procedure which has been widely used in the analysis of mathematical models of excitable tissue and the study of experimental preparations. The system was first paced with a regular train of suprathreshold S1 stimuli at a given basic cycle length (BCL or time interval (S1-S1) between the onset of consecutive stimuli). Then, following the last action potential produced by the S1 of the train, the threshold of excitability recovery (I_{thr}) was determined by the application of a premature stimulus (S2) at various coupling intervals

(S1-S2). Various combinations of S1 parameters (I_{stim1}, T_{stim1}, S1-S1) were studied, but the BCLs were restricted to a range giving stable 1:1 responses. Stability was tested by requiring, for ten successive responses, a difference of less than 1% for V_{min}, V_{max}, I_p and all variables measured at the onset of stimulation. I_{thr}(S1-S2) was calculated using the same criteria employed for I_{thR} in the preceding section. Results with T_{stim1} = 1 ms, I_{stim1} = 1.25 I_{thR} and (S1-S1) = 1000 ms are presented first to discuss the effect of the duration of S2 (T_{stim2}) on I_{thr}(S1-S2), and to serve as a reference to discuss the effects of changing the S1 parameters.

2.4.1 I_{thr}(S1-S2, T_{stim2}), Reference Case

I_{thr}(S1-S2, T_{stim2}) was obtained for T_{stim2} ranging from 1 to 45 ms. Curves for I_{thr}(S1-S2, T_{stim2})/I_{thR} are plotted in Figure 2.4.1.1 for various values of T_{stim2}. The values of I_{thR} are given in Table 2.4.1.1 for different values of T_{stim1} (see also Fig. 2.3.4).

Table 2.4.1.1:. I_{thR} for different value of T_{stim1}.

T_{stim1} (ms)	1	5	15	25	35	45
I_{thR} ($\mu A/cm^2$)	31.4139	7.4706	3.5764	2.8415	2.5417	2.3869

For comparison, the curves of Fig. 2.4.1 were divided into three categories: short ($T_{stim2} \leq$

5 ms), intermediate ($5 < T_{stim2} \leq 35$ ms), and long ($T_{stim2} > 35$ ms) stimulus durations.

1. Short T_{stim2}

Starting from a large (S1-S2), $I_{thr}(S_1\text{-}S_2)$ first decreases slightly and then drops sharply near (S1-S2) = 320 ms to reach a minimum of about 50% of I_{thR} at $(S_1 - S_2)$ = 279 ms. It then increases abruptly to infinity (not shown) over an interval of less than 1 ms. For $(S_1 - S_2) < 273$ ms, it was impossible to measure an active response since the system had reached its absolutely refractory period (ARP).

2. Intermediate T_{stim2}

$I_{thr}(S_1 - S_2)$ increases beyond I_{thR} as $(S_1 - S_2)$ is reduced, reaches a finite maximum (I_{thrmax}) and then decreases to a minimum (I_{thrmin}) before going to infinity when the ARP is reached. Relative to I_{thR}, I_{thrmax} increases as T_{stim2} increases, but I_{thrmin} increases more rapidly. Thus there is a finite range of (S1-S2) intervals for which the system is more excitable than in the resting state, a phenomenon known as absolute supernormality (Chialvo et al., 1990).

3. Long T_{stim2}

For a long T_{stim2}, I_{thrmin} becomes greater than I_{thR} and gradually approaches the value of I_{thrmax}. At still longer T_{stim2} (not shown), I_{thr}(S1- S2) becomes a monotonically decreasing curve.

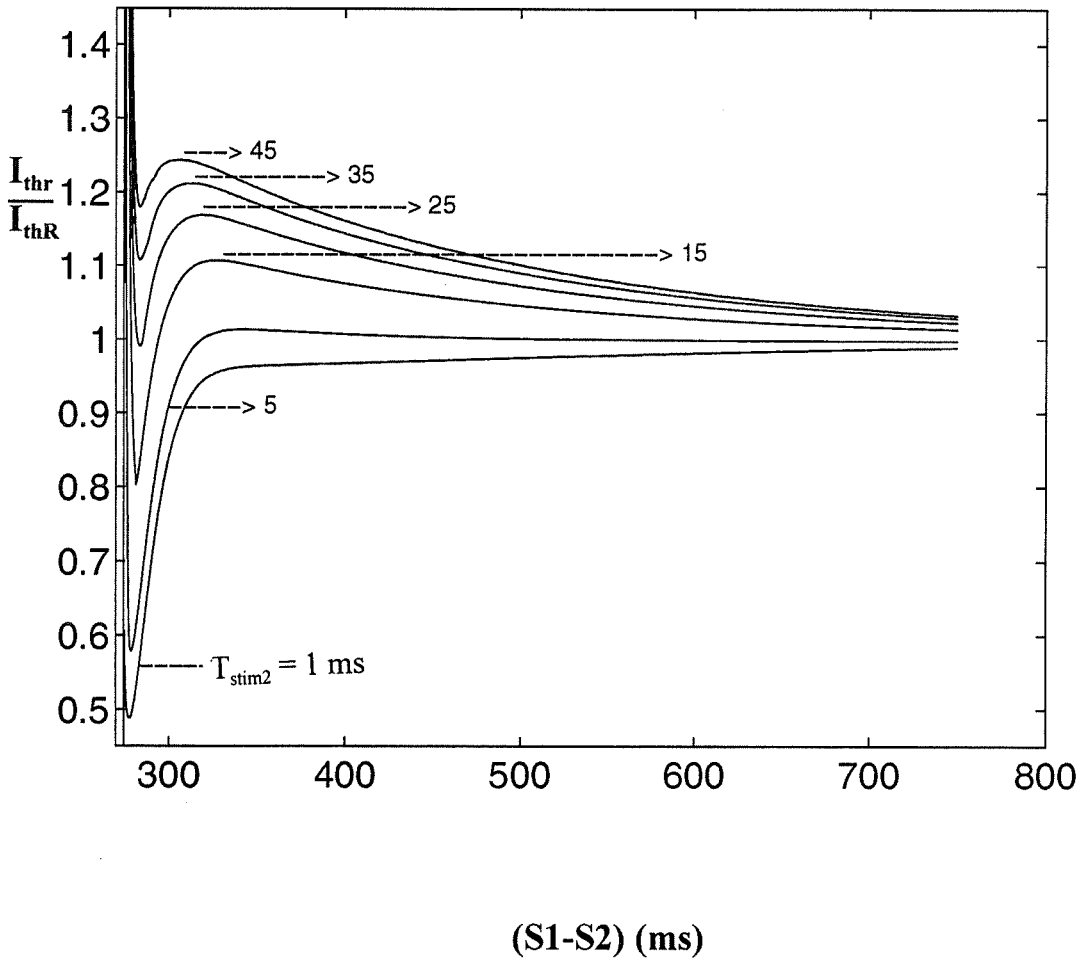

Figure 2.4.1.1: Normalized threshold curves (I_{thr}(S1 - S2)/ I_{thR}) for differentT_{stim2} values; (S1-S1) =1000 ms, T_{stim1} = 1 ms, I_{stim1} = 1.25 I_{thR}.

2.4.2 Effect of (S1-S1) on I_{thr}(S1-S2, T_{stim2})

To examine the effect of the (S1-S1) interval, we compared the results of the reference case ((S1-S1)= 1000 ms) to those obtained with a (S1-S1) of 300 ms, which is near the limit of the 1:1 entrainment region, while keeping T_{stim1} = 1 ms and I_{stim1} = 1.25 I_{thR} as in the reference case. Both cases are illustrated together in fig. 2.4.2.1 The most visible difference is a shift of the ARP which moves from 278 ms in the reference case to 198 ms in the (S1-S1) = 300 ms case.

The differences in ARP for different (S1-S1) intervals reflect the changes in conditioning action potentials. Faster pacing results in shorter action potentials (Fig. 2.4.2.2.). However, aligning the different action potentials to make the end of their ARP correspond shows that they have identical repolarization time courses below -20 mV (Fig. 2.4.2.3). Hence the crossing time at any potential level $\leq$ -20 mV can be taken as a fiducial point to redefine the time axis in order to superimpose the threshold curves corresponding to different ARPs. We have repeated the comparison for different values of the stimulus parameters T_{stim1} and I_{stim1} (results not shown). For each set of [T_{stim1}, I_{stim1}] parameters, the threshold curves obtained with the same pair of T_{stim1} and I_{stim1} values, but different (S1-S1) intervals, were virtually identical when (S1-S2) - T_{-50} was used as the time axis (T_{-50} represents the time measured between the onset of S1 and the time at which the membrane potential reaches -50 mV during repolarization). Following the notation of Vinet et al. (1990; 1994), **the quantity [(S1-S2) - T_{-50}] is called the**

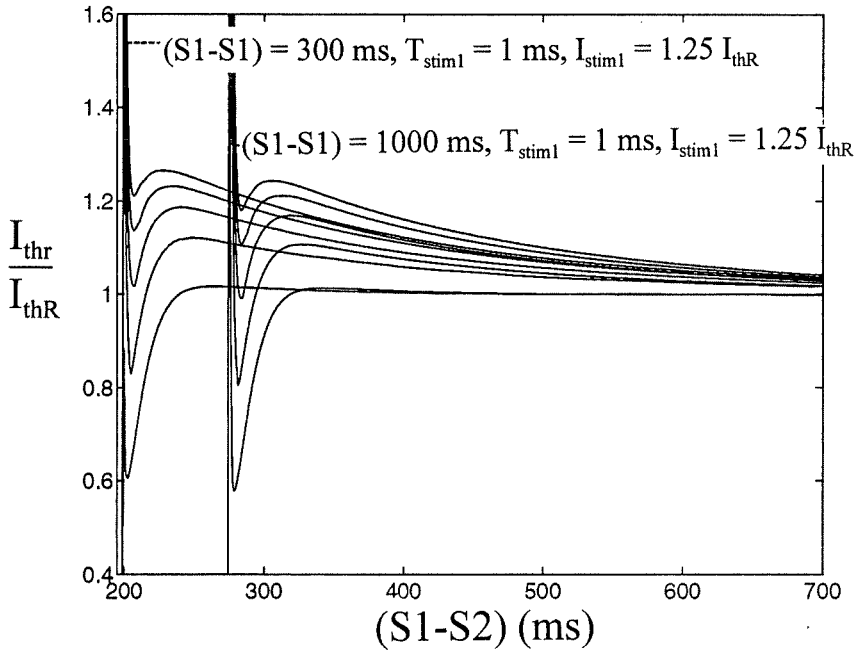

Figure 2.4.2.1: The effect of S_1-S_1 on $I_{thr}(S_1$-$S_2)$.

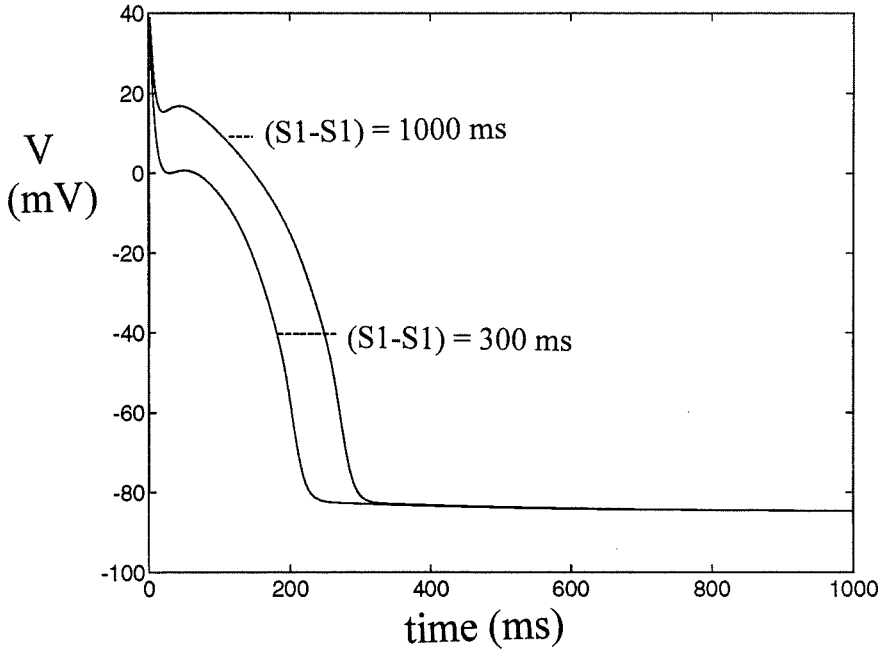

Figure 2.4.2.2: Conditioning action potentials for (S1-S1) 1000 and 300 ms, T_{stim} = 1ms, I_{stim} = 1.25 I_{thR}.

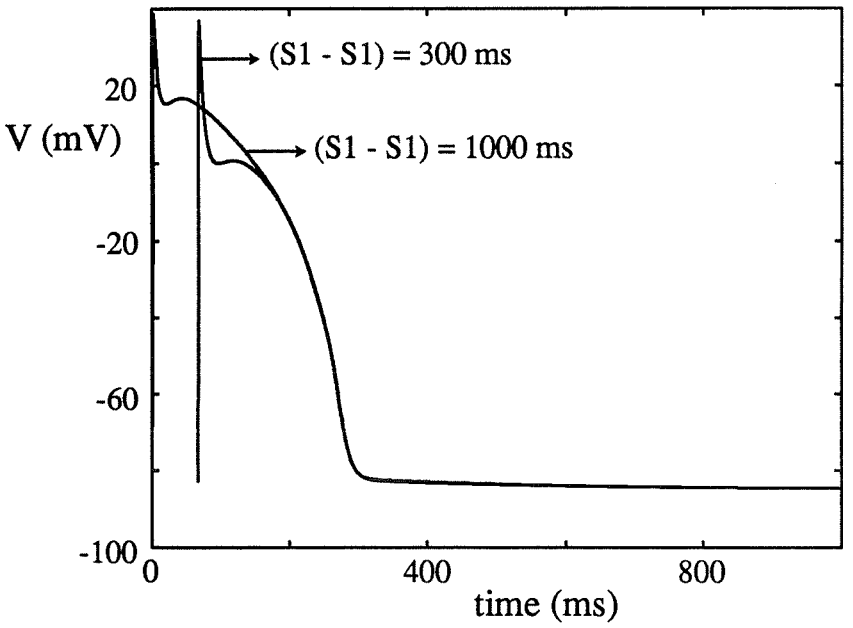

Figure 2.4.2.3: Aligning the action potentials of Fig.2.4.2.2 at V_{-50} = -50 mV.

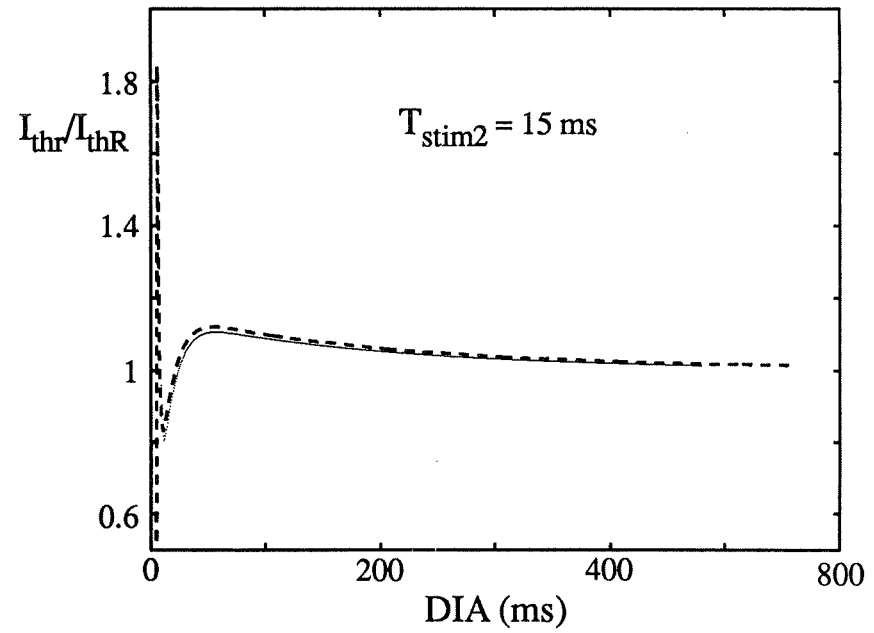

Figure 2.4.2.4: When I_{thr}/I_{thR} is plotted as a function of DIA for a given T_{stim2}, the curves for (S1 - S1) = 1000 ms (full curve) and 300 ms (broken curve) are almost exactly superimposed.

diastolic interval (DIA), and we set DIA = 0 at T_{-50}. Results for T_{stim2} = 15 ms are shown as an example in Figure 2.4.2.4 where the threshold curves for (S1- S1) = 1000 ms and 300 ms are almost exactly superimposed.

In conclusion, threshold curves obtained with the same T_{stim1} and I_{stim1} values are virtually identical if the repolarization time below approximatley -20 mV is used to reexpress the time axis. We have chosen -50 mV as fiducial point, in part because this potential corresponds to the level at which $h_\infty(V)$ starts to increase, leading to the post-upstroke resetting of the I_{Na} current and excitability recovery (Vinet el al., 1990; Chialvo et al., 1990).

2.4.3 Effect of T_{stim1} on $I_{thr}((S1\text{-}S2), T_{stim2})$

To study the effect of T_{stim1}, we compared threshold curves obtained with a constant (S1-S1) interval and a fixed I_{stim1} = 1.25 I_{thR} as in Fig. 2.4.2.1. First, we noticed that increasing T_{stim1} increased both T_{-50} and the ARP. This effect is discussed in detail in the next chapter. Here, we concentrate on the comparison of the threshold curves expressed as a function of DIA.

In Fig. 2.4.3.1 the duration of the test pulse was fixed at T_{stim2} = 15 ms, (S1-S1) at 1000 ms, and the threshold curves were constructed from action potentials obtained

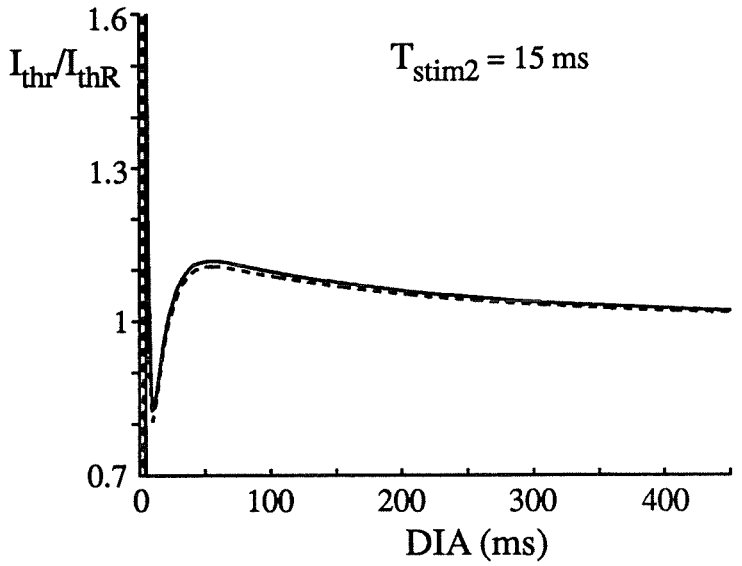

Figure 2.4.3.1: The effect of T_{stim1} on I_{thr}/I_{thR} (DIA) for T_{stim2} = 15 ms. T_{stim1} = 1ms (broken curve), T_{stim1} = 45 ms (continuous curve).

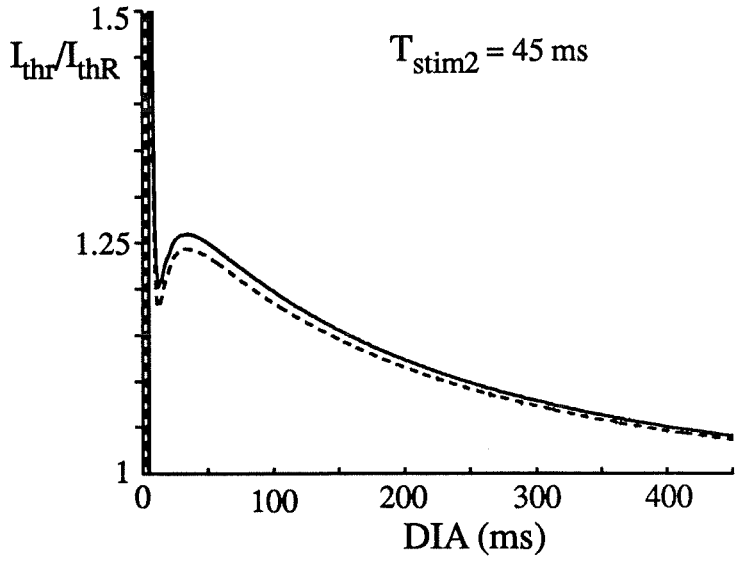

Figure 2.4.3.2: The effect of T_{stim1} on I_{thr}/I_{thR} (DIA) for T_{stim2} = 45 ms. T_{stim1} = 1ms (broken curve), T_{stim1} = 45 ms (continuous curve)..

with T_{stim1} = 1 and 45 ms, and I_{stim1} = 1.25 I_{thR}. Fig. 2.4.3.2 is similar, except for T_{stim2} which was fixed at 45 ms. In all cases the ARP ends at nearly the same DIA value ($\approx$ 14 ms), with variations of only a few milliseconds. The shape of the threshold curves is thus little affected by T_{stim1}, contrary to the strong effect of T_{stim2} illustrated in Fig. 2.4.1.1 (compare also Fig. 2.4.3.1 for T_{stim2} =15 ms and Fig. 2.4.3.2 for T_{stim2} =45 ms). In summary, T_{stim1} may be taken to have a negligible effect on the ARP of the response to S2 and the associated threshold curve.

2.4.4 Effect of I_{stim1} on I_{thr}((S1-S2), T_{stim2})

To study the effect of I_{stim1}, we compared threshold curves obtained with I_{stim} of I_{thR} and 4.25 I_{thR} for the same (S1-S1) interval and the same T_{stim1}. Differences are barely noticeable at short T_{stim1} ($<$ 15ms , results not shown). The variations become more important with T_{stim1} $>$ 15 ms. Figure 2.4.4.1 shows that a large I_{stim1} of 4.25 I_{thR} induces an important ARP reduction (about 90 ms). The normalized Thr(DIA) (i.e. I_{thr}/I_{thR} vs DIA) curves (Fig. 2.4.4.2) show that a large I_{stim1} increases the amplitude and that a longer T_{stim2} enhances the effect of I_{stim1}.

Hence, increasing I_{stim1} clearly increases the threshold for the S2 stimulus. This effect was not considered in previous work in which a moderate range of I_{stim1} ($\approx$ from I_{thR} to 1.25 I_{thR}) and T_{stim1} ($\leq$ 25 ms) were mainly considered. The present study shows a

noticeable increase of Thr(DIA) especially for $T_{stim2} > 15$ ms with large I_{stim1} and T_{stim1}.

We noted earlier that different conditioning action potentials may lead to different T_{-50} and ARP values. Decreasing (S1-S1) or increasing T_{stim1} decreased T_{-50}, while increasing I_{stim1} did not lead to any change when the stimulus duration was short. However, for larger T_{stim1}, changes in I_{stim1} had also an influence on T_{-50} and the ARP. To elaborate on this, we compared the variations in gating variables x and f for the following cases: (S1-S1) = 1000 ms, T_{stim1} = 45 ms, I_{stim1} = 1.25 and $4.25I_{thR}$ which were the conditions exhibiting the largest Thr(DIA) differences in Fig. 2.4.4.2. Two conditioning action potential waveforms are shown in Fig. 2.4.4.3A, for I_{stim1} = 1.25 I_{thR} (continuous curve) and 4.25 I_{thR} (broken curve), with respective ARPs of 271 ms and 202 ms. The two action potentials are aligned at their T_{-50} values and the corresponding changes in x and f gating variables are plotted in panels B and C. At DIA =0, the magnitude of x (panel B) is increased much more than the value of f (panel C), such that the differences in the excitability recovery curves for two I_{stim1} values (differences between curves A and C, Fig. 2.4.4.2) are governed mainly by the behaviour of x. During the application of S1, a large and long lasting pulse (I_{stim1} = 4.25 I_{thR} and T_{stim1} = 45 ms) causes the membrane potential to increase to a high level (near +100 mV, Fig. 2.4.4.3 A) such that x increases rapidly (panel B) due the short τ_x at this potential level (Fig. 2.1.1 C). Consequently, the resulting large I_k induces a very rapid repolarization which yields a substantially shorter T_{-50} and ARP. To recover, I_{thR} must also be higher in order to counterbalance the supplementary outward current resulting from an increased x value.

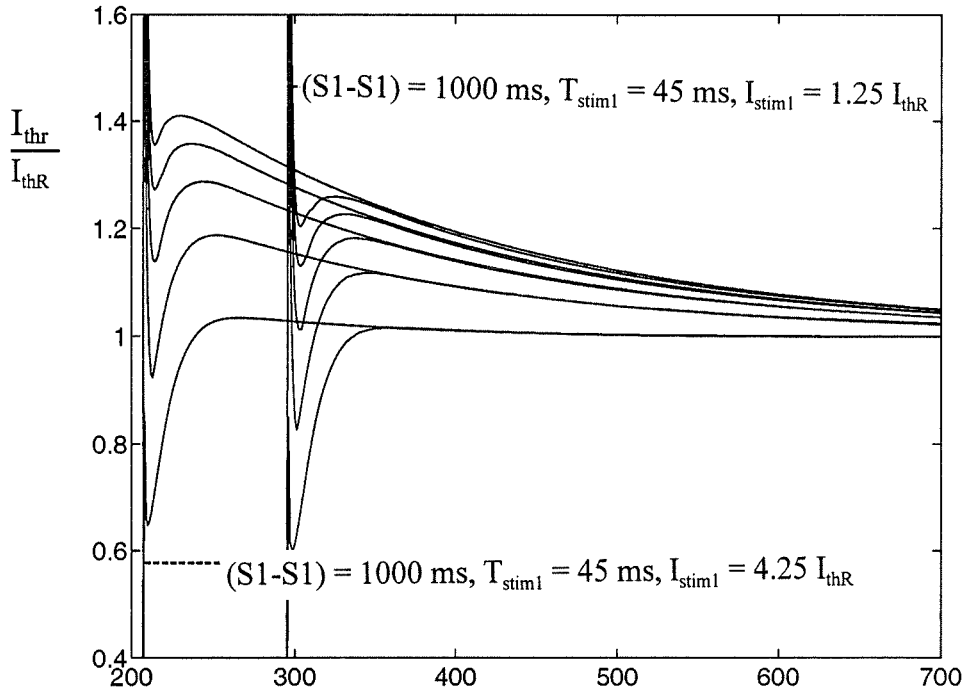

Figure 2.4.4.1: The effect of I_{stim1} on $I_{thr}(S1\text{-}S2)/I_{thR}$ when T_{stim1} = 45 ms. I_{stim1} was increased from 1.25 to 4.25 I_{thR}. The amplitude increases near in the vicinity of ARP when I_{stim1} is increased

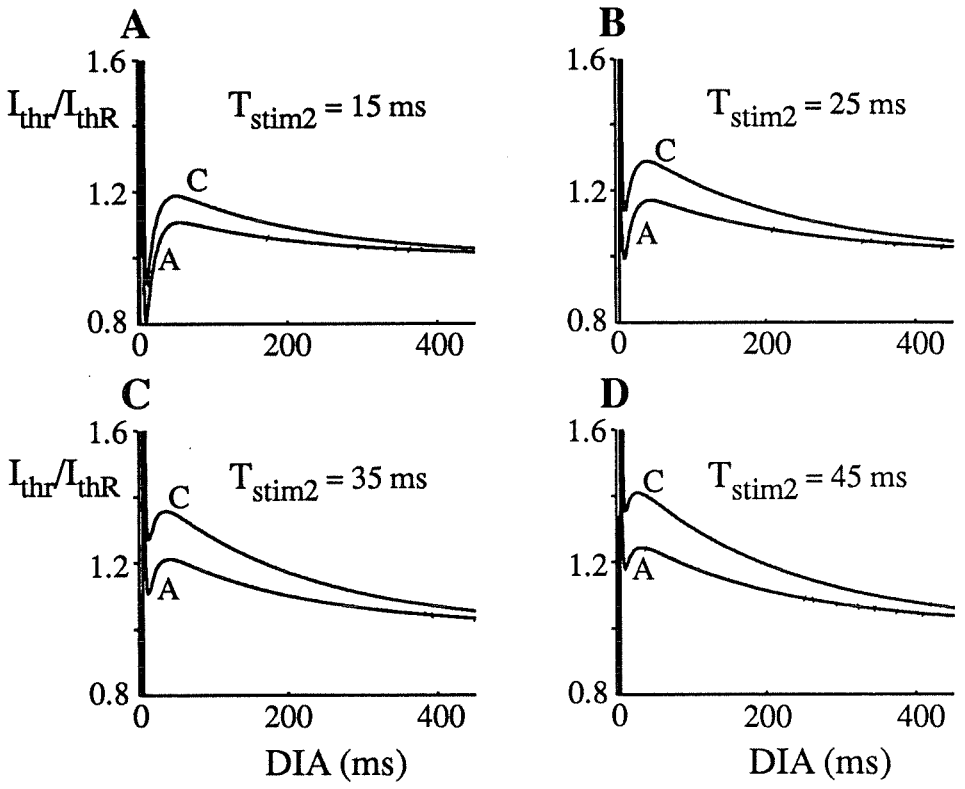

Figure 2.4.4.2: The effect of T_{stim1} on Thr (DIA) curves for (S1 - S1) = 1000 ms and T_{stim1} = 45 ms, while I_{stim1} was either 1.25 I_{thR} (A curves) or 4.25 I_{thR} (C curves). Values of T_{stim2} are shown on each panel.

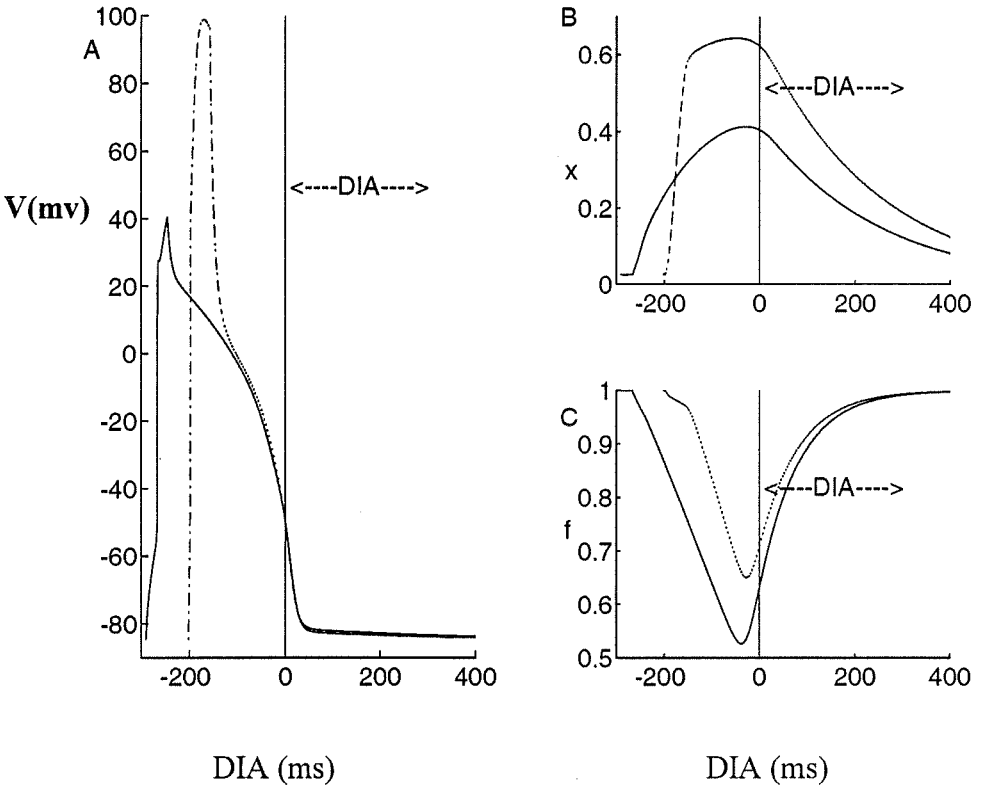

Figure 2.4.4.3: Action potential (panel A) and gating variable changes (x in panel B and f in panel C) for $I_{stim1} = 1.25\ I_{thR}$ (continuous curves) and $4.25\ I_{thR}$ (broken curves). In all cases we have (S1-S1) = 1000 ms and $T_{stim1} = 45$ ms.

2.5 Summary and Conclusion

This study is based on the modified Beeler-Reuter (MBR) model without a slow inactivation gate (j-gate, having a time constant of the order of 100 ms, Beeler & Reuter, 1977). Under nominal conditions, this model has a single global stable resting state (Vinet, &Roberge, 1990; Chay & Lee, 1985, 1992). It exhibits a sharp pseudo-threshold owing to its large maximum Na conductance and its fast Na activation (gating variable m). Peak I_{Na} at threshold is at least two orders of magnitude larger than any other ionic current component. At threshold, a slight increase of the stimulus current amplitude (ΔT_{stim}) causes a large increase in peak ionic current (ΔI_P) such that $(\Delta I_P/\Delta T_{sim})_{max}$ is a reliable indicator of threshold action (Vinet & Roberge, 1994). An equivalent indicator can be based on the maximum incremental increase of the time to repolarization of the action potential (ΔTR) such that the threshold indicator could be expressed as $(\Delta TR/\Delta T_{stim})_{max}$ (Vinet & Roberge, 1994). In practice, however, the threshold phenomenon is so prominent that it can be simply detected from the amplitude of I_P over a sufficiently short time duration. During stimulation from rest, we defined the threshold as the minimum I_{stim} which induced a net surge of I_P for more than 0.55 ms (Fig. 2.3.4).

The absence of the j-gate in the present MBR formulation contributes to make the changes in maximum depolarization (V_{max}) and peak I_{Na} a little more jerky near the end of the ARP. It shortens the ARP slightly since recovery from rapid inactivation (h-gate) does

not need to be as advanced when j-gate inactivation is present. In practice, the absence of the j-gate enhances supernormality at short coupling intervals (viz., Fig. 2.4.1.1) (Vinet et al., 1990; Luo & Rudy, 1991).

A major feature of the MBR model is the relative invariance of its excitability threshold with respect to the conditioning action potential waveform (memory-free threshold function, Vinet & Roberge, 1994). First we found that the threshold current at rest (I_{thR}) and the form of the threshold curves as function of premature stimulation were highly sensitive to the duration (T_{stim2}) of the premature stimulus. The shape of the curves was shown to change from a monotonically increasing form at short T_{stim2}, to a supernormal form at intermediate T_{stim2}, and to a monotonically decreasing form at high T_{stim2}. The threshold curves as a function of premature stimulation were also shown to change with the parameters of the S1 stimulus: (S1-S1) interval, T_{stim1} and I_{stim1}. The most obvious effect was the shift of the threshold curves with the change in ARP. Fast (S1-S1) pacing, high T_{stim1} and high I_{stim1} reduced the APD and the ARP. The shift due to (S1-S1) pacing can be eliminated by taking DIA as the new time axis. We have chosen to use T_{-50} as the reference point to calculate DIA. However, the choice of DIA as a common time axis did not eliminate all the differences. High T_{stim1} and high I_{stim1} we seen to increase Thr(DIA) as a result of the higher potentials.

The results are summmarized in Table 2.5.1. Each row refers to a given protocol and the shaded area indicates the particular parameter that is varied. In the first protocol, for

example, (S1-S1), T_{stim1} and I_{stim1} were held at the indicated values while T_{stim2} was set successively at one of the 6 values shown. The effect on I_{thr}(S1-S2) or Thr(DIA) is briefly summarized in the rightmost column and the corresponding figure number is given.

The main results are as follows:

1. T_{stim2} has an important influence on Thr(DIA). Increasing T_{stim2} causes a substantial upward shift of the curve (Protocol #1, Fig. 2.4.1.1).
2. While changes in (S1-S1) modify the ARP and APD substantially,expressing the threshold in terms of DIA makes it possible to neutralize completely the effect of different (S1-S1). In other words, Thr(DIA) is virtually invariant with respect to (S1-S1) for a given T_{stim2} (Protocol # 2, Fig. 2.4.2.4).
3. Changes in T_{stim1} have no effect on Thr(DIA) if T_{stim1} is short. A slight increase in Thr(DIA) is observed when T_{stim1} is long (Protocols # 3, Figs 2.4.3.1 and 2.4.3.2).
4. For a given T_{stim2}, variations of I_{stim1} have substantial effects on Thr(DIA) (Protocol # 4, Fig. 2.4.4.2), which are in the same direction as the effects of T_{stim2}.

We can conclude from these results that Thr(DIA) is practically insensitive to the conditioning stimulus parameters (T_{stim1} and I_{stim1}) if the stimulus strength is not too large. On the other hand, Thr(DIA) is sensitive to a large increase in I_{stim1}; when I_{stim1} is much above I_{thR}, the excitability recovery process is delayed (Thr(DIA) shifted upward in Fig. 2.4.4.2)

owing to upward shifts in x and f by I_{stim1} (Fig. 2.4.4.3). The shift is enhanced by larger T_{stim1}.

Table 2.5.1: Protocols used to study the effects of the stimulus parameters on I_{thr}(S1-S2) or Thr(DIA). In each row, the shaded area indicates the parameter variations under examination while the other parameters are fixed.

Protocols #	(S1-S1) (ms)	T_{stim1} (ms)	I_{stim1} ×(I_{thR})	T_{stim2} (ms)	Effect on I_{thr}(S1S2) or Thr(DIA).
1	1000	1	1.25	1, 5, 15, 25, 35, 45	Fig. 2.4.1.1 The form of I_{thr}(S1-S2) is changed as T_{stim2} is increased.
2	1000 300	1	1.25	1, 5, 15, 25, 35, 45	Fig. 2.4.2.1 Both I_{thr}(S1-S2) at the two (S1-S1) values are virtually identical but they are shifted by the ARP difference: 278 to 198 ms. Taking DIA as the independent variable allows to superimpose the two Thr(DIA) at the two (S1-S1)s.
3	1000	1 & 15 1 & 45	1.25	15 45	Only a small effect on Thr(DIA) Fig. 2.4.3.1 Effect is slightly enhanced as T_{stim2} is increased, Fig. 2.4.3.2.
4	1000	45	1.25 4.25	15, 25, 35, 45	Amplitude of Thr(DIA) is increased with larger I_{stim1}. A longer T_{stim2} causes an increased Thr(DIA), Fig. 2.4.4.2.

CHAPTER III

RESTITUTION CURVE FOR A SINGLE CELL

3.1 Introduction

In the previous chapter, the diastolic interval (DIA) was introduced to obtain excitability recovery curves which are independent of the absolutely refractory period (ARP) duration and action potential duration (APD) associated with the shortening of the (S1-S1) pacing interval. This chapter describes the influence of the S1 and S2 stimuli on the APD. As in previous publications (Bass, 1975; Boyett et al., 1978; 1980; Elharrar, 1983; Chialvo et al., 1990; Lewis et al., 1990; Vinet et al.,1990, 1994), all APD restitution curves are presented as function of DIA. The APD(DIA) relation has been obtained with different versions of the BR model (Vinet et al., 1990; 1994). Most of these studies were done with nominal ionic model parameters, with short to intermediate stimulus durations (up to 25 ms), and with I_{stim} below 2 I_{thR}. In this context APD(DIA) was shown to be largely independent of the S1 and S2 stimulus parameters. Some memory effect (influence of the previous APD

on the current APD) were also shown to exist at high pacing rates. However, except for a few cases (Delmar et al., 1991; Vinet et al., 1990), the effect of a large T_{stim} has not been thoroughly discussed in the literature. Here, we have included the effect of long T_{stim} durations because they are important to understand the dynamics of loosely coupled cell pairs, where a long lasting coupling current may exist at the onset of the action potential.

3.2 Method

The protocol to study APD changes is similar to that used to study threshold variations in the preceding chapter. The APD was measured from the onset of S1 to V_{-50}, and thus includes the latency. Results are compared for a long (1 sec) and a short (300 ms) (S1-S1) interval. The latter was chosen because it is close to the lowest basic cycle length (BCL) of stable 1:1 entrainment under nominal conditions. For all combinations of S1 stimulus parameters, pacing was maintained until stability was diagnosed according to the criteria defined in the previous chapter. Then the APD(S1-S2) curves were constructed by premature stimulation in the wake of each conditioning action potential for T_{stim2} durations given in Table 2.4.1.1 of Chapter II and values of I_{stim2} ranging from 1 to 4.18 I_{thr}(S1- S2, T_{stim2}) (Fig. 2.4.1.1). The APD curves were then reexpressed as function of DIA for comparison.

3.3 Effect of $S_2(T_{stim2}, I_{stim2})$ on APD(DIA) Curves

The effects of I_{stim2} and T_{stim2} on APD(DIA) are described using the conditioning action potential obtained with (S1- S1) = 1 sec, T_{stim1} = 1 ms and I_{stim1} = 1.25 I_{thR}.

3.3.1 Effect I_{stim2} on APD(DIA)

Figs 3.3.1.1 to 3.3.1.4 give a comparison of APDs obtained with $I_{stim2} = I_{thr}$ and 4.18 I_{thr} for T_{stim2} = 1, 5, 25 and 35 ms. The large I_{stim2} = 4.18 I_{thr} was chosen arbitrarily to ensure that the distortions caused by the stimulus were clearly visible.

For short T_{stim2} = 1 ms (Fig. 3.3.1.1), the larger I_{stim2} gives larger APDs at short DIA (< 70 ms). The APD is nearly doubled near the end of the absolute refractory period (ARP), and the difference decreases gradually and vanishes at DIA = 100 ms. Hence, a high stimulation amplitude reduced the slope of the APD(DIA) curve over the steep portion at low DIA.

When T_{stim2} is increased to 5 ms (Fig. 3.3.1.2), the effect of the larger I_{stim2} can also be seen at larger DIA where the APD is now shorter than for the lower I_{stim2}. The shortening of the APD at high DIA is accentuated as T_{stim2} is increased further (Figs 3.3.1.1, and 3.3.1.4). As a result, as T_{stim2} is increased, there is large range of DIA values where a higher

I_{stim2} induces a reduction of the APD slope and a lower dispersion of APD values. At T_{stim2} = 5 ms, the curves obtained with high and low I_{stim2} intersect at DIA = 55 ms and APD = 140 ms.

At T_{stim2} = 25 ms (Fig. 3.3.1.3), the intersection is moved toward a set of lower DIA and APD values. At T_{stim2} = 35 ms (Fig. 3.3.1.4) the transition is complete and the high I_{stim2} curve is wholly below the low I_{stim2} one. Therefore, when the stimulus duration is large, the APD(DIA) curve is globally displaced toward lower APDs as the stimulus intensity is increased.

In summary high amplitude stimulation reduce the APD(DIA) dispersion, either by increasing the APD at low DIA when T_{stim2} is relatively short, or by decreasing the APD at higher DIA when T_{stim2} is longer. Previous work has shown, in BR-type models, that the initial steep increase in APD value was a consequence of the activation delay of gating variable d, while the late APD variation involved the slow gating variables f and x (Vinet & Roberge, 1994). High amplitude stimulation affects both processes.

At low DIA, high I_{stim2} increases the level of the initial depolarization, such that d has more time to activate under conditions where τ_d is near its minimum value (see Fig. 2.1.1). This reduces the effect of the activation delay of d on the APD. At high voltage, τ_x also reaches a minimum which is around 50 ms see Fig. 2.1.1). For longer T_{stim2}, x will thus activate during the stimulation. This explains the reduction of APD which is apparent at

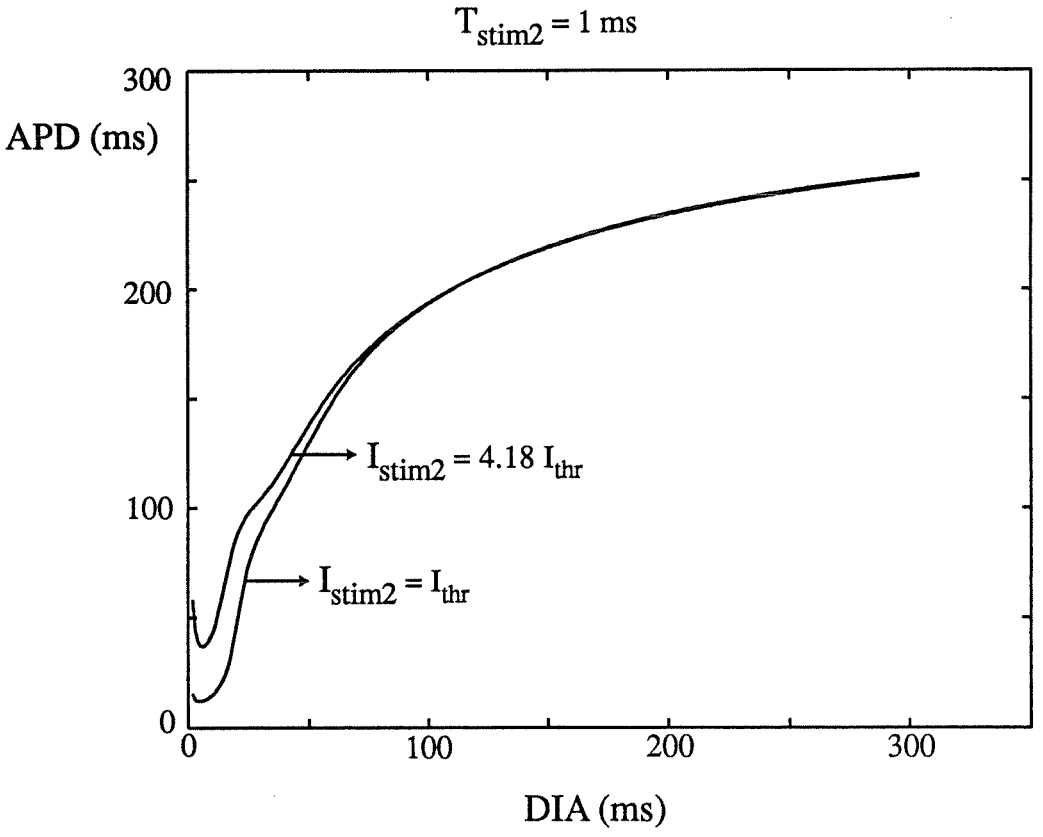

Figure 3.3.1.1: APD (DIA) curves for $I_{stim2} = I_{thr}$ or 4.18 I_{thr} withT_{stim2} as indicated.

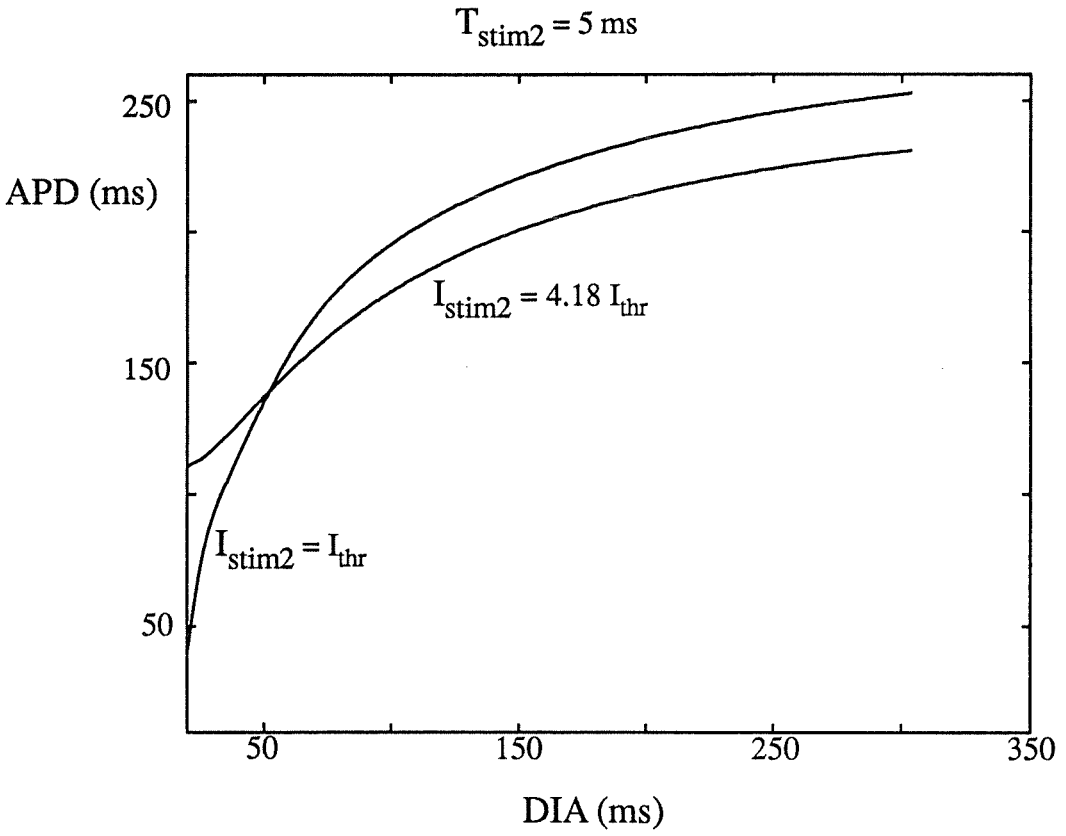

Figure 3.3.1.2: Same legend as in Figure 3.3.1.1.

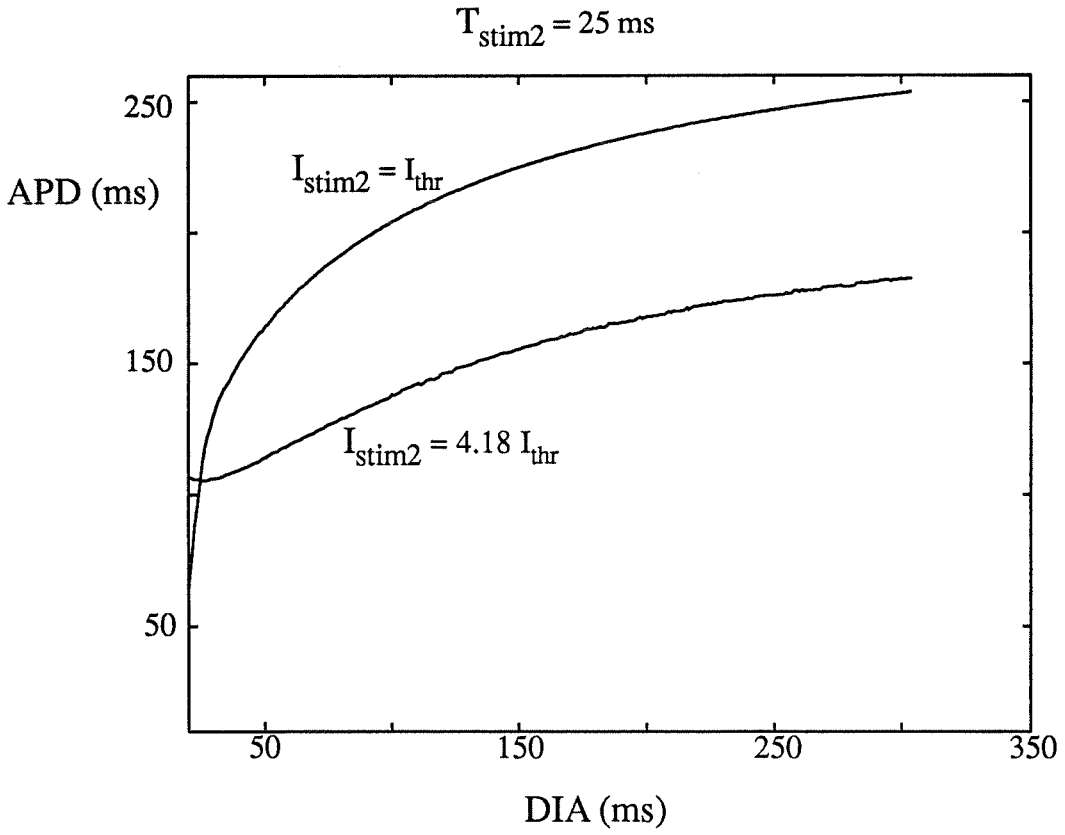

Figure 3.3.1.3: Same legend as in Figure 3.3.1.1.

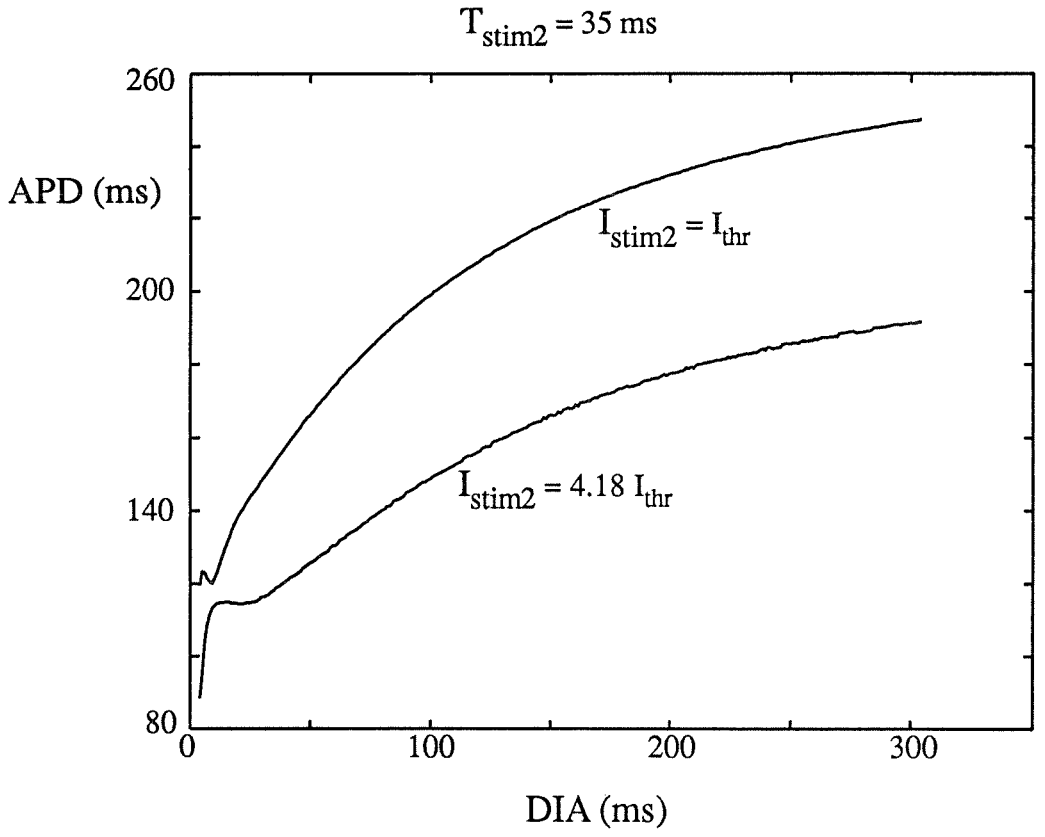

Figure 3.3.1.4: Same legend as in Figure 3.3.1.1.

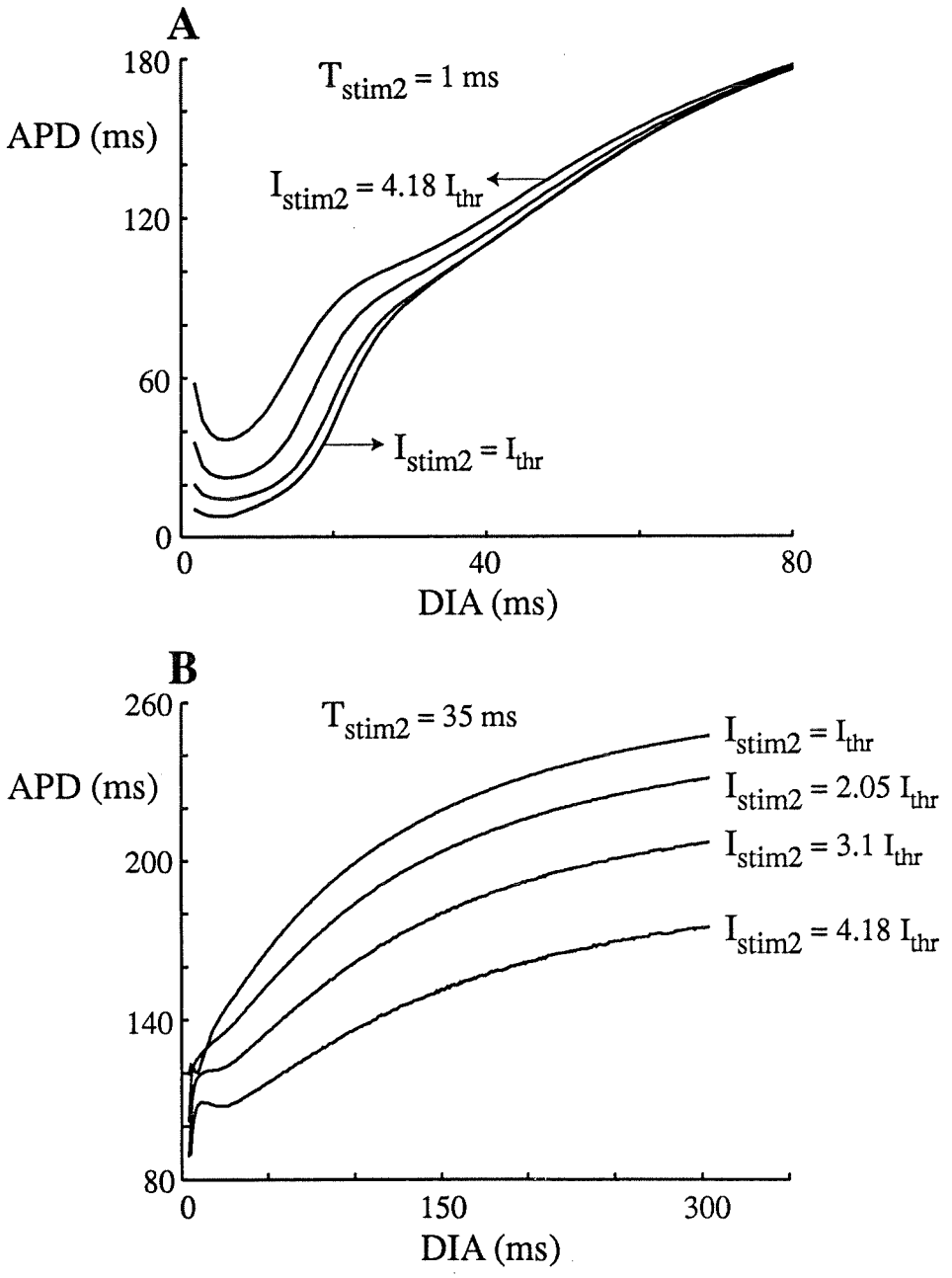

Figure 3.3.1.5: A) APD(DIA) curves with I_{stim2} = 1, 2.05, 3.1, and 4.18 I_{thr} and T_{stim2} = 1 ms. B) Same I_{stim2} values and T_{stim2} = 35 ms

larger DIA.

By comparing $I_{stim2} = I_{thr}$ and 4.18 I_{thr} for different T_{stim2}, we were able to demonstrate more clearly the effect of the stimulation amplitude on the APD restitution curves. At short stimulus duration (T_{stim2} = 1 ms, Fig. 3.3.1.5A) there is a gradual transformation of the APD curve with increasing I_{stim2} such that the APD(DIA) relation can still be approximated by a single curve if the I_{stim2} variation is not too large (<0.5 I_{thr}) around a given level. This is no longer true when the stimulus duration is large (T_{stim2} = 35 ms, Fig. 3.3.1.5B).

3.3.2 Effect of T_{stim2} on APD(DIA)

The effect of T_{stim2} can be more directly grasped by comparing the APD curves obtained with the same I_{stim2}, but different T_{stim2}. Results are presented in Figs 3.3.2.1 and 3.3.2.2 respectively for low ($I_{stim2} = I_{thr}$) and high (I_{stim2} = 4.18 I_{thr}) stimulus amplitudes. At low stimulation amplitude (Fig. 3.3.2.1), the main effect of prolonged T_{stim2} is to reduce the initial steep APD increase associated with the activation delay of gating variable d. The APDs at low DIAs are then larger for longer T_{stim2}.

At larger I_{stim2}, the d retardation effect is minimal for all T_{stim2} because the high potential reached during stimulation is by itself sufficient to suppress it. Enlarging T_{stim2} (Fig. 3.3.2.2) then induces a global lowering of the APD curves, except at very short DIAs. These changes are associated with the activation of x occurring during the stimulation,

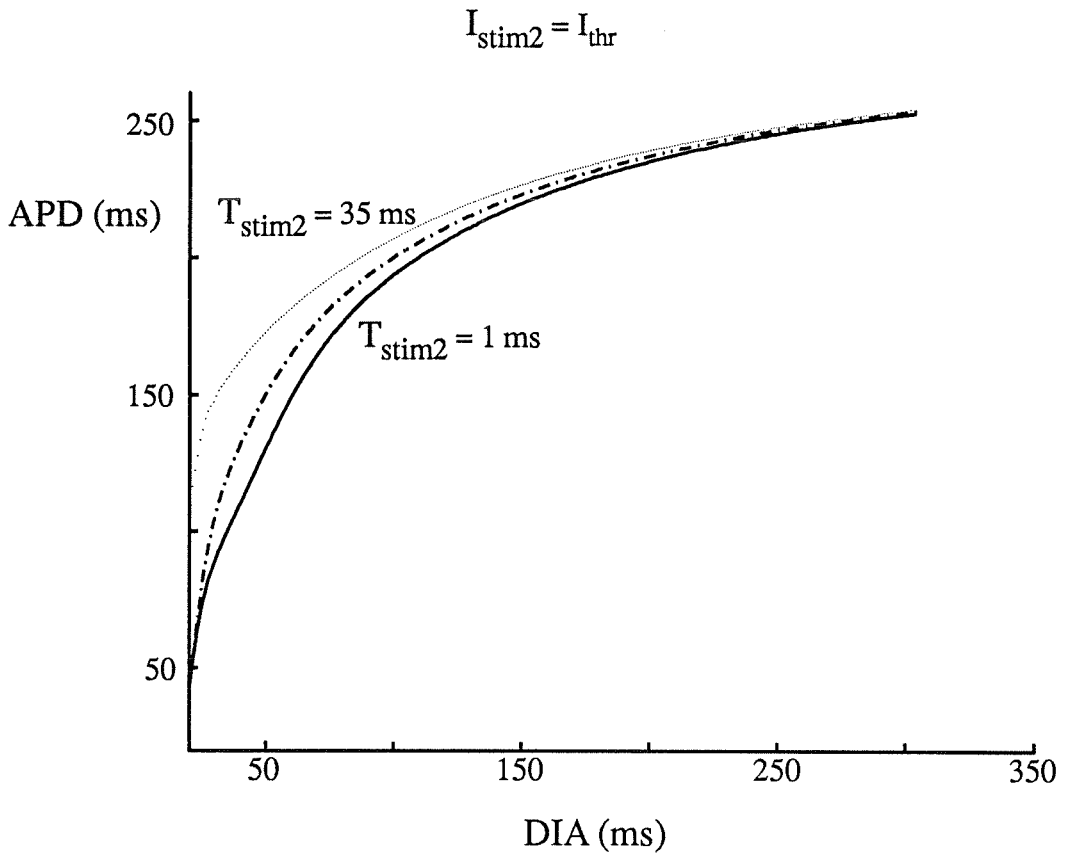

Figure 3.3.2.1: APD(DIA) curves for T_{stim2} = 1 ms (full curve), 15 ms (broken curve), and 35 ms (dotted curve), and I_{stim2} as indicated.

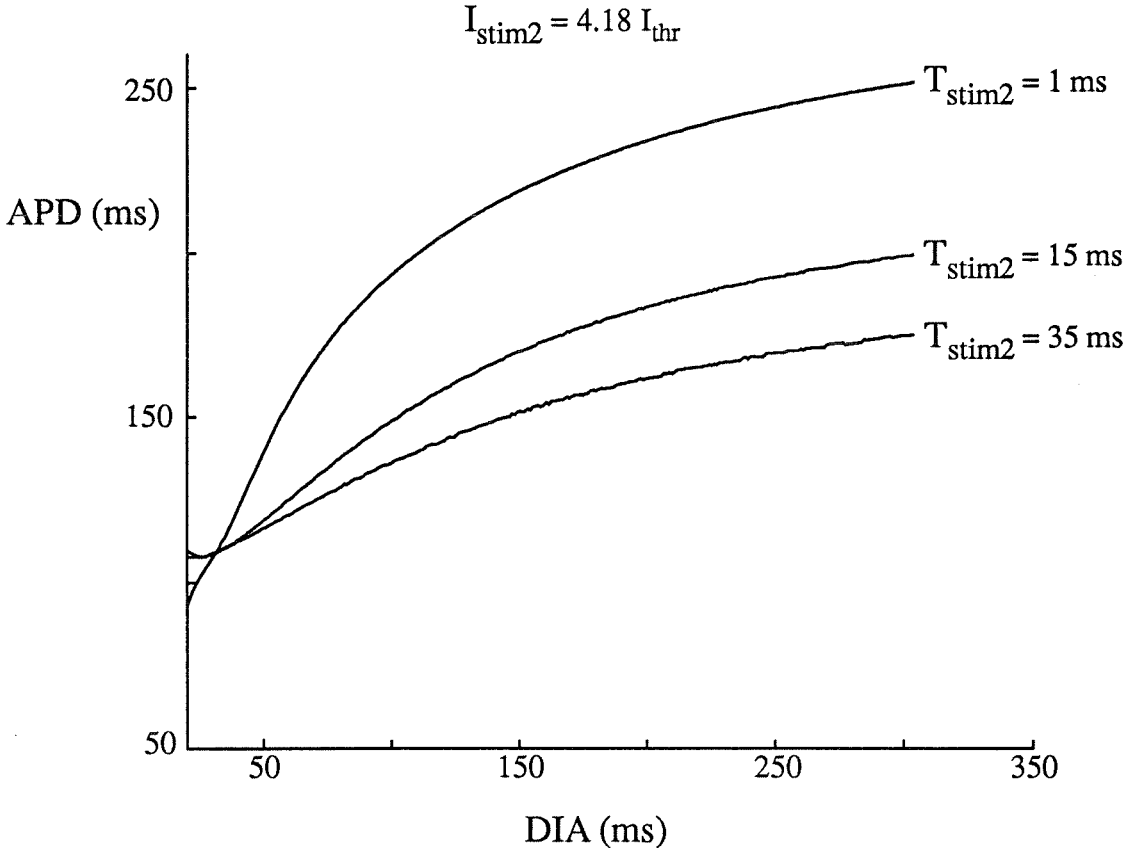

Figure 3.3.2.2: Same legend as in Figure 3.3.2.1.

giving a higher potassium repolarisation current.

3.4 Effect of $(S_1\text{-}S_1)(T_{stim1}, I_{stim1})$ on APD(DIA)

A shorter (S1-S1) interval results in briefer APD and ARP values because the stimulus is applied at shorter DIA. Expressing threshold and APD as function of DIA serves to eliminate this effect. Clearly, any combination of T_{stim1} and I_{stim1} that would induce long term effects on the state of the gating variables during repolarisation would change the form of the APD(DIA) function obtained by premature stimulation. Long term effects can only be due to the slow gating variables x and f.

The discussion of the last two sections has emphasized the role of a high I_{stim2} and a long T_{stim2}. The resulting effects can be explained by considering the variations of x (Fig. 3.4.1) and f (Fig. 3.4.2). In Fig. 3.4.1, curve B is above curve A (slightly larger x values) due to the lower BCL of 300 ms, while curve D is above curve A owing to the large T_{stim1} of 45 ms. On the other hand, curve C is far above curve D because of the higher I_{stim1} of 4.25 I_{thR}. The behaviour of gating variable f is fairly similar (Fig. 3.4.2), particularly with respect to curve C which is far above curves A, B, or D (i.e., larger f values) because of the stronger I_{stim1} of 4.25 I_{thR}. It is clear therefore that I_{stim1} is much more potent than T_{stim1} or (S1-S1) to increase both x and f. This is in accord with Fig. 2.4.4.3 which depicted similar results over a wider range of DIA values.

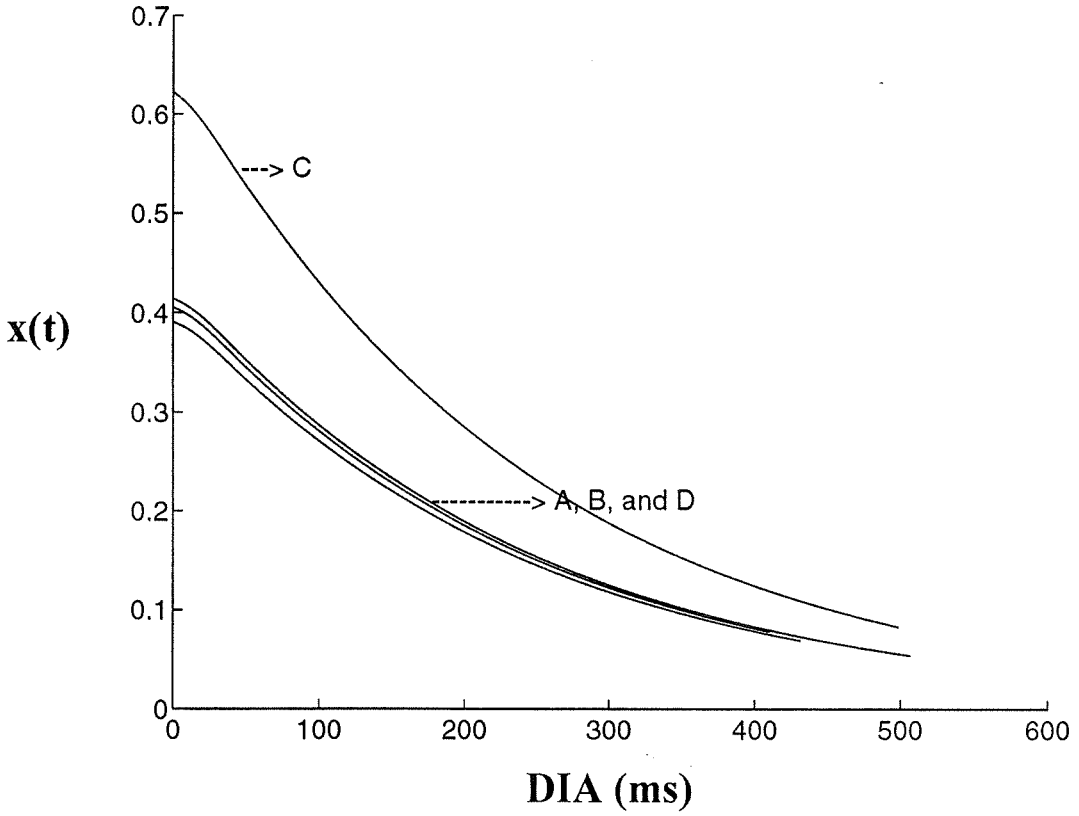

Figure 3.4.1: Curves A-D decribed activation gating variable x during different protocols of S_1 stimulation. A) (S1-S1) = 1000 ms , T_{stim1} = 1 ms, and I_{stim1} = 1.25 I_{thR}. B) (S1-S1) = 300 ms , T_{stim1} = 1 ms, and I_{stim1} = 1.25 I_{thR}. C) (S1-S1) = 1000 ms , T_{stim1} = 45 ms, and I_{stim1} = 4.25 I_{thR}. D) (S1-S1) = 1000 ms , T_{stim1} = 45 ms, and I_{stim1} = 1.25 I_{thR}.

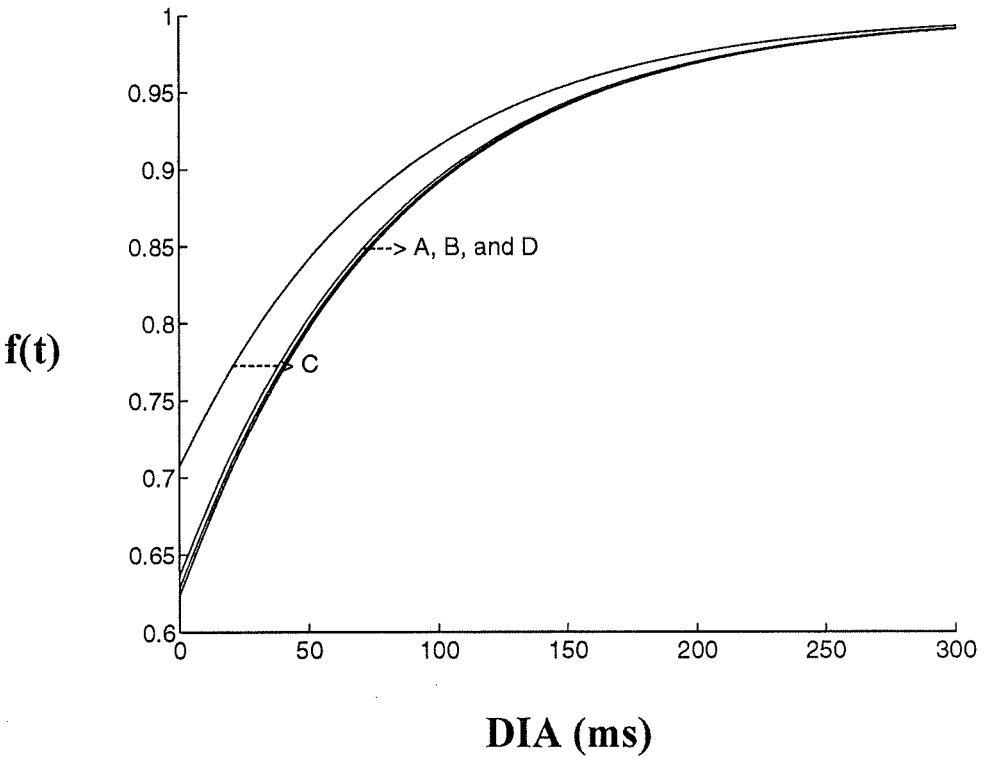

Figure 3.4.2: Same protocols as in Fig. 3.4.1 for the inactivation f-gate.

These differences in the state of the slow variables x and f illustrate the mechanism by which I_{stim2} and T_{stim2} affect the APD during premature stimulation. For short T_{stim2} and low I_{stim2}, x and f are relatively unaffected by the stimulus and the intrinsic APD dispersion is not changed. An increased T_{stim2} reduces the APD dispersion somewhat (Fig. 3.3.2.1), and it does so mainly by increasing the APD at short DIA without affecting the APD values at long DIA. This is consistent with the fact the x becomes larger at relatively short DIAs when T_{stim2} is large (Fig. 3.4.1). Similarly, the dramatic decrease in APD dispersion with large T_{stim2} and I_{stim2} (Fig. 3.3.2.2) results from the same mechanism.

3.5 Summary and Conclusion

The time to repolarization (TR) considered in Chapter II defines the APD which is taken to end at V_{-50}. An analysis of TR (or APD) variations in the MBR model has shown the quasi-all-or-none behaviour of this quantity, in close parallel with changes in I_p at threshold (Chapter II and Vinet &Roberge 1994). There is then a clear and abrupt transition between a short and a long APD at threshold. Changes in APD(DIA) with the stimulation parameters were obtained using the protocols listed in Table 3.5.1.

The APD(DIA) curve and APD dispersion are essentially independent of the stimulus parameter if I_{stim2} is close to the threshold intensity and T_{stim2} is short enough. Increasing T_{stim2} shortens the APD mainly at low and medium DIAs. The most potent modifier of the

APD(DIA) relation is the amplitude I_{stim2} of the stimulus. The largest effects are obtained when both T_{stim2} and I_{stim2} are large.

Table 3.5.1: Protocols used to study the effects of the stimulus parameters on APD(DIA). In each row, the shaded area indicates the parameter variations currently under examination while the other parameters are fixed.

Protocols #	S1-S1 (ms)	T_{stim1} (ms)	I_{stim1} × (I_{thR})	T_{stim2} (ms)	I_{stim2} × (I_{thr})	Effect on APD(DIA).
1	1000	1	1.25	1 5 25 35	1.0 4.18	Fig. 3.3.1.1- 3.3.1.5: Increasing I_{stim2} changes the shape of APD(DIA) curves. APDs are increased at low DIA when T_{stim2} >5 ms. At T_{stim2} = 5 or 25 ms the APDs are decreased at high DIA and increased at low DIA. With T_{stim2} >25 ms, APDs are shifted downward at all DIA values
2	1000	1	1.25	1 15 35	1	Fig. 3.3.2.1 The increases of T_{stim2} increase the APDs at lower DIA.
3	1000	1	1.25	1 15 35	4.18	Fig. 3.3.2.1 The increases of T_{stim2} decreases the APDs at all DIA > 30 ms.
4	1000 300	1	1.25 4.25	No S2 stimulus		Figs. 3.4.1 and 3.4.2 Large increases in x and f values are obtained when I_{stim1} is increased

CHAPTER IV

ENTRAINMENT RESPONSE OF THE MEMBRANE MODEL

Action potential duration, APD(DIA), and threshold, Thr(DIA), curves constructed from responses to premature pulse stimulations provide a global characterization of the membrane model dynamical properties. These functions summarize the result of the interplay of the stimulation current with the different ionic currents on the time scale of one action potential. In the previous chapters, we have characterized both Thr(DIA) and APD(DIA) for various stimulus durations, amplitudes, and conditioning action potentials. In summary, the form of the Thr(DIA) curve was shown to change continuously with the prolongation of T_{stim2}. For short T_{stim2} ($\sim$5 ms), Thr(DIA) is less than the resting threshold (I_{thR}) for all DIAs, except in a small interval near the absolute refractory period. For long T_{stim2} ($\sim$ 50 ms), Thr(DIA) becomes a monotonically decreasing function of DIA. For intermediate T_{stim2}, absolute and then relative supernormality exists in an interval of DIA. Thr(DIA) curves are virtually independent of the characteristics of the (S1-S1) protocol preceding the S2 premature stimulation. This is not true for APD(DIA) curves since a high I_{stim2}, and to a lesser extend a long T_{stim2}, were found to decrease the APD(DIA) steepness, involving an APD

increase at low DIA and an APD decrease at high DIA and thus a large decrease in APD dispersion.

A different approach to global characterization is to apply repetitive pulse stimulation at various basic cycle lengths (BCLs) to study the transformation of the entrainment responses of the model as a function of the stimulus parameters and BCL. The nature and succession of the stable entrainment patterns provide information about the long term behaviour of the model. In many nonlinear excitable membrane models, continuous variations of the stimulation parameters resulted in a cascade of discontinuous changes in the different response patterns (Lewis et al., 1990; Chialvo et al., 1990; Vinet et al., 1990). The cascade of transitions defines the bifurcation structure of the model. The existence of specific generic patterns of bifurcations, like period doubling or period adding (see below), gives strong indication about the fundamental dynamical characteristics of the model and permits to relate them to a more general class of models displaying similar bifurcation structures.

The first goal of the present chapter is to examine the bifurcation structure of the entrainment response of the MBR model as a function of the three parameters of regular repetitive stimulation: T_{stim}, I_{stim}, and BCL. Since high I_{stim} values were shown to be associated with large changes in the APD function in Chapter III, this condition will be included in our study of bifurcation, thus expanding the range of stimulation parameter values that have been considered in the literature.

There is a relationship between the short term behaviour of the model, characterized by APD(DIA) and Thr(DIA) (Chapters II and III), and the long term behaviour described by the bifurcation structure. The relationship has been formalized by the means of a finite difference model. Although different versions of the model have been proposed (Chialvo et al., 1990; Lewis et al., 1990, Vinet et al., 1990, 1994), the simplest version includes only the Thr(DIA) and APD(DIA) functions. Such a simple formulation has been shown to reproduce many key features of the BR bifurcation structure under different values of the stimulation parameters. The second goal of this chapter is to examine whether the finite difference relationship holds when a larger range of stimulation parameters is used.

4.1 Protocols and Simulations

The stimulus durations used were either 1 ms or from 5 to 45 ms in steps of 10 ms. In all cases, I_{stim} was varied from I_{thR} to 1.3 I_{thR} by steps of 0.025 I_{thR}. Furthermore, for T_{stim} = 1, 25, 35, and 45 ms, I_{stim} was increased as high as 5.25 I_{thR}, most often by steps of 0.075 I_{thr}. For each combination of T_{stim} and I_{stim}, BCL was varied from 350 to 100 ms by steps of 1 ms. The system was reset at rest at the beginning of pacing for each BCL. Pacing was continued until stability was found, or a maximum of 550 stimulations were applied. Criteria for periodicity are those which were used to establish (S1-S1) stability in Chapter II (Section 2.2). Depolarization following each stimulation was classified as active, i.e. producing an action potential, if there was an inward ionic

current ($I_{ion} < 0$) for more than 0.55 ms.

We define the activation ratio (AR) as a pair of numbers, m:n, in which m is the number of stimuli in the periodic sequence and n the number of active responses. An AR is defined only for a stable pattern (e.g. 1:1, 2:2, 4:3, etc), otherwise the response is aperiodic and was classified as irregular dynamics (I.D.). The period number of a stable rhythm corresponds to the number of stimuli: period 1 (or P=1) refers to 1:1 and/or 1:0 rhythm, period 2 (or P=2) to 2:2 and/or 2:1 rhythm, period 3 (or P=3) to 3:2 and/or 3:1 rhythm, etc. A sequence of rhythms (or bifurcation structure) is called period doubling when it includes only a series of consecutive doublings of period numbers (e.g. 1:1, 2:2 or 2:1, 4:3 or 4:2, 8:6 or 8:5, etc). A sequence is said to be period adding when the series of consecutive period numbers follows the sequence of successive integers (e.g. 1:1, 2:2 or 2:1, 3:3 or 3:2 or 3:1, 4:4 or 4:3 or 4:2 or 4:1, etc).

4.2 Bifurcation Maps

4.2.1 Short T_{stim}

Figures 4.2.1.1 and 4.2.1.2 show the bifurcation structure of the period (P) and activation ratio (AR) for T_{stim} = 1 ms and I_{stim} ranging from 0.997 to 1.25 I_{thR}. For I_{stim}

$\leq I_{thR}$, period 1 passive responses are found for all BCLs (thin dark blue band along the abscissa in Fig. 4.2.1.1). Then, at a slightly higher stimulus strength, the bifurcation structure changes abruptly to a cascade of successive period doubling (P = 1→2 → 4 → 8, and 3 → 6) interrupted by intervals of irregular dynamics (I.D.). In Fig. 4.2.1.1, the corresponding colour sequence is dark blue (P=1), light blue (P=2), dark green (P=4), yellow (P=8), turquoise (P=3) and red (I.D.). Some small windows of periodicity (e.g. P=5) were found in the I.D. zones. The ARs also follow a typical pattern. Starting from 1:1 at a BCL of 350 ms, AR changes to 2:2 at BCL = 290-254 ms when $I_{stim} < 1.18\ I_{thR}$, and 282-231 ms when $I_{stim} > 1.18\ I_{thR}$. A further decrease in BCL leads to 2:1 and then to 4:2, which is followed by 4:3. Some of these bifurcations are shown in Fig. 4.2.1.2 as follows: blue (1:1), green (2:2), blue (2:1), etc. Note that 8:6 (yellow) is the last pattern observed before the I.D. zone (black). In the I.D. zone, the mean AR ranges from 530:495 to 530:325. Small islands of 5:4 (yellow) and 5:3 (green) appear within the I.D. region for $I_{stim} > 1.18\ I_{thR}$. Similar bifurcation structures were reported by other investigators (Vinet et al., 1990; Lewis & Guevara, 1990).

It has been shown that the main features of the above bifurcation scenario of period doubling and chaos (1:1 → 2:2 → 2:1 → 2n:n → chaos → 3:1) can be explained by a difference equation (iterative) model based on Thr(DIA) and APD(DIA). In the simplest version, the relation between the DIA at the onset of the (i+1)th stimulus and the previous one is given by the following set of equations:

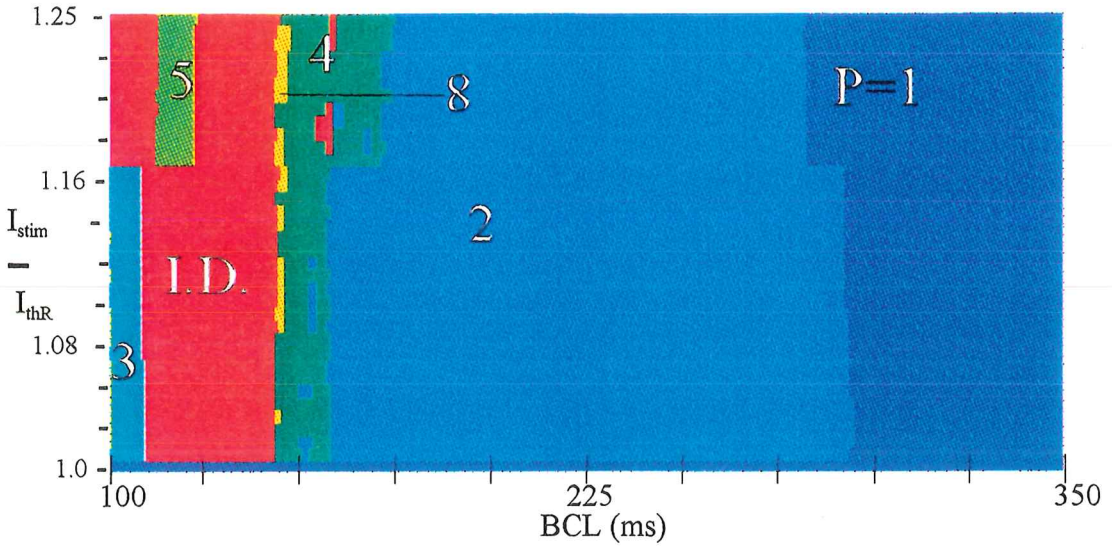

Figure 4.2.1.1: Period bifurcation structure of the MBR model for T_{stim}=1 ms. BCL was changed from 350 to 100 ms and I_{stim} from 0.997 to 1.25 I_{thR}.

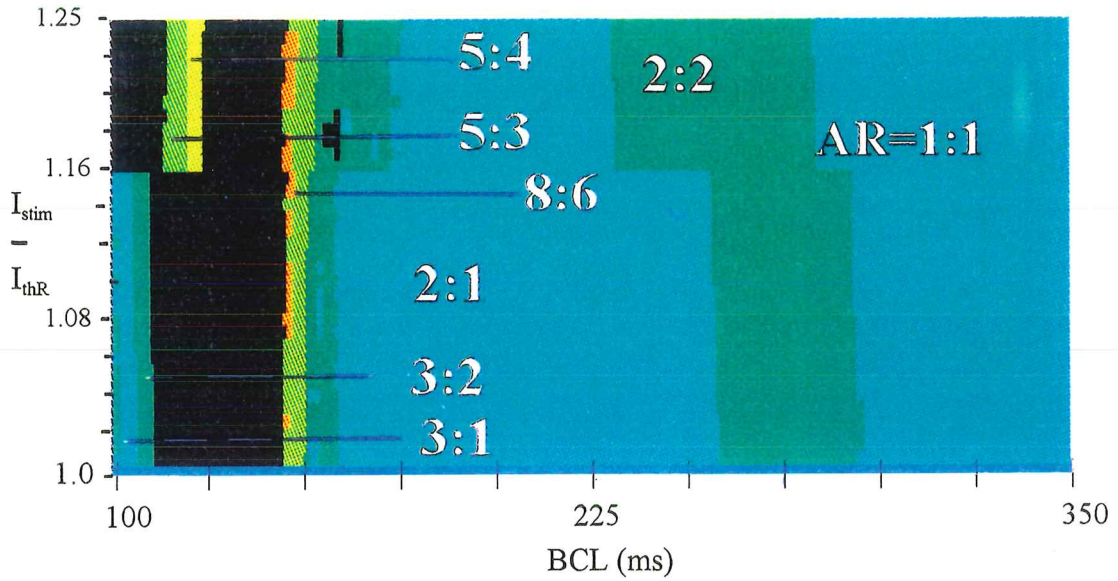

Figure 4.2.1.2: AR bifurcation structure of the MBR model for T_{stim}=1 ms. BCL was changed from 350 to 100 ms and I_{stim} from 0.997 to 1.25 I_{thR}.

$$DIA_{i+1} = BCL - APD(DIA_i) \quad , \quad if\ I_{stim} \geq Thr(DIA_i) \tag{4.2.1.A}$$

$$DIA_{i+1} = BCL + DIA_i \quad , \quad if\ I_{stim} < Thr(DIA_i) \tag{4.2.1.B}$$

Our purpose is not to provide a detailed comparison of the bifurcation structures predicted by the ionic and iterative models, since this was done previously for some versions of the BR model (Vinet et al., 1994). Our objective is to illustrate how the iterative model can be used to understand certain selected features of the dynamic behaviour of the MBR model.

In the iterative model, the DIA value associated with a 1:1 response satisfies the relations:

$$\begin{aligned} BCL &= DIA_o + APD(DIA_o) \\ I_{stim} &\geq Thr(DIA_o) \end{aligned} \tag{4.2.1.C}$$

where DIA_0 is the stable DIA at the corresponding BCL. It is stable if the slope of APD(DIA) evaluated at DIA_o is less than one (Vinet et al., 1991). For a monotonically increasing APD(DIA) curve, which includes a portion with slope > 1 at low DIA, there is a value DIA_{lim} where dAPD/dDIA =1. Therefore the 1:1 response loses its stability at

$$BCL_{lim} = DIA_{lim} + APD(DIA_{lim}) \tag{4.2.1.D}$$

For BCL < BCL_{lim}, stable 2:2 responses exist and are characterized by two values of DIA, one larger (DIA_h) and one smaller (DIA_{low}) than DIA_{lim}. As the BCL decreases, the amplitude of the alternation increases. The 2:2 response persists until it loses its stability, or until the smaller DIA of the 2:2 response becomes smaller than the absolute refractory period, leading to a blocked response (Watanabe et al., 1995). The DIA following a blocked response is then given by Eq. 4.2.1.B.

The 2:1 response appears when one DIA is larger than ARP(DIA_h) and the next DIA is less than ARP(DIA_{low}). DIA_h satisfies the relation 2BCL = DIA_h + APD(DIA_h), and the 2:1 response is stable as long as dAPD(DIA_h)/dDIA < 1. Accordingly, the 2:1 response looses its stability at $BCL_{lim}/2$, where a stable 4:2 appears and persists on a BCL interval half as long as that of the 2:2 interval.

The upper panel of Fig. 4.2.1.3 a shows the APD(DIA) curve obtained with premature stimulation of the MBR model, stimulus with I_{sim}= 1.25 I_{thR} and T_{stim}= 1 ms, following an action potential produced by pacing with I_{stim} =1.25 I_{thR} = 39.27 $\mu A/cm^2$. It was fitted by a double exponential function (broken curve) using Matlab software (1992). The value of DIA_{lim} was calculated from the fitted function (crosses), and BCL_{lim} was evaluated using eq. 4.2.1.D. We obtained a BCL_{lim} = 284 ms, which is close to the value of 282 ms corresponding to the 1:1→ 2:2 transition in Fig. 4.2.1.2.

The end of the 2:1 regime was found at 157 ms, that is at a value somewhat

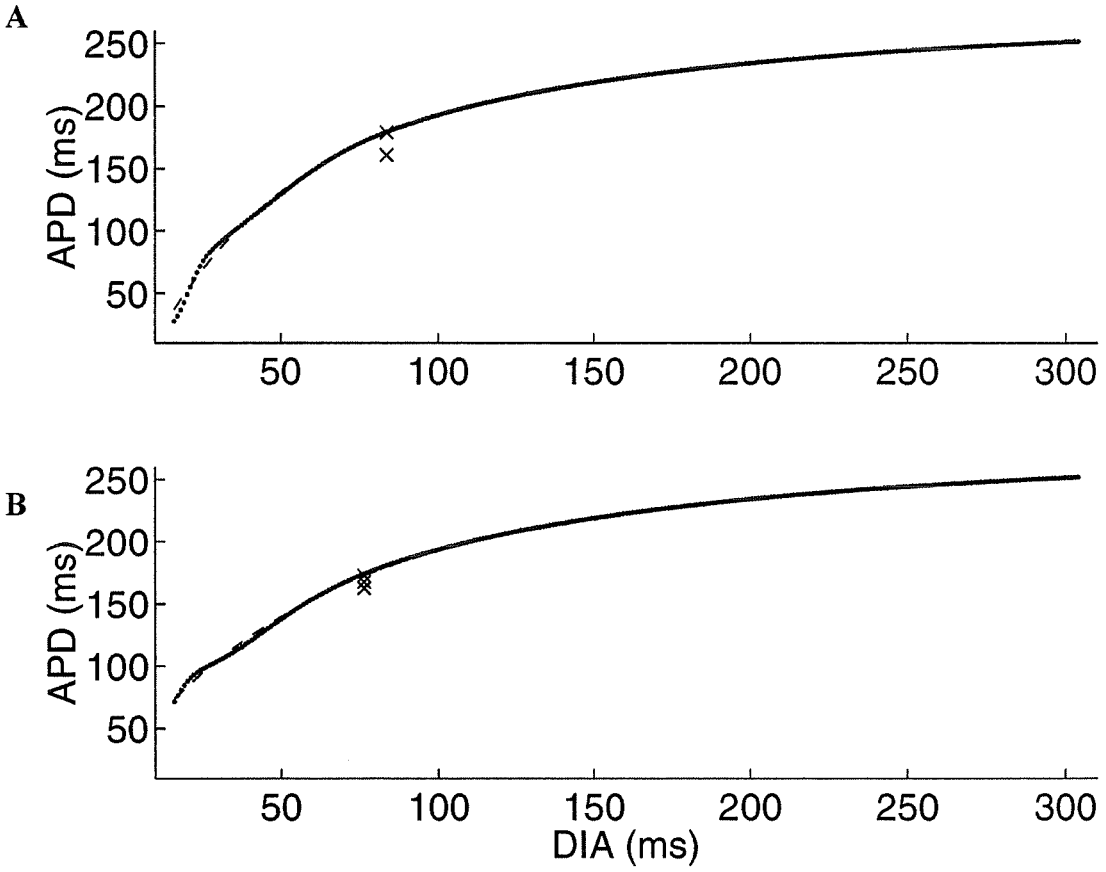

Figure 4.2.1.3: MBR model APD(DIA) curves for T_{stim} = 1 ms and I_{stim} = 1.25 I_{thR} (upper panel), or I_{stim} = 4.25 I_{thR} (lower panel). Broken curve is the double-exponential fit to the APD(DIA) curve in each panel, and the crosses indicate the slope dAPD/dDIA = 1.

higher than the $BCL_{lim}/2$ = 142 ms predicted by the iterative model. This can be explained by the resetting effect of the blocked response which introduces a delay in the repolarization (not taken into account by eq. 4.1.2.B). It has been proposed to treat this delay as an instantaneous resetting of the DIA interval (DIA→DIA- Δ) to be included in the iterative model (Vinet and Roberge, 1994). Because of the resetting, the DIA that follows the blocked response is smaller than the value predicted by eq. 4.1.2.B. The 2:1 response will then be characterized by the sequence:

$$DIA_{low} = BCL - APD(DIA_h) \quad (4.2.1.D)$$
$$DIA_h = BCL + DIA_{low} - \Delta \quad (4.2.1.E)$$

or

$$DIA_h = 2 \times BCL - \Delta - APD(DIA_h) \quad (4.2.1.F)$$

where Δ is a small time interval. Since stability is lost when DIA = DIA_{lim}, it occurs at BCL = $(DIA_{lim} + APD(DIA_{lim}) + \Delta)/2 = (BCL_{lim} + \Delta)/2$. Hence the resetting increases the BCL values at which the stability of the 2:1 rhythm is lost. Furthermore, the locus of the 2:1→ 4:2 transitions would change with the amplitude of the stimulation since Δ is a function of I_{stim}. Both features are observed in the MBR model.

In fact, the influence of the reset is even more complex. Following Eq. 4.2.1.F, the 2:1 rhythm is stable if $d(APD + \Delta)/dDIA$ is < 1 at DIA_h. The Δ function has been shown to be a non-monotonic function of DIA_{low} and I_{stim} (see Fig. 2 in Vinet and

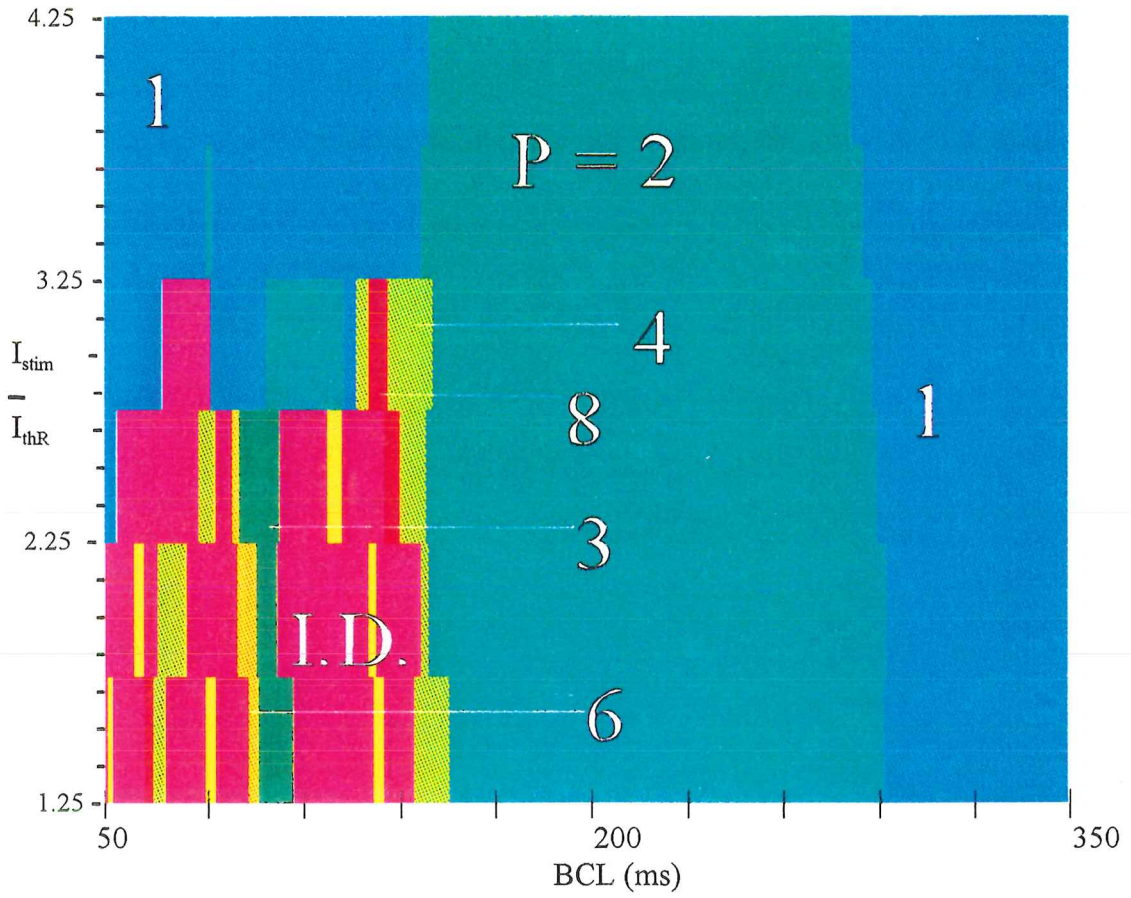

Figure 4.2.1.4: Period bifurcation structure of the MBR model for T_{stim}= 1 ms. BCL was changed from 350 to 50 ms and I_{stim} from 1.25 to 4.25 I_{thR}.

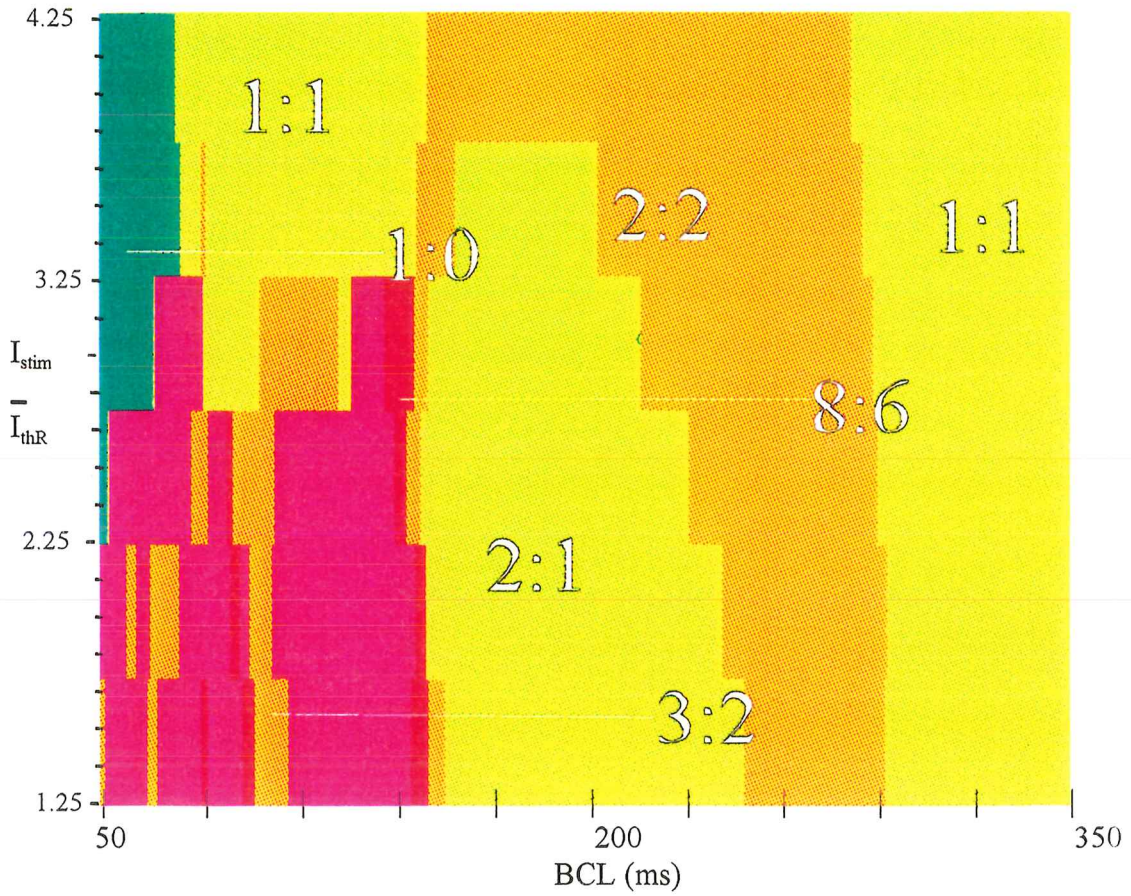

Figure 4.2.1.5: AR bifurcation structure of the MBR model for T_{stim}= 1 ms. BCL was changed from 350 to 50 ms and I_{stim} from 1.25 to 4.25 I_{thR}.

Roberge, 1994). The stability criterion, evaluated at DIA_h can then be written as:

$$\left(1-\frac{d\ \Delta(DIA_{low})}{d\ DIA}\right)\ \frac{d\ APD(DIA_h)}{d\ DIA} \leq 1 \qquad (4.2.1.G)$$

Besides moving DIA_h toward DIA_{lim}, Δ can also stabilize (positive slope for Δ) or destabilize (negative slope for Δ) the 2:1 rhythm. This may explain the occurrence of small zones of irregular rhythm in the 4:2 and the 2:1 regions (e.g. small red areas within P=4 in Fig. 4.2.1.1), and windows of periodicity in the I.D. region at relatively high I_{stim}.

We have also investigated the bifurcation structure for I_{stim} ranging from 1.3 to 4.2 I_{thR}. The BCL was changed from 50 to 350 ms. The results are depicted in Figures 4.2.1.4 and 4.2.1.5. With larger I_{stim} values, the period doubling zone and the I.D. zones decrease and then disappear (e.g. P=4 (green), P=6 (yellow), P=8 (green) are lost at I_{stim}= 3.25I_{thR} in Fig. 4.2.1.4). A new bifurcation sequence then appears, where the rhythm changes from period 1 to period 2, and then returns to period 1 again (upper part of Fig. 4.2.1.4). The first transition still occurs at BCLs between 284 and 290 ms, while the second occurs in the range where period 4 was appearing at lower I_{stim}. The AR transitions follow the sequence 1:1→ 2:2 → 2:1→2:2 → 1:1 → 1:0, with missing 1:1 and 1:0 components when the stimulus strength is sufficiently low. The 2:1 region shrinks gradually and disappears for $I_{stim} > 3.82\ I_{thR}$.

In the preceding chapter, we showed that high I_{stim} reduces the dispersion of the

APD(DIA) curve, simultaneously by shifting the DIA_{lim} toward lower DIA values and reducing the slope below DIA_{lim}. This is illustrated again in Fig. 4.2.1.3.A. These changes explain why both the beginning and the end of the 2:2 region are moved toward a lower BCL as I_{stim} increases.

To understand the transition from period 2 to period 1 at high stimulus amplitude, we constructed the APD(DIA) curve using as conditioning action potential one of the 1:1 responses of this region: BCL = 140 ms, I_{stim}= 4.2 I_{thR}, and T_{stim} = 1ms. The same value of I_{stim} and T_{stim} were taken for the S2 stimulations. The results are depicted in Figure 4.2.1.6. The lower panel shows that the derivative > 1 for DIA = [33-77 ms], and then returns to values < 1 for DIA < 33 ms. This explains why the system may return to a 1:1 response after an interval of 2:2.

The final occurrence of 1:0 can be explained by the influence of the blocked response for high amplitude stimuli. The value of Δ becomes so high that, at low BCL, DIA_h given by eq. 4.1.2.E still falls in the refractory period. A new fixed DIA_o is created below the refractory period if BCL = $\Delta(DIA_o)$ and if $\| d\,\Delta(DIA_o)/ d\,DIA \| <$ 1. The system is then locked in a period 1 rhythm, with no active response. The effect of a blocked response had been included in some version of the difference equation model (Vinet & Roberge 1994), but the range of stimulus amplitudes where reset becomes dominant and controls the pattern of response had not been previously described.

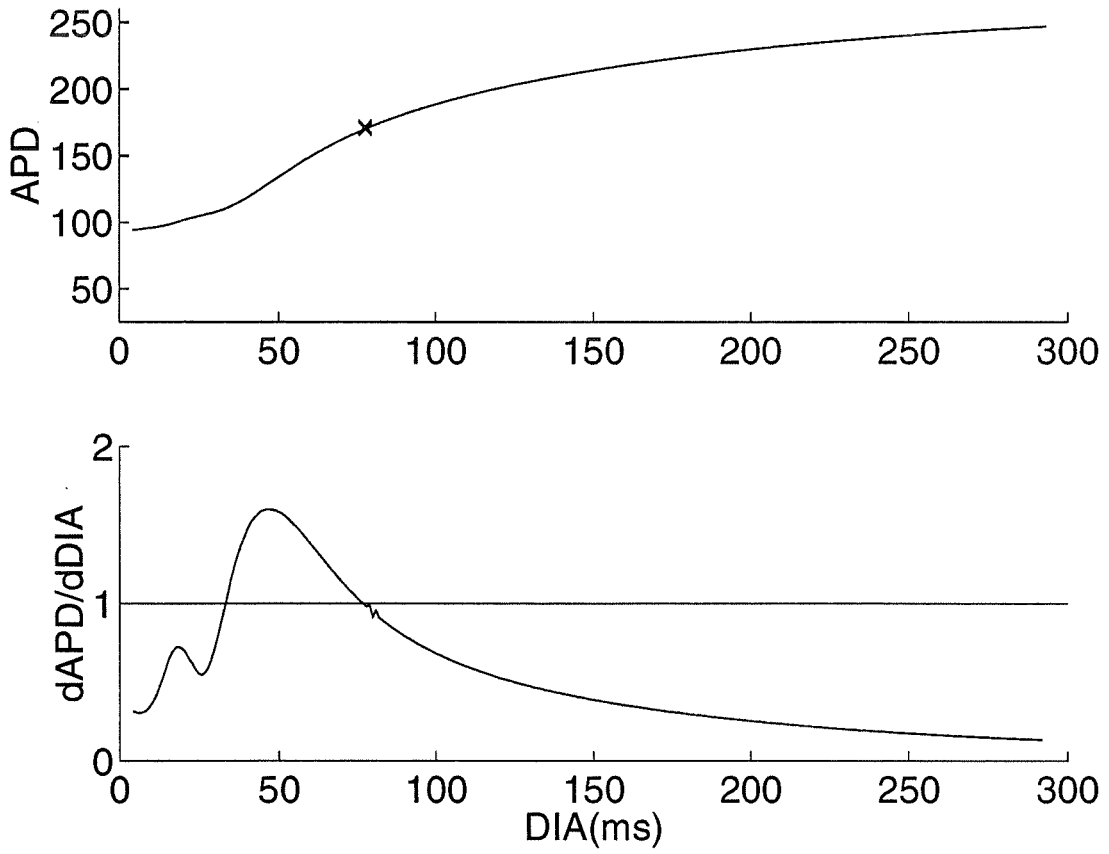

Figure 4.2.1.6: For (S1-S1)= 140 ms, the APD(DIA) curve for T_{stim} = 1 ms and I_{stim} = $4.2I_{thR}$ (upper panel) has a transition from period 1 to period 2 indicated by a cross. Lower panel shows dAPD/dDIA.

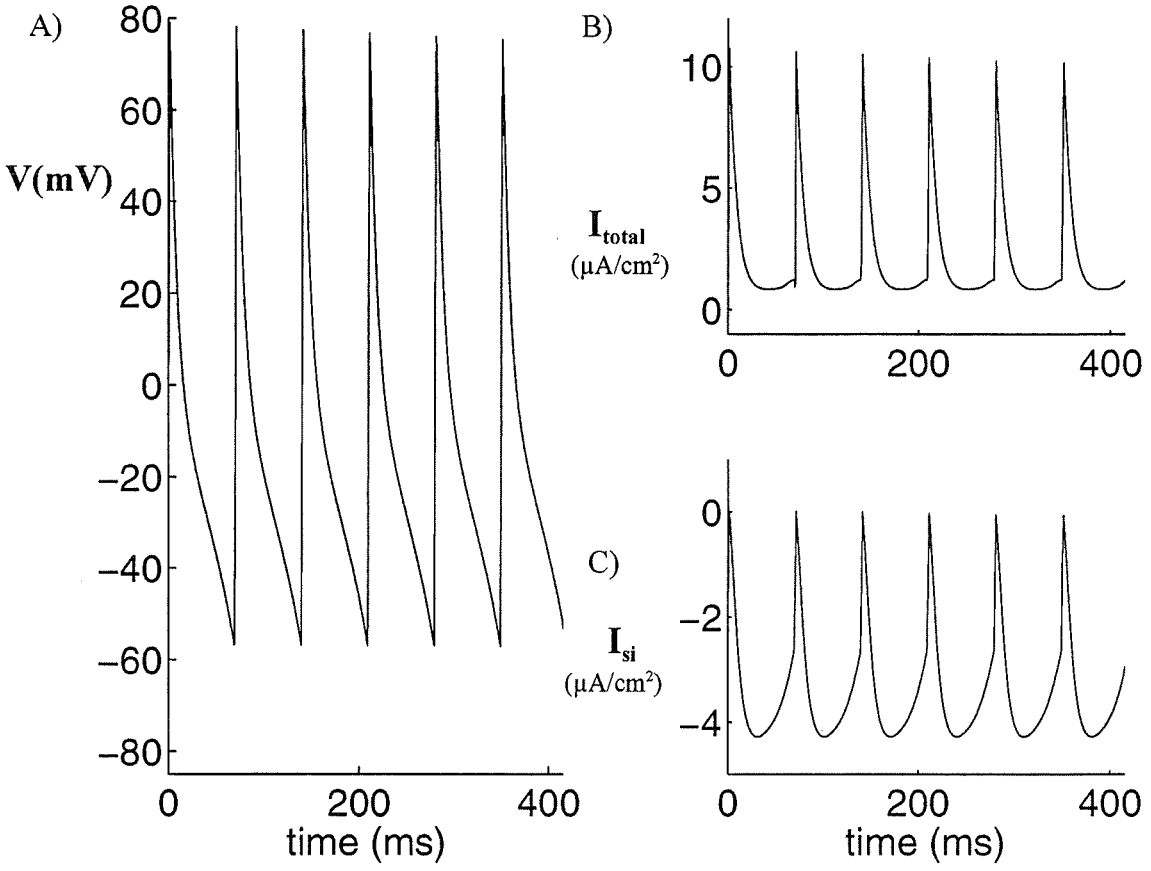

Figure 4.2.1.7: Membrane potential responses (panel A) for T_{stim}=1 ms, I_{stim} = 4.2 I_{thR} and BCL = 70 ms. Corresponding membrane current responses (panel B) and I_{si} waveforms

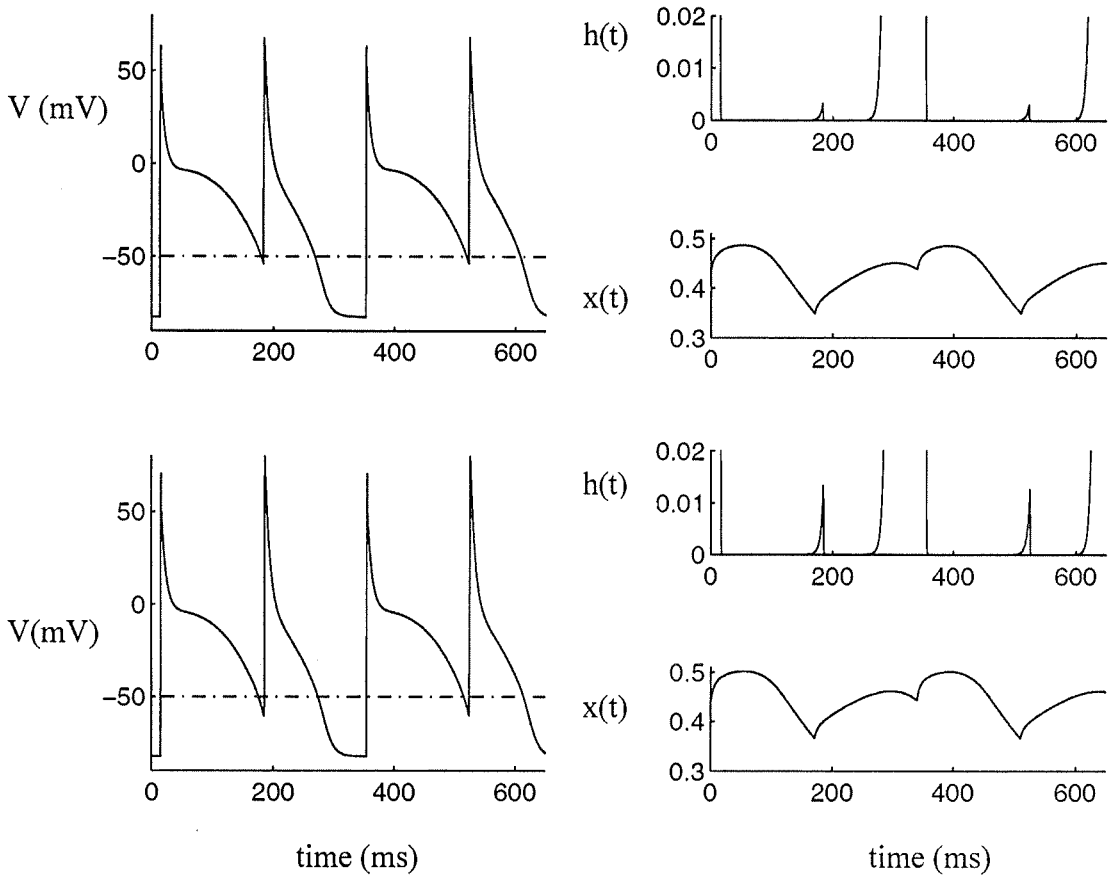

Figure 4.2.1.8: For (S1-S1) = 170 ms, T_{stim} = 1 ms and $I_{stim} = 3.57I_{thR}$ (upper panels), and $4.18I_{thR}$ (lower panel). In both cases the system is in period 2. ARs are 2:1 (upper panels) and 2:2 (lower panel).

In terms of ionic current, the system does not have enough time between 2 stimuli to repolarize to a low enough potential for the sodium current to be reactivated (h gate, reactivated for V < -70 mV). Fig. 4.2.1.7 shows the 1:0 response for T_{stim} = 1 ms, I_{stim} = 4.2 I_{thR} and BCL = 70 ms. Although the responses look like action potentials (panel A), the ionic current (I_{total}) is always outward (panel B). Thus, these responses are considered passive, even if the slow inward current (I_{si}) is fully activated (panel C).

The set of transitions 1:1→2:2→1:1 existing at high I_{stim} can thus be explained by the monotonic evolution of the APD curve which, in this range of stimulation, starts with a segment that has a slope less than 1 at low DIA. It remains to understand why the transitions 2:2→2:1→2:2 also exist in a limited range of stimulus amplitudes. Figure 4.2.1.8 shows the action potential responses and the evolution of h and x for I_{stim} = 3.57 I_{thR} and 4.18 I_{thR}. For the first I_{stim} (upper panels), there is still an interval of 2:1 responses, while there are 2:2 responses for the second (lower panels). The horizontal broken line in the left column shows the V_{-50}. Both cases exhibit a long and a short response, and in both cases the responses have the same duration, whether they correspond to the passive (2:1) (upper panel) or the active (2:2) response (lower panel). Moreover, x is slightly higher for I_{stim} = 4.18 I_{thR}, leading to a faster repolarization. In addition, I_{Na} is reset and the small burst of sodium current occurring during the stimulation leads us to classify the beat as active (panel 4, right column). However, this small burst of sodium current does not change V_{max} and the following time course of repolarization. This situation is completely different from that observed at lower I_{stim},

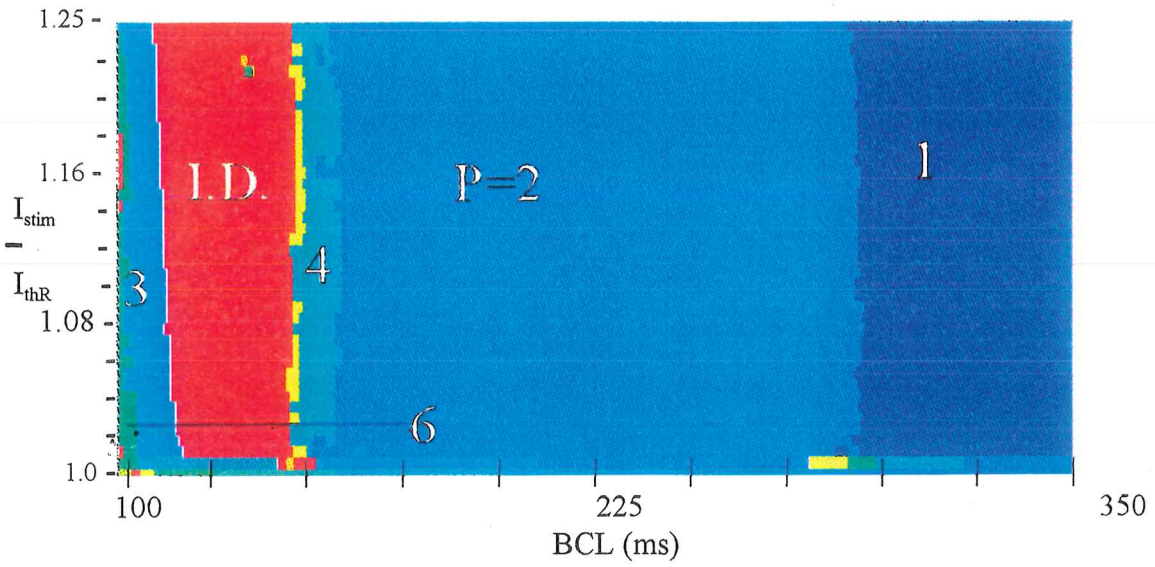

Figure 4.2.1.9: Period bifurcation structure of the MBR model T_{stim}= 5 ms. BCL was changed from 350 to 100 ms and I_{stim} from 1 to 1.25 I_{thrR}.

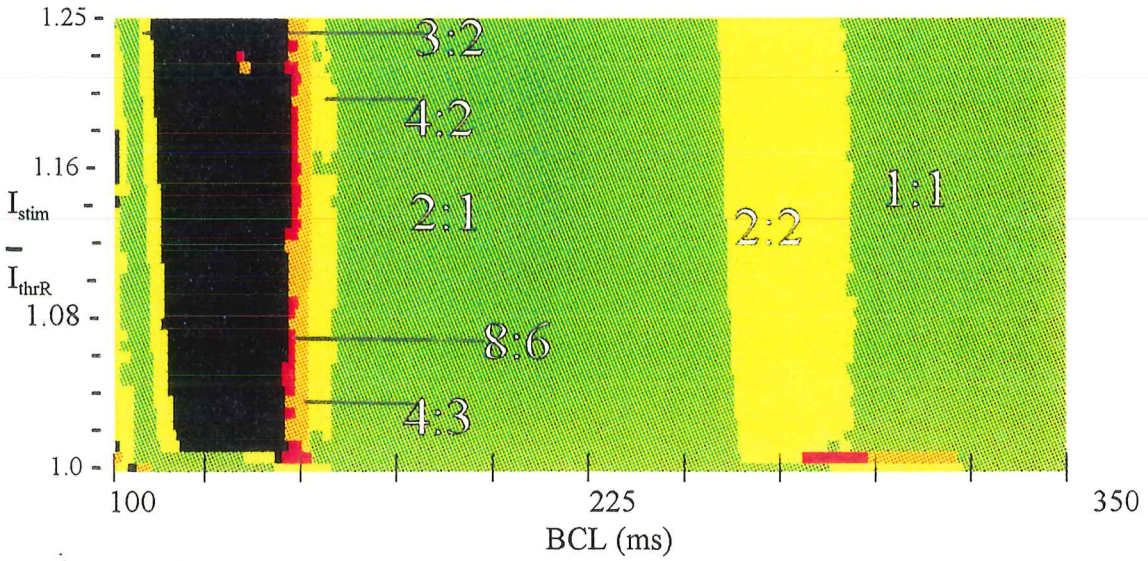

Figure 4.2.1.10: AR bifurcation structure of the MBR model for T_{stim}= 5 ms. BCL was changed from 350 to 100 ms and I_{stim} from 1 to 1.25 I_{thR}.

where supra and subthreshold responses were associated with different repolarization time courses, and where the peak ionic current (I_p) and time to repolarization were equivalent indicators of threshold behaviour (Vinet & Roberge, 1994). Hence at low BCL and high I_{stim}, the distinction between a short active or passive response becomes arbitrary and does not reflect distinct repolarization time courses.

For T_{stim} = 5 ms, the major structures of the bifurcation map are similar to those obtained with T_{stim} = 1 ms (Figs 4.2.1.9 and 4.2.1.10). The only difference is a small region of period adding bifurcations (1 → 2 → 3, . . .) with decreasing activation ratios (1:1 →2:1 →3:1) which appear for I_{stim} near I_{thR}. This particular bifurcation structure will be discussed in the next section since it appears over a larger I_{stim} interval with a larger T_{stim}.

In summary, for short $T_{stim} \leq 5$ ms, the iterative model can predict and explain the bifurcation structure and transition periods. However, for high I_{stim} and low BCL (Figs 4.2.1.4 and 4.2.1.5), the resetting due to a blocked response and the transformation of the APD(DIA) curve shape cause important changes in the bifurcation maps.

4.2.2 Intermediate $T_{stim.}$

For I_{stim} ranging from I_{thR} to 1.3 I_{thR}, the 15 and 25 ms T_{stim} durations exhibit three different bifurcation structures corresponding to successive ranges of I_{stim}, Region I for

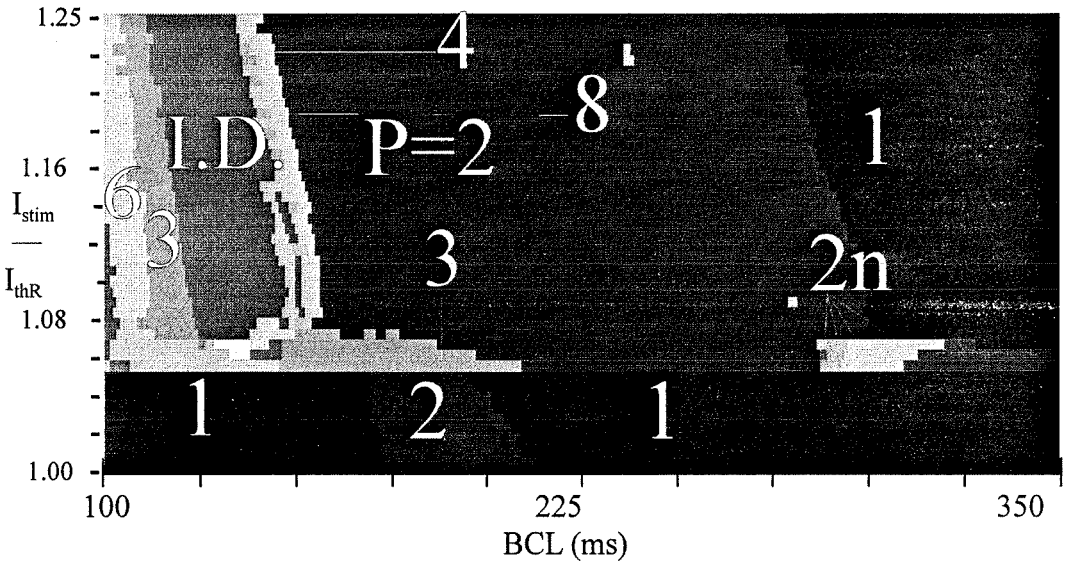

Figure 4.2.2.1: Period bifurcation structure of the MBR model for T_{stim}= 15 ms. BCL was changed from 350 to 100 ms and I_{stim} from 1 to 1.25 I_{thR}.

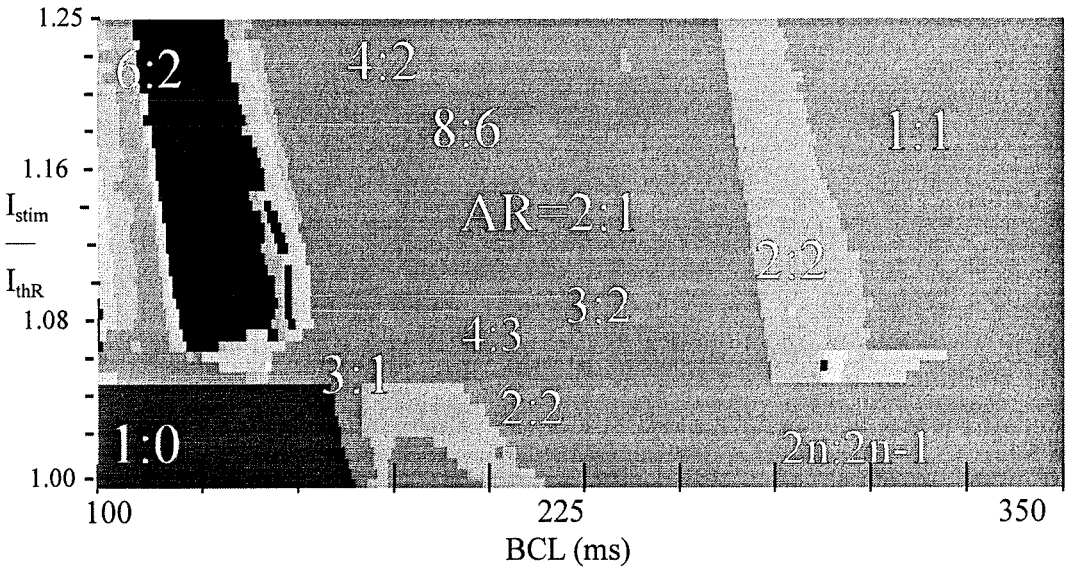

Figure 4.2.2.2: Activation bifurcation structure of the MBR model for T_{stim}= 15 ms. BCL was changed from 350 to 100 ms and I_{stim} from 1 to 1.25 I_{thR}.

$I_{stim} < 1.07\ I_{thR}$, Region II for $1.07\ I_{thR} < I_{stim} < 1.18\ I_{thR}$, and Region III for $I_{stim} > 1.18\ I_{thR}$. The results are presented in Figs 4.2.2.1 and 4.2.2.2, for T_{stim} = 15 ms, and in Figs 4.2.2.3 and 4.2.2.4 for T_{stim} = 25 ms. They are quite similar to those described by Vinet et al. (1990) and Chialvo et al. (1990). Since Region I-III are larger and can be seen clearly for T_{stim}= 25 ms, this case is analyzed in more detail. The bifurcation structure in Region I is similar to that seen with low I_{stim} and T_{stim} = 5 ms (Figs 4.2.1.9 and 4.2.1.10). It is characterized by period adding (1→ 2 → 3 → 4 . . .), Fig. 4.2.2.3, and decreasing n:1 AR, Fig. 4.2.2.4.

Region II presents a very complex bifurcation structure. During slow pacing (BCL = 350 ms) the system is already in period 2, as was the case in Region I. Period 2 then increases to period 4, 6, 8 , 10. The AR of the period 2 zone is 2:2 and 2n:2n-1 in period 4, 6, 8 and 10 zones. Related transitions can be found in the period 3 zone. In Region III ($I_{stim} > 1.18\ I_{thR}$), the bifurcation structure is the same as for T_{stim} = 1 ms and 5 ms, with a cascade of period doublings leading to irregular dynamics.

The succession of bifurcation scenarios found in Region I and Region III can be explained by the interaction of the supernormal Thr(DIA) curve with APD(DIA) (Chialvo et al., 1990; Vinet et al., 1990). As seen in Fig. 4.2.2.5, stimulation with DIA >230 ms is subthreshold if I_{stim} is below $1.07\ I_{thR}$. All suprathreshold stimuli (DIA > 230ms) fall in the region where the derivative of APD(DIA) is less than one (Fig. 4.2.1.3.A). Hence, for each I_{stim} near I_{thR}, there is a value $DIA_f(I_{stim})$ below which the stimulus

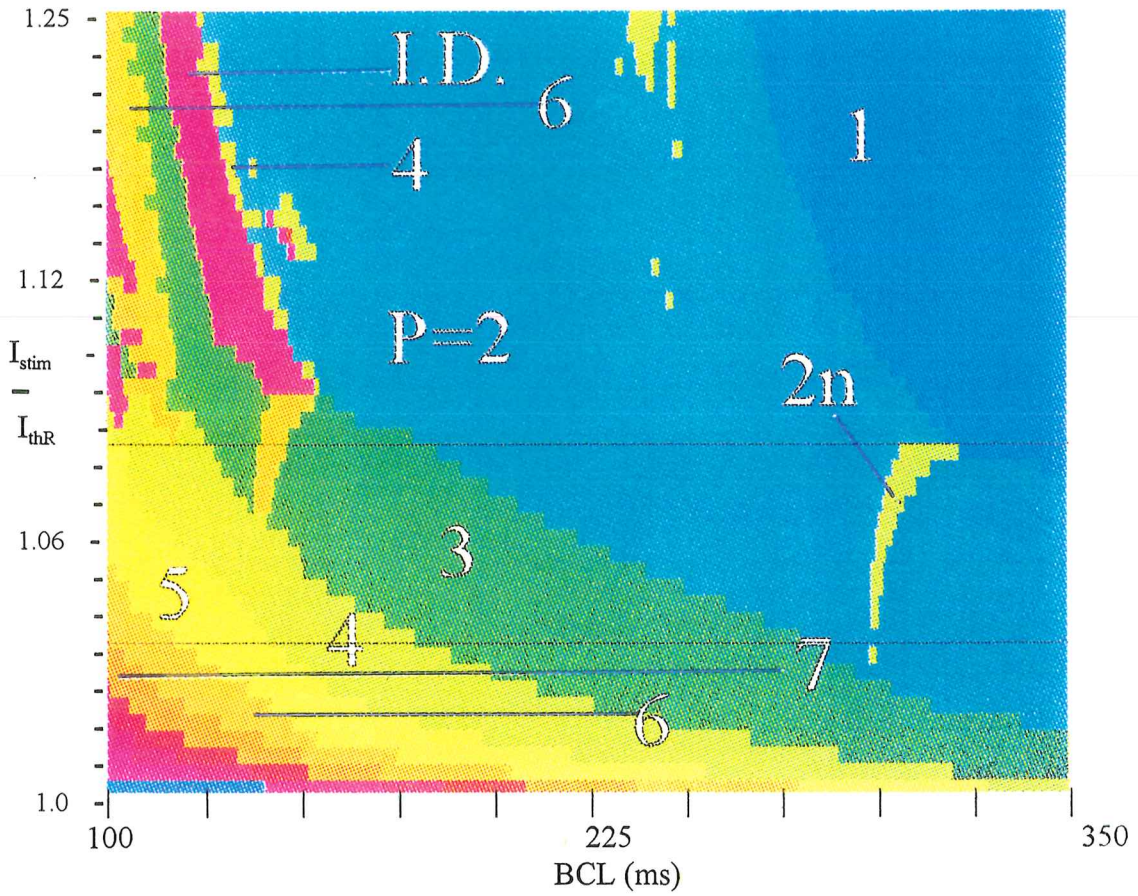

Figure 4.2.2.3: Period bifurcation structure of the MBR model for T_{stim}= 25 ms. BCL was changed from 350 to 100 ms I_{stim} from 1 to 1.25 I_{thR}.

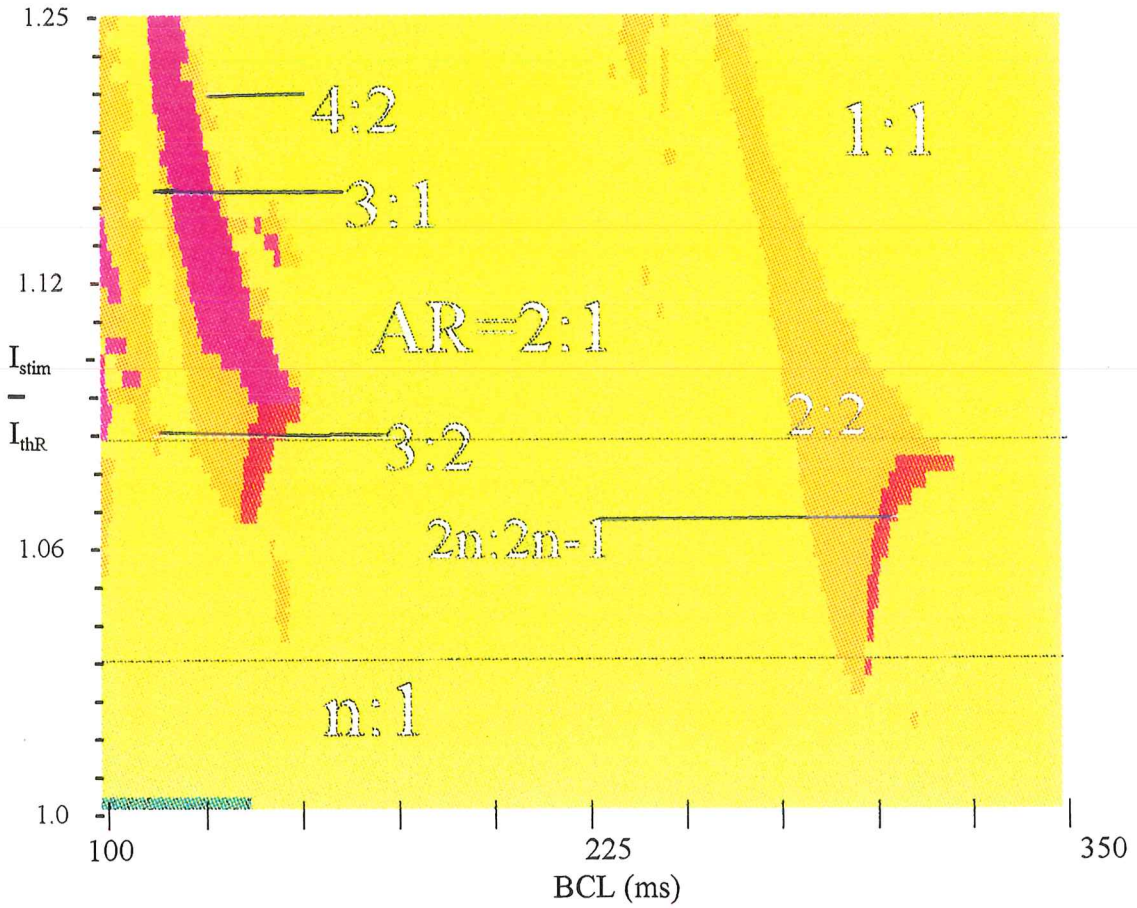

Figure 4.2.2.4: AR bifurcation structure of the MBR model for T_{stim}= 25 ms. BCL was changed from 350 to 100 ms and I_{stim} from 1 to 1.25 I_{thR}.

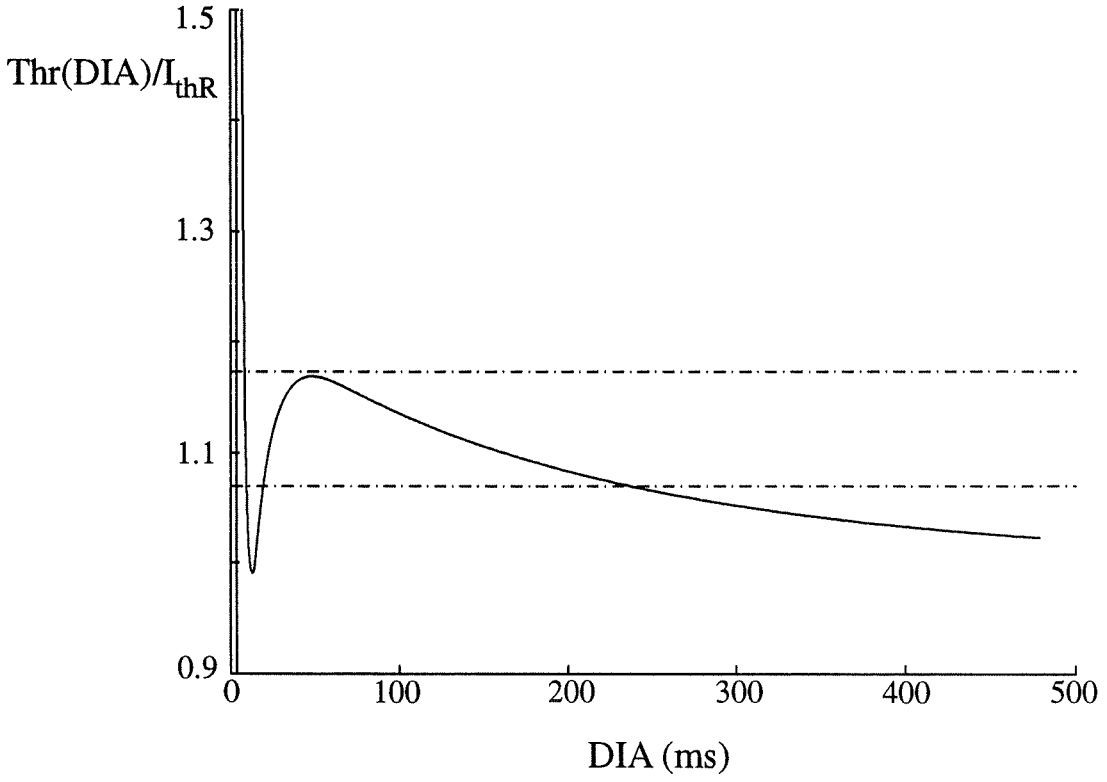

Figure 4.2.2.5: Thr(DIA) for T_{stim} = 25 ms, the horizontal broken lines indicate the value of I_{stim} = 1.07 I_{thR} (bottom line) and I_{stim} = 1.18 I_{thR} (upper line).

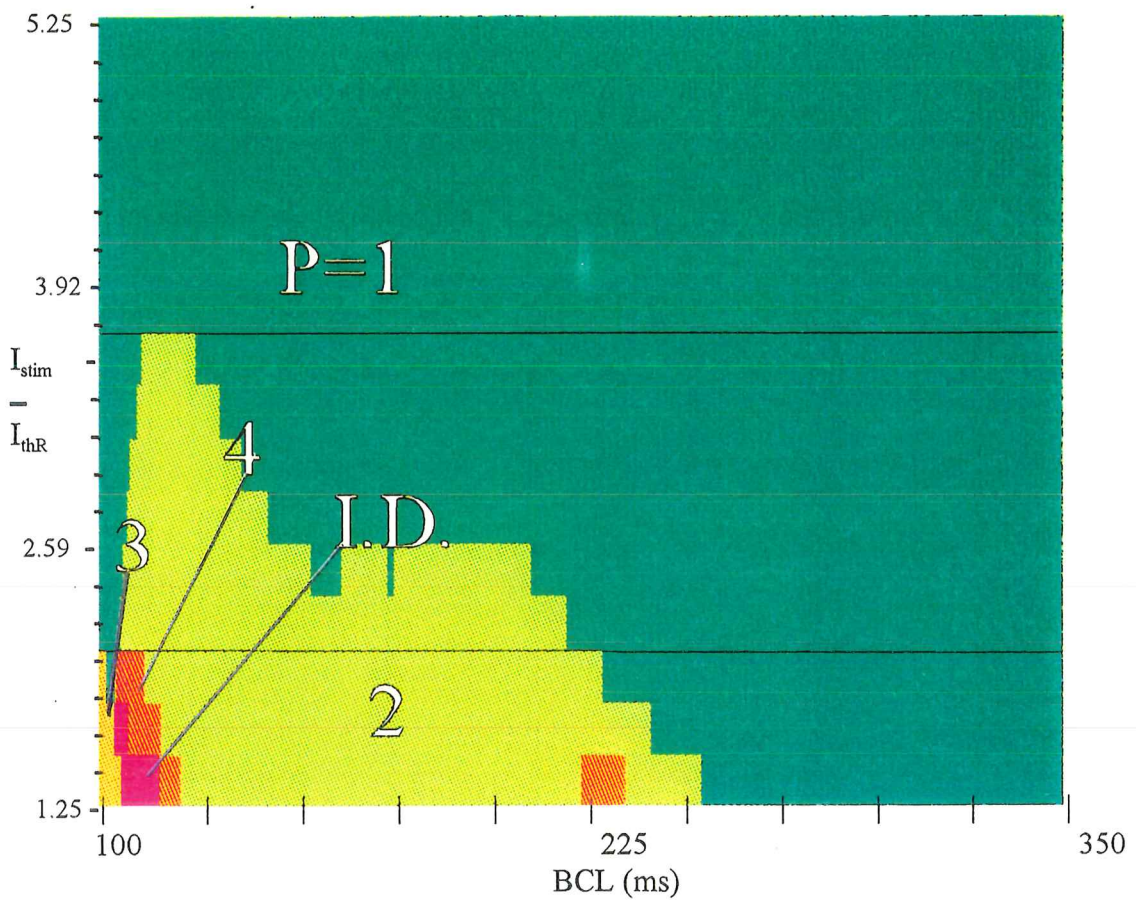

Figure 4.2.2.6: Period bifurcation structure of the MBR model for T_{stim}= 25 ms. BCL was changed from 350 to 100 ms and I_{stim} from 1.25 to 5.25 I_{thR}.

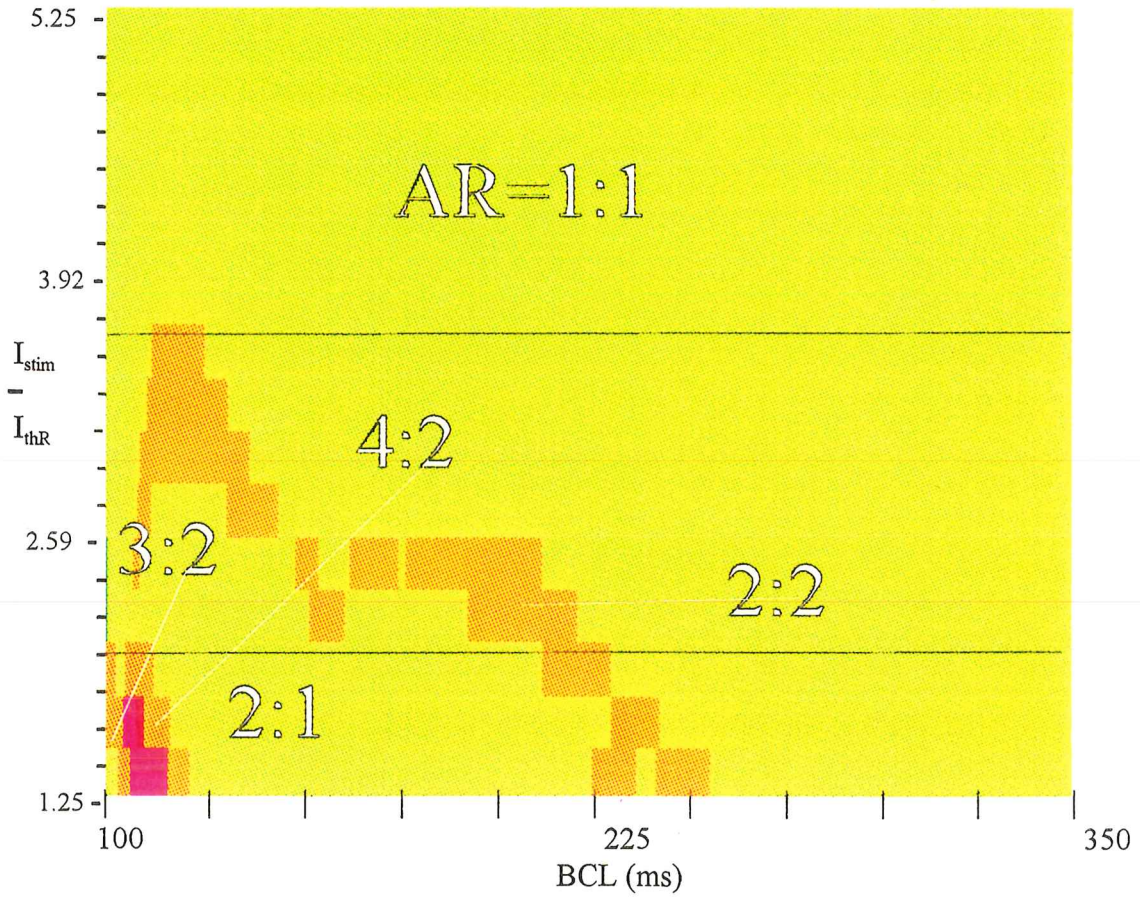

Figure 4.2.2.7: AR bifurcation structure for the MBR model for T_{stim}= 25 ms. BCL was changed from 350 to 100 ms and I_{stim} from 1.25 to 5.25 I_{thR}.

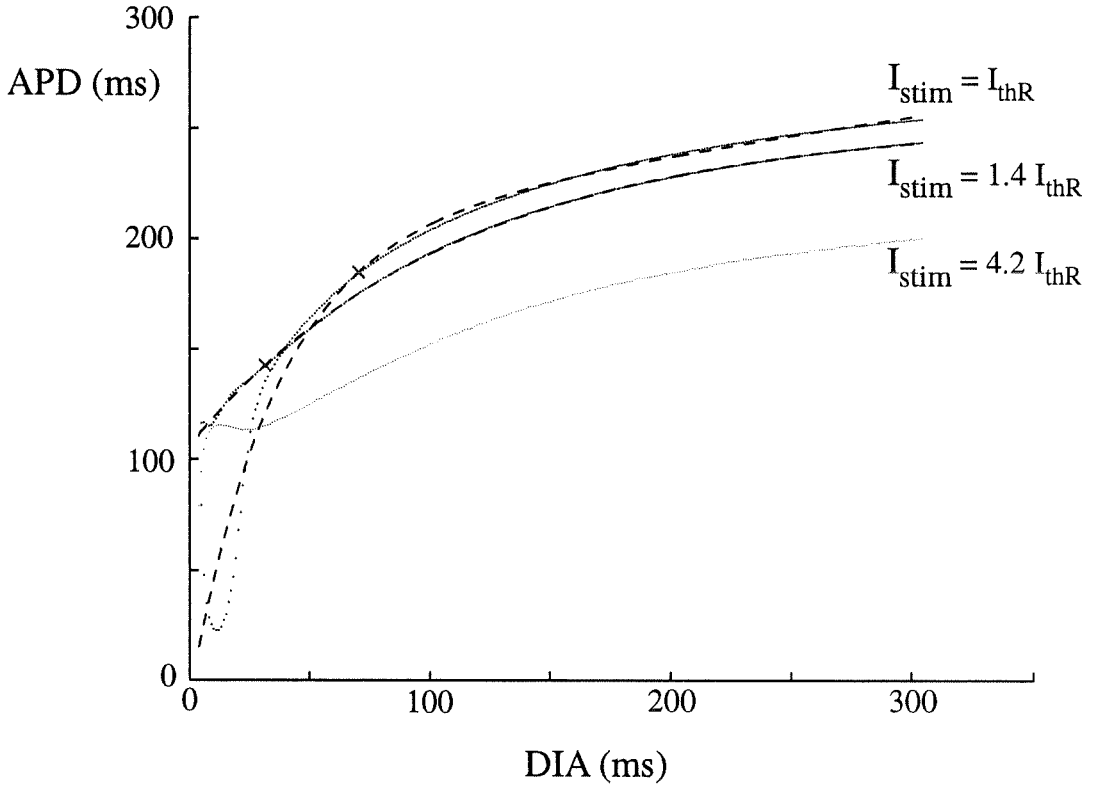

Figure 4.2.2.8: APD(DIA) curves for T_{stim} = 25 ms and I_{stim} = 1, 1.4, and 4.2 I_{thR} (dotted curves). The broken curve represents the fit of the double exponential.

becomes subthreshold. Since the slope of APD(DIA) is < 1 for all DIA > DIA_f, the 1:1 response persists until $BCL_f = DIA_f + APD(DIA_f)$, where the 2:1 responses appear. The iterative model predicts that successive n:1 entrainment responses exist in the BCL interval [BCL/n, BCL/(n-1)].

In Region II (1.07 I_{thR} < I_{stim} < 1.18 I_{thR}), the stimulus strength exceeds Thr(DIA) over two distinct DIA intervals separated by a gap where the stimulus is subthreshold. Stimuli falling in this DIA interval lead to blocked responses which eliminate some APD values and this creates a hole in the APD(DIA) curve (Vinet et al., 1990). The complex bifurcation structure seen in Region II is due to this phenomenon.

Finally, near the lower part of Region III, the stimulus is suprathreshold for all DIA larger than a minimum value. It includes a DIA interval where dAPD/dDIA > 1. The difference equation model then predicts period doubling and chaos, in close agreement with the bifurcation structure of Region III for T_{stim}= 15 or 25 ms, and also with that observed for T_{stim} = 1 and 5 ms.

We have completed the study of the bifurcation structure for T_{stim}=25 ms by increasing I_{stim} up to 5.2I_{thR} The BCL was changed between 100 and 350 ms. The continuous increase of I_{stim} above 1.25 I_{thR} provided a new set of bifurcation structures which are presented in Figs 4.2.2.6 and 4.2.2.7. The maps are similar to those obtained with a large I_{stim} for T_{stim} = 1ms (Figs 4.2.1.4 and 4.2.1.5). First, the period doubling

and I.D. zones shrink and finally disappear for $I_{stim} > 1.85\ I_{thR}$. Then a 1:1 zone appears at low BCL, and the 2:1 zone (between 1:1 and 2:2) diminishes gradually. Finally, for $I_{stim} > 3.075\ I_{thR}$, only 1:1 rhythm can be found for all BCLs. Similar to the T_{stim}= 1 ms case, the transformation of the bifurcation structure can be explained by the changes of the APD(DIA) curve at high I_{stim} (see Fig. 4.2.2.8) which have already been discussed in Chapter III.

The bifurcation structures presented in this intermediate range of stimulus durations are generic since they are found in a variety of membrane model formulations. Their main characteristics are period adding at low stimulus amplitude, irregular dynamics and period doubling stages at intermediate amplitude, and period 1 rhythm at high amplitude. As indicated earlier, these bifurcation structures were expected because of the shape of the APD(DIA) and Thr(DIA) curves for each stimulus amplitude. The only unanticipated results are the sustained stable 1:1 rhythm at high stimulus amplitude and the 1:0 rhythm resulting from blocked responses even when the stimulus amplitude is large. In the latter case, such stimulus amplitudes perturb the action potential generating mechanism to such an extent that the normal recovery of excitability is prevented.

4.2.3 Long T_{stim}

No new entrainment zone was found when T_{stim} was increased beyond 25 ms. However, three transformations of the bifurcation structure were noticeable: 1) a gradual

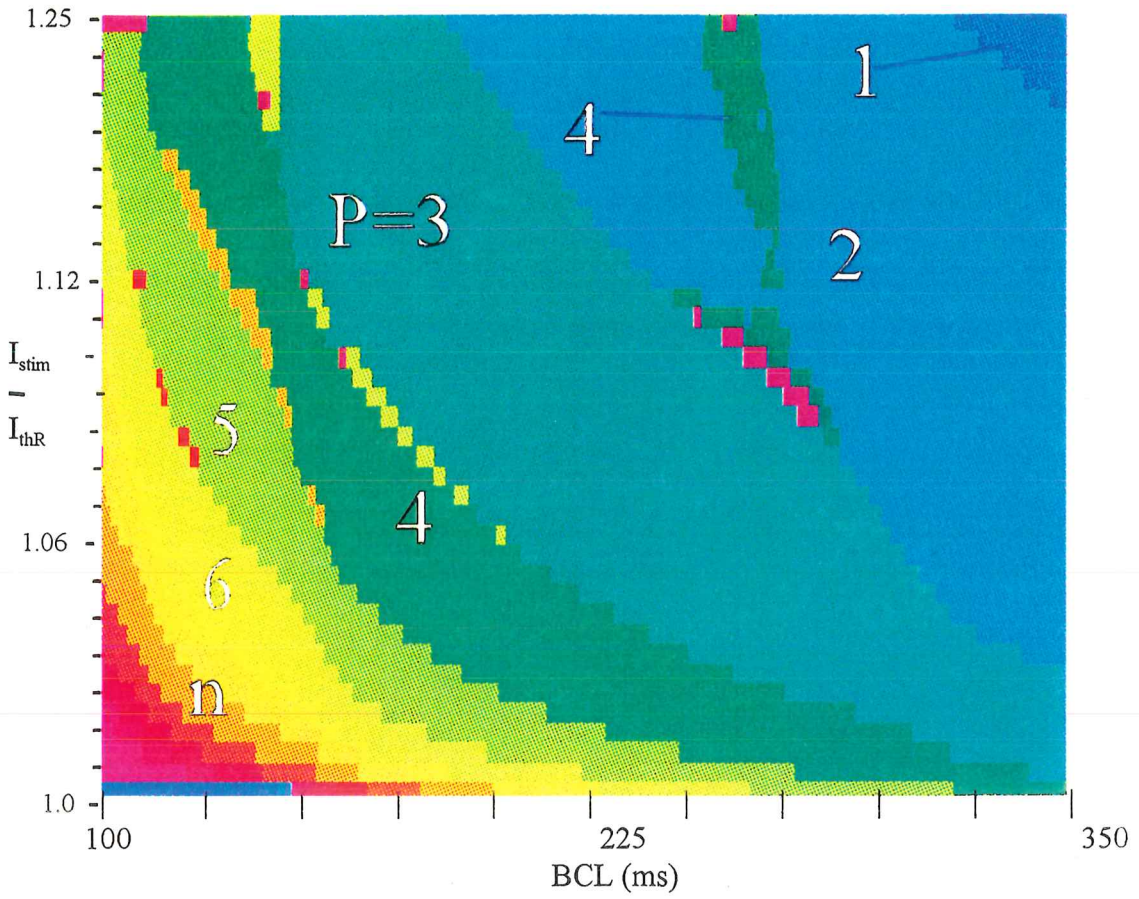

Figure 4.2.3.1: Period bifurcation structure of the MBR model for T_{stim}= 45 ms. BCL was changed from 350 to 100 ms and I_{stim} from 1 to 1.25 I_{thR}.

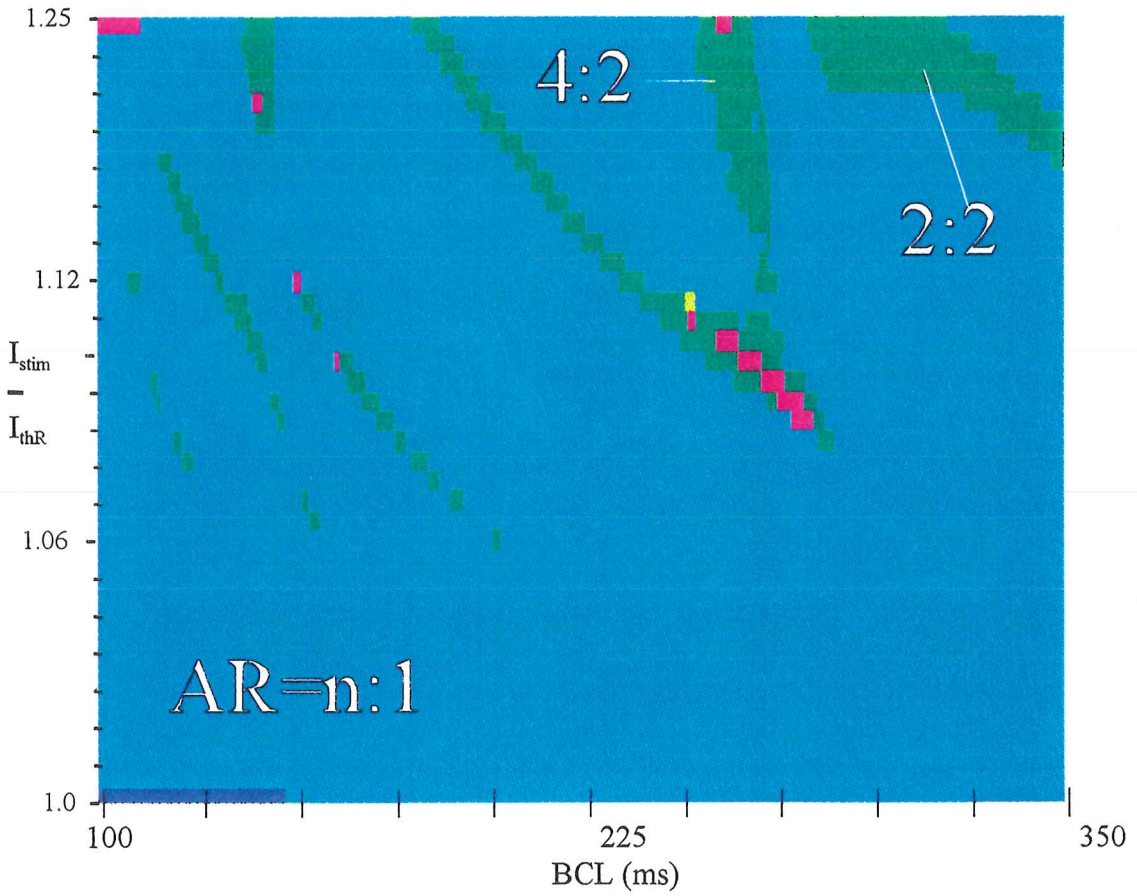

Figure 4.2.3.2: AR bifurcation structure of the MBR model for T_{stim}= 45 ms. BCL was changed from 350 to 100 ms and I_{stim} from 1 to 1.25 I_{thR}.

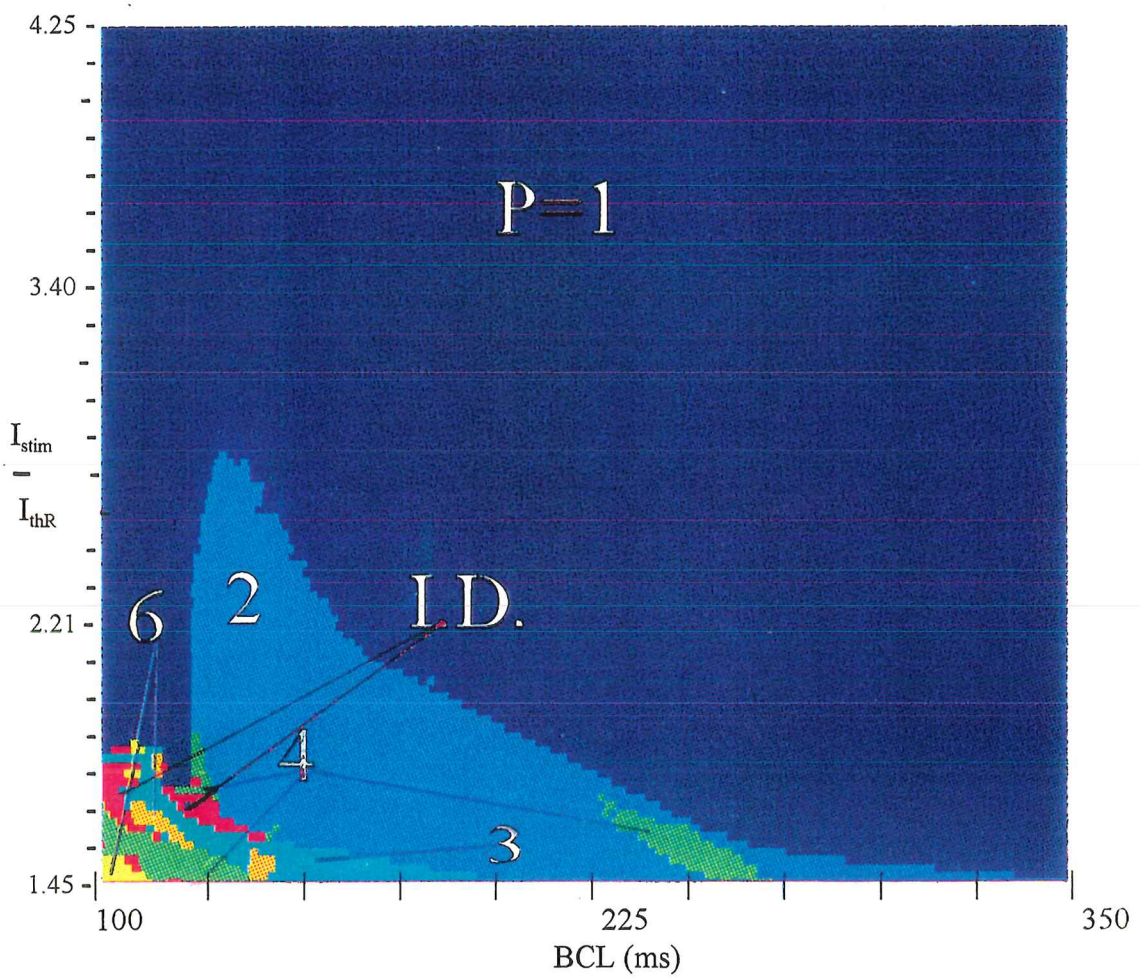

Figure 4.2.3.3: Period bifurcation structure of the MBR model for T_{stim}= 45 ms. BCL was changed from 350 to 100 ms and I_{stim} from 1.45 to 4.25 I_{thR}.

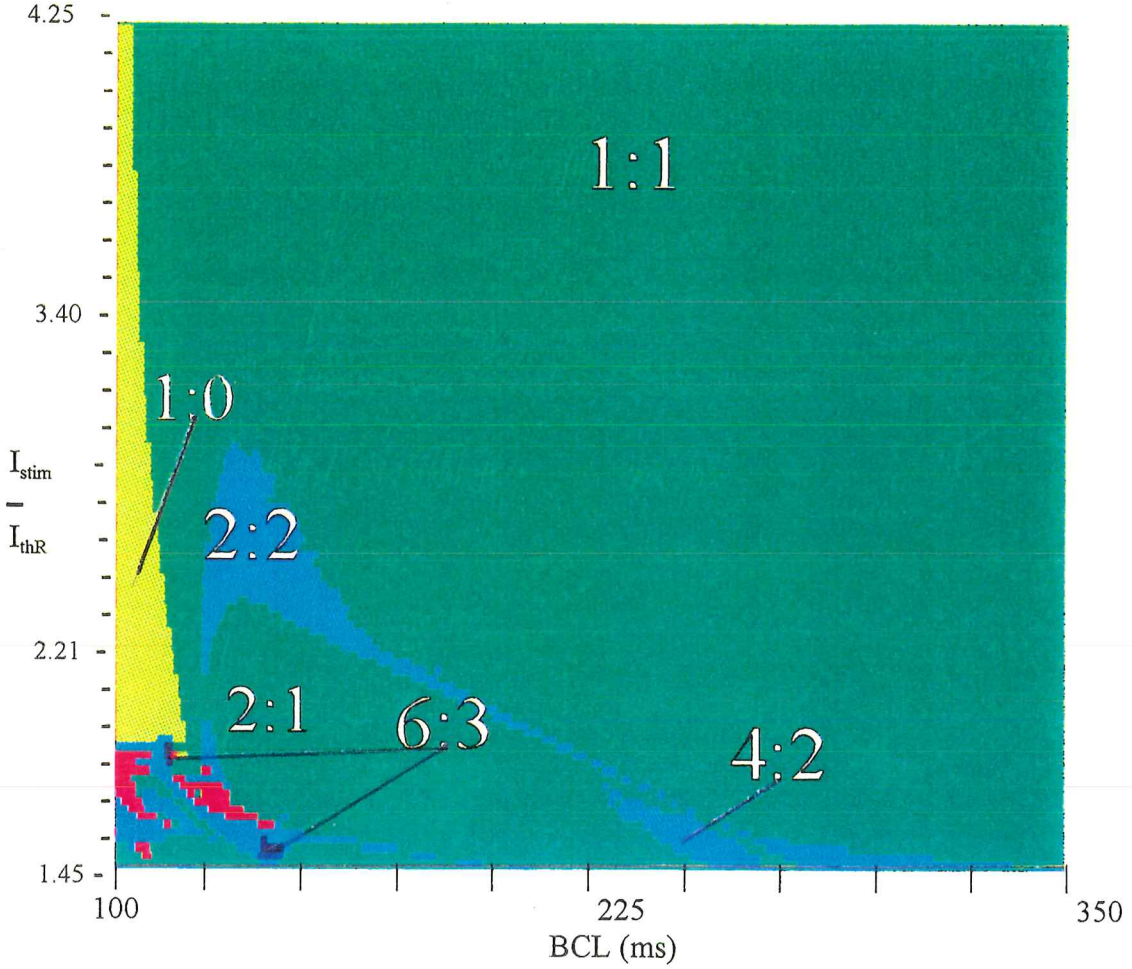

Figure 4.2.3.4: AR bifurcation structure of the MBR model for T_{stim}= 45 ms. BCL was changed from 350 to 100 ms and I_{stim} from 1.45 to 4.5 I_{thrR}.

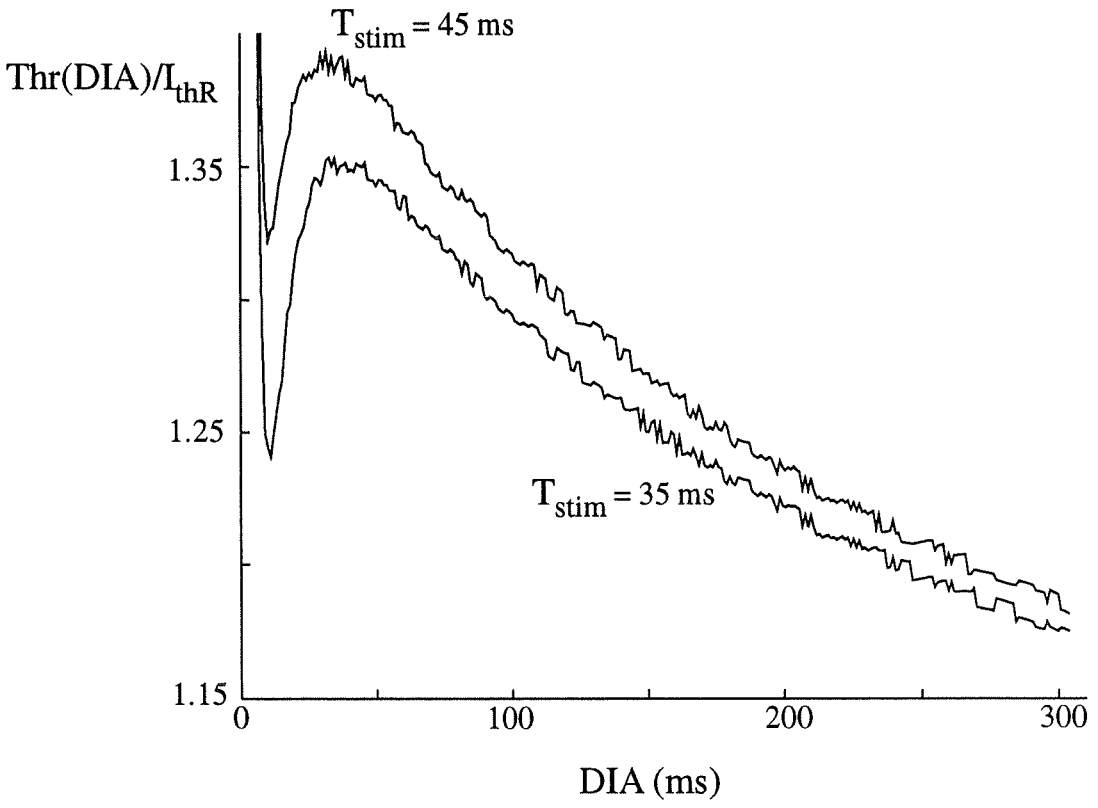

Figure 4.2.3.5: Normalized Thr(DIA) for T_{stim} = 35 and 45 ms.

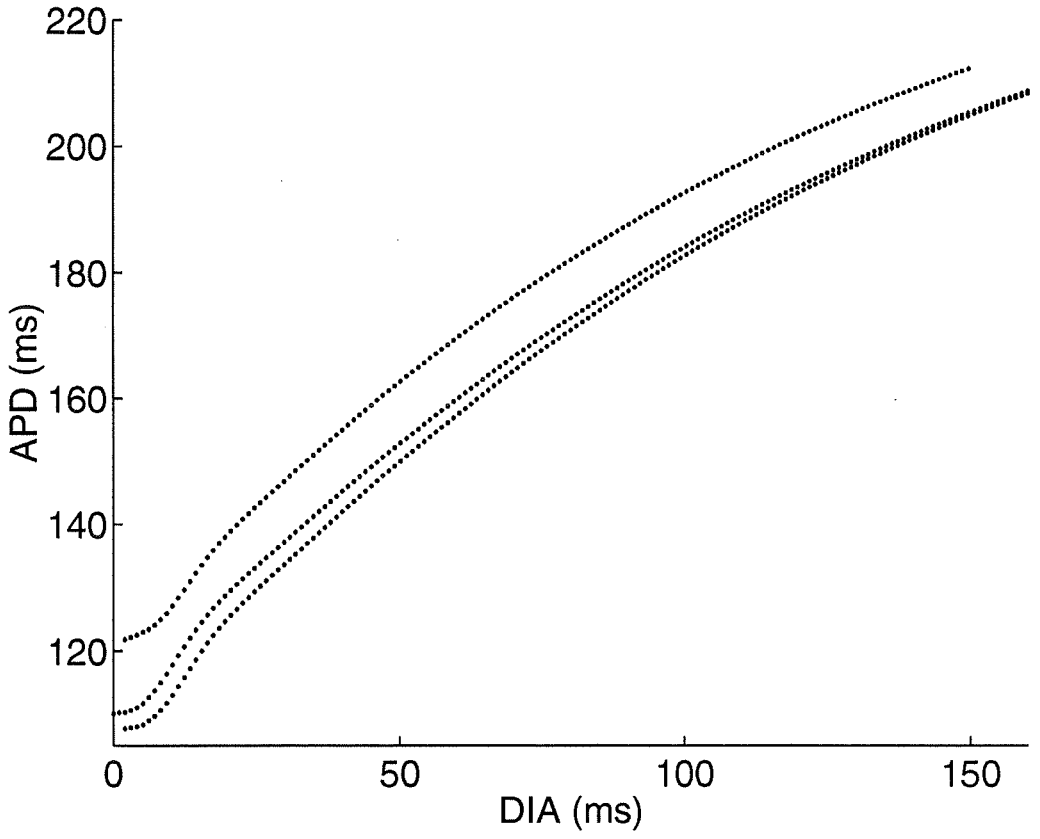

Figure 4.2.3.6: APD(DIA) with T_{stim} = 45 ms, I_{stim} = 2.01 I_{thR}, (S1-S1) = 300 ms (upper curve), (S1-S1) = 135 ms (middle curve), and (S1-S1) = 125 ms (lower curve).

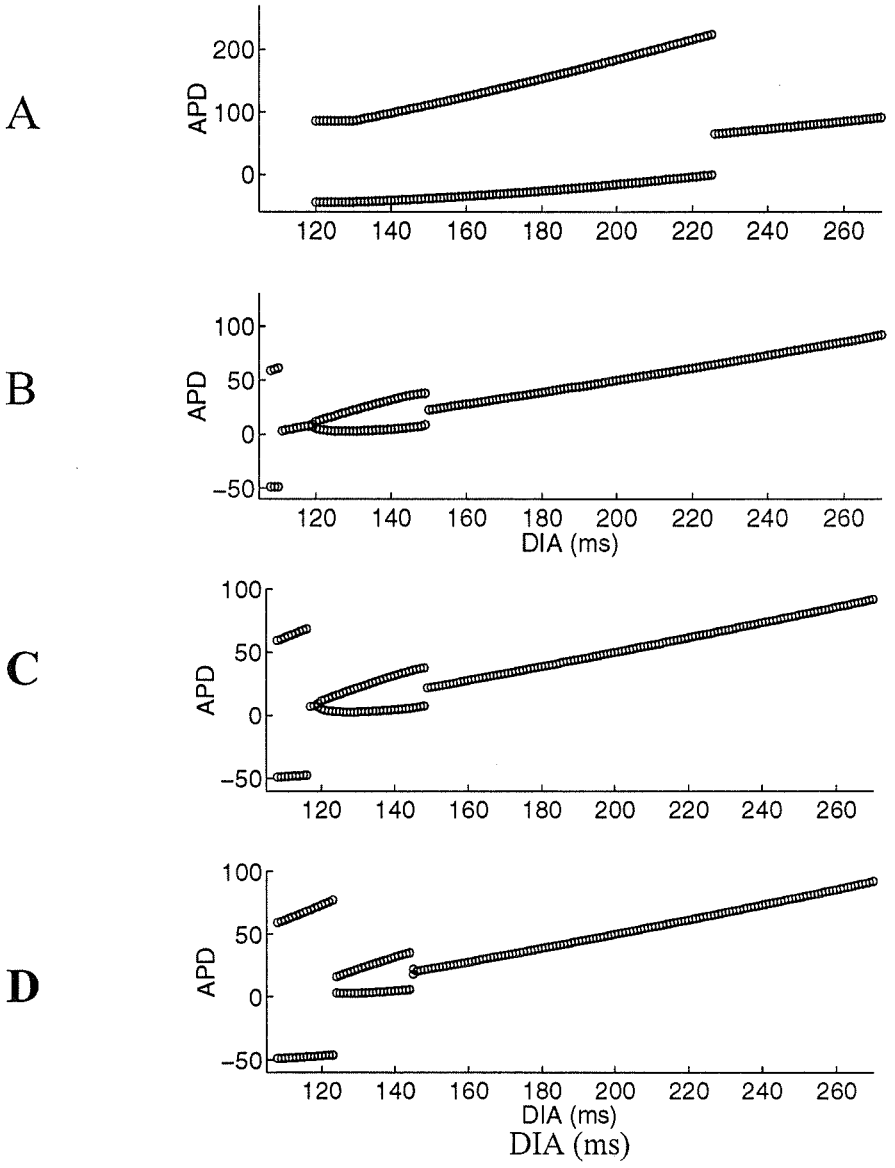

Figure 4.2.3.7: Maps obtained from the iterative model for APD(DIA) for different BCLs. A and B: (S1-S1) = 300 ms and 135 ms, respectively, with initial conditions at rest, C and D: (S1-S1) = 300 ms with initial conditions established by BCLs of 135 and 125 ms, respectively.

enlargement of the period adding zone for I_{stim} just above I_{thR}; 2) a disappearance of the intermediate Region II existing between the period adding and the period doubling zones, and 3) a reduction of the extent of the period doubling and I.D. zones. These features are depicted in Figs 4.2.3.1, 4.2.3.2, 4.2.3.3, and 4.2.3.4 for T_{stim}= 45 ms.

The map characteristics can be understood through the transformation of the Thr(DIA) and APD(DIA) curves with longer T_{stim}. As shown in Fig. 4.2.3.5, the normalized Thr (DIA) is shifted upward as T_{stim} increases. This explains the extension of the period adding zone and the disappearance of Region II which was a result of the supernormality seen in Chapter II (e.g. Fig. 2.4.1.1). One can observe also the flattening of the APD(DIA) curves associated with the increase of I_{stim}, as described in Chapter III (e.g. Fig. 3.3.1.5.B), and DIA intervals with a high APD slope occur over a much reduced range. Hence there is a reduction of the BCL interval over which period doubling and I.D. occur (compare Figs 4.2.3.1 and 4.2.3.3 with Fig. 4.2.1.4). All other bifurcation features at higher I_{stim} (Figs 4.2.3.3 and 4.2.3.4) can also be linked to the flattening of the APD(DIA) curve seen with T_{stim} = 25 ms.

Large T_{stim} values also amplify the dependence of the APD(DIA) curve on the previous paced action potential. Fig. 4.2.3.6 shows the APD curves constructed from the 1:1 response at BCL = 300, 135 and 125 ms, with T_{stim} = 45 ms and I_{stim}= 2.01 I_{thR}. The bifurcation structures predicted by the iterative model used with each APD(DIA) curve are very different (Fig. 4.2.3.7). Depending of the choice of BCL and initial

conditions, there may be an interval of 1:1 between 2:2 and 2:1 rhythms. Thus, for long T_{stim} and high I_{stim}, some kind of memory effect links the APD changes with the preceding action potential and this property must be included in the iterative model in order to make it more accurate.

4.4 Summary and Conclusion

The stimulus duration and amplitude have a strong influence on the period bifurcation structure of the MBR membrane model. Three major types of bifurcation structures were found. The first is period doubling, the second is period adding, and the third is the 1:1→ 2:2 → 1:1 → 1:0 bifurcation cascade.

Period doubling is present at low and middle intensity for short stimulus durations, and middle intensity for longer stimulus durations. According to the simple difference equation model (Eqs. 4.2.1.A and B), period doubling and irregular dynamics (I.D.) should occur in cases where the APD(DIA) curve has a region with dAPD/dDIA > 1 and where I_{stim} is suprathreshold over a continuous interval starting in the region were dAPD/dDIA > 1. In the MBR ionic model, however, the effect of blocked responses becomes important at large I_{stim}, such that the bifurcation cascade is interrupted after period 2 and the system then moves to 1:0 entrainment. Period adding exists both at low and high I_{stim} for large stimulus durations. In these cases, the Thr(DIA) function is either monotonically decreasing ($T \geq 35$ ms) or has a strictly decreasing part over a

range of DIA values. Hence there is an interval of I_{stim}, starting at I_{thR}, where the stimulus is suprathreshold for a narrow DIA interval over which dAPD/dDIA < 1 everywhere, which yields period adding bifurcations. Since strong stimuli of long duration reduce the APD dispersion (Chapter III), the region where dAPD/dDIA > 1 may be eliminated (e.g. lower curve in Fig. 3.3.1.3) to yield a period adding bifurcation structure.

The 1:1 region at low BCL exists when I_{stim} is increased, leading to faster depolarization fostered by the x variable (see Fig. 2.4.4.3).

The analysis has shown that the simple iterative model with APD(DIA) and Thr(DIA) functions can be used to explain many of the different regimes of entrainment occurring in the MBR ionic model. It is clear, however, that a single APD(DIA) curve cannot be used to predict the behaviour of the MBR model for sufficiently large I_{stim} and T_{stim} values. In particular, once T_{stim} is increased above 35 ms, the iterative model is no longer appropriate at high stimulus amplitude. Moreover the effect of blocked responses must be incorporated into the iterative model (as in Vinet et al.,1994), particularly for very large I_{stim}.

CHAPTER V

ENTRAINMENT RESPONSE OF A PAIR OF CARDIAC CELLS WITH A FIXED GAP JUNCTION RESISTANCE

In the previous chapters, we explained the entrainment response of a space-clamped MBR model of the cardiac myocyte. In the present chapter, we investigate the response of a pair of identical cardiac cells coupled by a fixed gap junction resistance (R). Stimulation is applied to one of the cells and the entrainment response is described for a wide range of gap junction resistances. Increasing R reduces the coupling current and may prolong the time spent by the non-paced cell in the subthreshold regime. The situation is qualitatively similar to the change in the pulse stimulus characteristics (I_{stim} and T_{stim}) studied in Chapter IV and should yield comparable results, unless the presence of the gap junction resistance introduces additional dynamic characteristics into the two-cell system.

5.1 Model of the Cell Pair

The cell pair model is diagrammed in Fig. 5.1.1. We consider two identical cells with

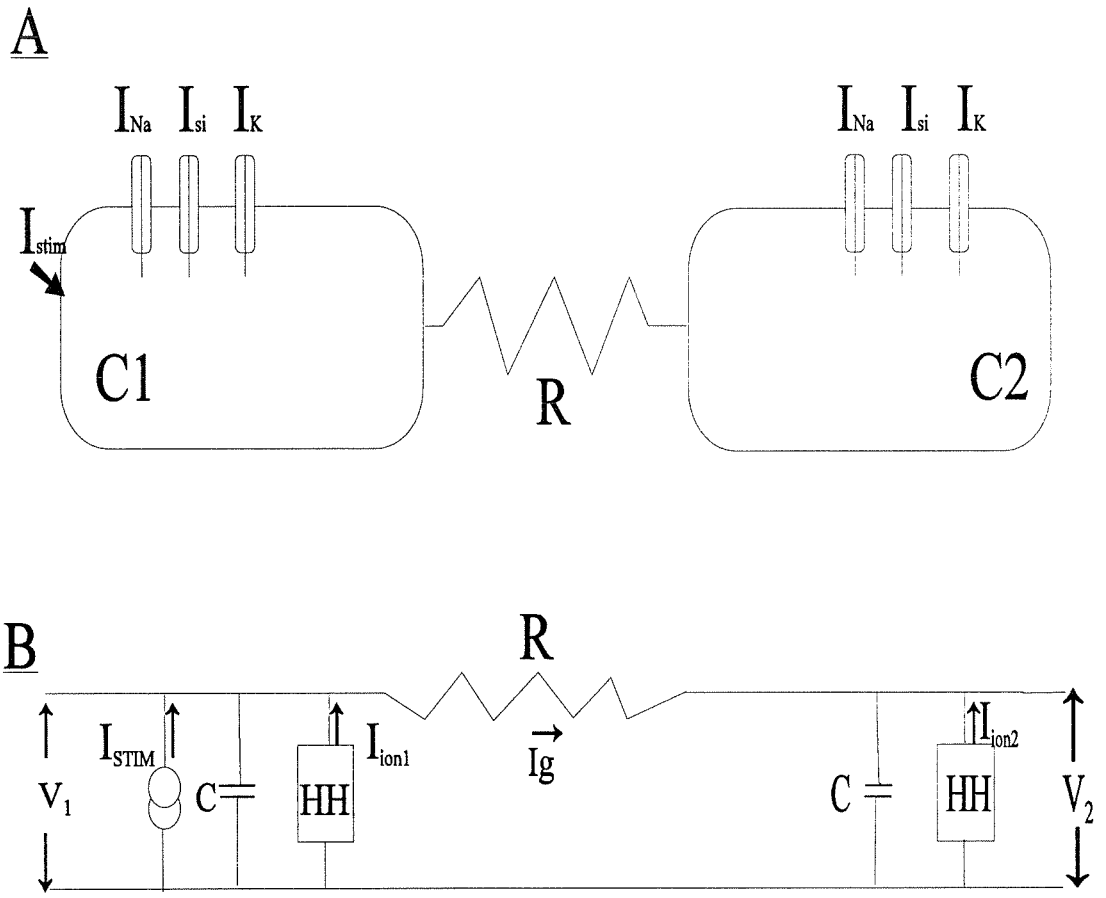

Figure 5.1.1: Diagram of the cell pair and equivalent electrical circuit. HH represents the MBR ionic membrane model.

membrane ionic properties given by the MBR model described in Chapter II. The two cells are interconnected by a fixed gap junction resistance (R). Considering that stimulation is applied only to the first cell of the pair (C1) and that each cell has a spatially uniform potential, the evolution of the membrane potential is described by the following set of equations:

$$C\frac{dV_1}{dt} = -I_{ion1} + I_{stim} - Ig \tag{5.1}$$

$$C\frac{dV_2}{dt} = -I_{ion2} + Ig \tag{5.2}$$

where $C = 1\mu F/cm^2$ is the membrane capacitance, V_1 or V_2 is the membrane potential in mV, t is the time in ms, I_{ion1} or I_{ion2} is the ionic current density in $\mu A/cm^2$, I_{stim} is the stimulation current density, and Ig is the gap junction current density expressed as:

$$Ig = \frac{(V_1 - V_2)}{R\ A} \tag{5.3}$$

where $A = 4.19 \times 10^{-5}$ cm^2 is cell membrane area, and R is the gap junction resistance. In addition to Eqs. 5.1 to 5.3, the description of the system involves equations for the five gating variables (m, h, d, f, x) and changes in the intracellular calcium concentration $[Ca]_{in}$ of each cell.

5.2 Numerical Method

The system was solved numerically with a fixed time step δt of 1μs. Using such a small time step, Eqs. 5.1 and 5.2 were discretized beyond the end of I_{stim} as:

$$V_1(t+\delta t) = V_1(t) - (I_{ion1}(t) + Ig(t)) \times \frac{\delta t}{C}$$

$$V_2(t+\delta t) = V_2(t) - (I_{ion2}(t) - Ig(t)) \times \frac{\delta t}{C}$$

The ionic currents I_{ion1} and I_{ion2} were calculated by the hybrid method of Victorri et al. (1985).

5.3 Protocols and Simulations

A rectangular pulse stimulus of 1 ms in duration was used throughout. First the threshold current was estimated for C1 at rest while R was varied from 0 to 600 MΩ. The cell response was considered active when there was a surge of inward ionic current exceeding 0.55 μA/cm^2 for more than 0.01 ms. The threshold current was estimated with a precision of 0.0001 μA/cm^2. The state of C2 was determined by measuring its membrane potential (V_2') just prior to the firing of C1.

The entrainment response of the system was investigated for different R values and

BCL variations between 100 to 2000 ms. For each R, I_{stim} was fixed at 1.25 times the resting threshold current of cell C1 of the two-cell system (I_{thRC1}). The choice of T_{stim} (1ms) is in agreement with the observation that the axial current triggering cell to cell propagation in a discontinuous cable model of a cardiac strand is of the order of a few milliseconds when the gap junction resistance ranges from 1 to 5 MΩ. When an active response occurs in C1 or C2, the cycle length is divided into three parts: latency, action potential duration (APD), and diastolic interval (DIA). The latency is the time elapsed from the stimulus onset to the instant at which dV/dt of the upstroke reaches its maximum, while APD and DIA are as defined in Chapter II. In all cases of regular pacing, the stimulus strength is large enough to keep the latency of C1 at a small value which is incorporated into APD_1 by measuring from the stimulus onset.

Following a given stimulus, the maximum membrane current (I_P), maximum membrane potential (V_{max}), minimum diastolic potential (V_{min}), latency, APD and DIA were collected for both cells. A sequence of responses was considered stable if each of these quantities did not differ by more than 10^{-3} for 10 successive repetitions of the sequence. Otherwise, the sequence was considered aperiodic after 800 stimuli.

5.4 The Effect of R on the Resting Threshold

Fig. 5.4.1 shows the threshold current in C1 (I_{thRC1}) as R is varied between 0.250 and

600 MΩ. The coupling current Ig acts as a stimulus for C2. The state of C2 following the stimulus onset and prior to the firing of C1 is described by measuring its membrane potential (V_2'). The changes in V_2' vs R are plotted in Fig. 5.4.2, together with the resting threshold voltage (V_{thRC1}) corresponding to I_{thRC1} (upper horizontal line). At low resistance, the two cells are well coupled and fire together, such that I_{thRC1} is twice the current needed for a single isolated cell. For R > 520 MΩ, the cells are uncoupled and firing occurs only in the first cell. Then the value of I_{thRC1} converges toward the current needed to stimulate a single isolated cell. In between I_{thRC1} falls exponentially with R.

Fig. 5.4.2 shows that C1 has always the same threshold potential for different R values. This potential (≃-55 mV) is the potential at which m_∞ (V) is increased sharply to activate I_{Na} in the first cell. The fall of I_{thRC1} is paralleled by the fall of V_2'. As R increases, C2 is farther away from its threshold at the end of the stimulation and requires an additional current arising from the activity of C1 to become excited. However, the increased potential in C2 must occur at a rate which is fast enough to prevent the deactivation of I_{Na} by the closure of the h gate (note that $\tau_h \cong 12$ ms at this potential level, Fig. 2.1.1). Since Ig is proportional to 1/R, there is a value of R for which the C2 potential is too low to prevent the deactivation of I_{Na}. From there, C2 remains silent even if C1 has fired.

In order to better understand the behaviour of C1 and C2 when the system is stimulated from the resting state, we examine in Fig. 5.4.3 the time course of the early phase of the action potential triggered in C1 by a just suprathreshold stimulus. There is then a

substantial latency in both C1 and C2 which varies with R. For R = 4 MΩ, Ig has the form of a large brief pulse (1 ms × 31 μA/cm^2) and both cells behave in exactly the same manner, including a latency of about 7 ms before firing. For R = 35 MΩ, C1 exhibits a long latency (28 ms) during which Ig remains quite low (about 1 μA/cm^2); C2 then fires slightly before C1 to give rise to a brief Ig negative spike. For R = 100 MΩ, C1 fires with a short latency (3 ms) and then generates a large Ig increase (about 22 μA/cm^2) which elicits firing in C2 with a latency of about 5 ms. For R = 355 MΩ, C1 fires with a short latency (4 ms) and generates a rather small Ig increase (about 6 μA/cm^2) which triggers C2 after a delay of about 7 ms. For R = 520 MΩ, C1 fires early (latency of about 15 ms) and generates a small Ig increase (about 3.5 μA/cm^2) which is insufficient to trigger an action potential in C2; the loading effect of C2 on C1 brings down the plateau potential of C1. Then the membrane potential of C2 drifts slowly toward more depolarized values during the C1 plateau and thus progressively inactivates I_{Na} and activates I_{si} such that only small local active response is seen in C2 when threshold is reached at a latency about 90 ms. Except for the large latency values which become quite small when a strong stimulus is used, these events occur in a similar manner when C1 is driven at various regular pacing rates.

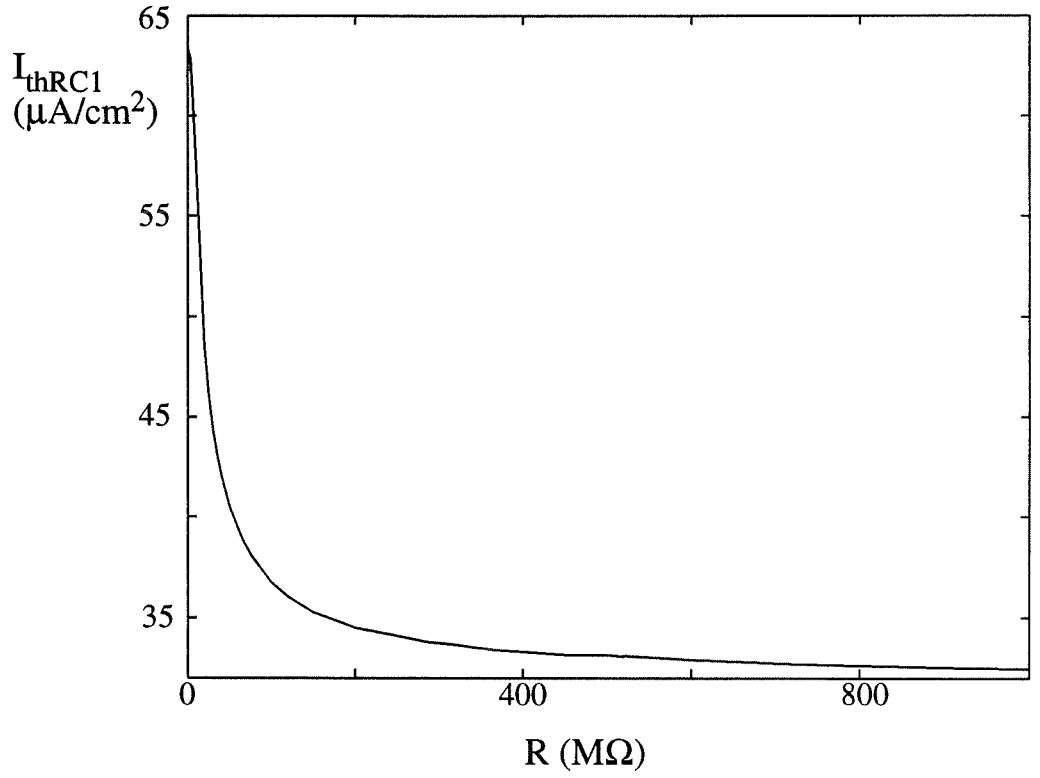

Figure 5.4.1: The threshold current at rest for C1 (I_{thRC1}) as a function of R.

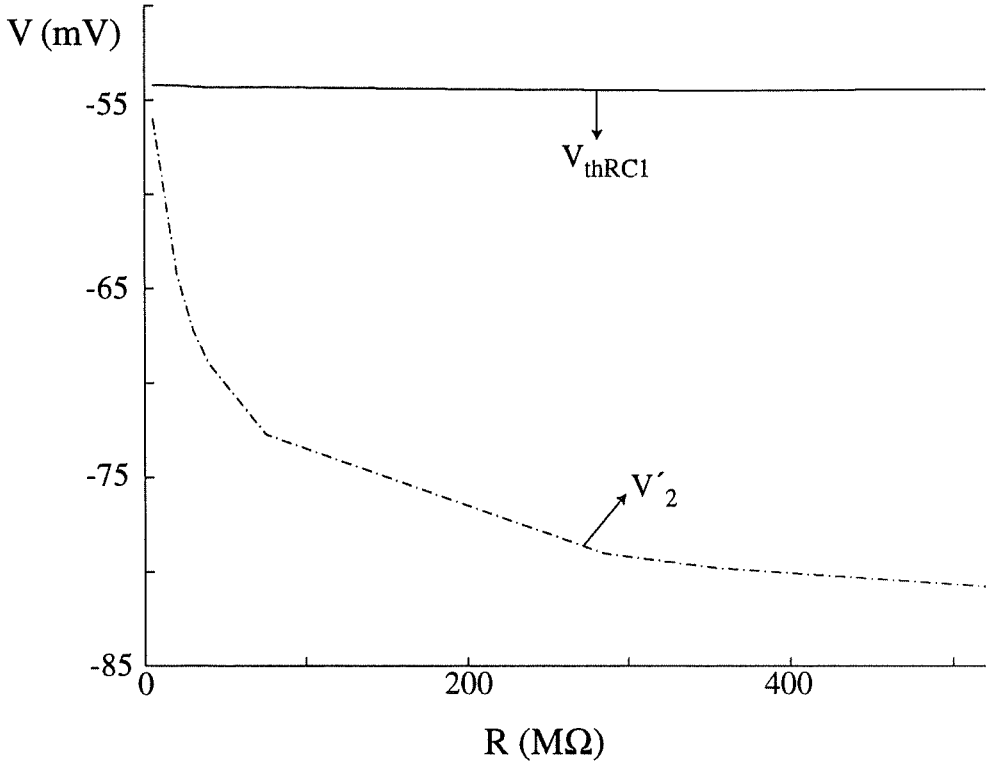

Figure 5.4.2: Threshold voltage at rest (V_{thRC1}) in C1 when coupled to C2, and membrane potential of C2 (V'_2, broken curve) when I_{thRC1} is applied to C1 and R is varied.

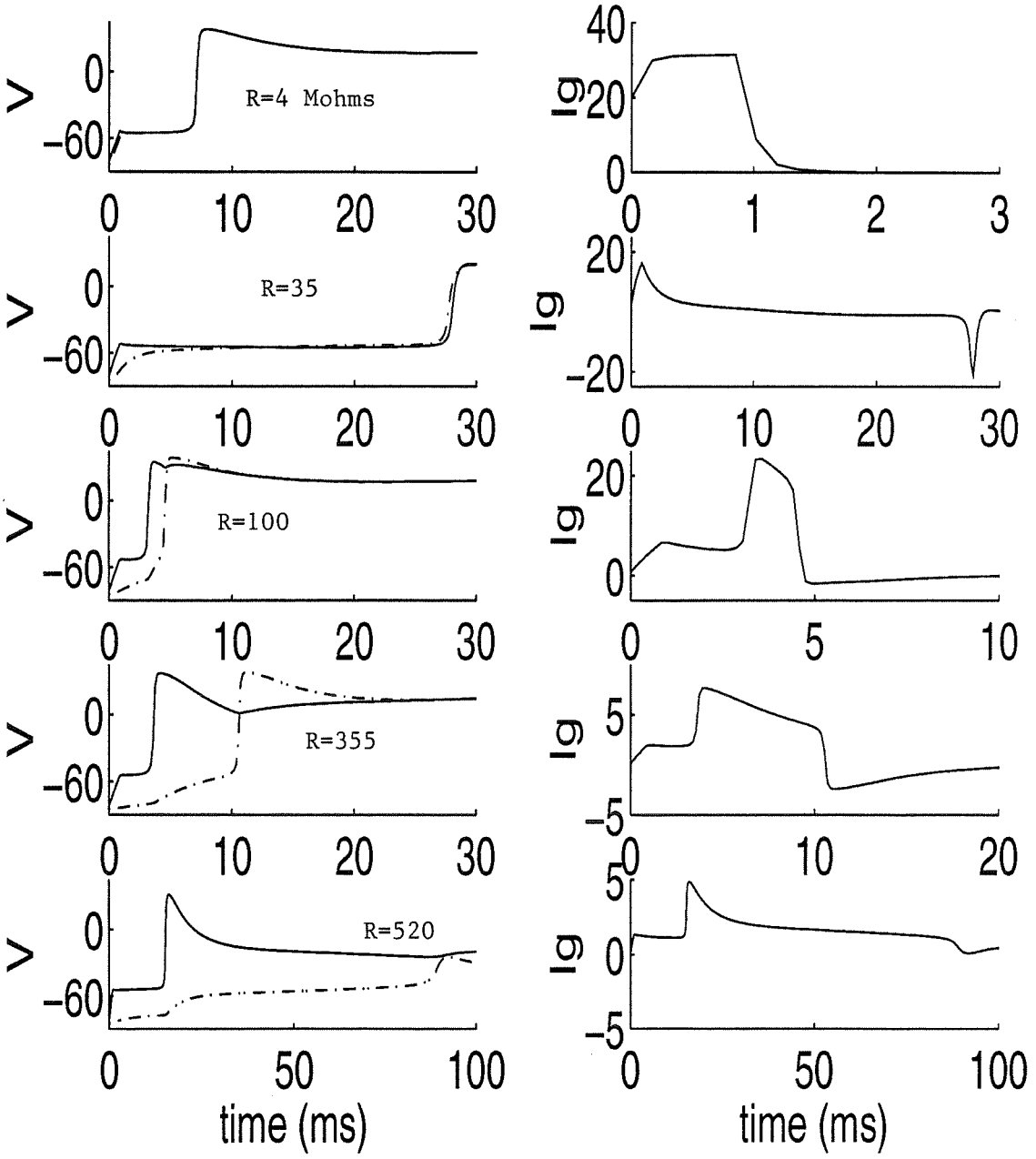

Figure 5.4.3: Membrane potential (V, left column) of C1 (continuous tracing) and C2 (broken tracing) with R = 4, 35, 100, 355 and 520 MΩ (top to bottom). The corresponding coupling current (Ig) prior to and following the action potential upstroke in C1 and C2 is plotted in the right column.

5.5 Active Response in a Pair of Cells

It was seen in Chapter IV that the entrainment response of the space-clamped membrane changed widely as function of T_{stim} and I_{stim}. With a decreasing BCL (stimulation from rest at each BCL value), different bifurcation sequences (period doubling, period adding, or more complex scenarios) were observed for different T_{stim} and I_{stim} combinations. In the light of these results, we can suspect that the entrainment response of C1 may be affected by the loading of C2 through the coupling resistance (R). It can be expected also that the entrainment response of C2 will differ from that of C1 because the efficacy of the driving stimulus (current Ig supplied to C2) will change with R.

Regular pacing was applied to C1 (stimulus of 1 ms × 1.25 I_{thRC1}) in order to drive the cell assembly at BCLs between 100 and 2000 ms. This was done for a choice of coupling resistances between 0.25 and 520 MΩ. Pacing was maintained until stability was detected, or a maximum of 800 stimulations was reached. For each R and BCL values the system was reset at rest at the beginning of pacing. In this section, we compare the maximum ionic currents (Ip_1 , Ip_2) of both cells. For R < 35 MΩ, the active response (firing of an upstroke) of both cells are identical at all BCLs and Ip_1 and Ip_2 are barely distinguishable. The bifurcation sequence, with period doubling and I.D. or chaos, is similar to that obtained with a single cell when similar pacing parameters are used (Fig. 4.2.1.1). A typical result is shown in Fig. 5.5.1 for R = 25 MΩ.

R = 25 MΩ

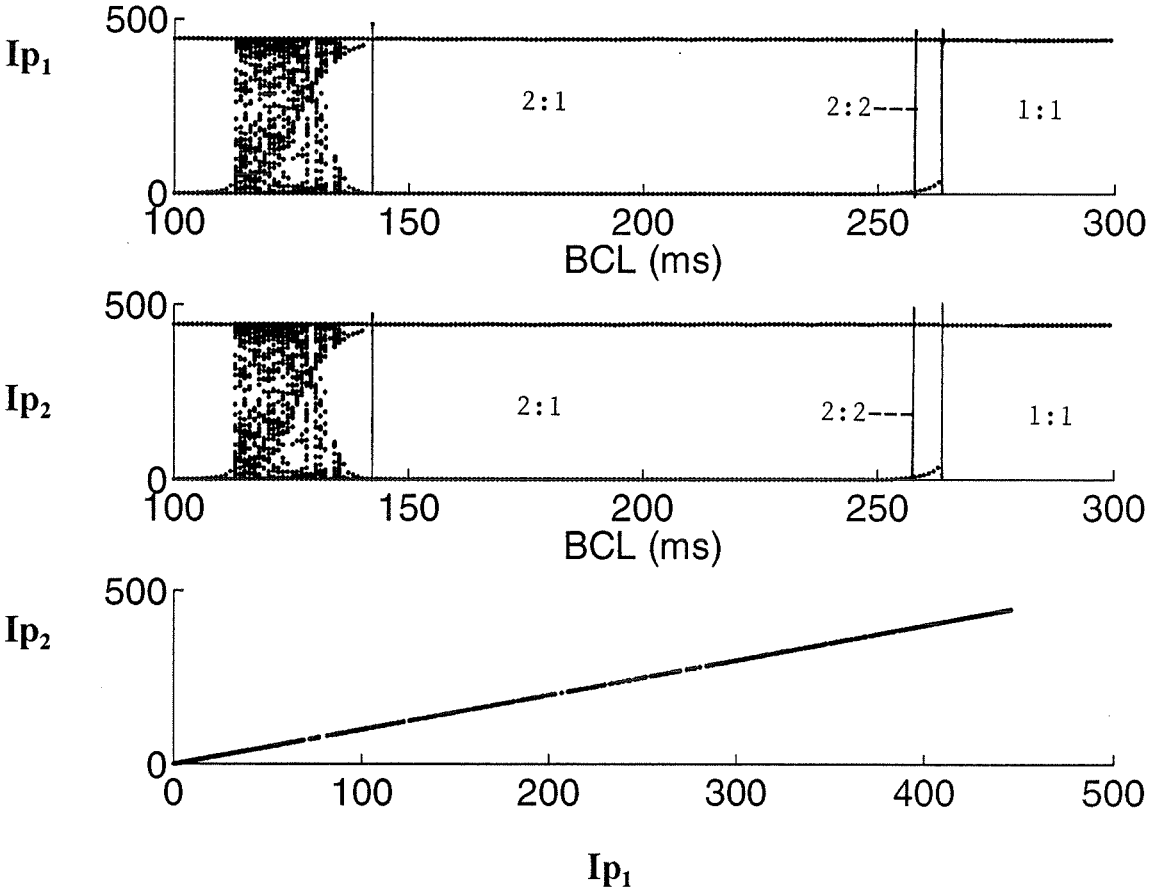

Figure 5.5.1: Bifurcation sequence from the amplitude of Ip_1 and Ip_2 with decreasing BCL values and stimulation from rest at each BCL. Rhythm sequence is 1:1→2:2 →2:1 →I.D. (Irregular Dynamics) for each cell. Bottom panel shows Ip_2 vs Ip_1. Ip_1 and Ip_2 are in $\mu A/cm^2$.

R = 50 MΩ

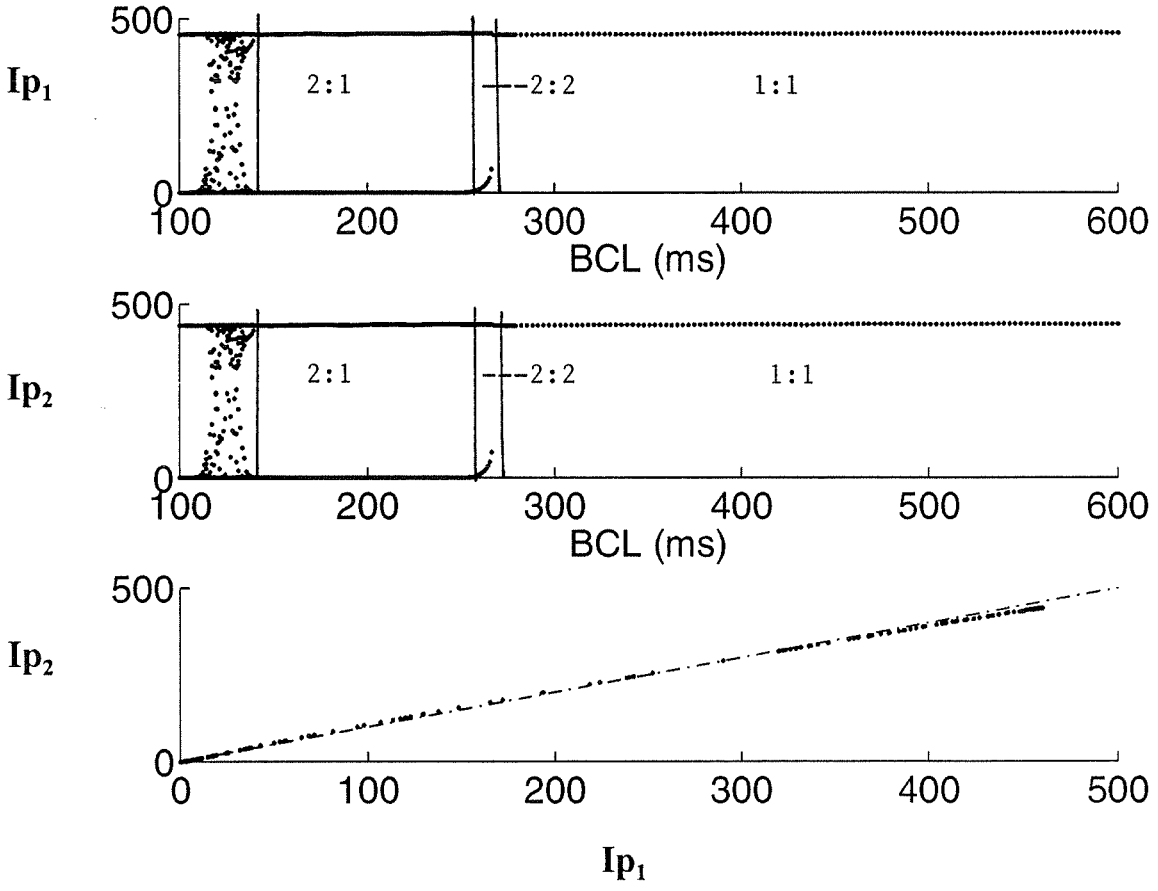

Figure 5.5.2: Bifurcation sequence from the amplitude of Ip_1 and Ip_2 with decreasing BCL values and stimulation from rest at each BCL. Rhythm sequence is 1:1→2:2 →2:1 →I.D. (Irregular Dynamics) for each cell. Bottom panel shows Ip_2 vs Ip_1. Note in bottom panel that the Ip_2 vs Ip_1 curve deviates slightly from the identity line (dash-dot line).

R = 250 MΩ

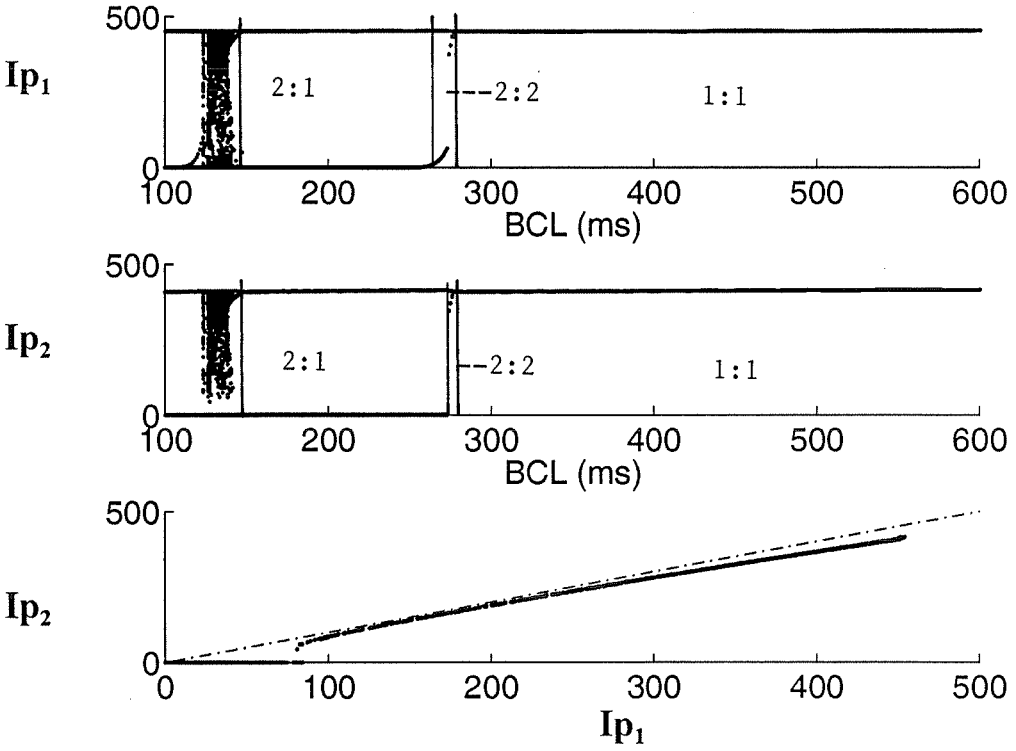

Figure 5.5.3: Bifurcation sequence from the amplitude of Ip_1 and Ip_2 with decreasing BCL values and stimulation from rest at each BCL. Rhythm sequence is 1:1→2:2 →2:1 →I.D. (Irregular Dynamics) for each cell. Bottom panel shows Ip_2 vs Ip_1. Ip_1 and Ip_2 are in $\mu A/cm^2$. Note in bottom panel that the Ip_2 vs Ip_1 curve deviates from the identity line (dash-dot line).

The same bifurcation sequence with identical active response in the two cells is observed until R = 170 MΩ. However, as shown in Fig. 5.5.2 for R = 50 MΩ, the Ip_2 vs Ip_1 relationship deviates slightly from the identity line ($Ip_2 = Ip_1$).

For R > 170 MΩ, Ip_2 is everywhere smaller that Ip_1, and the active responses with a low Ip_1 begin to yield passive responses in C2. This is illustrated in Fig. 5.5.3 for R =250 MΩ. As seen in the lower panel, active responses in the first cell with $Ip_1 < 90$ $\mu A/cm^2$ cannot trigger active responses in the second cell. The bifurcation sequence is still period doubling and chaos. As R is increased further, the minimum Ip_1 required to get an active response in C2 continues to increase such that the range of Ip_2 corresponding to active C2 responses gradually decreases.

For R > 355 MΩ, the response of C1 and the bifurcation sequence also begin to be affected. All period doubling bifurcations (see Fig. 5.5.4 for R = 385 MΩ), beyond period 2 (e.g. 4, 6, etc) disappears and the bifurcation sequence becomes period adding. The number of C2 responses with low Ip_1 is much reduced. The value of Ip_1 as a function of BCL also decreases. As a result, C2 can only respond actively to the highest Ip_1 in each entrainment zone and only displays n:1 rhythms.

At a still higher R value, as with R = 519 MΩ in Fig. 5.5.5, the picture is completely different. The second cell remains silent with no active response for all BCLs below 1140

R = 385 MΩ

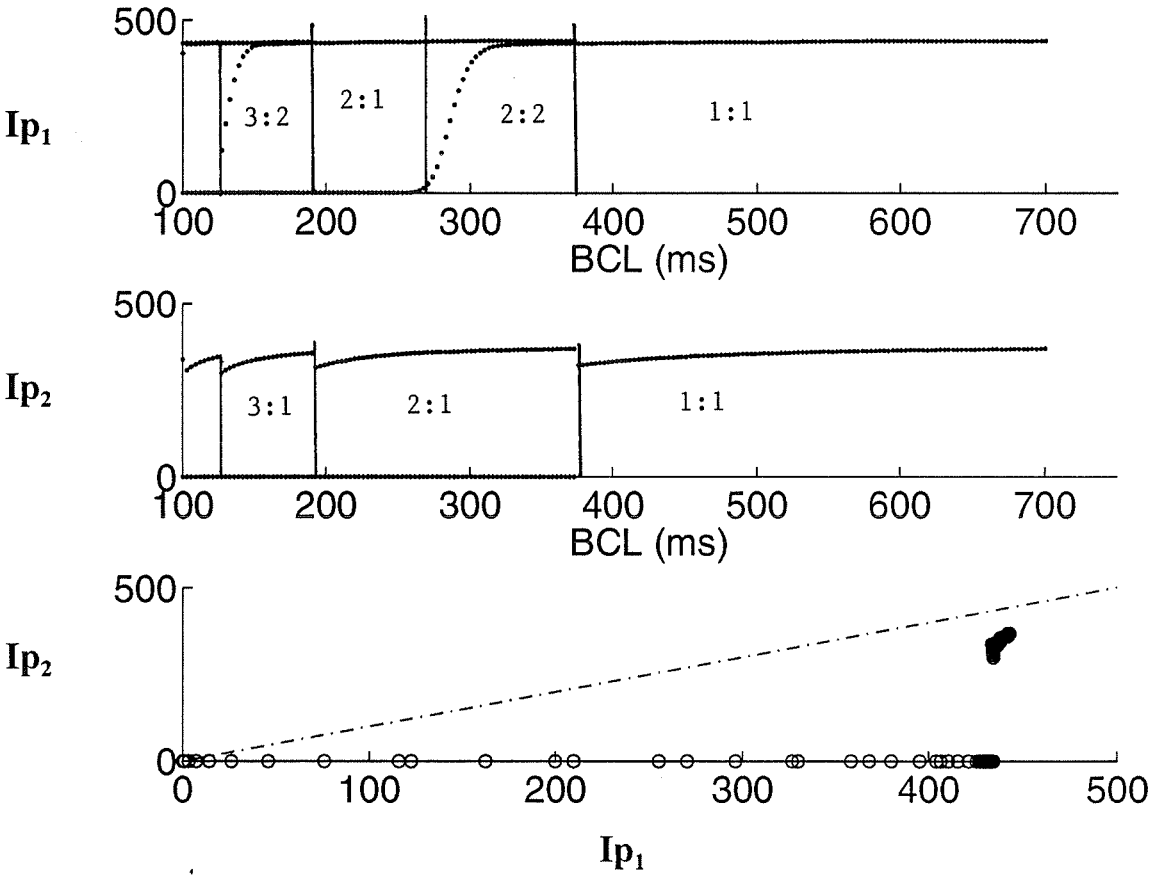

Figure 5.5.4: Bifurcation sequence from the amplitude of Ip_1 and Ip_2 with decreasing BCL values and stimulation from rest at each BCL. Rhythm sequences are indicated for each cell. Bottom panel shows Ip_2 vs Ip_1. Ip_1 and Ip_2 are in $\mu A/cm^2$. Note in bottom panel that the Ip_2 vs Ip_1 curve is far from the identity line (dash-dot line).

R = 519 MΩ

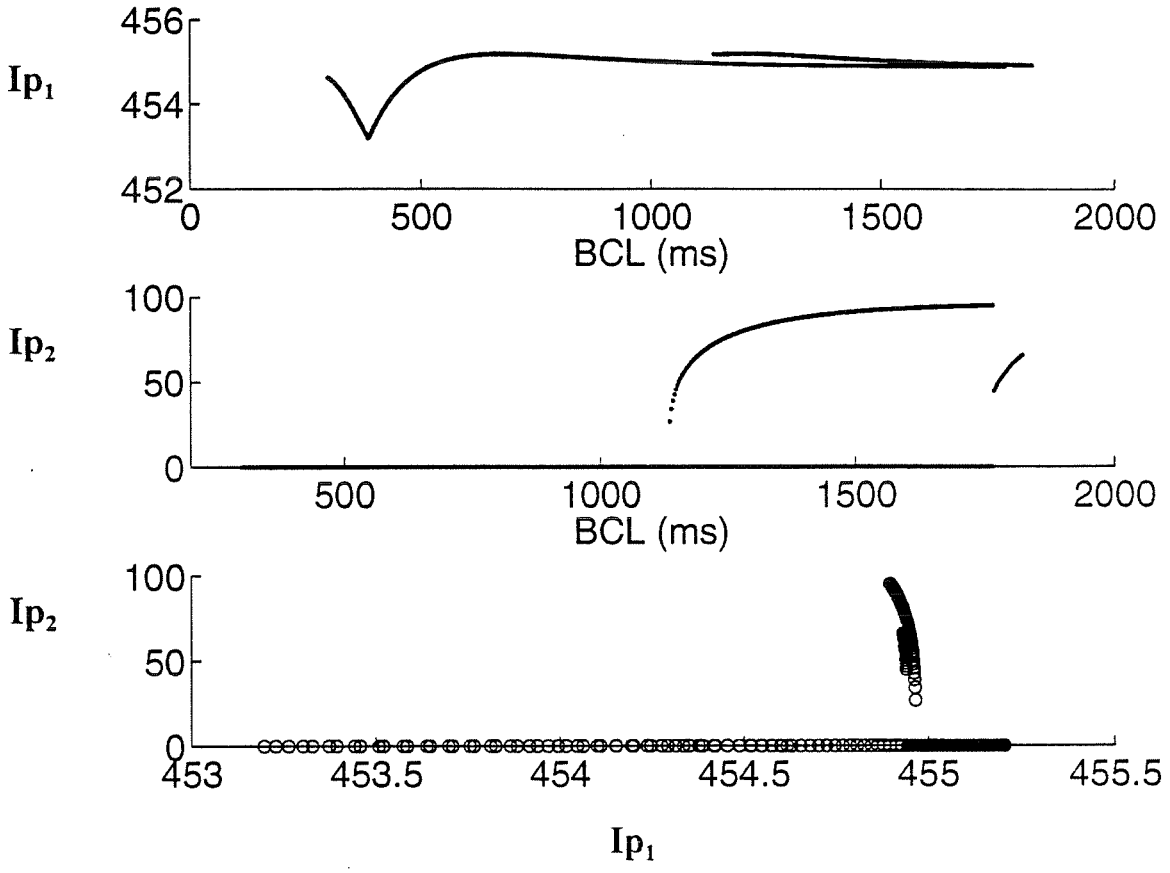

Figure 5.5.5: Bifurcation sequence from the amplitude of Ip_1 and Ip_2 with decreasing BCL values and stimulation from rest at each BCL. Rhythm sequences are indicated for each cell. Bottom panel shows Ip_2 vs Ip_1. Ip_1 and Ip_2 are in $\mu A/cm^2$.

ms. Once C2 becomes silent after an interval of 2:1 responses, C1 returns to period 1 and this rhythm can be maintained for BCLs as low as 100 ms (top panel in Fig. 5.5.5). The Ip_2 vs Ip_1 relationship is also changed since some large Ip_1 values occurring in the final 1:1 range do not induce active responses in C2 (see lower panel, Fig. 5.5.5). The change of Ip_1 with BCLs in the low 1:1 zone also becomes non-monotonic. To understand the dynamics, we must also study the influence of R on repolarization. This is done by studying, in the next section, the APD(DIA) relationship of both cells.

5.6 Effect of R on the Restitution Curves

The DIA and APD values were collected for all the entrainment patterns studied in the preceding section. As indicated previously (Chapter III), APD_i is the duration of the action potential following the application of the i_{th} stimulus while DIA_{i+1} is the time from V_{-50} to the onset of the $(i+1)_{th}$ stimulus. When the i_{th} stimulus did not elicit an active response and V did not cross the -50 mV level, DIA_{i+1} was calculated as $BCL+DIA_i$. If the i_{th} stimulus raised the potential above -50 mV without eliciting an action potential, DIA_{i+1} was set at the time elapsed between V_{-50} and the next stimulus. Thus the effect of resetting due to the subthreshold stimulus was not calculated if the membrane did not depolarized above -50 mV, such that DIA was slightly over estimated in these cases. When a stimulus was applied before repolarization had reached V_{-50}, the APD of the preceding response was not calculated and the response was discarded.

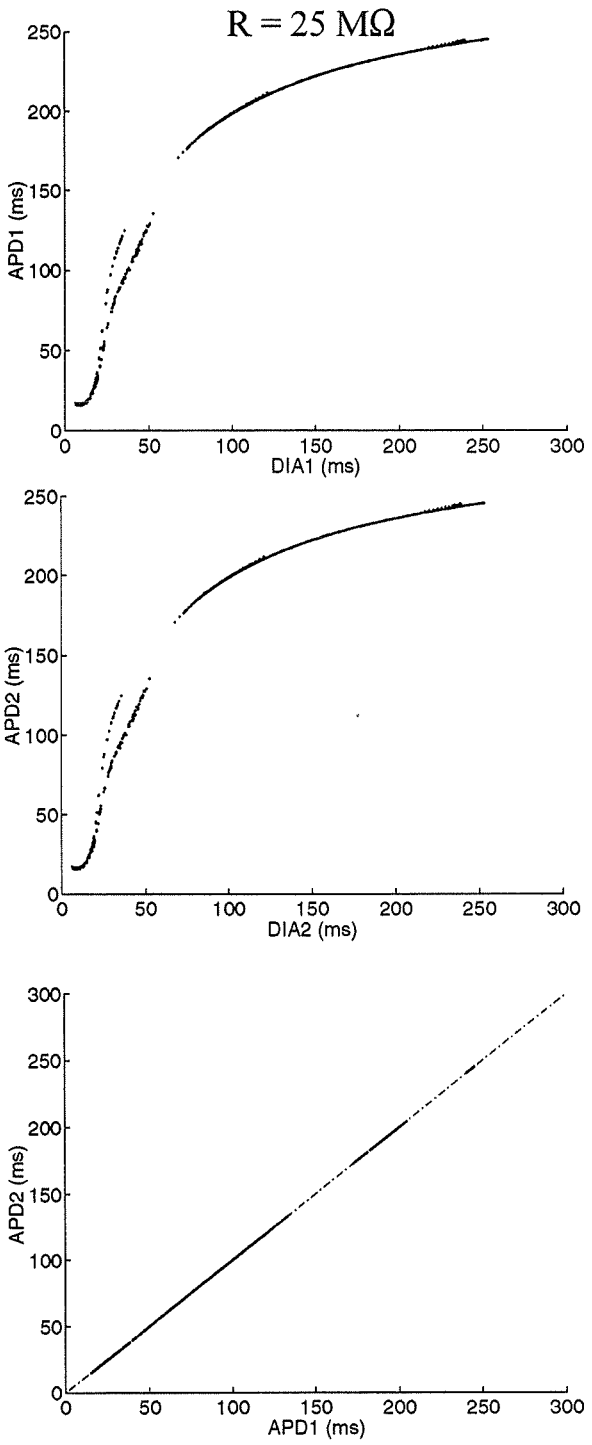

Figure 5.6.1: APD(DIA) of C1 (upper panel) and C2 (middle panel). APD_1 vs APD_2 in the bottom panel.

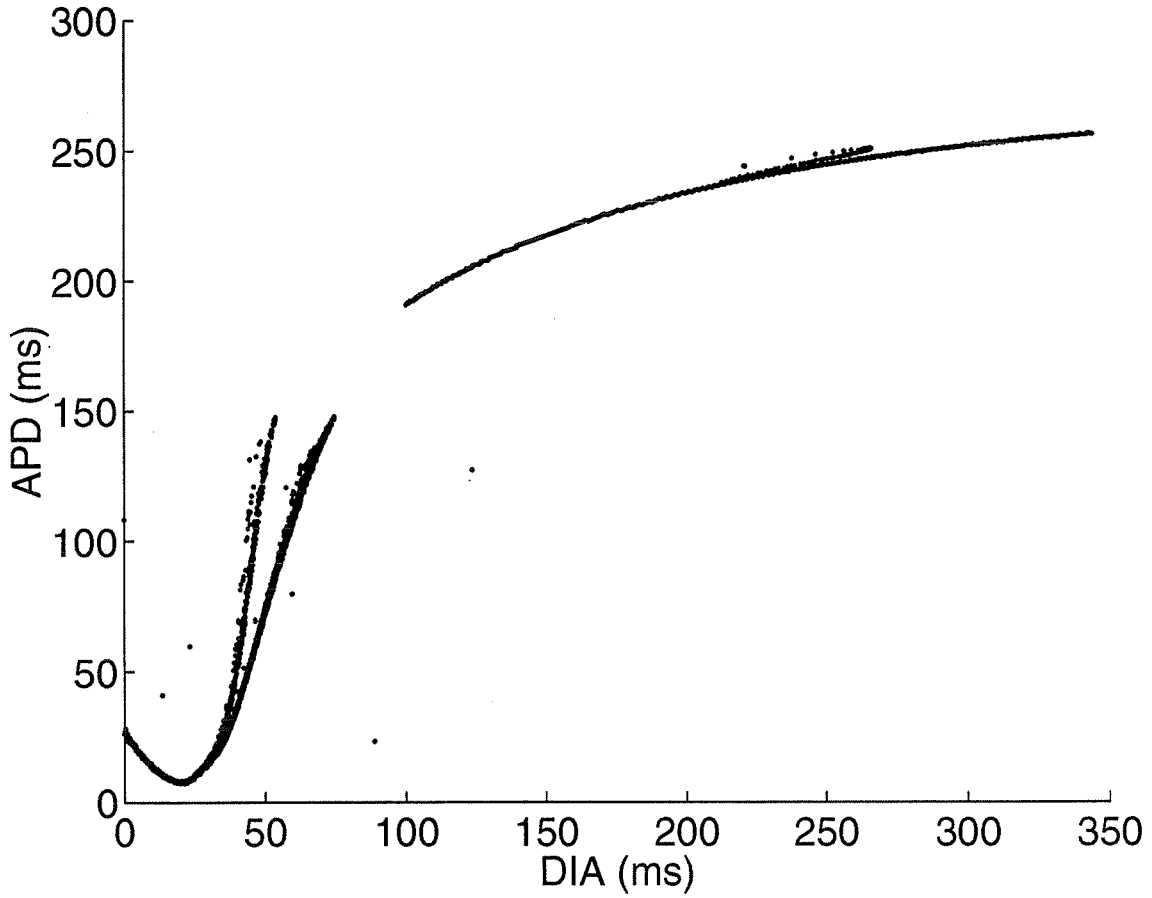

Figure 5.6.2: APD(DIA) scatter diagram for an isolated cell. Stimulus of 1 ms in duration and 1.25 I_{thr} in amplitude with a BCL range of 600 to 100 ms.

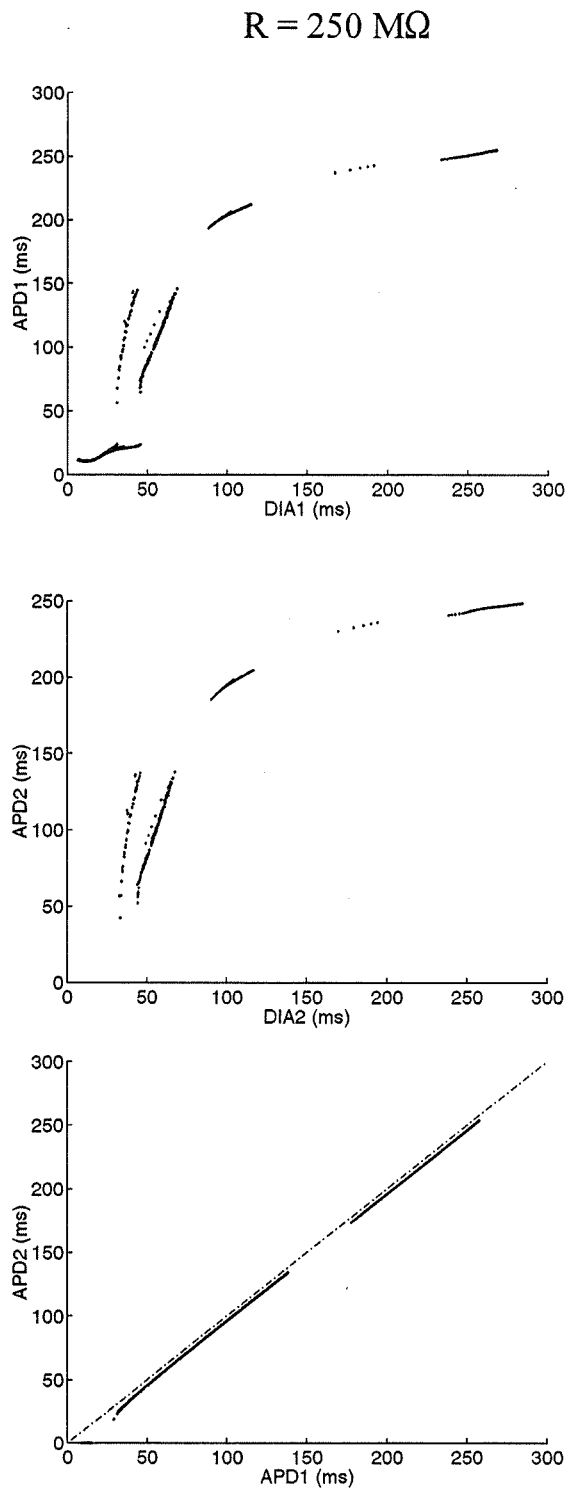

Figure 5.6.3: APD(DIA) of C1 (upper panel) and C2 (middle panel). APD_1 vs APD_2 in the bottom panel, the dash-dot line in bottom panel is the identity line $APD_1 = APD_2$.

For each R value, results from entrainment at all BCLs were pooled for each cell and the APD values were plotted as a function of their preceding DIA to obtain $APD_1(DIA_1)$ and $APD_2(DIA_2)$. Overall, the effects of changing R on the APD(DIA) relationship of the stable responses are similar to those on I_p. For $R < 35$ MΩ, both cells have identical APD(DIA) curves. For $35 < R < 355$ MΩ, $APD_1(DIA_1)$ and $APD_2(DIA_2)$ have a similar form, but the APD_2 values are lower. For $R > 355$ MΩ, there are major transformations in the form and amplitude of APD(DIA) curves of both cells.

Fig. 5.6.1 shows $APD_1(DIA_1)$ and $APD_2(DIA_2)$ for R = 25 MΩ. The two scatter diagrams are identical and similar to those obtained from the space-clamped model stimulated with T_{stim}= 1 ms and I_{stim}= 40 μA/cm^2 over the same 100 to 600 ms BCL range (Fig. 5.6.2). The general form is also similar to that obtained by premature stimulation of the space-clamped model using a short stimulus duration (Fig. 3.3.1.1), which was suitable to explain the period doubling and I.D. bifurcation associated with a BCL decrease (Chapter IV).

However, the APD(DIA) of frequency entrainment shows, two separate branches for DIA between 30 and 60 ms, and a lesser separation for DIA around 250 ms. For DIA > 90 ms, the lower thick branch of Fig. 5.6.2 corresponds to 1:1 responses, while the upper branch (which emerges between DIA = 200-250 ms) comes from other rhythms. For DIA between 30 and 70 ms, APDs from the BCL region with irregular dynamics are distributed over the

two well defined branches, while APDs from regions with periodic activity are concentrated around the lower branch. This dual-branch structure of APD(DIA) is a consequence of the memory effect whereby an APD is not strictly a function of the preceding DIA, but depends also on the past pacing history of the system (Vinet & Roberge, 1994). In Chapter III, APD(DIA) obtained from different conditioning action potentials have been used to study the memory effect. For short T_{stim}, only a slight memory effect was seen because the choice of conditioning action potentials was restricted to BCLs giving 1:1 responses.

For R = 250 MΩ (Fig. 5.6.3), the APD_1 and APD_2 scatter diagrams are similar, except for the loss of active C2 responses for $DIA_2 \leq 25$ ms. This was also seen in the analysis of Ip_2 in the preceding section. The loss of an active C2 response shortens the APD_1 and introduces a discontinuity in $APD_1(DIA_1)$. All APD_1 values corresponding to an absence of C2 response are very short and are located on the small isolated flat lower segment at low DIA. For all other DIA values, APD_2 is generally a few milliseconds shorter than the corresponding APD_1, as shown by the position of the APD_2 vs APD_1 curve slightly below the identity line in the bottom panel of Fig. 5.6.3.

For R > 355 MΩ, we recall (see Fig. 5.5.4) that only n:1 responses with high Ip_2 exist in C2, while n:1 and n:2 responses occur in C1. This situation is reflected in the APD vs DIA diagrams since $APD_2(DIA_2)$ exists only at large DIA (> 150 ms) and has a slope less than 1 everywhere (Fig. 5.6.4). $APD_1(DIA_1)$ shows a discontinuity around DIA = 140 ms where C2 fails to respond. The discontinuity was already present at R = 250 MΩ (Fig. 5.6.3)

and is shifted to higher DIA values as R is increased. This result is caused by the abrupt shortening of the action potential of C1 when C2 fails to respond. Note that APD_1 values at DIA > 140 ms are not appreciably affected by R variations (Figs 5.6.1 to 5.6.4), whereas APD_2 values are shorter than corresponding APD_1 values (bottom panel Fig. 5.6.4) due to the latency of the response of C2. In Fig. 5.4.3, during this latency, current is pumped from the first cell, which is active, to the second cell which is still passive. Soon after the second cell reached threshold, the two cells have the same potential and repolarize together.

Fig. 5.6.5 shows the APD(DIA) relationships for R = 519 MΩ. At this high resistance, C2 has 1:1 responses only for BCL > 1800 ms and 2:1 responses for a minimum BCL of 1140 ms, as shown in Fig. 5.5.5. In the same BCL interval, C1 has 1:1 responses followed by 2:2 responses, and then returns to 1:1 rhythm. The small segment of $APD_2(DIA_2)$ corresponds to 1:1 responses, and the longer one to 2:1 responses (Fig. 5.6.5). It should be noted that the DIA_2 values of the 2:1 segment are over estimated since they are not corrected for the resetting effect of blocked responses. The upper small segment of $APD_1(DIA_1)$ corresponds to 1:1 responses at high BCL, the pair of well separated segments at DIA_1 > 800 ms to 2:2 responses, and the leftmost lower segment to 1:1 responses at low BCL. The two higher segments of $APD_1(DIA_1)$ are both slowly decreasing with increasing DIA_1. This feature was not seen in the other cases and is a consequence of the latency associated with the firing of C2 which prolongs APD_1. The closer the state of C2 is to the value of DIA_2 at which it will not fire, the longer is its latency and the greater is the prolongation of APD_1.

The change of R from 0.25 to 355 MΩ produced a continuous transformation of the APD(DIA) scatter diagrams of both cells. As the value of R is changed, so are the coordinates DIA_c and APD_c defining the point where the slope of APD(DIA) = 1. DIA_{c1} and APD_{c1} were estimated by using a double exponential fit on the upper portion of the $APD_1(DIA_1)$ curves. Thus, only the n:1, 1:1, and the 2:2 regions were considered for the fit. Results are given in table 5.6.1 for a set of R values between 25 and 320 MΩ. DIA_{c1} is shifted toward higher values as R is increased, APD_{c1} is not changed appreciably, and BCL_T is increased (where BCL_T is the cycle length at which the 1:1 rhythm ceases). This phenomenon is opposite to that observed in a single cell when I_{stim} is increased for the same T_{stim}. For instance, in the case of T_{stim} = 25 ms, as I_{stim} was increased from 1.1 to 1.25 I_{thR}, the border of the 1:1 and 2:2 zones shifted to a lower BCL (Fig. 4.2.2.3).

Increasing R has another important influence on APD_1 and APD_2. DIA_{min2}, the minimum DIA_2 over which C2 has active responses, increases and the portion of $APD_2(DIA_2)$ having a slope > 1 shrinks and eventually disappears. Consequently, all C2 responses with an AR different from n:1 become also restricted to short BCLs before disappearing completely. The loss of active responses in C2 for $DIA_2 < DIA_{min2}$ induces a break in $APD_1(DIA_1)$ at DIA_{min1}. Then C1 has a low flat $APD_1(DIA_1)$ which extends from its ARP to DIA_{min1}, and a higher portion for $DIA > DIA_{min1}$. Since DIA_{min1} follows DIA_{min2}, the high slope portion of $APD_1(DIA_1)$ is also reduced as R is increased.

Table 5.6.1: Changes in DIA_{c1}, APD_{c1}, and BCL_T as R is increased.

R (MΩ)	DIA_{c1} (ms)	APD_{c1} (ms)	BCL_T (ms)
25	80	249	339
50	82	257	339
130	87	254	341
250	95	253	348
320	100	252	352

From $R \cong 355$ MΩ, neither APD_1 nor APD_2 has a steep portion with slope higher than 1 (Fig. 5.6.4). DIA_{min2} corresponds to the ARP of C2 and can be used to calculate the BCL where changes of regime occur. Results are given in Table 5.6.2 . Because APD2 is flat and stops at DIA_{min2}, C2 can exhibit only successive n:1 transitions. Since APD_1 consists of two flat portions, one with low APDs for $DIA < DIA_{min1}$, and one with high APDs for $DIA > DIA_{min1}$, it will have higher n:k ($k > 1$) activation ratios.

At high R values, C2 exhibits 1:1 rhythm followed by 2:1 rhythm and ends up with 1:0 responses (Fig. 5.5.5). This is the result of the resetting. DIA_{min2} becomes very large and a response can occur only if $DIA_2 > DIA_{min2}$.

In summary, increasing R prolongs the latency of the response in C2 and augments the DIA_{min2} which makes the activation possible. Hence the prolonged latency has the effect of a long low-amplitude stimulus, and it tends to decrease APD_2 values and to reduce their dispersion. As shown in Chapter IV, a reduced APD dispersion favours a period adding

bifurcation structure. As indicated earlier, the potential of the two cells becomes identical soon after the firing of C2 and both C1 and C2 then repolarize together. As a consequence, the latency of the second cell contributes to increase APD_1. Therefore APD_1 values will tend to remain high and their dispersion will be reduced as long as C2 fires. On the other hand, when C2 is not activated, it drains current during the action potential of C1. Because of this load, APD_1 may be much reduced and C1 may become able to give 1:1 responses at much shorter BCLs than would be the case if it were isolated or tightly coupled to C2.

Table 5.6.2: Changes in DIA_{min2}, DIA_1 and BCL_T as R is increased.

R MΩ	DIA_{min2} (ms)	DIA_1 (ms)	BCL_T (ms)
385	231	159	388
400	237	175	414
450	264	322	587
505	285	721	1009
510	288	822	1108

To illustrate the behaviour of the system as a function of R, we increased R for a given BCL of 500 ms. The C1 response was initially 1:1 with a large APD_1 for $R < 420$ MΩ, changed to 2:2 for $420 < R < 520$ MΩ, and reverted to 1:1 with a short APD_1 for $R > 520$ MΩ (top panel, Fig. 5.6.6). C2 followed the 1:1 rhythm of C1, jumped to 2:1 when C1 was in 2:2 rhythm, and stopped responding for $R > 520$ MΩ (middle panel, Fig. 5.6.6). Changes in APD_1 and APD_2 during 1:1 rhythm for $R < 420$ MΩ are illustrated in the bottom panel of

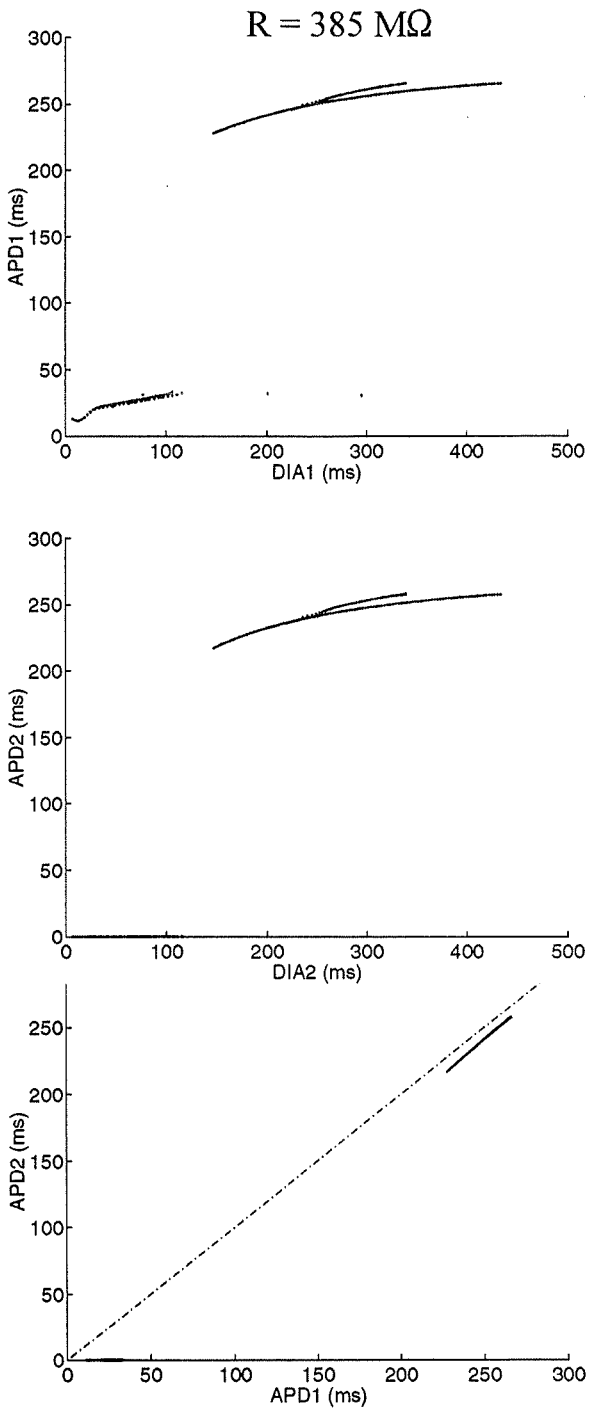

Figure 5.6.4: APD(DIA) of C1 (upper panel) and C2 (middle panel). APD_1 vs APD_2 in the bottom panel, the dash-doted line in bottom panel is the identity line $APD_1 = APD_2$.

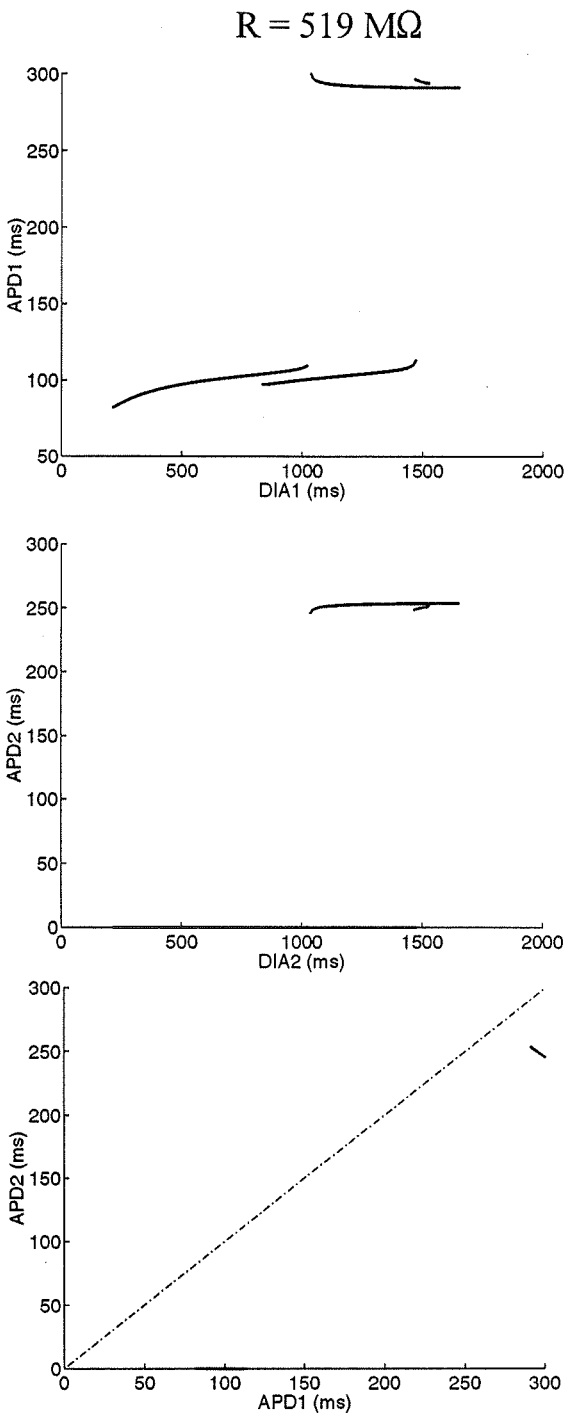

Figure 5.6.5: APD(DIA) of C1 (upper panel) and C2 (middle panel). APD_1 vs APD_2 in the bottom panel, the dash-doted line in bottom panel is the identity line $APD_1 = APD_2$. 1:1 and 2:2 rhythm give rise to APD_1 vs DIA_1 segments, while 1:1 and 2:1 occur in C2.

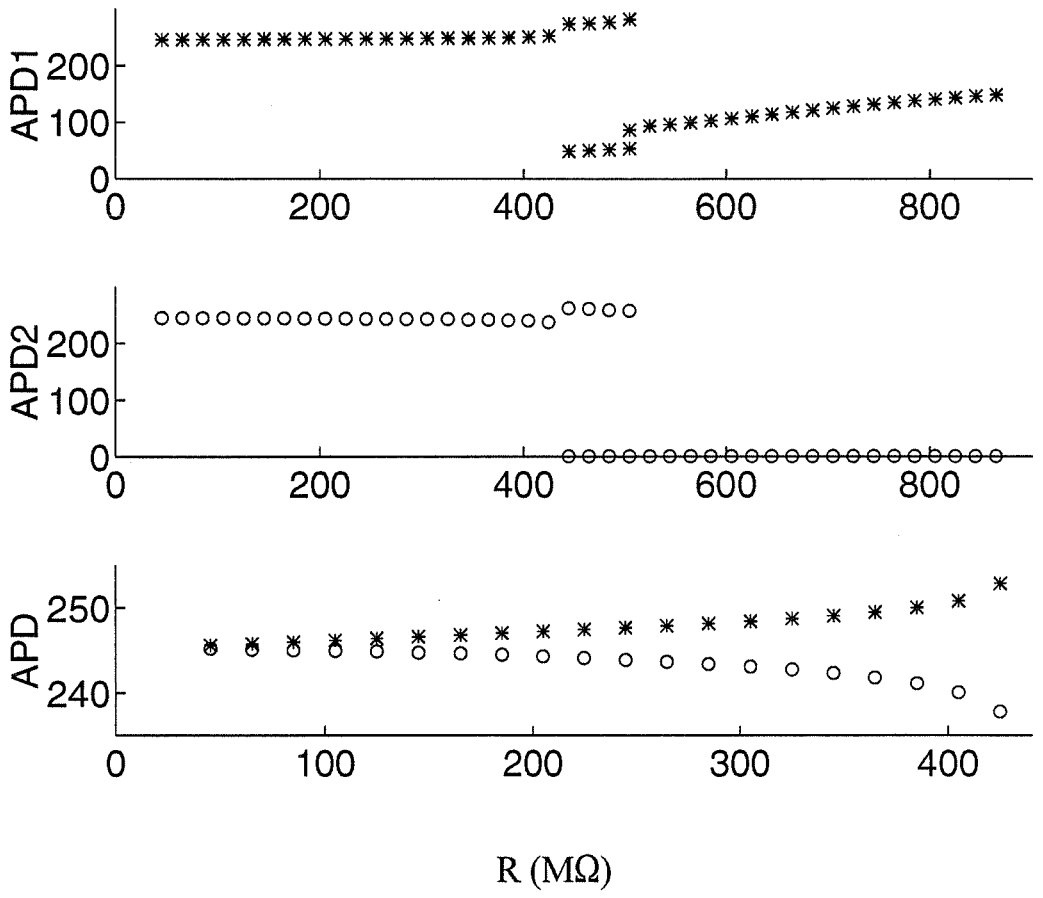

Figure 5.6.6: At BCL = 500 ms, R was increased by steps of 20 MΩ. APD_1 and APD_2 are depicted in the upper and middle panel, respectively. APD_1 and APD_2 are plotted versus R in the bottom panel (* = APD_1, o = APD_2).

Fig. 5.6.6, showing a progressive increase in APD_1 and a progressive decrease in APD_2 as R is increased. With R = 430 MΩ, the separation is largest with APD_1= 254 ms and APD_2 = 237 ms. Once C2 stops firing, at R > 520 MΩ, APD_1 decreases dramatically. At R = 530 MΩ, APD_1 is no more than 95 ms, while it is almost 150 ms at R = 880 MΩ. In this range of very high R values, the effect of C2 on C1 diminishes since the two cells are nearly uncoupled.

5.7 Period Bifurcation Structure

In the two preceding sections, the bifurcation structure of the entrainment response of the pair of cells was studied for a subset of R values, and it was related to the transformation of Ip, DIA and APD. We now present a global picture of the bifurcation structure as a function of R and BCL. Values of R were changed from .025 to 520 MΩ in steps of 10 MΩ. For each R value, the BCL was varied from 100 to 3000 ms in steps of 1 ms, and the system was reset to rest at the beginning of pacing for each BCL. The BCL at which changes in the pattern of entrainment were detected and used to construct the bifurcation map presented in Fig. 5.7.1

At low R, we find the usual sequence, period 1 (1:1 rhythm), period 2 (2:2 and/or 2:1 rhythm), successive period doubling transitions leading to I.D., and then period 3 (3:2 and/or 3:1 rhythm). The most noticeable effect of R is to shift the border of each zone toward a

higher BCL. This can be better appreciated in Fig. 5.7.2 which provides an enlargement at low BCLs. As discussed in the previous section, this result can be explained by the fact that DIA_{c1} (point where the slope of $APD_1(DIA_1) = 1$) is shifted toward higher DIA_1 values (Table 5.6.1). Moreover, the interval over which period doubling and irregular dynamics (I.D.) is observed decreases. This has been discussed in the previous section and has been related to the narrowing of the range of DIAs for which APD_1 and APD_2 have a slope greater than one (compare Figs 5.6.3 and 5.6.1).

At $R > 355$ MΩ , the transitions follow a period adding pattern . An illustration of the change of the bifurcation sequence from period doubling to period adding (around the horizontal broken line in Fig. 5.7.1) is depicted in Fig. 5.7.3. The period doubling and I.D. zones existing between period 2 and period 3 regions disappear completely at $R > 355$ MΩ.

Moreover, as R is increased beyond 360 MΩ, tongues of increasing period number successively appear (Fig. 5.7.3). These zones are the prolongation of the n:1 zones existing below BCL= 100 ms for lower R values. Because of the bending associated with the shift of DIA_{c1}, their borders successively cross the BCL=100 ms line used as the limit of our simulations. For example, the period 4 region is visible from R=362 MΩ. Period adding zones from period 1 to period 8 are shown in Figure 5.7.4. Tongues up to period 13 have been detected, but are not shown because of the small BCL and R intervals over which they exist. They are indicated by a zone of period n in Fig. 5.7.5. However, moving along the vertical line BCL= 100 ms, there is a limit to the progression of the period adding pattern

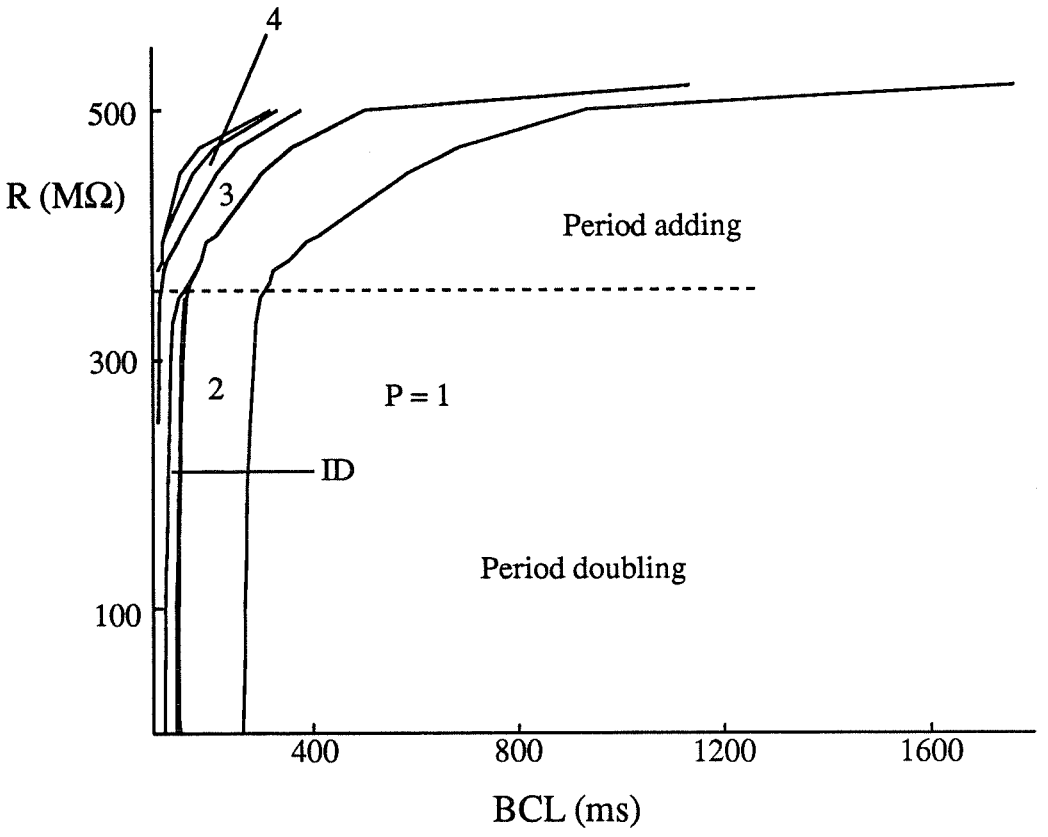

Figure 5.7.1: The bifurcation map of the period (P) of the system (C1 and C2) as a function of the coupling resistance R (25 - 520 MΩ) and BCL (2000 - 100 ms).

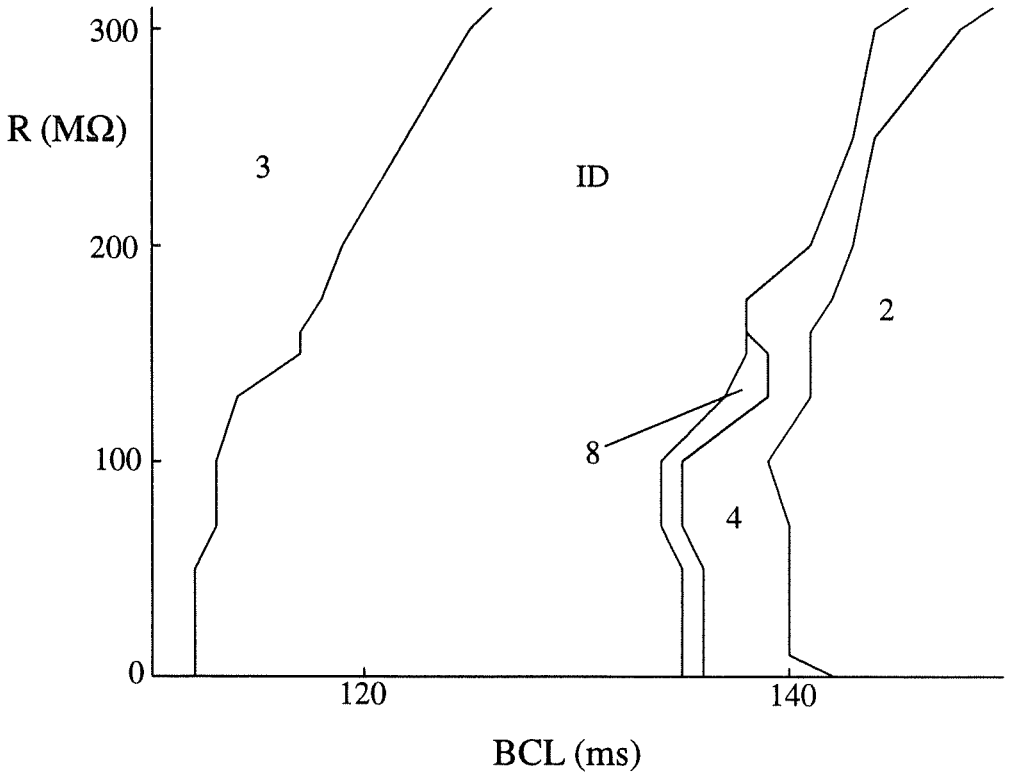

Figure 5.7.2: Enlargement of the bottom left portion of Fig.5.7.1. Period doubling region.

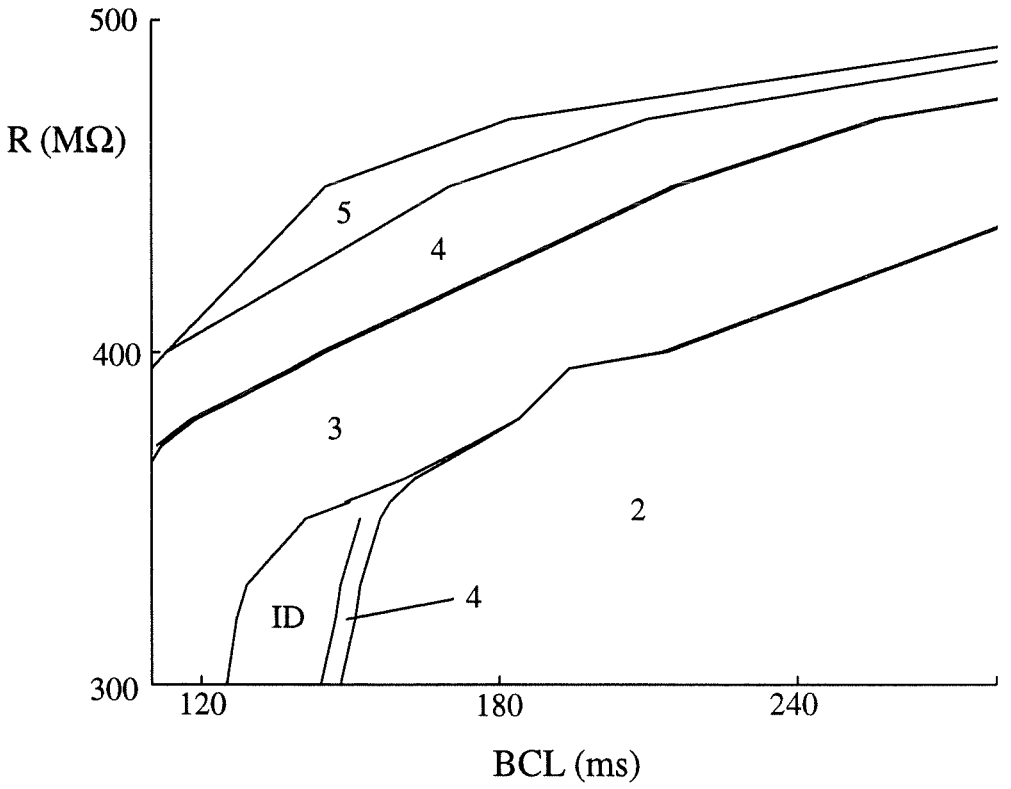

Figure 5.7.3: Same legend as in Fig.5.7.1. Junction between period doubling and period adding regions.

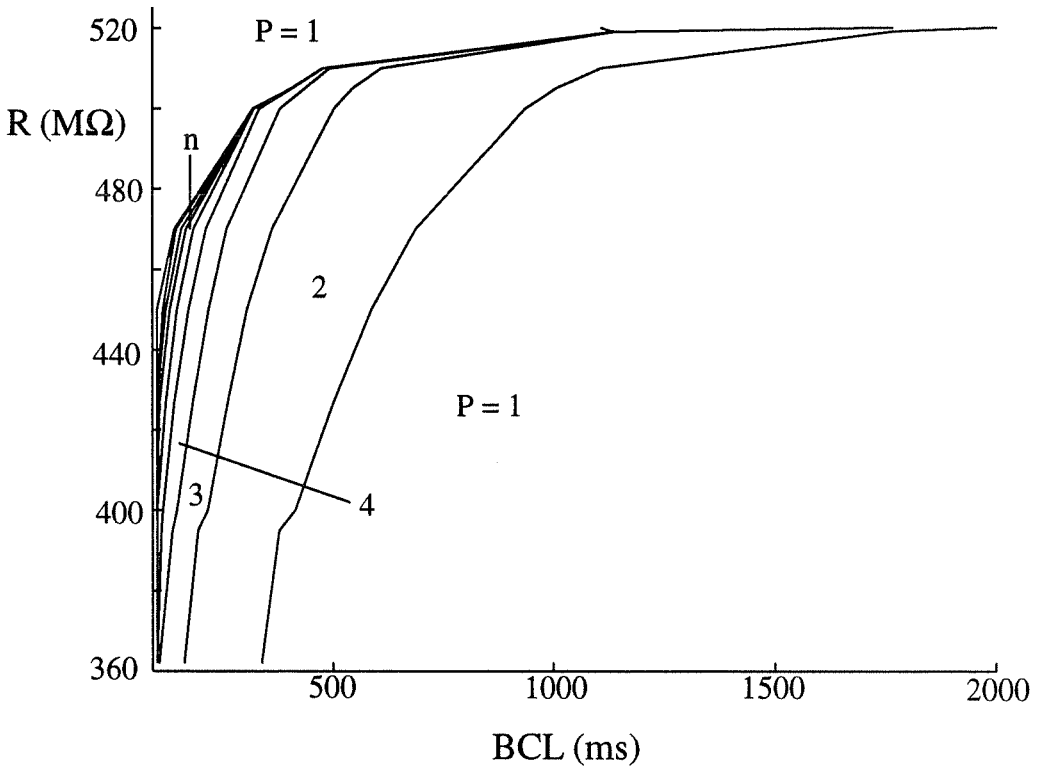

Figure 5.7.4: Same legend as in Fig.5.7.1. Period adding region.

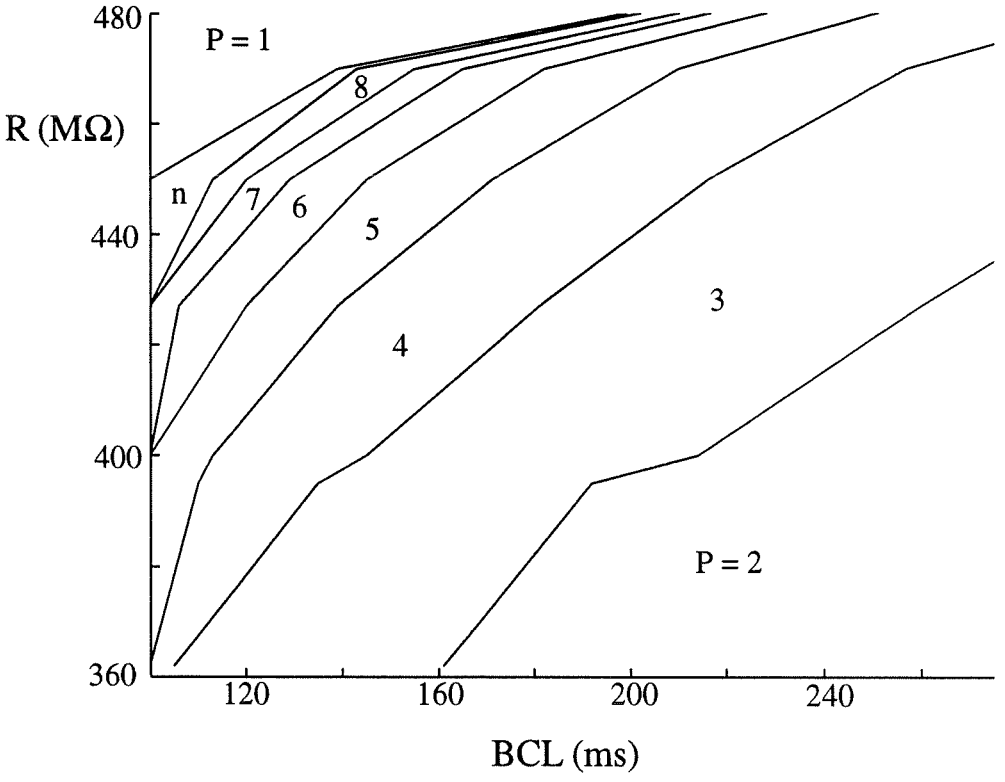

Figure 5.7.5: Same legend as in Fig.5.7.1. Period adding region.

since, for R > 450 MΩ , a new period 1 was detected. As R is increased beyond 500 MΩ , all the periods disappear one after the other, starting from the higher n. The bifurcation cascade has the form 1→2→....→n→1, with n decreasing toward n = 2 which is the only case remaining at R =519 MΩ.

5.8 Activation Ratios

The bifurcation sequences based on I_{p1} and I_{p2} values, as described in Fig. 5.5.1 to 5.5.5, give rise to well defined transitions between successive activation ratios (ARs). The BCLs corresponding to some of these transitions are listed in Table 5.8.1 for a choice of R values. For R< 50 MΩ both C1 and C2 have the same sequence of AR transitions: 1:1→2:2→4:3→4:2→8:6→I.D.→3:2→3:1. As indicated in Table 5.8.1, the 1:1→2:2 transition occurs at a BCL of 262-265 ms, the 2:2→ 2:1 transition at a BCL of 249-251 ms, the 2:1→ 4:3 or 4:2 transition at a BCL of 140-141 ms.

Once R exceeds 50 MΩ, the two cells exhibit different sequences of AR transitions and the sequence of C1 always includes an extra step where the AR is higher than in C2. For example, with R = 70 MΩ and BCL = 253 ms, C1 has a 2:2 and C2 a 2:1 AR. With R = 70 MΩ and BCL = 107 ms, C1 has a 3:2 AR and C2 a 3:1 AR.

At any given transition, there is also a progressive shift of the BCL value toward a

larger BCL as R is increased. This shift is similar in both cells. For instance, the 1:1→2:2 transition in both C1 and C2 is at a BCL of 262 ms for R = 25 MΩ, and it is raised to 265 and 277 ms, respectively, for R= 50 and 250 MΩ (Table 5.8.1); in C1 this transition is shifted further to 330 ms for R = 385 MΩ and to 1763 for R = 519 MΩ. Similarly, the 2:2→2:1 transition in C1 is shifted from a BCL of 249 ms for R = 25 MΩ to 251, 256, and 259, respectively for R= 50, 250 and 385 MΩ (Table 5.8.1).

Increasingly larger R values reduce the size of the 2:2, 4:3, and 3:2 regions in C2. For example, with R = 250 MΩ, the BCL range for the 2:2 region in C1 is 21 ms (between 277 and 256 ms) compared to 4 ms in C2 (between 277 and 273 ms); and with R = 385 MΩ, the 2:2 BCL range is 71 ms in C1 and zero in C2 (Table 5.8.1). In fact, when R is large enough (> 355 MΩ), several transitions are abolished in C2 and the sequence becomes n:1 (i.e, 1:1→ 2:1→ 3:1→ 4:1→etc). Finally, at R values close to complete decoupling (e.g. R = 519 MΩ, Table 5.8.1), the C2 sequence is simplified to 1:1→ 2:1→ 1:0 and that of C1 to 1:1→ 2:2→ 1:1. Increasing R further above 520 MΩ allows C1 to maintain a 1:1 rhythm at very low BCL (Fig. 5.5.5) since the extra load imposed by the passive C2 shortens the APD of C1.

Table 5.8.1: Critical BCLs at the transitions between ARs in C1 and C2 for various R values. Figures correspond to the Ip_1 and Ip_2 bifurcation sequences of Figs 5.5.1 to 5.5.5.

R(MΩ)	Bifurcations in C1		Bifurcations in C2	
	Transitions	BCL (ms)	Transitions	BCL (ms)
25	1:1 - 2:2	262	1:1 - 2:2	262
	2:2 - 2:1	249	2:2 - 2:1	249
	2:1- 4:2	141	2:1- 4:2	141
50	1:1 - 2:2	265	1:1 - 2:2	265
	2:2 - 2:1	251	2:2 - 2:1	251
	2:1- 4:2	140	2:1- 4:2	140
250	1:1 - 2:2	277	1:1 - 2:2	277
	2:2 - 2:1	256	2:2 - 2:1	273
	2:1- 4:2	145	2:1- 4:2	145
385	1:1 - 2:2	330	1:1 - 2:1	330
	2:2 - 2:1	259	2:1-3:1	189
	2:1 - 3:2	189	3:1- 4:3	119
	3:2 - 4:3	119		
519	1:1 - 2:2	1763	1:1 - 2:1	1763
	2:2 - 1:1	1136	2:1 - 1:0	1136

5.9 Summary and Conclusion

In the system of two coupled cells, the two cells interact via the coupling current (Ig). When R is low (e.g., R < 50 MΩ) the threshold of C1 is raised by the loading effect of C2 (Fig. 5.4.1), and the stimulus pulse current applied to C1 generates a substantial depolarization in C2. Both cells can be entrained in a 1:1 mode as long as the BCL exceeds 262 ms (Figs 5.5.1 and 5.5.2) and R remains below about 325 MΩ (Fig. 5.7.1). The APD(DIA) scatter diagrams (Fig. 5.6.1) are then identical for the two cells.

Since the C1 upstroke generates the current which stimulates C2 above threshold, the efficacy of the coupling current (Ig) is reduced as R is increased. There is then an increased delay between the firing of C1 and that of C2 as R becomes larger, and the feedback effect of the action potential of C2 can modify the value of APD_1. An increased APD_1 is expected if the delay is not too long, whereas a shorter APD_1 will occur if the delay is long enough or if the C2 spike is absent. We have not investigated the quantitative aspects of this delay during pacing and it was taken into account through APD variations (Figs 5.6.3 to 5.6.5).

At BCLs shorter than 262 ms, both cells loose their 1:1 rhythm and adopt a period 2 rhythm (Fig. 5.7.1) which may exist over a wide range of R values (see also Table 5.8.1). At R = 250 MΩ, for example, the behaviour begins to be altered appreciably since the C2 upstroke current (I_{p2}) is substantially reduced in comparison with I_{p1} (Fig. 5.5.3, bottom

panel), and many C2 responses are blocked when the C1 rhythm is sufficiently rapid. APD_2 exists only if DIA_2 exceeds a minimum value which increases with R. $APD_1(DIA_1)$ is divided into two disjoint portions, each corresponding to the presence or absence of responses in C2.

These phenomena become more apparent at higher R values as illustrated for R = 385 MΩ in Figs 5.5.4 and 5.6.4, and the sequences of AR transitions in both cells are altered. When R is close to the limit for C2 excitation (R = 520 MΩ), responses occur in C2 only at very slow pacing rates (BCL > 1140 ms, Fig. 5.5.5 and Table 5.8.1) and the behaviour of C1 is much simplified. However, even in the absence of a C2 response, the small Ig continues to affect the excitability of C1 and the 1:1 response can be maintained for BCLs as low as 100 ms (Fig. 5.5.5., panel 1). This is quite different from the behaviour seen in the space-clamped membrane where the limit for 1:1 pacing was a BCL of 262 ms under comparable conditions (Chapter IV, Fig. 4.2.1.1).

Globally, it is possible to understand the sequence of entrainment responses for different R values by referring to the form of the APD curves. Once the APD curves are known for a given R, the bifurcation map can be understood. However it is impossible to predict the form of the curves and consequently the bifurcation structure.

For the second cell, increasing R is somewhat equivalent to increasing the duration of the stimulation current while decreasing its amplitude. For a single cell, it was shown in

Chapter III that such changes transform the bifurcation structure as a function of BCL from period doubling to period adding , and eventually to purely passive 1:0 responses. This is precisely what is observed in C2. In some sense, the bifurcation structure of C2 in the [R × BCL] parameter space can be seen as following a trajectory in the three-dimensional [T_{stim} × I_{stim} × BCL] parameter space of a single cell. The idea is useful to explain *a posteriori* what is observed, but an *a priori* calculation of trajectory appears to be impossible since the stimulation received by C2 through Ig is very different from a rectangular pulse as soon as R becomes fairly large.

The situation is more complex for C1 since its APD is influenced by the response of C2. APD_1 is prolonged if C2 fired, and shortened if C2 did not. Again, when $APD_1(DIA_1)$ is known, the bifurcation map can be understood. But it is impossible to calculate its features in advance.

Understanding the bifurcation structure of a single cell and its relation to APD(DIA) and Thr(DIA) has helped us to understand the frequency entrainment characteristics of the two-cell system. However, it seems difficult to envisage an iterative formulation to describe the behaviour of the pair of coupled cells over a range of coupling resistance values. The major impediments are the existence of distinct APD(DIA) curves for the two cells and their variations with R.

CHAPTER VI

CARDIAC GAP JUNCTION MODEL

The purpose of the present chapter is to describe a mathematical model of the calcium-dependent cardiac gap junction resistance. This model will serve to study the entrainment response of a pair of cells in Chapter VII.

6.1 The Experiments of Noma and Tsuboi

Noma's group, in experiments on pairs of guinea pig ventricular cells (Noma and Tsuboi, 1987), showed that the gap junction resistance has a linear current-voltage relationship. Moreover, an increase in $[Ca]_{in}$ increased the gap junction resistance. Similar observations were reported by other investigators (Dahl et al., 1980, Spray et al., 1981, De Mello, 1982, Metzger et al., 1985, White et al., 1990).

A closer examination of the experiments of Noma's group is essential since our model of the gap junction channel is based on their results. Isolated cell pairs of the guinea pig left ventricle were used in all experiments. One of the cells was voltage clamped using two electrodes. After clamping the membrane potential, the bath solution was switched from

the control Tyrode solution (1.8 mM-Ca^{2+}) to a low-Ca^{2+} solution and then part of the surface membrane of the partner cell was disrupted. This procedure allowed the bath solution to affect the cytoplasmic aspect of the gap junction facing the partner cell. Under such conditions the measured current flowed from the clamped cell mostly through the gap junction into the partner cell whose interior was short-circuited to ground. The equivalent circuit after the disruption of the membrane of the partner cell is illustrated in Figure 6.1.1.

The input conductance (G_i) is given by:

$$G_i = G_{m1} + G_j.(G_{m2}+G_s)/(G_j+G_{m2}+G_s) \qquad (6.1)$$

where G_j is the gap junction resistance, G_s the conductance through the hole made in the partner cell, and G_{m1} and G_{m2} the respective non-junctional membrane conductances of the clamped cell and partner cell. If G_s is much greater than G_j and G_{m2}, G_j is given by:

$$G_j \cong G_i - G_{m1} \qquad (6.2)$$

The value of G_{m1} was approximated as half the conductance of the total non-junctional membrane ($G_{m1}+G_{m2}$) measured before perforating the partner cell. When the bath solution was switched to pCa_{in} = 7.1, 6.8 or 6.4, there was a temporal evolution of the gap junction conductance. The conductance stabilized at a steady state whose value was decreasing with the augmentation of $[Ca]_{in}$ or the decrease of pCa_{in} (Fig. 6.1.2).

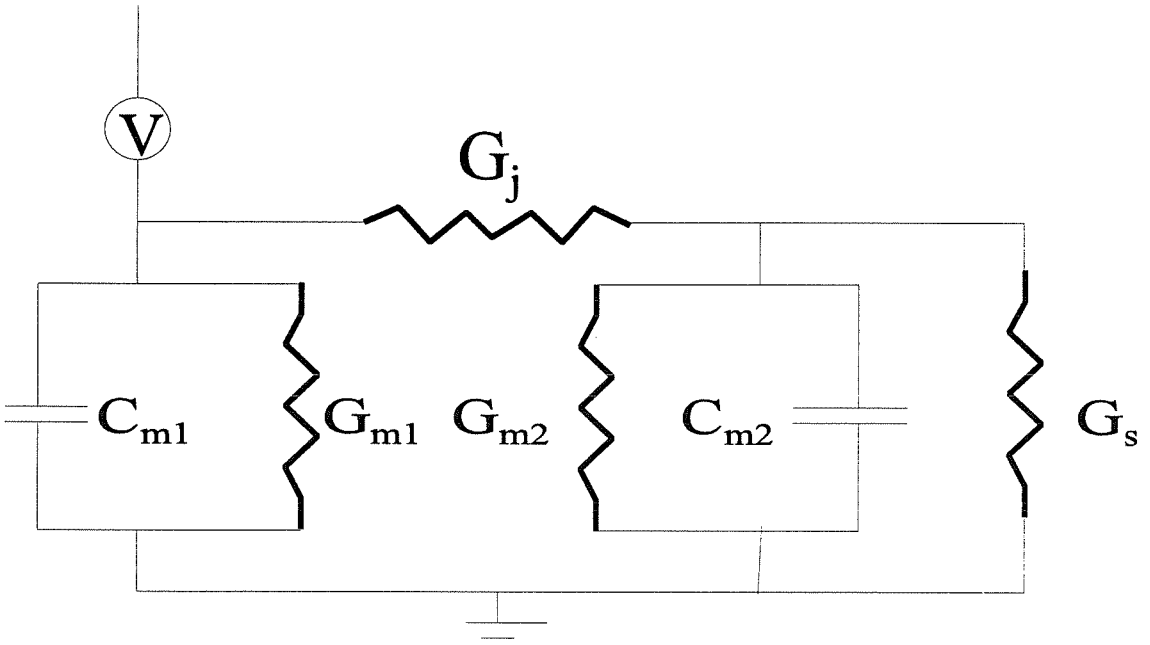

Figure 6.1.1: Equivalent circuits for Noma and Tsuboi experimental setting. G_m is the membrane conductance, C_m the membrane capcitance, G_j the gap junction conductance, and G_s the openning conductance.

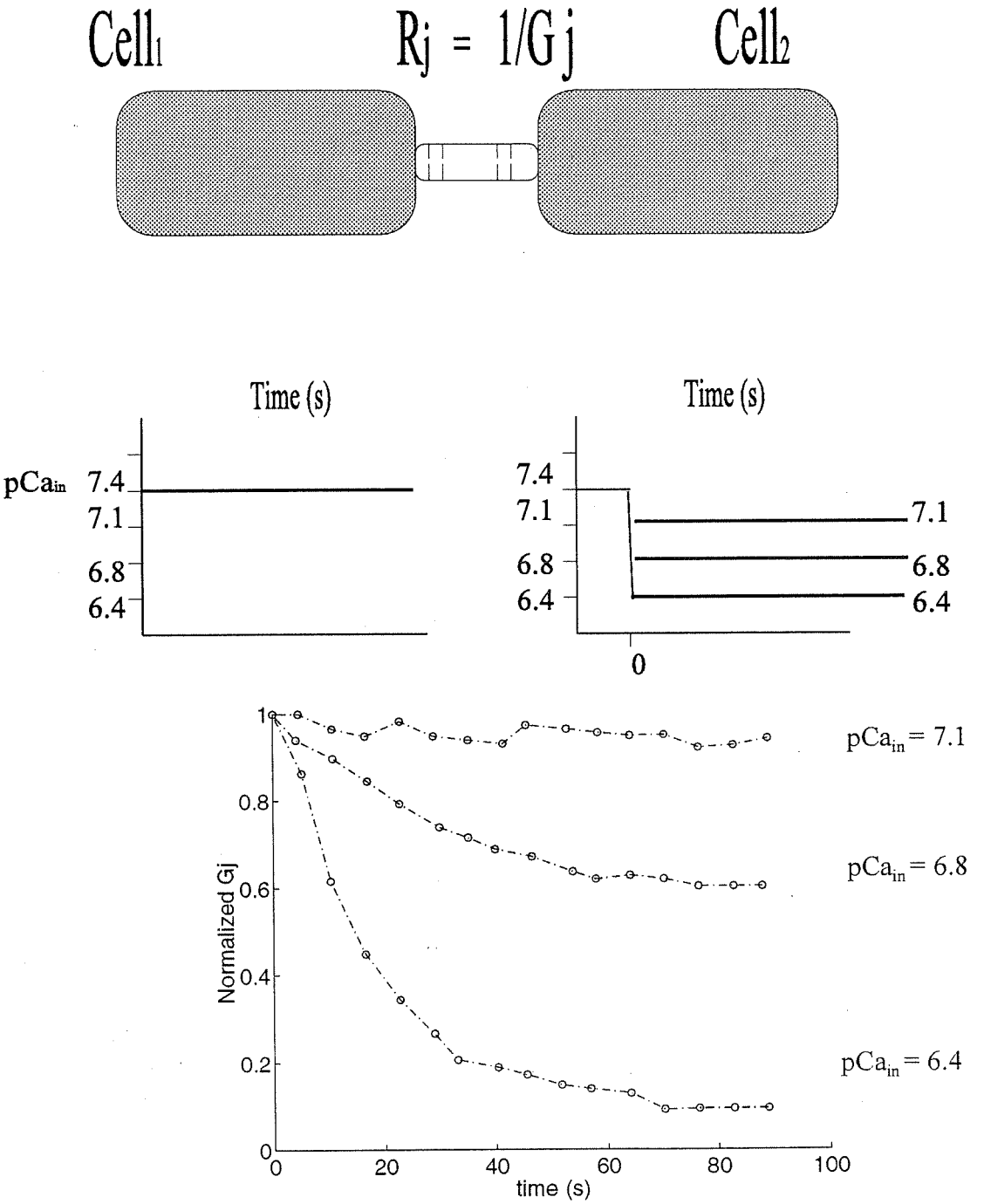

Figure 6.1.2: Experimental results of Noma and Tsuboi (1987) for step changes in pCa_{in} as shown. Time is in seconds.

6.2 Model Assumptions

Based on the results of various experimental studies showing that the gap junction resistance is regulated by the intracellular concentration of calcium ions ($[Ca]_{in}$), we can assume the following:

-The gap junction is formed by the assembly of a large number of identical channels. Each channel is gated either in an open state or a closed state.

-The channel gate is regulated by $[Ca]_{in}$.

-The channel may have more than one gate, and the dynamic behaviour of each gate is independent of the others.

-All gates are similar.

-The channels are symmetrical. A channel is made of two connexons, each one being attached to one of the adjacent cells of a pair.

6.3 Model Formulation

We hypothesize that there is a single transition between an open and a closed state, and that binding of Ca^{2+} to the connexon is instantaneous. If we designate by r the probability that the calcium-dependent gate is open and by (1-r) the probability that it is closed, the process can be described by the first order reaction:

$$1\text{-}r \underset{\alpha_r}{\overset{\beta_r}{\rightleftharpoons}} r \qquad (6.3)$$

where α_r and β_r are rate constants dependent on pCa_{in}. At a fixed pCa_{in}, the typical evolution of r is given by:

$$dr/dt = \alpha_r(1-r) - \beta_r.r \qquad (6.4)$$

From Eq. 6.4, the pCa_{in}-dependent time constant τ_r and steady-state value r_∞ are given by:

$$\tau_r = 1/(\alpha_r + \beta_r) \qquad (6.5)$$

$$r_\infty = \alpha_{r/}(\alpha_{r+} \beta_r) \qquad (6.6)$$

When pCa_{in} is clamped at a fixed value, the solution of Eq. 6.4 is:

$$r(t) = r_\infty - (r_\infty - r_0) \exp(- t / \tau_r) \qquad (6.7)$$

where r_0 is the initial value.

We assume that each channel is regulated by two identical gates, such that its conductance can be written as:

$$G_c = r^2 \times gb \qquad (6.8)$$

where gb is the maximal connexon conductance in (nS). Since each gap junction channel is made up of two connexons, and since each connexon in a pair of cells is controlled by the $[Ca]_{in}$ of each cell, the total conductance of the gap junction channel is the sum of two connexon conductances in series. For the total number of channels forming the overall gap junction conductance (Gj), we write the resistance Rj = 1/Gj as:

$$Rj = Rb \frac{(r_1^2 + r_2^2)}{(r_1^2 r_2^2)} \qquad (6.9)$$

where Rb is the minimum resistance of all connexons attached to the two cells, and r_1, r_2 are the connexon gating variables related to cell 1 and cell 2, respectively.

6.4 Calculation of α_n and $ß_n$

The experimental results of Noma and Tsuboi (1987) are used to determine the rate constant α_r and $ß_r$ for the gap junction channels. The curves showing the $[Ca]_{in}$-dependent decrease of the junctional conductance G_j (Fig. 6.1.2) provide us with an estimation of τ_r and r_∞. Based on our assumptions listed in Section 6.1 and on Eqs 6.5 and 6.6, we can write:

$$\tau \times r_\infty^{-1} = \alpha^{-1} \qquad (6.10)$$

$$ß = \tau^{-1} - \alpha \qquad (6.11)$$

where α and $ß$ are matrices representing the different value of α_r and $ß_r$ at different pCa_{in}.

Using the Marquardt's method, which is a compromise between the Gauss-Newton

and the steepest descent methods (Clarke, 1987), the best approximation of the values for α_r and $ß_r$ at different pCa_{in} are represented by the following sigmoidal functions:

$$\alpha_r = 0.0292 / (1 + \exp(-(pCa_{in}-6.624)/0.3067)) \quad (6.12)$$

and

$$ß_r = 0.030847 / (1 + \exp((pCa_{in}-6.6195)/0.13764)) \quad (6.13)$$

Equations 6.12 and 6.13 describe the activation and deactivation rate constants of the gap junction channels at different pCa_{in}. Curves showing the pCa_{in} dependence of τ_r and r_∞ for the cardiac myocyte gap junction are shown in Figure 6.4.1. At very high pCa_{in} (e.g. 7.9), we have $r_\infty = 1$ and the r gate is fully open. At very low pCa_{in} (e.g. 5) we have r_∞ near zero and the r gate is nearly closed. Note that τ_r is large and varies between 18 and 35 seconds. A comparison between experimental and model results is depicted in Figure 6.4.2. Temporal variations of the gap junction conductance (1/(Rj/Rb)) between two identical cells are shown in Fig. 6.4.3. In each curve, pCa_{in} is changed from 7.4 at t = 0 to the pCa_{in} level indicated. At pCa_{in} = 6.2, the conductance becomes nearly zero about 100 seconds after the step change, while the time required for nearly complete decoupling is close to 60 seconds at pCa_{in} = 5.4.

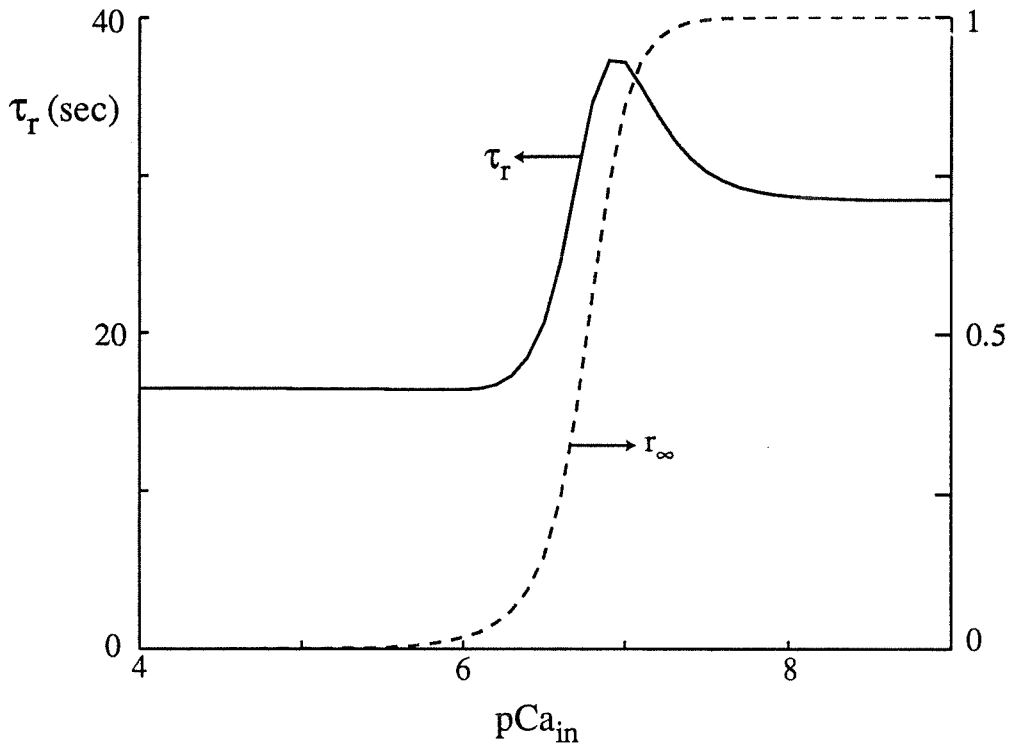

Figure 6.4.1: Model of gap junction connexon conductance: time constant (τ_r) and steady-state characteristic (r_∞) of gating variable r.

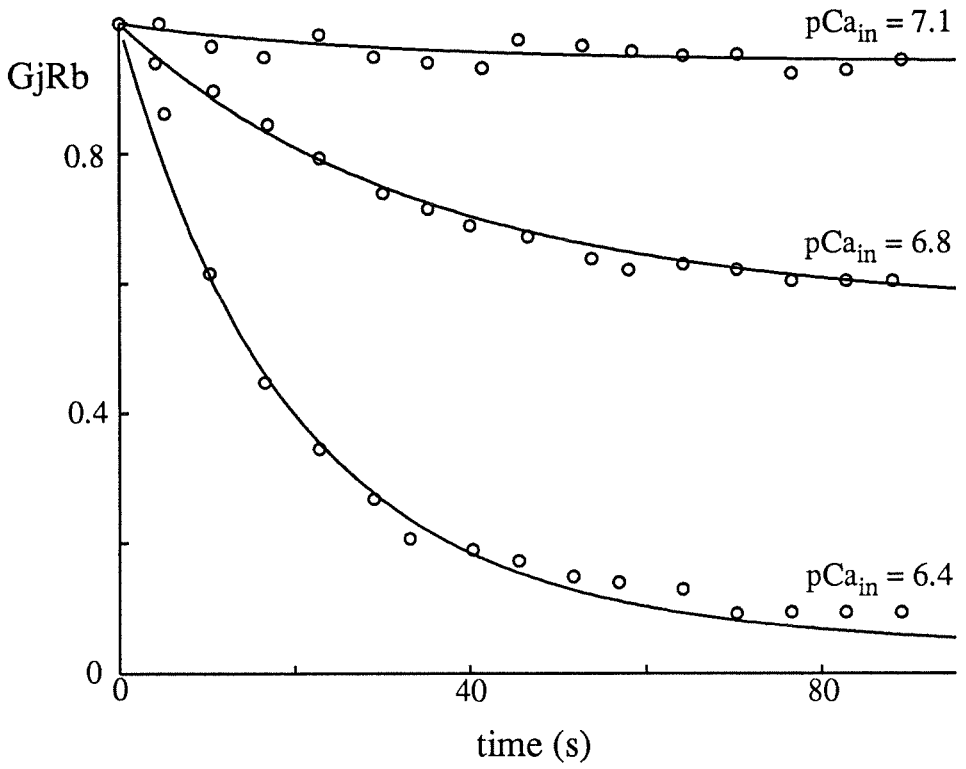

Figure 6.4.2: Comparison between the model behavior (continuous curves) and the experimental results (open circles) of Noma and Tsaboi (1987). Ordinate is the gap junction conductance (Gj) normalized by its maximum value (1/Rb).

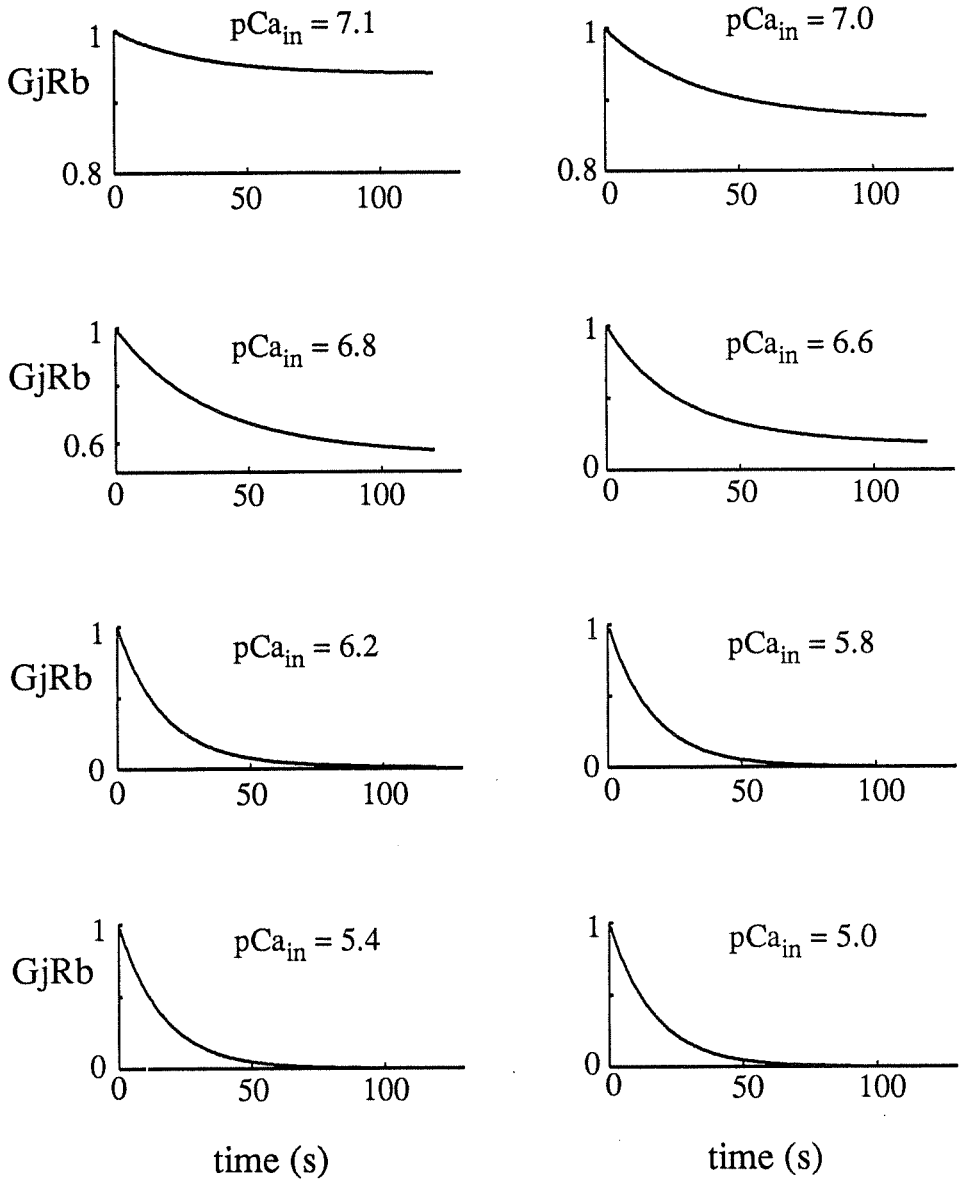

Figure 6.4.3: Illustration of the time course of GjRb changes as pCa_{in} is varied: in the left column pCa_{in} is changed from 7.1 to 5.4, in the right column pCa_{in} is changed from 7.0 to 5.0.

6.5 Summary and Conclusion

The gap junction model provides a close reconstruction of Noma and Tsuboi's data. The resting gap junction resistance depends on the resting pCa_{in} , which is chosen at 6.8 to yield $r_{1\infty} = r_{2\infty} = 0.747$ (Fig. 6.4.1). The dynamic behaviour of Rj is very slow (large τ_r of 18 to 35 seconds) and its magnitude is very sensitive to $[Ca]_{in}$ variations (Fig. 6.4.3). Since $[Ca]_{in}$ changes in a normal myocyte correspond to pCa_{in} between 7.1 and 6.2, we can expect that the corresponding gap junction resistance will remain fairly low. During sustained rapid repetitive activity, however, the model predicts that Rj will increase.

CHAPTER VII

ENTRAINMENT RESPONSE OF A SYSTEM OF TWO CARDIAC CELLS COUPLED BY A VARIABLE RESISTANCE

In the previous chapter we proposed a mathematical model for the cardiac gap junction (Rj) resistance modulated by $[Ca]_{in}$. The value of Rj is determined by the minimum resistance Rb and by a very slow calcium-dependent gating variable with a peak time-constant in the range of 38 seconds. The repetitive activity of the two cells produces important changes in Rj which in turn modifies the response of the two-cell system to regular pacing. Our goal is to describe the behaviour of the system over a range of BCL and Rb values

7.1 Pair of Cells Coupled Through a Variable Resistance

In the present chapter we consider again the two-cell system of Fig. 5.1.1, with the fixed coupling resistance (R) replaced by the Rj mechanism described in Chapter VI.

We use protocols similar to those of Chapter V, based on the application of regular pulse trains to one of the two cells, and record the activity of each cell. Both cells have identical properties and the stimulus is applied to the first cell (C1) which influences the second cell (C2) through the coupling current Ig.

The coupling current (Ig) is expressed as:

$$Ig = \frac{(V_1 - V_2)}{R_j A} \tag{7.1}$$

$$R_j = R_b \left(\frac{1}{r_1^2} + \frac{1}{r_2^2}\right) \tag{7.2}$$

where A= 4.19×10^{-5} cm^2 is the cell membrane area, Rj is the total gap junction resistance, Rb is the minimum resistance of all connexons attached to the two cells, and r_1, r_2 are the calcium-dependent gating variables of C1 and C2, respectively. It follows, therefore, that Rj will be modulated by the $[Ca]_{in}$ changes of C1 through r_1, and by the $[Ca]_{in}$ changes of C2 through r_2. Note that the resting states of C1 and C2 corresponds to $pCa_{in} = 6.8$, such that $r_{1\infty} = r_{2\infty} = 0.747$ (Fig. 6.4.1).

Rectangular pulses of $T_{stim} = 1$ ms and $I_{stim} = 1.25\ I_{thRC1}$ were used throughout to stimulate C1, with the value of I_{thRC1} determined from Fig. 5.4.1. Given the resting values of $r_{1\infty} = r_{2\infty} = 0.747$, the Rj value used to set I_{stim} =1 .25 I_{thRC1} was Rj ≅ 3.5 Rb (Eq. 6.9). Rb was normally changed between 100 to 1000 KΩ, although some higher values were sometimes used. For each Rb, the BCL was changed between 125 and 1000 ms. The

value of Rj was determined at the onset of each pulse stimulus (Fig. 7.1.1). Definitions and other aspects of the procedures are as in Chapter V, except for the maximum number of applied stimuli (23,800) registered before the response pattern was considered aperiodic

Dynamic changes in gating variable (r) and coupling resistance (Rj) are illustrated in Fig. 7.1.1, where Rb = 300 KΩ and BCL = 500 ms. The two-cell system is stimulated from rest and only the first two action potentials of C1 are shown (column 1, panel 1). C2 exhibits exactly the same behaviour as C1, including the changes in $[Ca]_{in}$ (column 1, panel 2) and pCa_{in} (column 2, panel 1). There is a rapid initial build-up of $[Ca]_{in}$ at the beginning of the action potential, followed by a plateau and return to the base level. There is therefore no cumulative increase of $[Ca]_{in}$ during successive action potentials, even at very short BCLs, since the $[Ca]_{in}$ changes do not extend beyond the APD.

There is, however, a slow downward drift of the magnitude of r_1 or r_2 when the successive action potentials are sufficiently close to one another. With a BCL of 500 ms, this unidirectional drift is about 1.3% at each action potential (column 1, panel 3), or nearly 2% for r_1^2 or r_2^2 (column 2, panel 2). At the beginning of each action potential, pCa_{in} changes abruptly from 6.8 to 5.3, and stays at this level during the plateau of this action potential. $r_\infty(pCa_{in})$ is then shifted from its 0.747 resting level to zero (see Fig. 6.4.1), inducing a small decrease of r_1 and r_2, even if their time constant is around 18 seconds. Because of the asymmetric $\tau_r(pCa_{in})$ curve, (18 seconds at low pCa_{in} versus 38 seconds at high pCa_{in}), r_1 and r_2 return toward their basic level at a much slower pace

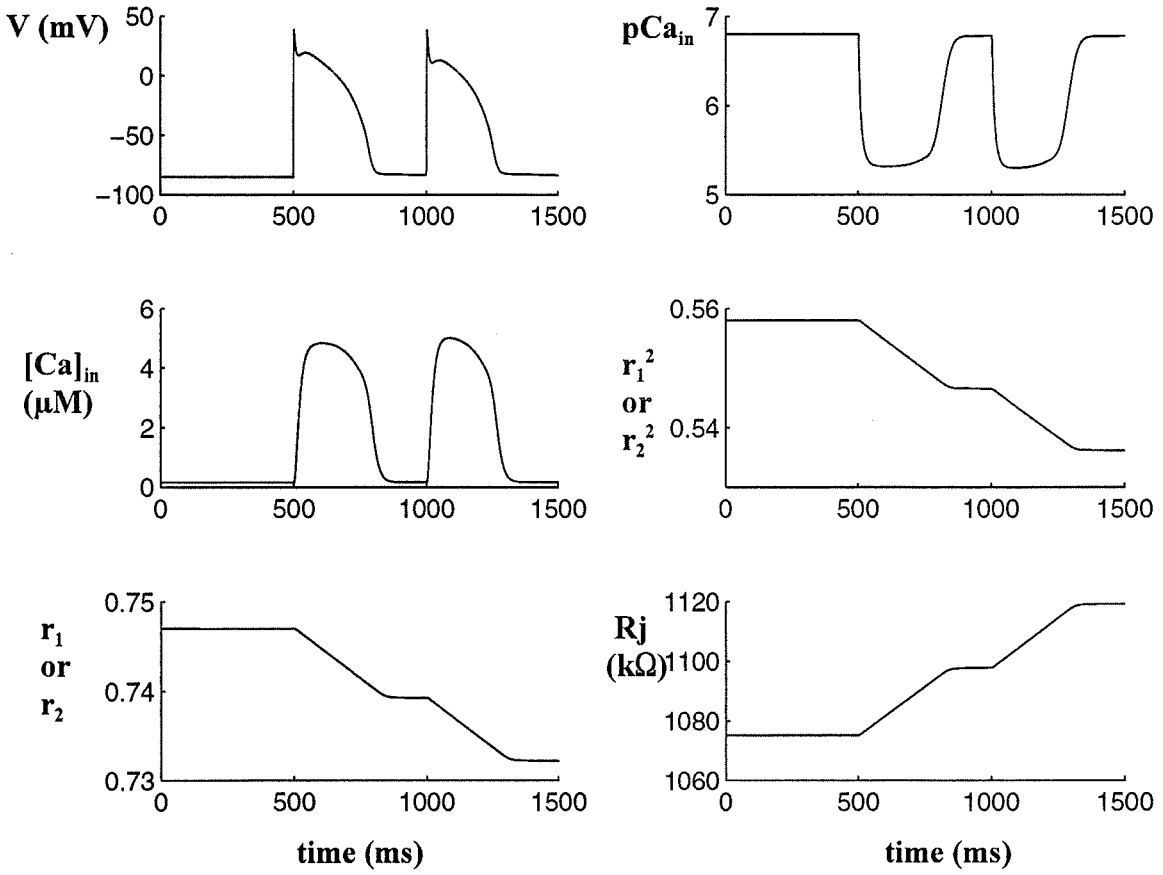

Figure 7.1.1: Dynamic changes of the coupling resistance (Rj) during successive action potentials. Left column: action potentials (panel 1), corresponding $[Ca]_{in}$ changes (panel 2), and resulting r_1 or r_2 variations (panel 3). Right column: corresponding pCa_{in} changes (panel 1), resulting r_1^2 (panel 2), and resulting Rj increase (panel 3).

during repolarization (viz. column 1, panel 3). The net result is a cumulative decrease in r_1 or r_2 in proportion to the rate of firing of C1 or C2. In view of Eq. 7.2, these gating variable changes give rise to corresponding Rj variations (column 2, panel 3).

7.2 Slow Rate of Pacing with Rb < 15,000 KΩ

When the two cells are tightly coupled (low Rb and thus low Rj) and the rate of pacing is fairly low (BCL of 500 to 1000 ms), C1 and C2 are synchronized. In the same range of BCL, the two cells of the fixed resistance model studied in Chapter V have nearly identical 1:1 responses for R < 425 MΩ (Fig. 5.7.1).

During regular pacing of the variable gap junction model, there is first a gradual decrease of r_1 and r_2 (Fig. 7.1.1) and Rj becomes larger. This is illustrated in Fig. 7.2.1 for BCL = 500 ms and Rb =300 or 900 KΩ, where Rj increases during the first hundred stimuli to finally stabilize at 10.55 or 31.6 MΩ, respectively. These saturation values are well below the value of R = 425 MΩ at the transition between 1:1 to 2:2 rhythm in Chapter V. The two cells have identical APD values which stabilize around 245 ms after the first few responses. The initial alternation in APD values is the same as that obtained in a single cell stimulated from rest. Since the action potentials and the $[Ca]_{in}$ variations observed for Rb = 300 or 900 KΩ are identical, the Rj saturation value is directly proportional to Rb.

A closer examination of the Rj variations during the early and late phases of entrainment is presented in Fig. 7.2.2, for Rb = 300 KΩ and BCL = 500 ms. At the beginning (left panel) the gap junction resistance is continuously increasing from a baseline of about 1.07 MΩ. After 1800 pulses, Rj reaches a steady state in the form of a periodic variation between 10.55 and 10.74 MΩ during each stimulation cycle (500 ms). Rj increases progressively during the action potential and decreases in a similar manner during the diastolic interval. Note that the rate of Rj increase around the steady state level is much larger (0.190 MΩ over the APD) than near the resting level (0.023 MΩ over the APD).

In this range of BCLs, the APD is close to its saturation value. A larger BCL then increases the APD only slightly and causes mainly an increase in DIA. Consequently, the saturation value of Rj decreases with a larger BCL since r_1 and r_2 have more time to increase toward their resting levels because of the longer DIA. This behaviour is depicted in Fig. 7.2.3 where a BCL of 870 ms gives a final Rj of 10.4 MΩ versus 31.6 MΩ for a BCL of 500 ms, with APDs of 245.7 and 266.7 ms, respectively. In addition, since the saturation value of Rj is lower with a larger BCL, the number of stimulus pulses required from the onset of pacing to reach stability (transient phase of Rj) is lower (411 pulses for Rj =10.4 vs 1014 pulses for Rj =31.6 MΩ). This type of behaviour was obtained as long as Rb was below 1000 KΩ.

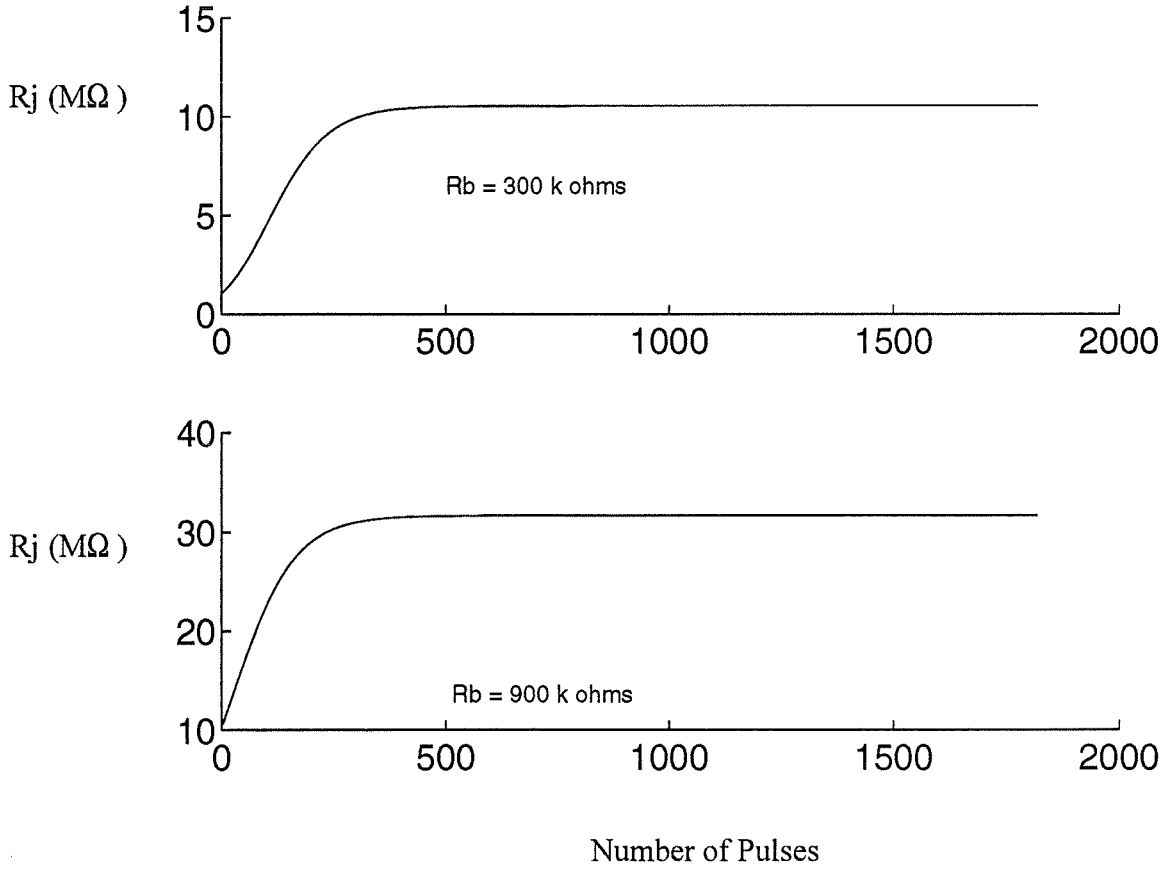

Figure 7.2.1.: Changes in Rj (values at the onset of pulse stimulus) for a BCL of 500 ms and Rb as indicated on each panel. The saturation values of Rj are 10.55 MΩ (top panel) and 31.6 MΩ (bottom panel).

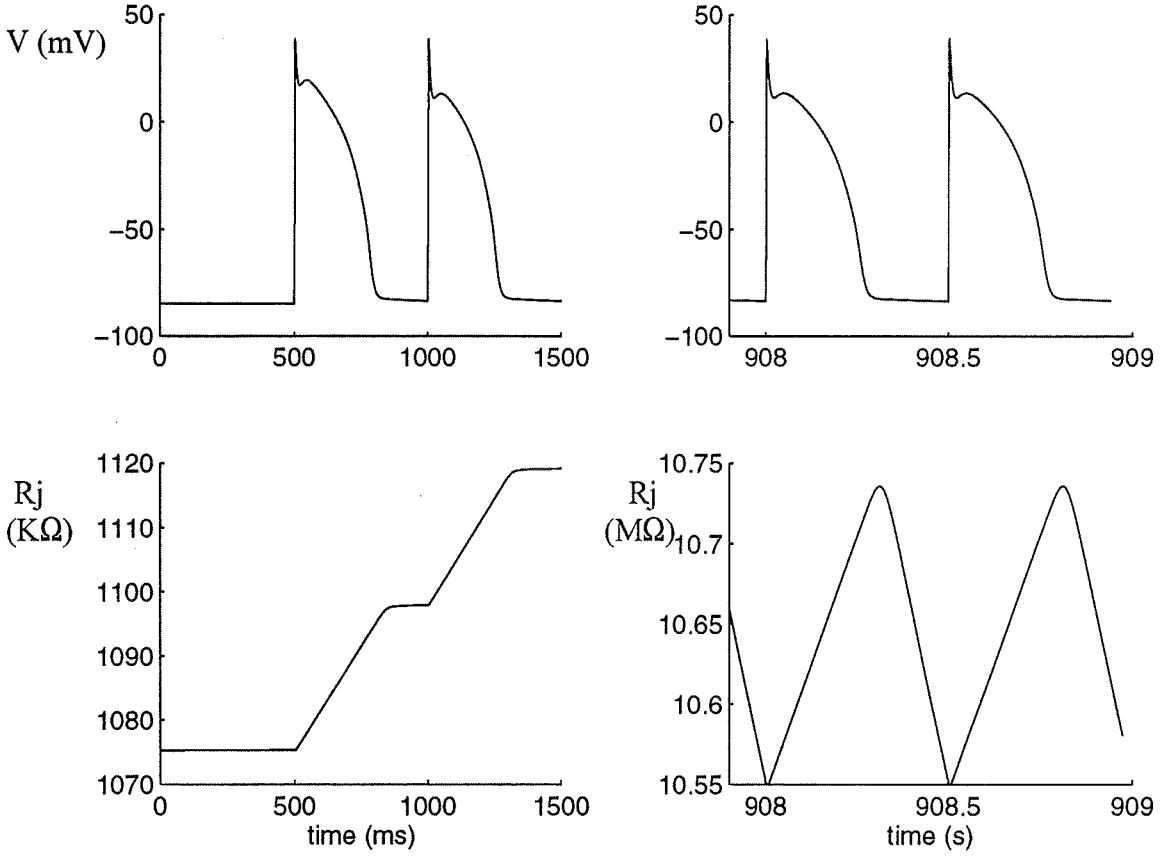

Figure 7.2.2 Typical action potential waveforms (top panels) and Rj variations with time elapsed from the onset of pacing at BCL = 500 ms and Rb 300 KΩ. Early time (ms) in the left column and late time (seconds) in the right column.

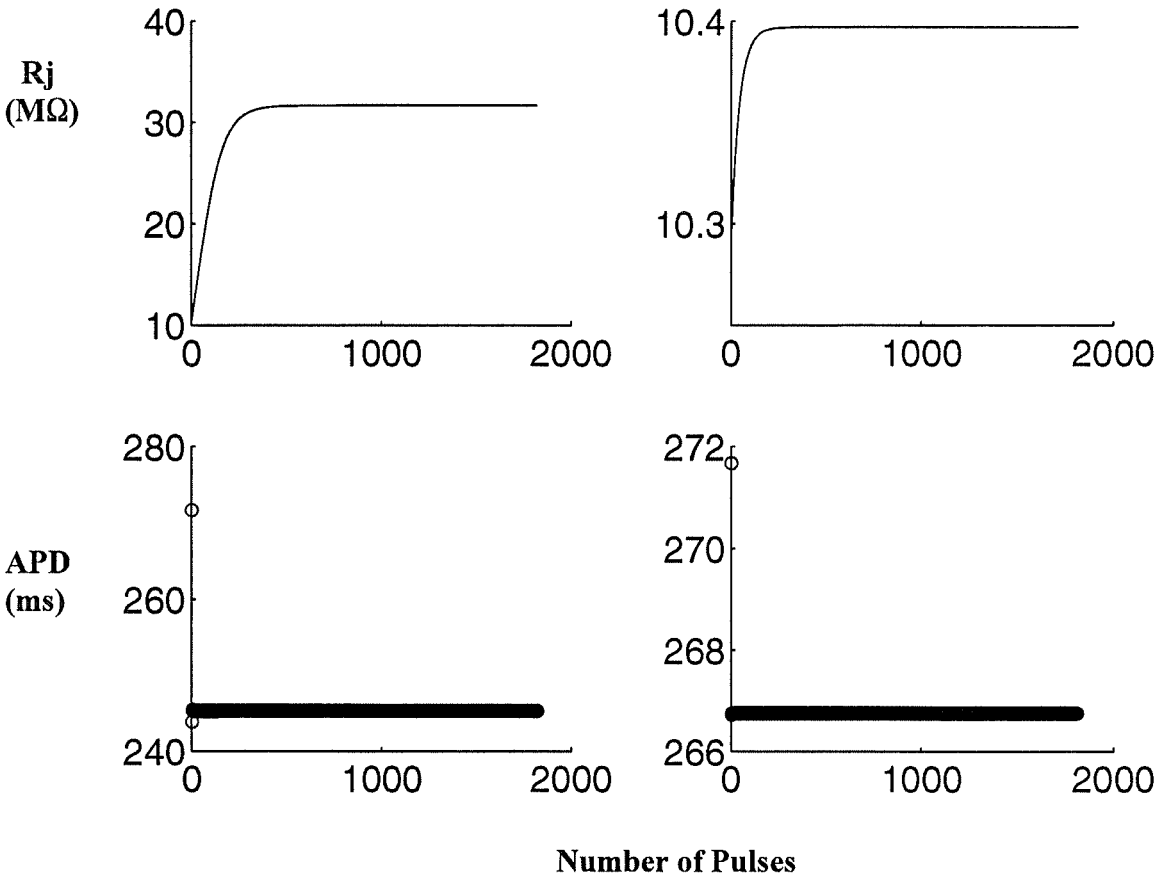

Figure 7.2.3 Comparaison of the effects of BCL = 500 ms (left column) and BCL = 870 ms (right column) for Rb = 900 KΩ. The saturation values of Rj are 31.6 and 10.4 MΩ, respectively, while the APDs are 245.7 and 266.7 ms, respectively.

7.3 Slow Pacing Rate with Rb > 15000 KΩ

With a BCL of 500 ms, the response of the pair of cells with a fixed coupling resistance (R) had a transition from period 1 to period 2 for R = 425 MΩ. For values of Rb < 15,000 KΩ, Rj never increased over 425 MΩ and the response of each cell remained in period 1 with nearly identical APDs in both cells.

With Rb $\geq$ 15,000 KΩ, Rj fluctuates around 425 MΩ and the structure of the C1 and C2 responses changes. When the BCL = 500 ms and Rb = 15,000 KΩ (Fig.7.3.1), Rj increases from its initial value of about 52 MΩ to above 418 MΩ after about 200 stimuli (panel 1). At the start of pacing, APD_1 and APD_2 jump almost immediately to a nearly constant value of 248 ms for APD_1 and 234 ms for APD_2 (panels 3 and 5). These APD values remain essentially unchanged during the transient Rj increase. However, when Rj approaches its maximum after about 210 pulses, the form of the response changes and Rj, APD_1 and APD_2 start to display periodic variations. The APD cyclic variations are shown on an enlarged scaled in Fig. 7.3.2. The new steady state cyclic behaviour is reached practically immediately after the initial Rj transient is completed.

In the steady state, Rj fluctuates regularly between 418 and 432 MΩ (panel 2 in Fig. 7.3.1). The steady state APD_1 pattern is a 59:59 rhythm, made of one 9:9 and five 10:10 sequences (panel 4 in Fig. 7.3.1), in exact correspondence with the Rj fluctuations.

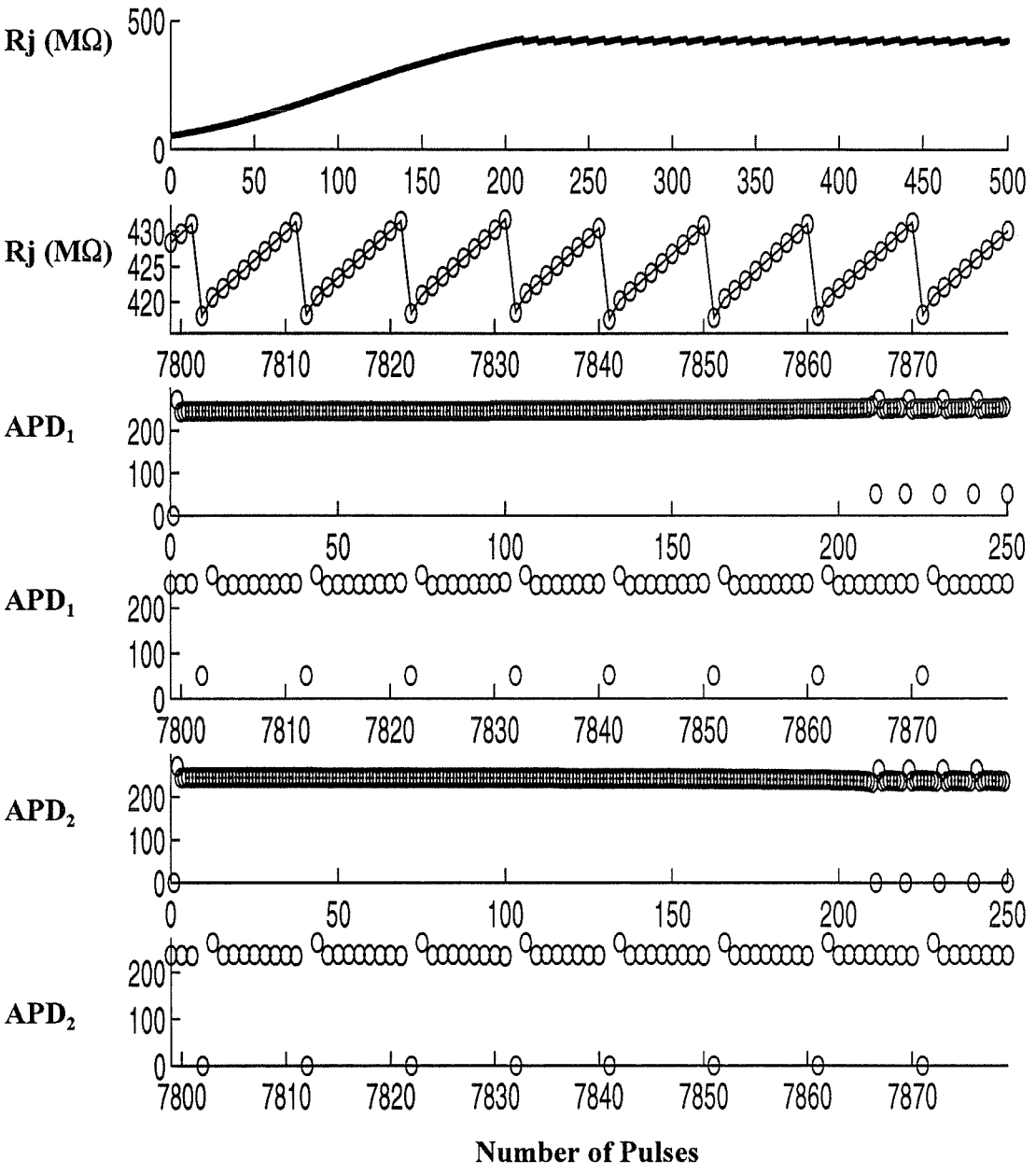

Figure 7.3.1: Transient change in Rj from the start of pacing (panel 1) and steady state alternations between 418 and 432 MΩ (panel 2). Panels 3 and 5 show APD_1 and APD_2 values from the start of pacing, while panels 4 and 6 show the corresponding steady state values. Sequences are 9,10,10,10,10,10 for Rj and APD_1, and 8, 9, 9, 9, 9, 9, for APD_2, as indicated. BCL = 500 ms, Rb = 15,000 KΩ, and APD values in ms.

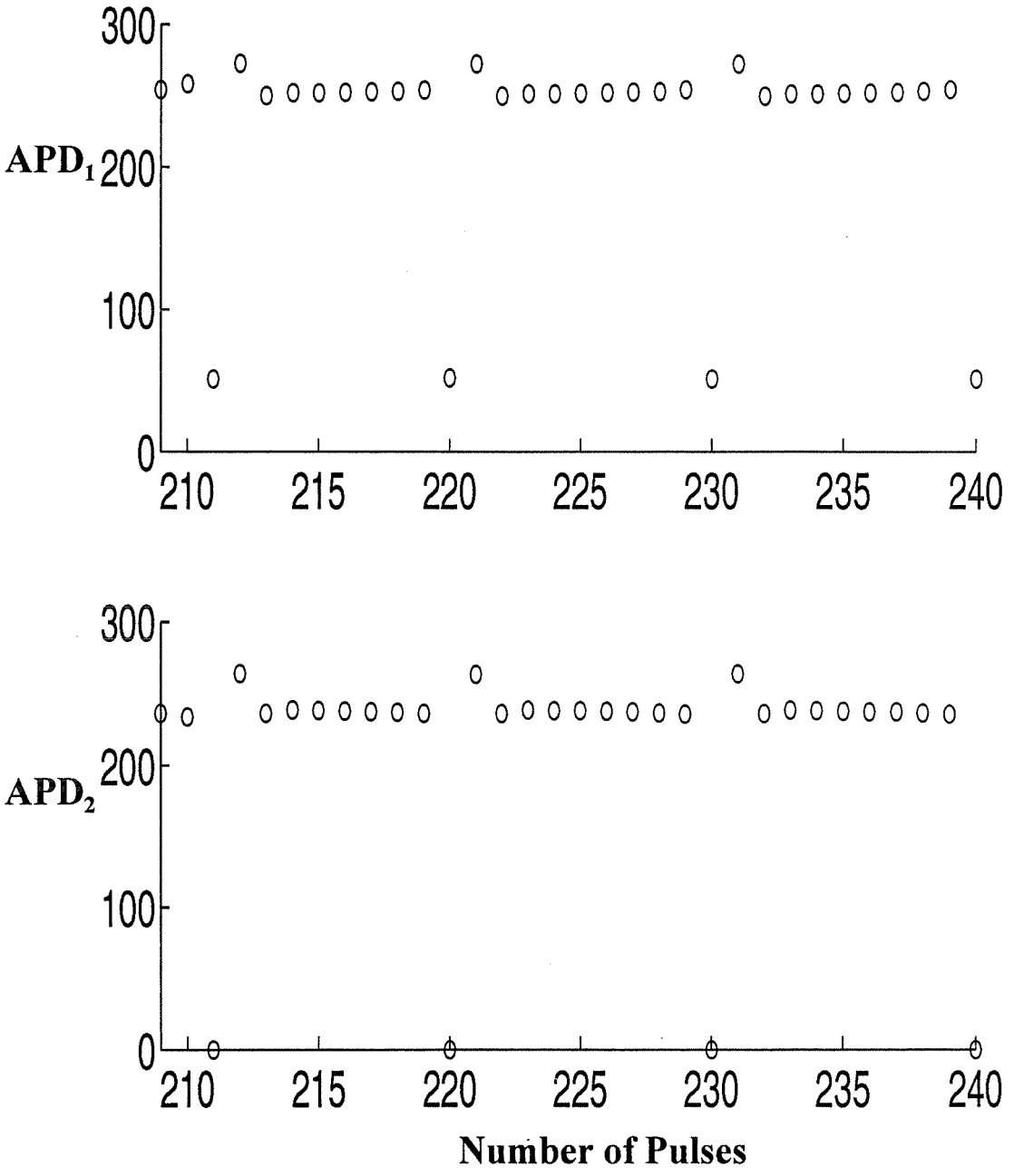

Figure 7.3.2.: Patterns of APD_1 and APD_2 responses at the end of the Rj transient on panels 3 and 5 of Fig.7.3.1. Sequences are exactly the same as in panels 4 and 6 of Fig. 7.3.1. BCL = 500 ms, Rb 15,000 KΩ, and APD values in ms.

When there is a sharp Rj drop from 432 to 418 MΩ, there is a corresponding APD_1 decrease from 251 to 51 ms, followed by a jump to a large APD as soon as Rj increases. As Rj increases progressively over the next 8 or 9 responses, APD_1 remains fairly constant. The APD_1 response could be seen as a mix of 1:1 and 2:2 responses. APD_2 follows a similar steady state pattern, except that a blocked response occurs in synchrony with the short APD_1 to cause a sudden drop of Rj (bottom panel in Fig. 7.3.1 where the blocked response corresponds to $APD_2 = 0$). As a result the APD_2 pattern is a 59:53 rhythm, made of one 9:8 and five 10:9 sequences. Because of the blocked responses, APD_2 shows a mix of 1:1 and 2:1 responses.

The behaviour of the system is qualitatively similar when Rb is increased to 20,000 KΩ (Fig. 7.3.3). Rj first increases from its initial 70 MΩ value to 420 MΩ, as in the Rb = 15,000 KΩ case. However, the increase is faster and occurs over ≃ 145 pulses (panel 1). APD_1 and APD_2 are almost constant during all the increasing phase of Rj, and begin to oscillate when Rj comes close to its maximum value. The periodic solution stabilizes rapidly after its first appearance.

During the stable oscillations, Rj varies between 420 and 434 MΩ (compare to 418 and 432 MΩ for Rb = 15,000 KΩ). There is a gradual build-up of Rj, followed by an abrupt drop, and the increase starts again. During the build-up, both APD_1 and APD_2 remain around a fixed high value. The Rj drop corresponds to the occurrence of a blocked response in C2 and a short APD_1 in C1 (Fig. 7.3.4). The considerable decrease

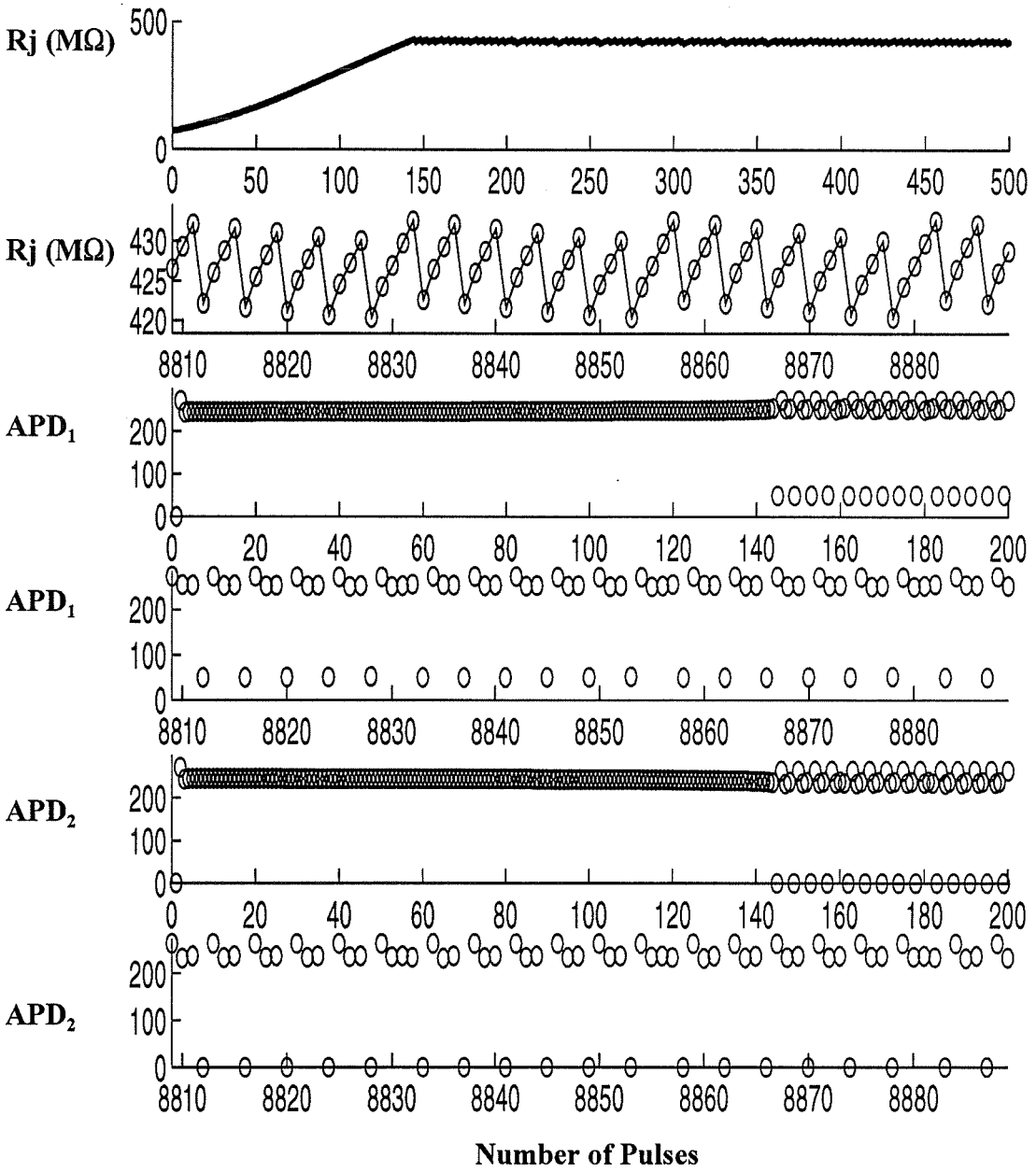

Figure 7.3.3: Transient change in Rj from the start of pacing (panel 1) and steady state alternations between 420 and 434 MΩ (panel 2). Panels 3 and 5 show APD_1 and APD_2 values from start of pacing, while panels 4 and 6 show the corresponding steady state values. Sequences are 5,4,4,4,4,4 for Rj and APD_1, and 4, 3, 3, 3, 3, 3, for APD_2, as indicated. BCL = 500 ms, Rb = 20,000 KΩ, and APD values in ms.

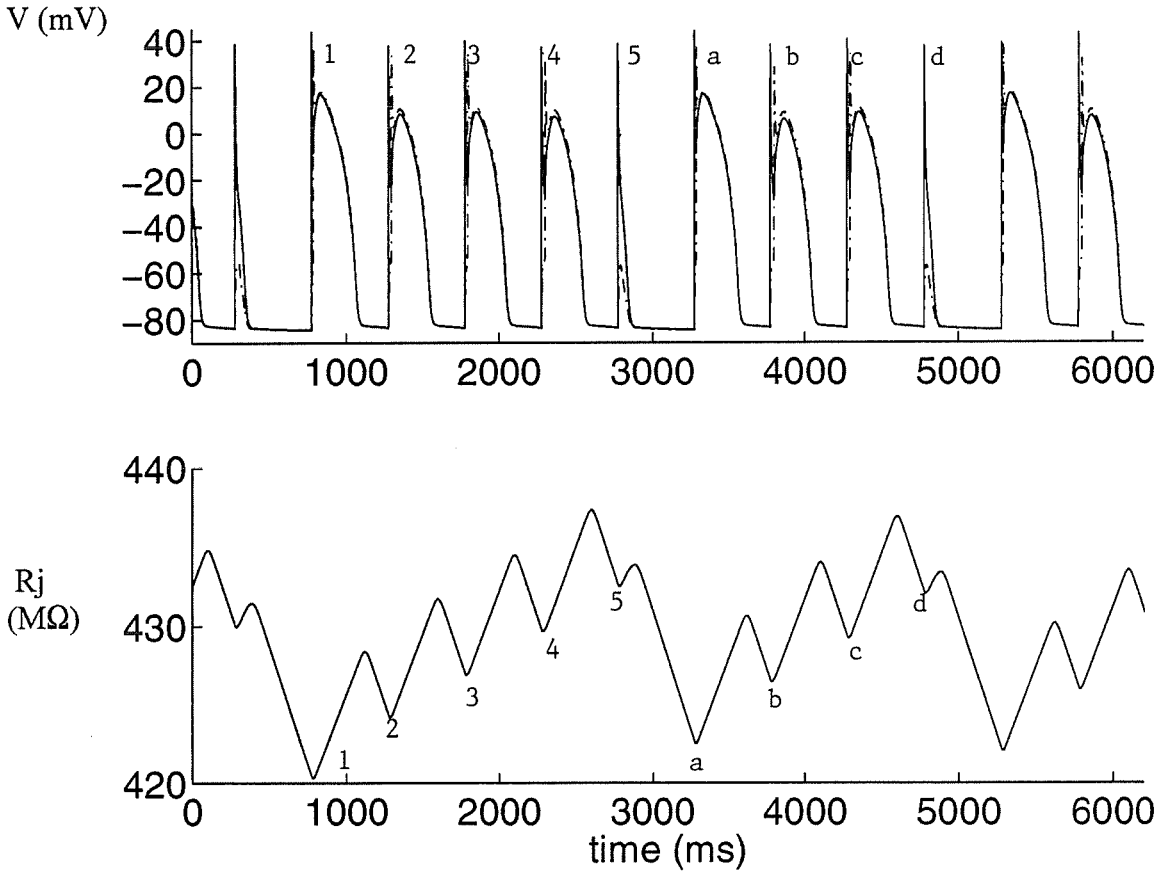

Figure 7.3.4: Action potentials (top panel) of C1 (continuous tracing) and C2 (broken tracing) and correponding Rj variations (bottom panel). A sequence of 5 action potentials (numbered 1 to 5) is followed by a sequence of 4 action potentials (numbered a to d). Note that the short APD_1 coincides with a blocked C2 responses. Rj increases during the APD and decreases during DIA. BCL = 500 ms and Rb = 20,000 KΩ.

of APD_1 when C2 is inactive is the result of a large increase of Ig (Eq. 7.1) due to the fact that V_2 is then quite low. This large outward C1 current causes a sudden drop of V_1 which prevents the occurrence of the APD_1 plateau.

The total period of the oscillation in Fig. 7.3.4 includes 25 responses (compared to 59 for Rb = 15,000 KΩ). Looking at APD_1 or APD_2, it is seen that these 25 responses consist of one sequence of 5 responses, followed by 4 sequences of 4 (i.e, 25 = 1×5+ 4×4, compared with 59 = 1×9 + 5×10 for Rb = 15,000 KΩ). Each sequence starts with a blocked response in C2 and a short APD_1 in C1. The next response has a large APD in both cells. Hence, the first two responses of each sequence could be seen as forming a 2:2 AR in C1 or a 2:1 AR in C2. In the subsequent responses, the APD remains almost constant in C2, and increases slightly in C1. Hence these responses could be seen as successive 1:1s. Thus, the global cycle appears to be a mix of 1:1 and 2:2 or 2:1 ARs. As Rb increases, the relative proportion of 2:2 and 2:1 ARs in the cycle increases (from 6×2:2 for 47×1:1 (or 13% of 2:2s at Rb = 15,000 KΩ), versus 5×2:2 for 15× 1:1 (or 33% of 2:2s at Rb = 20,000 KΩ)).

As Rb is increased, the transformation is more pronounced. At Rb = 20,000 KΩ, Rj reaches 420 MΩ after 141 responses, and starts to oscillate between 420 and 434 MΩ, going a little deeper into the period 2 zone of the fixed resistance model (Fig. 7.3.3). The final stabilization of the oscillatory solution is now delayed. The stable cycle has a period of 26 responses divided into one period 4 sequence, followed by 11 period 2 sequences

(i.e, 25 = 1×4 + 11×2). All the period 2 sequences, as well as all the first two responses of the period 4 sequence, appear as 2:2 AR in C1 or 2:1 AR in C2. Hence, the global rhythm is almost purely 2:2 or 2:1 (11×2:2 or 2:1 and 2×1:1).

The dynamics can be understood by considering the behaviour of the R-coupled system (Chapter V). In that case, for a BCL = 500 ms, R = 420 MΩ is the boundary between the 1:1 entrainment zone and the 2:2 (in C1) and 2:1 (in C2) entrainment zones. When Rj reaches this boundary, it starts to oscillate between the two regimes. Each short APD_1 in C1 and blocked response in C2 move the system back toward 1:1. With a higher Rb, the feedback interaction between the APD and Rj increases, and the period of the global cycle diminishes. Rj also goes deeper into the high resistance zone of the bifurcation map. At some Rb, it is expected that the system will definitely cross the 1:1 boundary and display period 2 responses. The next oscillation should then occur at the boundary between period 2 and period 3 rhythms that exists near R = 500 MΩ in the R-coupled system.

With Rb = 40, 000 KΩ (Fig. 7.3.5), there is an initial steep Rj increase, reaching 420 MΩ after 60 responses, followed by a slower drift to 500 MΩ. During the first phase of the increase, the two cells have a 1:1 response, and 2:2 (in C1) and 2:1 (in C2) responses during the second phase. The final oscillatory pattern has a period of 55 responses made of six successive alternations between period 9 and period 7 sequences, followed by a supplementary period 7 sequence (i.e, 55 = 3×(9 + 7) + 1×7), each of

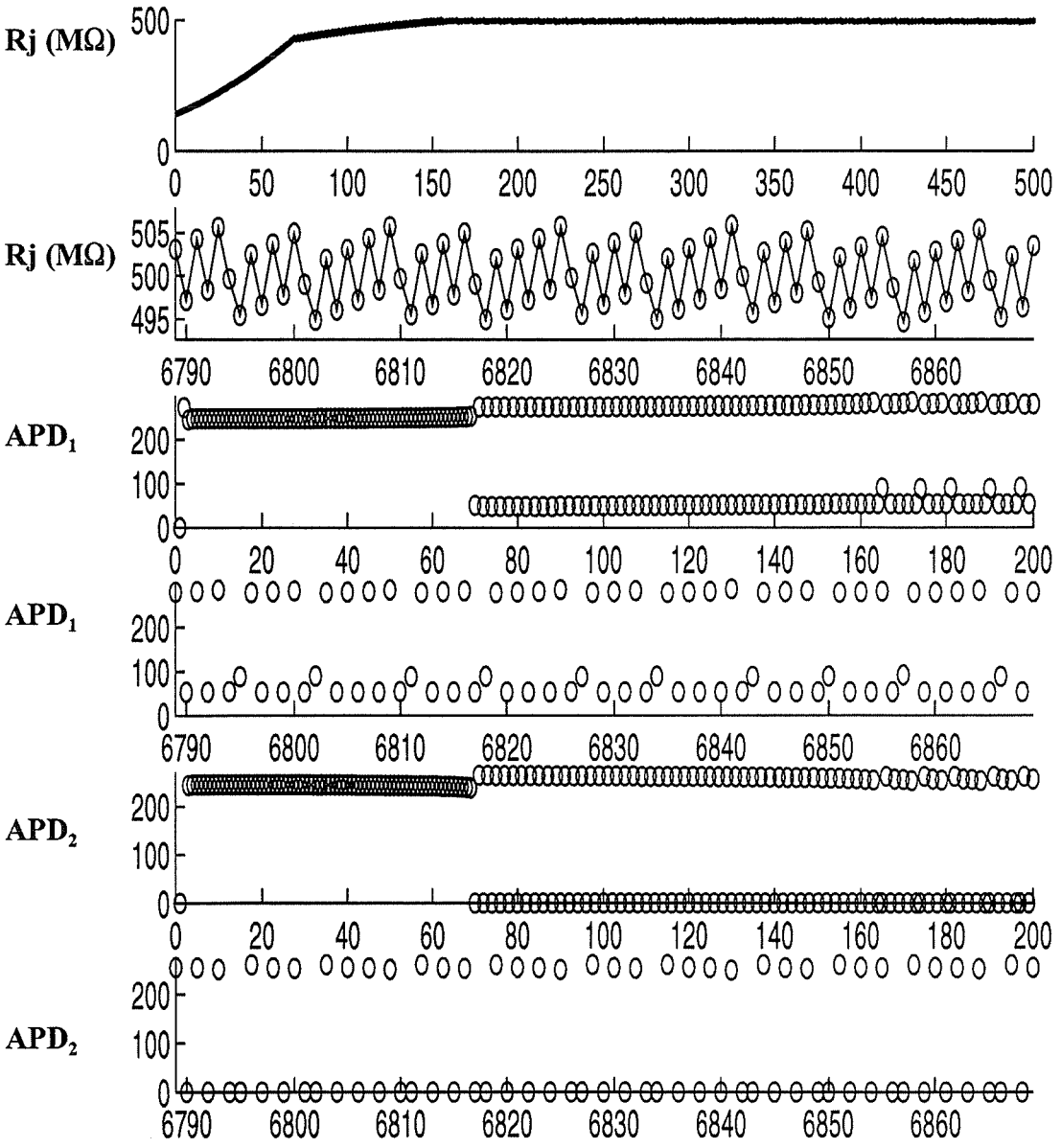

Figure 7.3.5 Transient change in Rj from the start of pacing (panel 1) and steady state alternations between 495 and 506 MΩ (panel 2). Panels 3 and 5 show APD_1 and APD_2 values from the start of pacing, while panels 4 and 6 show the corresponding steady state values. sequences are 16:16 for Rj and APD_1, and 16:7 for APD_2 as indicated. BCL = 500 ms, Rb = 40,000 KΩ, and APD values in ms.

these sequences are series of alternans terminated by supplementary low amplitude responses. In C2, there are 2 or 3×2:1 ARs, followed by one 3:1 AR (i.e, 7 = 2×2:1 + 1 ×3:1, and 9 = 3×2:1 + 1×3:1). As expected, the system oscillates near the boundary between period 2 and period 3 zones, where Rj varies between 495 and 506 MΩ.

7.4 Intermediate and Fast Pacing Rates

At faster pacing, the oscillation of the two-cell system continues for certain Rb values, and it appears at Rb $\leq$ 1000 KΩ. This oscillation was not limited to the crossing of the boundary between adjacent periods, but it also crossed the boundary between two ARs. At Rb $\leq$ 1000 KΩ and at faster pacing (intermediate range of BCL = 300 to 270 ms), there is a more rapid increase of Rj toward its steady state value which is expected since DIA is small. This may or may not disturb the 1:1 response of C1 and C2 depending on the final level of Rj. Table 7.4.1 provides data pertaining to the ranges of fixed coupling resistance (R) that defined the regions of period 1 and period 2 rhythms for BCLs of 300 and 270 ms in the R-coupled system (Chapter V). For instance, with a BCL of 300 ms, the 1:1 AR should be preserved in both C1 and C2 if Rj remains below 362 MΩ, while a Rj between 362 and 380 MΩ would be expected to yield a 2:2 AR in C1 and a 2:1 AR in C2.

Rj variations are plotted in Fig. 7.4.1 for a BCL of 300 ms and different Rb

values. As long as Rb is lower than about 990 KΩ , Rj saturates below 340 MΩ and the responses of C1 and C2 continue to correspond to a 1:1 AR. With Rb = 1000 KΩ, however, Rj comes close enough to the 362 MΩ barrier for the 1:1 rhythm to be altered. The new stable solution is an Rj oscillation between 320 and 372 MΩ (lower right panel, Fig. 7.4.1). The cycle of 373 pulses is depicted in Fig. 7.4.2. When Rj increases gradually from 320 MΩ, there are 1:1 responses in both C1 and C2 with constant APDs of 201 and 198 ms, respectively. When Rj reaches the critical value of 372 MΩ, C1 adopts a 2:2 AR, with increasing alternations between APD_1 values. APD_2 changes in a similar manner, until one response is blocked (APD_2 = 0 in Fig. 7.4.2). As a consequence, Rj drops sharply toward its lower value of 320 MΩ and the APD responses follow a sequence of decreasing alternations.

Table 7.4.1: Ranges of fixed coupling resistance values (R) in the two-cell system (Chapter V) defining the regions of period 1 and period 2 rhythm for BCL of 300 ms and 270 ms.

BCL = 300 ms			BCL = 270 ms		
R (MΩ)	AR1	AR2	R (MΩ)	AR1	AR2
0-362	1:1	1:1	0-155	1:1	1:1
362-380	2:2	2:2	155-240	2:2	2:2
380-420	2:2	2:1	240-410	2:2	2:1

The details of the initiation, duration, and aftermath of the aperiodic sequence are

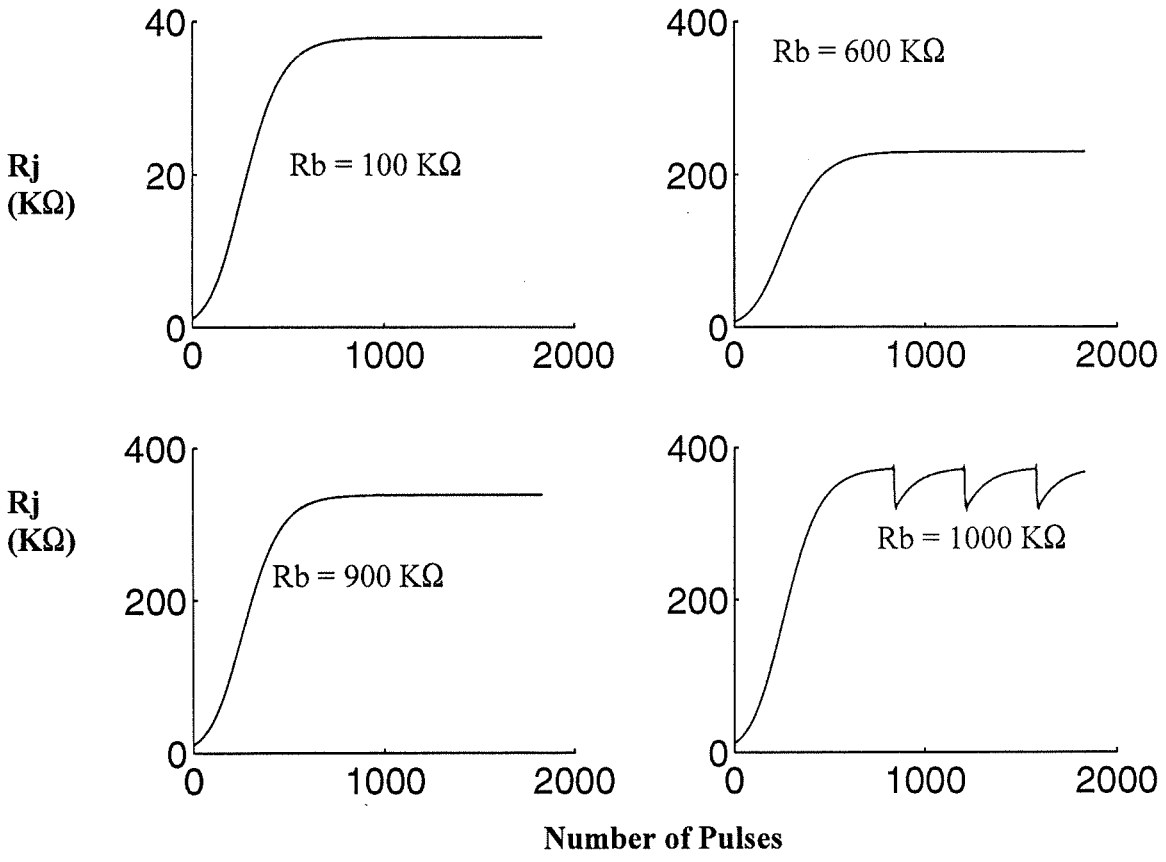

Figure 7.4.1: Changes in Rj with a BCL of 300 ms and Rb values as shown. Saturation values of Rj are 39, 230, and 339 MΩ for Rb = 100, 600 and 900 KΩ, respectively. Steady state alternations between 320 and 372 MΩ occur for Rb = 1000KΩ.

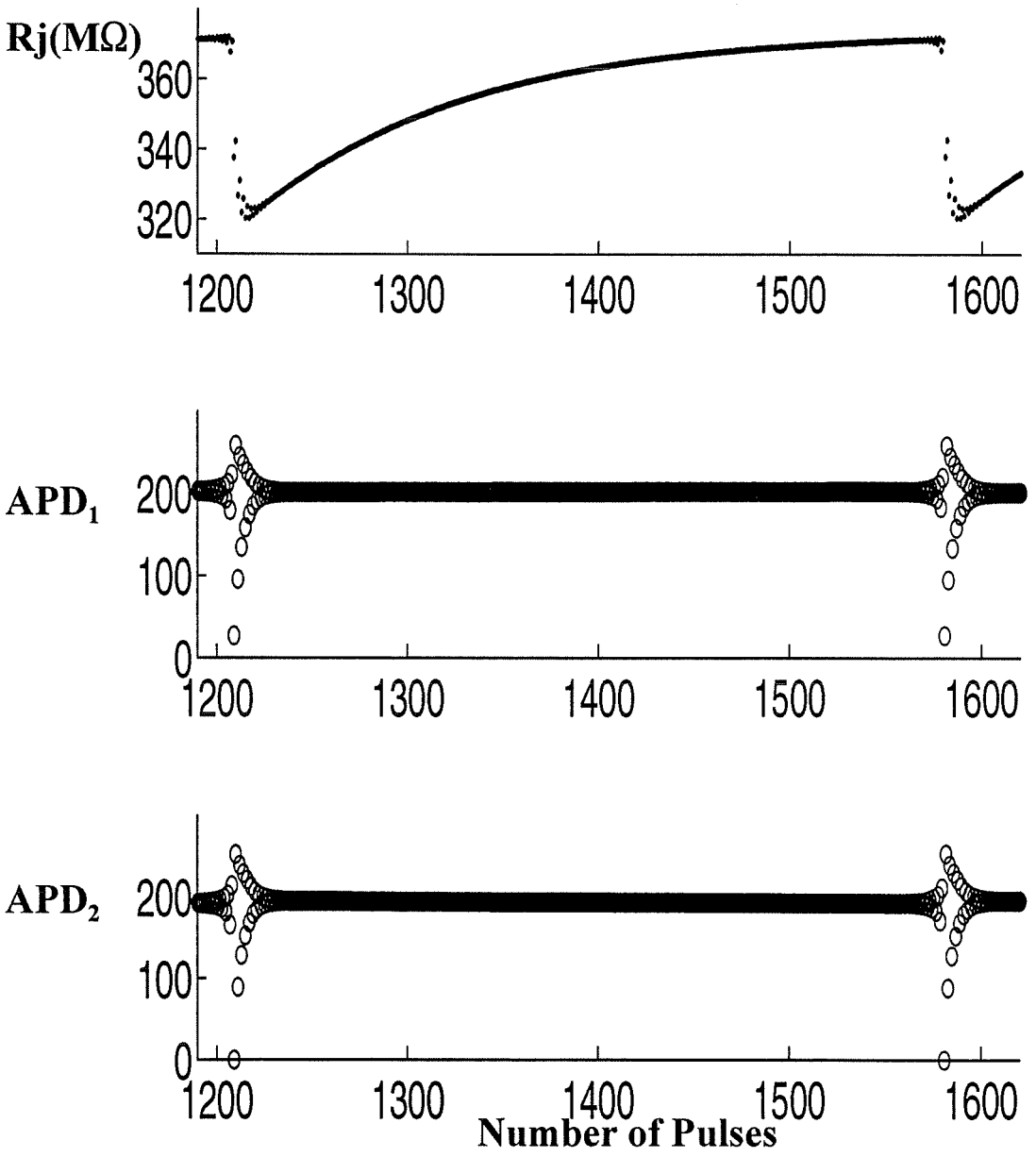

Figure 7.4.2: Steady state alternation of Rj (top), APD_1, (middle), and APD_2 (bottom). As Rj is increased gradually from 320 MΩ, both C1 and C2 respond in a 1:1 manner. When Rj reaches the critical value of 372 MΩ, the 1:1 rhythm of both cell is disrupted and Rj falls abruptly toward 320 M MΩ. BCL = 300 ms, Rb = 1000 KΩ, and APD values in ms.

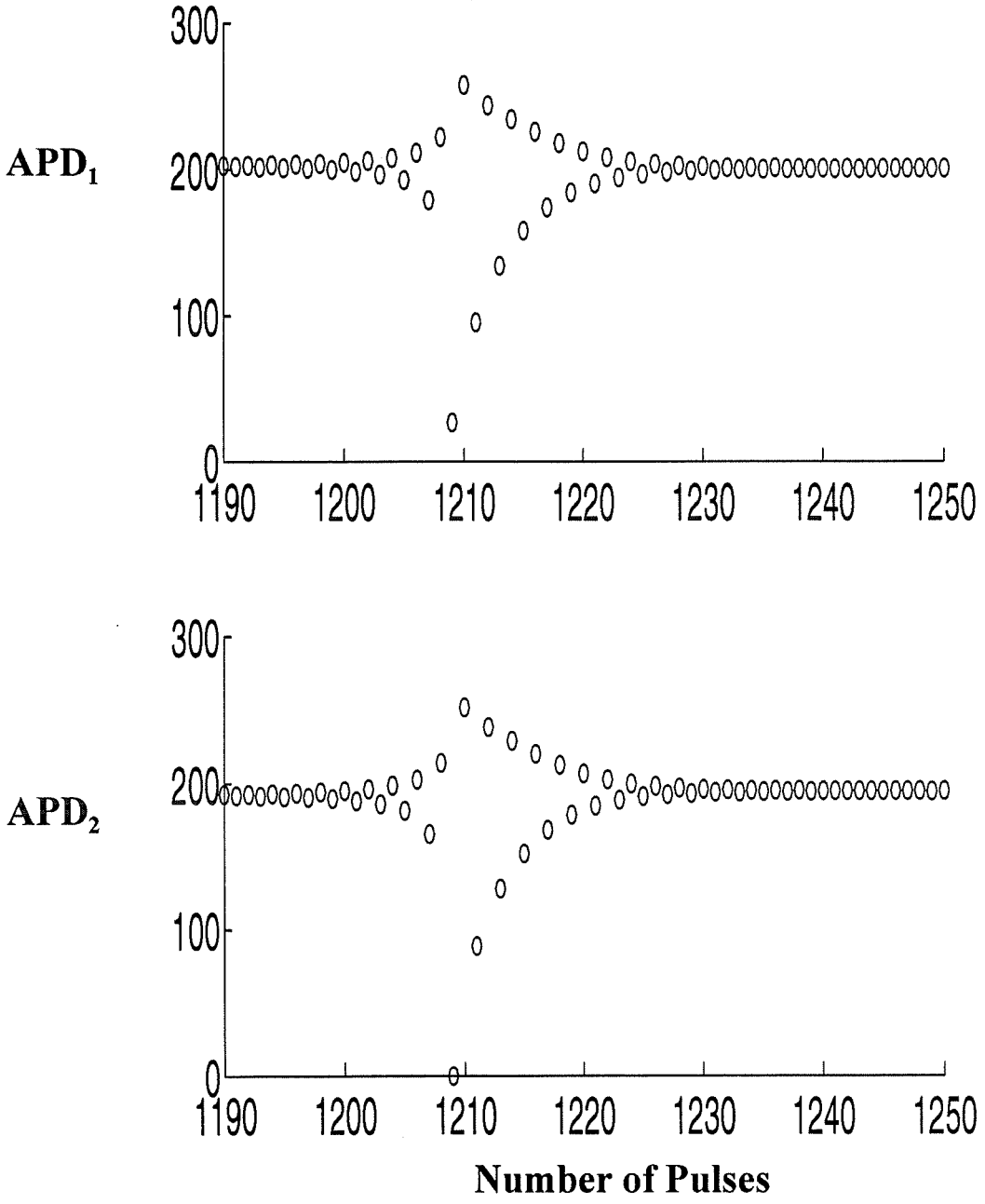

Figure 7.4.3: Expanded display of the rhythm disturbances occuring in the vicinity of the 1200th pulse in the two bottom panels of Fig.7.4.2.

shown on an expanded scale in Fig. 7.4.3. APD_1 and APD_2 begin to vary slightly just after the 1190th pulse, and the variations progressively increase in amplitude to reach a maximum at the 1209-1210 pulses; extreme APD_1 values are then 30 and 259 ms while extreme APD_2 values are 0 and 259 ms. Thereafter, the alternations gradually decrease in amplitude over about 20 pulses and the 1:1 rhythm is restored. Consequently, the predominant 1:1 rhythm of C1 is periodically broken by a burst of 2:2 rhythm, while that of C2 is broken mostly by 2:2 rhythm and one 2:1 response.

With a still higher pacing rate (BCL = 270 ms), Table 7.4.1 predicts that the breakup of the 1:1 rhythm will occur around Rj = 155 MΩ. This prediction is incorrect in view of the result of Fig. 7.4.4. With Rb = 100 KΩ, Rj saturates at 92 MΩ with APD_1 = 186.2 ms and APD_2 = 185.8 ms. With Rb = 210 KΩ, Rj saturates at 194 MΩ with APD_1 = 187 ms and APD_2 = 184.8 ms. There is therefore a stable 1:1 rhythm in both C1 and C2, even though Rj = 194 MΩ is much above the critical value of 155 MΩ predicted by the results of Chapter V (Table 7.4.1).

This discrepancy could be due to the fact that the fixed resistance (R) model was always reset to rest at the beginning of pacing, while there is a progressive increase of Rj in the variable gap junction model. To examine this possible explanation, we tried to mimic in the fixed resistance model the progressive changes of Rj seen in Fig. 7.4.1. As illustrated in Fig. 7.4.5, R was varied from 25 to 195 MΩ in steps of 5 MΩ. A total of 160 stimulations were applied at each step, and the resistance was changed using the final

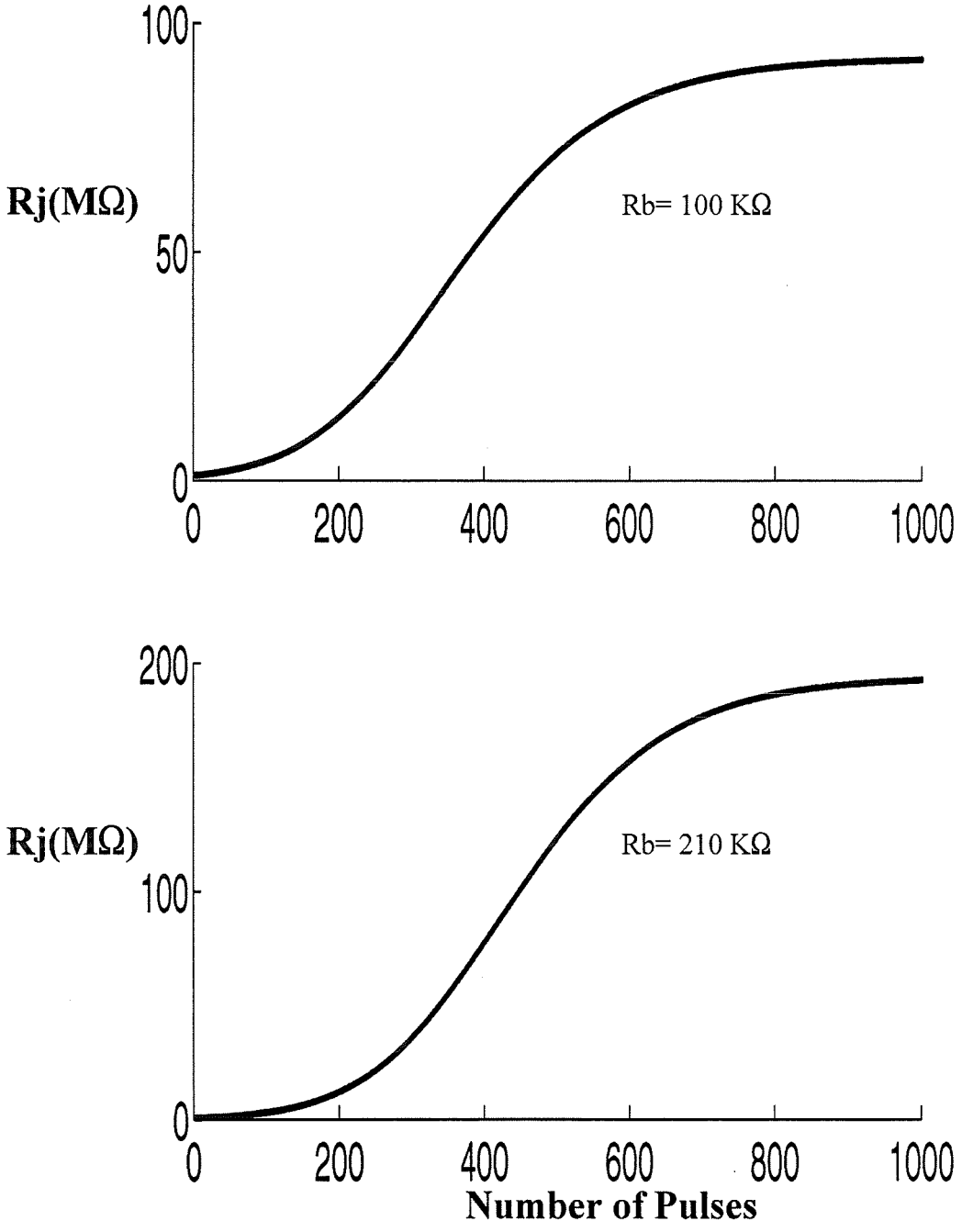

Figure 7.4.4: Changes in Rj with a BCl of 270 ms and Rb values shown. Saturation values of Rj are 92 and 194 MΩ, respectively, for Rb =100 and 210 KΩ.

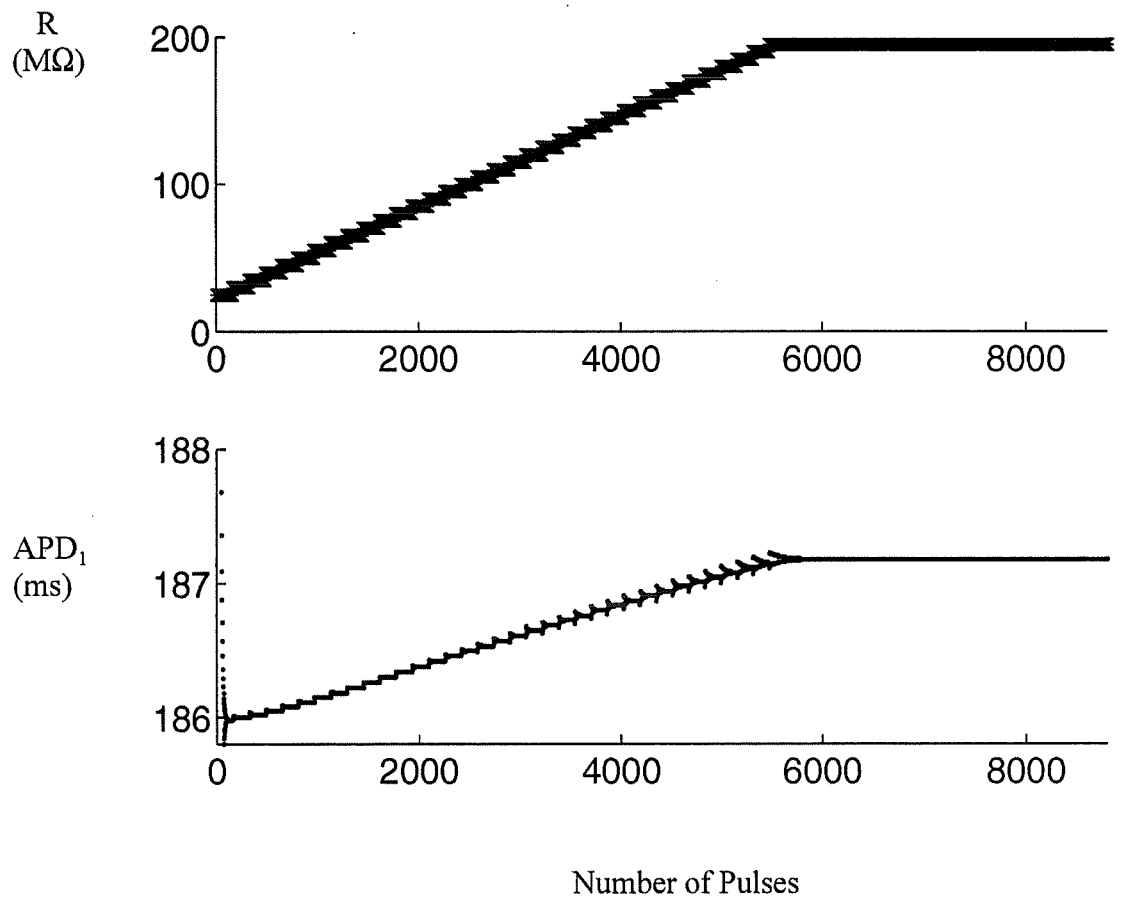

Figure 7.4.5: Progressive increase of R top from 25 to 195 MΩ in steps of 5 MΩ in the two-cell system with a constant coupling resistance (Chapter V), with C1 and C2 kept in their previous steady states at each R value. APD_1 (bottom) for a BCL of 270 ms.

C1 and C2 states as initial conditions. With this protocol, both C1 and C2 behaved in the same manner. There was either no break in the 1:1 or an initial 2:2 rhythm which returned to 1:1 after a small number of pulses, as shown by the APD_1 responses of Fig. 7.4.5. It is apparent, therefore, that the response pattern of the system is quite sensitive to the initial conditions at the start of pacing. The progressive changes in the coupling resistance allow Rj to reach higher values without the disruption of the 1:1 rhythm. However, when the steps of R were increased from 5 MΩ to 10 MΩ, there was a break of the 1:1 rhythm and the system converged into a 2:2 rhythm (results are not shown). Thus, for a low BCL, the fixed R system has hysteresis whereby a gradual increase of R pushes the transitions between entrainment patterns to a higher level in the bifurcation map (Fig. 5.7.1).

When Rb is chosen at a higher value, between 260 and 510 KΩ, the responses of C1 and C2 became oscillatory. With Rb = 260 KΩ, (Fig. 7.4.6), Rj reaches a saturation plateau of 238 MΩ after 800 pulses, remains at this level for more than 500 additional pulses, and then exhibits sustained slow oscillations between 156 and 223 MΩ with a period of 371 pulses. APD_1 and APD_2 exhibit similar patterns (top right, Fig. 7.4.6) which resemble those of Figs 7.4.2 or 7.4.3: a long stretch of quasi 1:1 response (alternans with less than 4 ms difference), followed by a phase of increasing and then decreasing alternations. There is no blocked response in C2 in this case so that both cells exhibit a full 2:2 rhythm. The major disruptions of the quasi 1:1 rhythm, where the largest APD alternations occur, correspond to the drop in Rj from 223 to 156 MΩ.

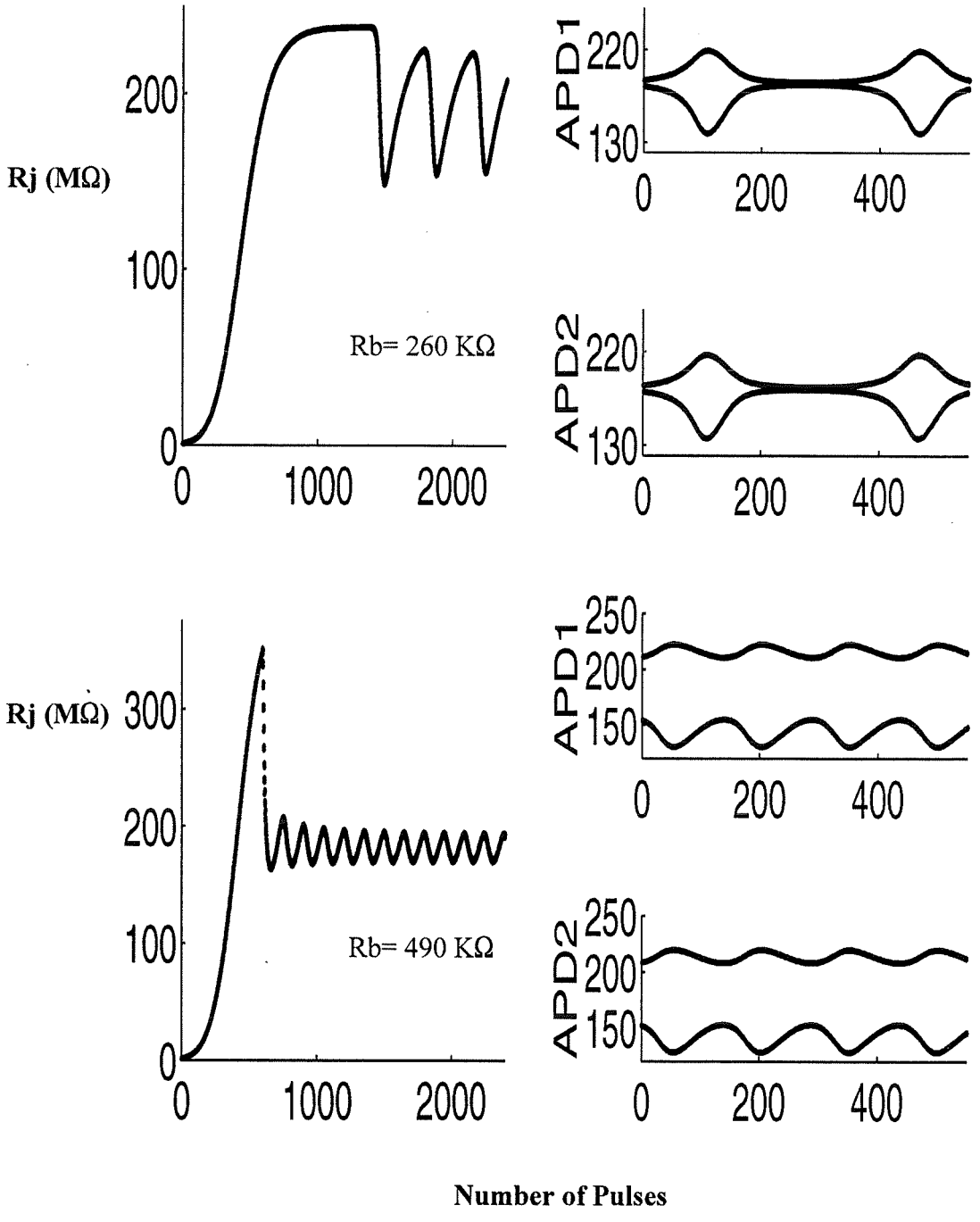

Figure 7.4.6: Behaviour of the two-cell system with BCL = 270 ms and Rb = 260 KΩ (top) or Rb = 490 KΩ (bottom). Transient and steady state Rj changes (left column) and corresponding APD_1, APD_2 responses (right column). APD values are in ms.

With Rb = 490 KΩ, Rj increases to a maximum of 351 MΩ (bottom left panel, Fig. 7.4.6), does not establish a plateau, and drops abruptly to adopt a slightly damped oscillatory mode between 170 and 194 MΩ, and a period of about 148 pulses. APD_1 and APD_2 exhibit a similar 2:2 pattern (bottom right, Fig. 7.4.6) which has the form of regular modulated alternations between short and long APDs. The maximum/minimum values are 222/128 ms for APD_1, and 220/126 ms for APD_2. Again both cells exhibit a full 2:2 rhythm. Here also, the largest APD alternations correspond to the drop in Rj from 194 to 170 MΩ.

For Rb = 260 or 490 KΩ, Rj drives the system within the 2:2 region. During the stable cycle, the amplitude of the APD alternation follows that of the Rj variations, reaching a maximum at the maximum value of Rj, and then decreasing as Rj approaches its minimum. However, because of the sensitivity to the initial conditions (Fig. 7.4.5), the system can transiently reach a high Rj value while maintaining a 1:1 response. This can be seen in Figs 7.4.7 and 7.4.8 which show the transition between the 1:1 and 2:2 patterns for Rb = 260 KΩ and 490 KΩ.

At still larger Rb values between 515 and 680 KΩ, the oscillatory pattern of Rj values is critically damped and the final steady state corresponds to period 2 alternations between fixed APD and Rj values (Fig. 7.4.9). Rj is now deep in the 2:2 region of the bifurcation map (Fig. 5.7.1), but the system does not display the oscillations which would be expected if its state were close to the boundary between two adjacent entrainment

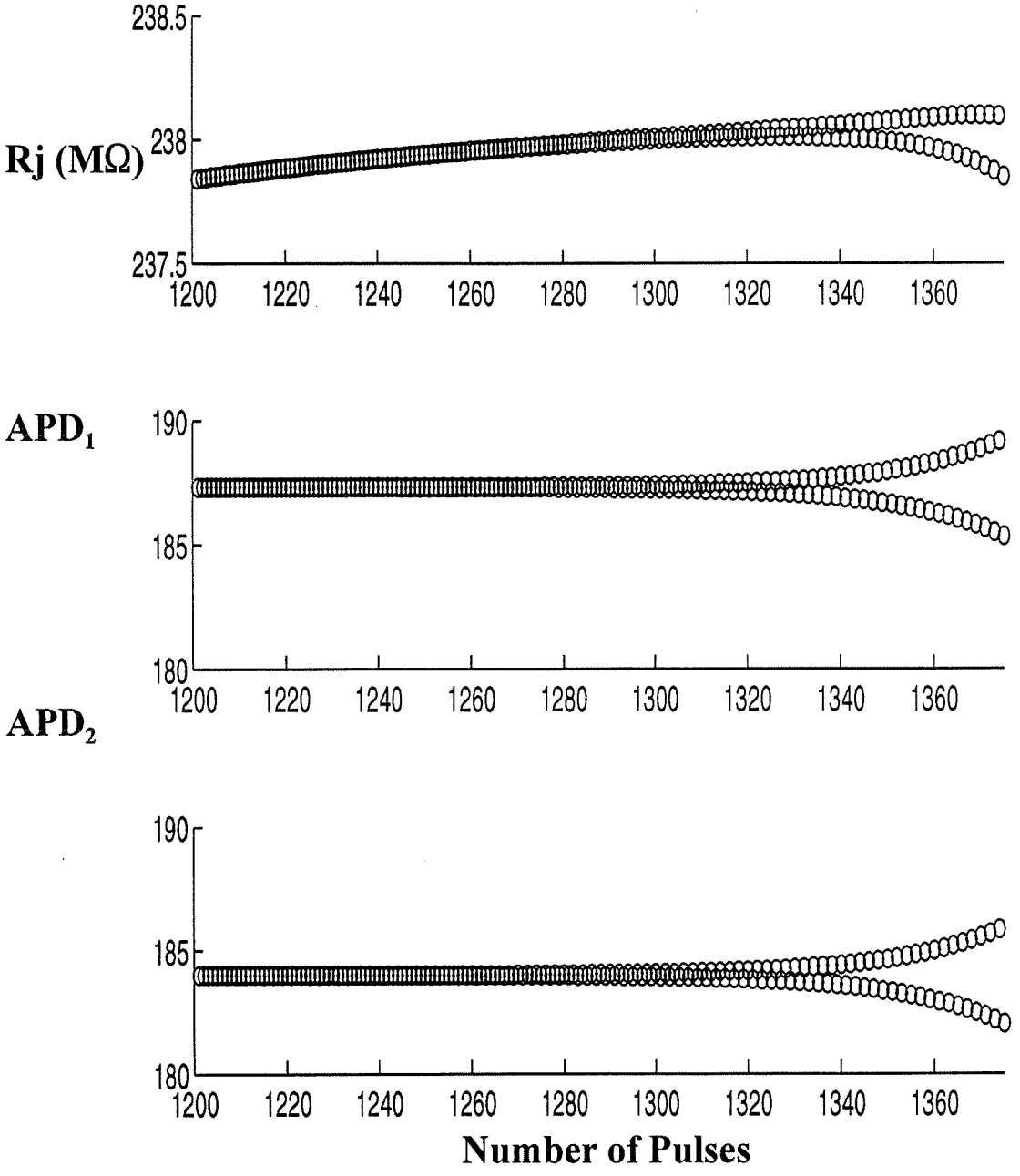

Figure 7.4.7: Patterns of Rj, APD_1 and APD_2 responses at the transition. BCL = 270 ms, Rb = 260 KΩ, and APD values in ms.

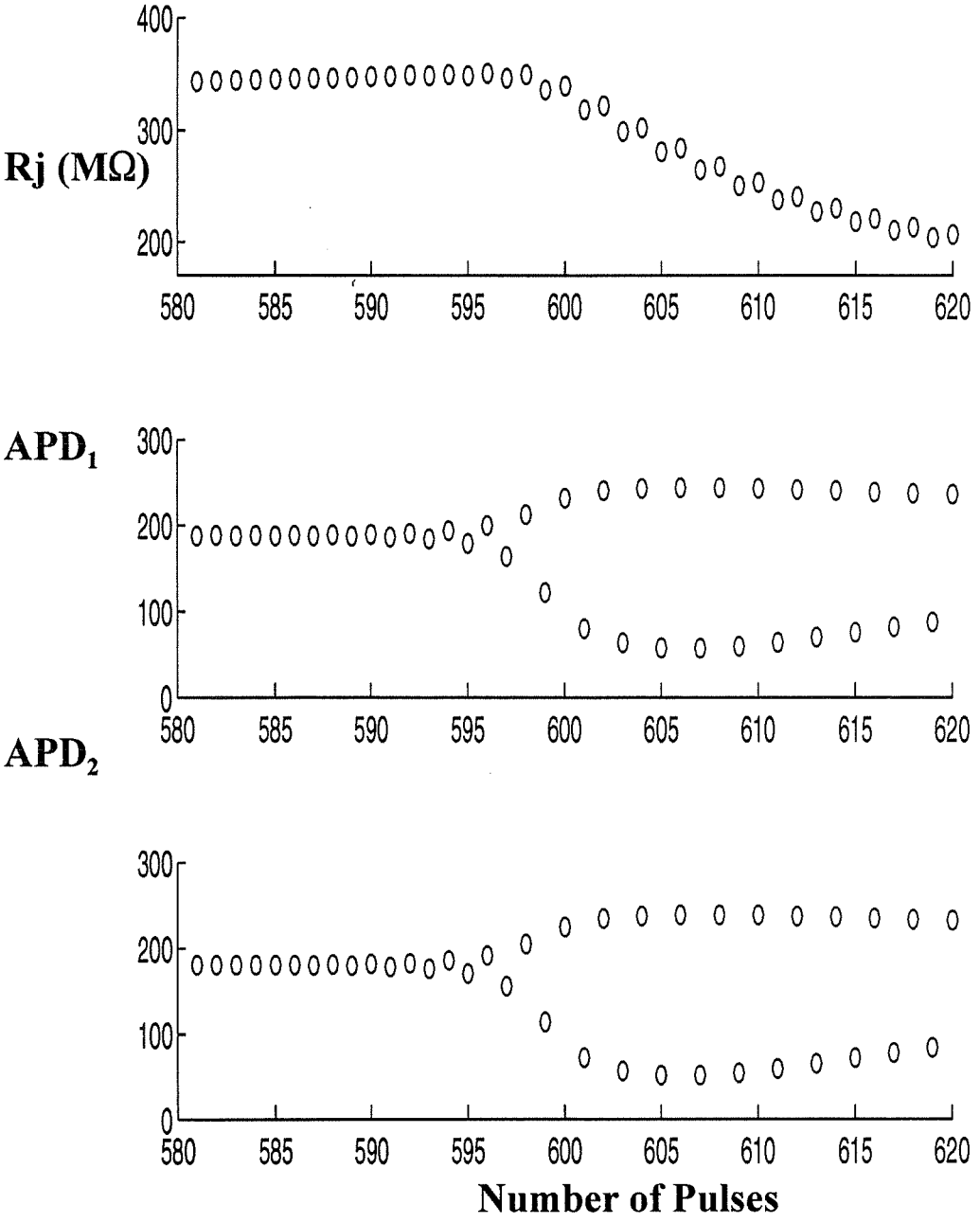

Figure 7.4.8: Patterns of Rj, APD_1 and APD_2 responses at the transition. BCL = 270 ms, Rb = 490 KΩ, and APD values in ms.

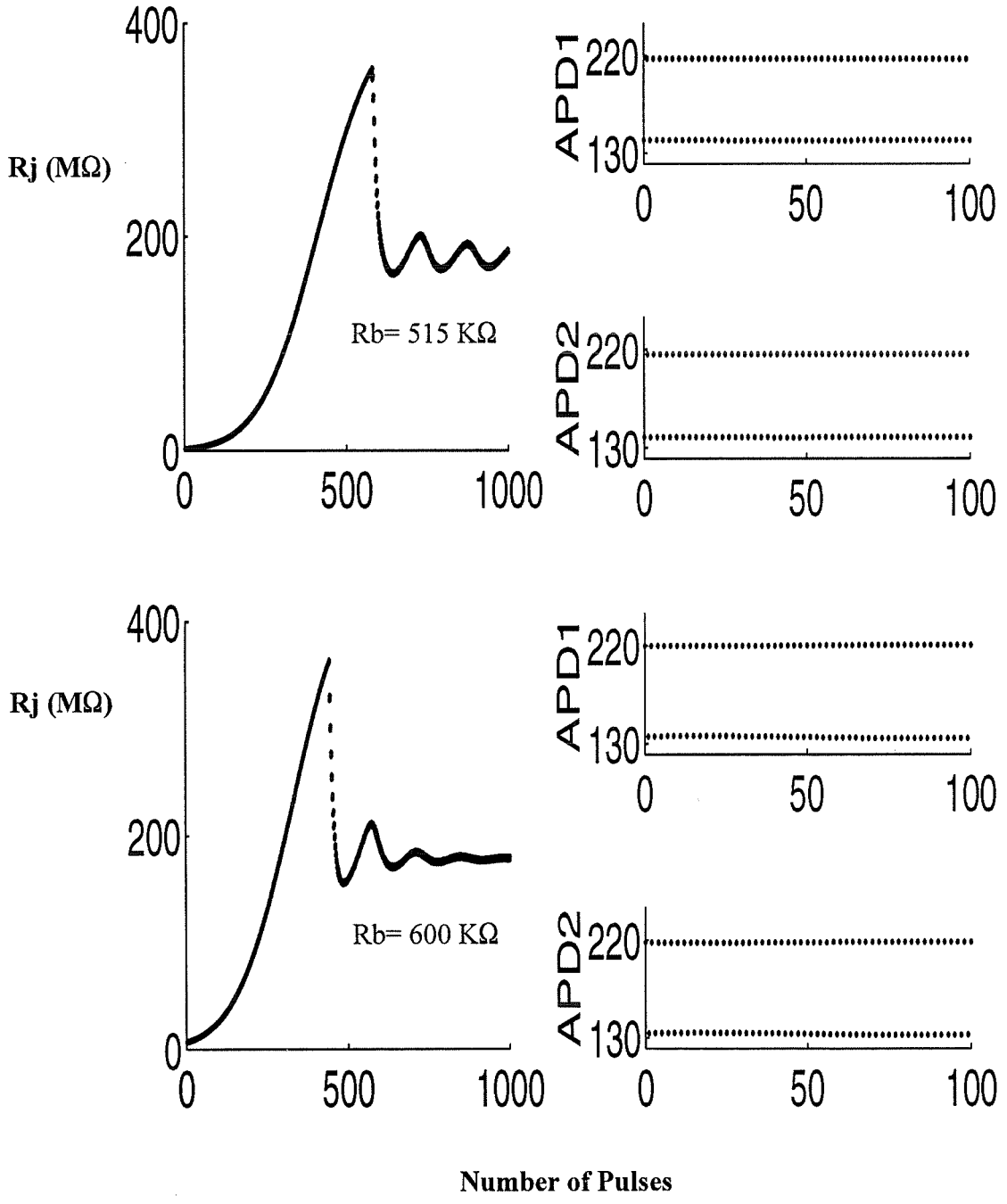

Figure 7.4.9: Behaviour of the two-cell system with BCL = 270 ms and Rb = 515 KΩ (top) or Rb = 600 KΩ (bottom). Transient and steady state Rj changes (left column) and corresponding APD_1, APD_2 responses (right column). APD values are in ms.

zones.

With Rb = 600 KΩ, the Rj oscillation is completely damped after less than 1000 pulses and the final alternation is between 177 and 179 MΩ. The steady state APD responses are regular alternations between 135 and 220 ms for APD_1, and between 133 and 217 ms for APD_2. The same type of behaviour for Rj and APD alternations occurs as Rb is increased further, as indicated in Table 7.4.2. In all cases, there is a transient increase to a maximum Rj, followed by a large sudden drop, with increasingly damped oscillations as Rb is increased.

Table: 7.4.2: Characteristics of 2:2 rhythm in C1 and C2 as Rb is changed with a BCL of 270 ms. Alternations in Rj and APD values correspond to the steady state after several thousand pulses. Note that stable 2:2 rhythm occurs with Rb ≥ 515 KΩ.

Rb (KΩ)	Maximum transient Rj (MΩ)	Alternation in Rj (MΩ)	Max / Min APD Values	
			APD_1 (ms)	APD_2 (ms)
260	238	156-223	218 / 138	215 / 135
490	360	170-194	222 / 128	220 / 116
515	361	178-181	217 / 141	215 / 139
600	363	177-179	220 / 135	217 / 133
900	371	185-188	226 / 121	223 / 118
1000	373	187-190	226 / 116	225 / 114
4000	375	259-263	244 / 55	240 / 50
6000	380	278-282	248 / 33	243 / 25

Since the maximum transient Rj is quite large and increases further as Rb is increased (Table 7.4.2), there are some blocked responses in C2 which cause an abrupt decrease of Rj (Figs 7.4.6 and 7.4.9) toward lower values which are in the vicinity of those reached during the steady state. This Rj adjustment may be oscillatory if the maximum Rj transient is not too large (Fig. 7.4.6) or more or less heavily damped if the maximum Rj transient is larger (Figs 7.4.9 and 7.4.10). The 2:2 rhythm is maintained in both C1 and C2, with increasing amplitude in the alternation. As indicated in Table 7.4.2, minimum APD_2 values of 50 or 25 ms are reached with Rb = 4000 or 6000 KΩ, with corresponding maximum APD_2 values of 240 or 243 ms.

It is apparent from the pattern of 2:2 responses of Table 7.4.2 that a further Rb increase above 6000 KΩ will lead to blocked C2 responses in view of the minimum APD_2 = 25 ms at Rb = 6000 KΩ. When that situation occurs, one can expect serious perturbation in the rhythm of both C1 and C2, which are likely to be of the type seen with Rb around 15,000 KΩ and BCL = 500 ms (Fig. 7.3.1.). The mix of rhythms is expected to be 2:2 and 2:1 in both C1 and C2.

Increasing Rb to a much larger value at BCL of 270 ms leads to a large Rj and complete cell decoupling, such that the behaviour of C1 will then approach that of the space-clamped membrane (Chapter IV). Fig. 7.4.11 illustrates the case for Rb = 50,000 KΩ which causes a transient Rj increase to a plateau at 18,000 MΩ after about 1500 pulses (column 1, panel 1).

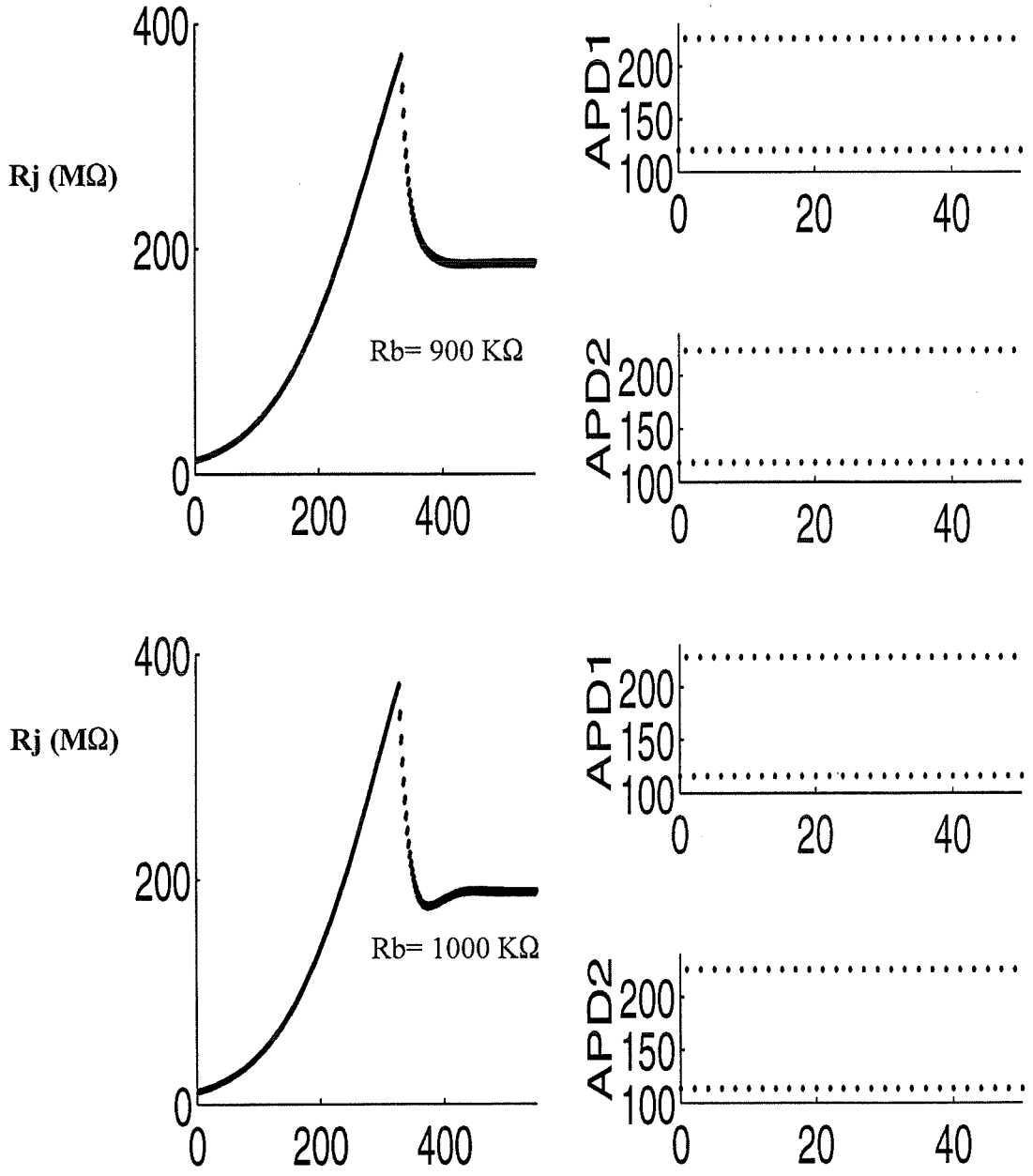

Figure 7.4.10: Behaviour of the two-cell system with BCL = 270 ms and Rb = 900 KΩ (top) or Rb = 1000 KΩ (bottom). Transient and steady state Rj changes (left column) and corresponding APD_1, APD_2 responses (right column). APD values are in ms.

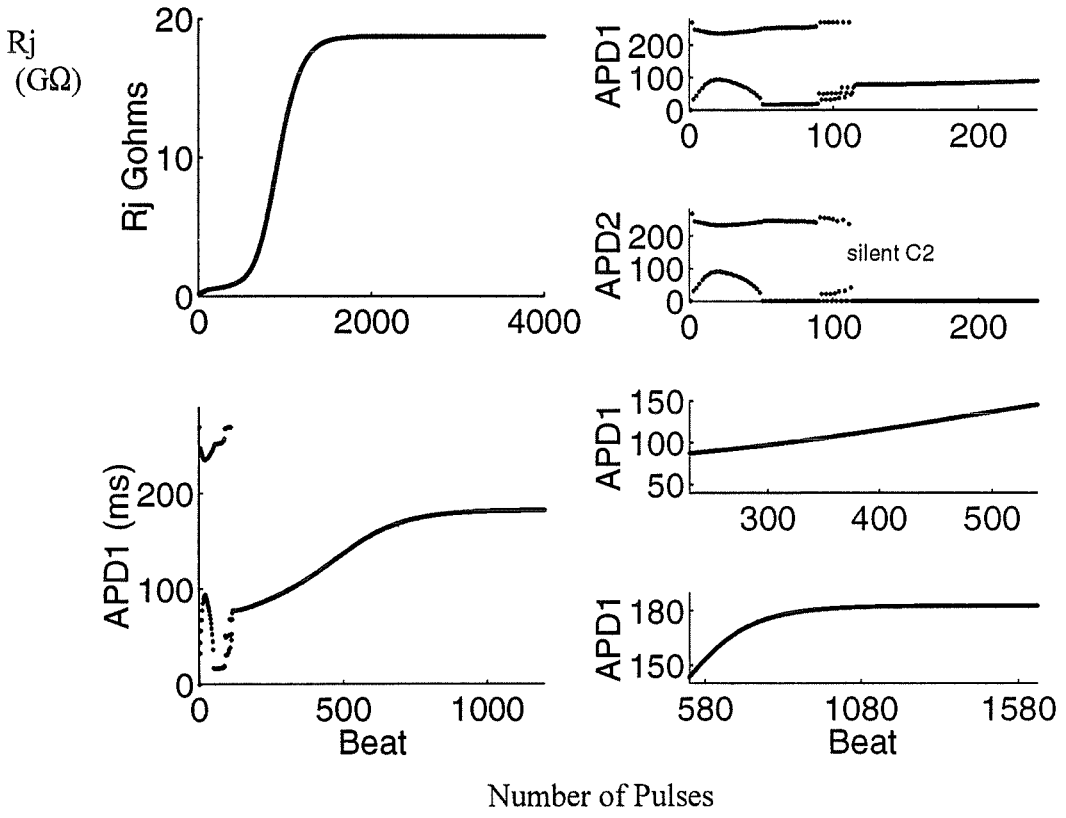

Figure 7.4.11: Same legend as in Fig. 7.4.6 with BCL = 270 ms and Rb = 50,000 KΩ.

7.5 Summary and Conclusion

In this chapter we described a $[Ca]_{in}$-dependent model of the cardiac gap junction resistance (Chapter VI) to study the entrainment behaviour of a pair of coupled myocytes. Although the gap junction model has a large time constant (varying between 18 and 35 seconds), its very high sensitivity to changes in pCa_{in} generates a sizable decrease (of the order of 1%) in the magnitude of the channel gating variable (r) during the action potential. Because of the asymmetric time constant values (18 seconds when pCa_{in} decreases from its resting level versus 35 seconds during the subsequent pCa_{in} increase, Fig. 6.4.1), the r value reached during the action potential plateau does not return to its initial level if the subsequent DIA is sufficiently short. In this way, there can be a cumulative decrease of r and a corresponding increase of Rj during pacing at a fast rhythm. Consequently, even if the MBR model lacks an appropriate mechanism of $[Ca]_{in}$ accumulation, there can be a build-up of Rj.

The behaviour of the dynamic gap junction model (Rj-coupled system) is best understood by comparison with the fixed resistance model (R-coupled system) described in Chapter V. For a BCL in the range of 500 ms, the response of the R-coupled system changes from period 1 to period 2 for $R > 425$ MΩ (Fig. 5.7.1). A similar phenomenon is seen in the Rj-coupled system. There is a range of Rb for which the stable response of the system is a mix of period 1 and period 2 responses, with Rj oscillating at the

transition between the two zones. As Rb increases, the periodic response becomes increasingly close to a period 2 response, until Rb becomes high enough to give a plain period 2 entrainment. When Rj is increased further, it approaches the value at which the next transition of the fixed resistance model occurs, this time between period 2 and period 3. The response of the Rj-coupled system then becomes a mix of period 2 and period 3 until Rb becomes high enough to escape the border of the transition zone.

At a shorter BCL of 300 ms, the fixed resistance model has a transition from an AR of 1:1 to an AR of 2:2 in C1 and to an AR of 2:1 in C2 when R = 362 MΩ. For Rb =1000 KΩ, Rj oscillates between 320 and 372 MΩ and the APD responses change from 1:1 to oscillatory. The global cycle has a long sequence during which the two cells have a 1:1 rhythm with almost constant APD, followed by a short sequence of growing alternations leading to a blocked response in C2, and a short sequence of decreasing alternations returning the APDs to a level where the response is sustained. Again, as Rb is increased, the relative contribution of 2:2 in C1 and 2:1 in C2 increases and eventually dominates.

At BCL = 270 ms, the R-coupled system exhibited a large zone of 2:2 in C1 and C2 with R between 150 and 240 MΩ. In the Rj-coupled system, the system displayed transitions from 1:1 rhythm at Rb less than 260 KΩ, to the modulated alternation rhythm at 260 < Rb < 490 KΩ, and then to 2:2 stable rhythm at Rb > 490 KΩ. The first modulated solution has a long stretch of almost 1:1 responses, interrupted by a short

sequence of low amplitude growing and then decreasing alternations. As Rb increases, the alternations increase in amplitude and the modulation becomes smaller, until the response becomes a pure 2:2 in both cells. However, the fixed resistance model has a marked hysteresis at this level of BCL. The transition from 1:1 to 2:2 occurs at a higher level in the bifurcation map (Fig. 5.7.1) when R is increased gradually during pacing instead of being always reset at rest. This procedure is closer to what happens in the Rj-coupled system where Rj increases gradually.

Consequently, the oscillatory behaviour found in the Rj-coupled system for a BCL of 270 ms corresponds to a different bifurcation map than the one depicted in Fig. 5.7.1. An additional phenomenon is also illustrated in this case, showing that a large overshoot of the Rj value beyond the bifurcation locus does not prevent the Rj-coupled system to end up in an oscillatory steady state around the critical Rj of 175-180 MΩ for a BCL of 270 ms. For example, in Fig. 7.4.6 (upper left panel), an overshoot to Rj = 260 MΩ is followed by a saturation plateau and then by large Rj oscillations between 156 and 223 MΩ with a period of about 370 pulse intervals. On the other hand, if the Rj overshoot reaches a higher value, the saturation plateau disappears and the oscillation amplitude is much smaller (between 170 and 194 MΩ, bottom left panel of Fig. 7.4.6) and attenuates much more rapidly. Indeed, a still larger overshoot may lead to a critically damped oscillation and a steady state oscillation of very small amplitude, such as in Fig. 7.4.10 These data are summarized in Table 7.4.2 which shows the magnitude of the Rj overshoot (maximum Rj transient) and the corresponding steady state oscillation amplitudes

(alternations in Rj). In this case also, one can reach the next bifurcation locus (between 2:1 and 2:2 rhythms) if Rb is raised to a sufficiently high value. This occurs for Rb > 6,000 KΩ.

The global picture that emerges is as follows. The Rj control mechanism operates via a negative feedback loop which adjusts Rj according to the rate and pattern of firing of both C1 and C2. For the range of BCLs explored in this chapter, the R-coupled system always ends up in a fixed entrainment rhythm, with relatively low period (1, 2, 3), simple firing ratio (1:1, 2:2, 2:1, ...), and multistability at low BCL. In the Rj-coupled system, any change of pattern involving the appearance of alternations or blocked responses always induced a decrease of Rj which tended to restore the former pattern of response. On the other hand, any sequence of responses with a more sustained activation ratio tended to increase Rj. As a result, the system oscillates between the two patterns, until the value of Rb becomes high enough to definitively escape the border region. The global Rb × BCL bifurcation map of the Rj-coupled system thus resembles that of the R-coupled system, except that the transition between the main entrainment zones are now gradual, with a set of intermediate periodic solutions.

CHAPTER VIII

GENERAL DISCUSSION

The anatomical structure of the myocardium as an assembly of discrete cells separated by periodic gap junctions was established more than 40 years ago. However, until recently the propagation of electrical excitation in cardiac muscle has been characterized as though it occurred in a syncytium. The effects of the structural discontinuities introduced by the junctions were not considered important, and activation was analyzed on the basis of continuous cable models utilized successfully for nerves (continuous cable theory) (Jack et al., 1975). Moreover, various normal and abnormal characteristics of propagation were traditionally associated with membrane properties alone, while effects of the anatomical structure of the myocardium were, for the most part, ignored. Such propagation phenomena include slow conduction, decremental conduction, conduction block, and changes in action potential duration and refractory periods. All of these characteristics are recognized as conditions that play an important role in causing reentrant arrhythmias.

Experimental results (Spach et al., 1981; 1982) have documented electrical properties of cardiac muscle that could not be explained on the basis on continuous cable theory. For example, the maximum dV/dt of the upstroke was observed to increase as

propagation velocity decreased due to a wider angle of propagation relative to the long cell axis. In addition, the importance of the anatomical structure of cardiac muscle in determining conduction velocity and source configuration (Plonsey & Barr, 1984; Barr and Plonsey, 1984; Roberge et al., 1986; Leon and Roberge, 1991), as well as its possible role in causing conduction abnormalities (Spach et al.,1981; 1990) were emphasized. It is clear that these effects and the possibility that they arise from the discrete cellular structure of the myocardium can only be examined using a model that includes microscopic discontinuities (gap junctions) at the cellular level. This philosophy was adopted in the present work for the study of a system of two coupled myocytes.

The effects of a discrete pattern of resistive barriers on propagation of the cardiac action potential were studied by Joyner (1982). In his study, the discontinuities were introduced by discretizing a continuous cable into elements (Δx) equal to the cell length and both the cytoplasmic resistance and junctional resistance were incorporated in an effective longitudinal resistance. Diaz et al. (1983) showed that the maximum dV/dt of the upstroke increased during slower propagation on a discontinuous cable, in agreement with experimental observations (Spach et al., 1981). Rudy and Quan (1987) studied propagation in a cardiac fibre model containing a periodic intercalated disk structure and showed, among other things, that the maximum dV/dt of the upstroke displayed a biphasic behaviour as a function of increasing intercalated disk resistance. Cole et al. (1988) compared computer simulations of propagation in cardiac tissue based on a discontinuous cable model with propagation along the longitudinal axis of small papillary

muscle under conditions of elevated intercellular resistance due to perfusion with octanol. Octanol reversibly reduced the velocity of propagating action potentials by some 53 to 6.6 cm/s before block occurred, and changed the maximum dV/dt of the upstroke in a biphasic manner (increasing from about 135 V/s in controls to 202 V/s when the velocity was 21 cm/s, and then declining to about 60 V/s just before block). These effects were successfully reproduced with a cable incorporating fixed gap junction resistances.

The focus of the present work is complementary to that of these earlier studies of discontinuous cardiac propagation. Our attention is centered on the long term behaviour of a system of two coupled myocytes, as documented through its response to regular pacing. The frequency entrainment features of the model are described as transitions (or bifurcations) between different types of stable or periodic model responses (or rhythms). The set of transitions obtained with variations of a given parameter and a range of BCL values constitutes a bifurcation map. The analysis of these bifurcation maps is a powerful means to gain insight into the dynamic characteristics of the system and to extrapolate the observations to cardiac tachyarrhythmias. We analyzed the space-clamped MBR model in Chapter IV and a pair of myocytes coupled by a fixed resistance in Chapter V. Following the description of a rate-dependent model of the gap junction resistance in Chapter VI, we proceeded to analyze the consequence of its presence in the two-cell system in Chapter VII.

8.1 Frequency Entrainment of the Space-Clamped MBR Model

The simulation results described in Chapters II-IV document the dependence of the MBR model on the stimulus parameters, and its behaviour during regular pacing (range of BCLs) for stimuli of various strength (I_{stim}) and duration (T_{stim}). Since the MBR model is a highly nonlinear dynamic system, its stable entrainment characteristics are sensitive to the conditions that prevail prior to the application of a given BCL. For reasons of simplicity, we have chosen to apply any given BCL when the system has returned to its resting state, thereby eliminating any residual effect of anterior repetitive activity. In correspondence with experimental studies of biological excitable membranes, we used a rectangular current pulse (duration T_{stim} and intensity I_{stim}) to produce an active response (action potential). Our study amply demonstrates the exquisite sensitivity of the MBR model response to these stimulus parameters.

The dynamic behaviour of the MBR model (see Chapter II and Appendix A) could be largely characterized by a threshold or excitability recovery function, Thr(DIA), and a restitution function, APD(DIA). With nominal parameter values, Thr(DIA) is invariant with respect to the preceding (or conditioning) action potential (i.e., memory-free excitability recovery) when the BCL is changed, provided that the test stimulus pulse duration (T_{stim2})

is not too long and that the conditioning stimulus pulse (T_{stim1} and I_{stim1}) is not too long nor too strong. Briefly, Thr(DIA) is practically insensitive to the conditioning stimulus parameters if the system is close to its resting state. Thus a strong I_{stim} of long duration affects Thr(DIA) by increasing the value of I_x at low DIA, so that Thr(DIA) needs to be larger in order to counterbalance a larger outward K^+ current. On the other hand, T_{stim2} has an important influence on Thr(DIA).

APD(DIA) corresponds to a smooth curve which is not importantly shifted when the BCL is changed, thereby indicating that the APD generating mechanism exhibits only a limited memory effect (Vinet and Roberge,1994). In addition, APD(DIA) and the dispersion of APD values are essentially independent of the stimulus parameters if the system is close to its resting state when the stimulus is applied (Chapter III, Section 3.5). Increasing T_{stim2} shortens the APD mainly at low and medium DIA values. The most potent modifier of the APD is I_{stim2}, with the largest effects obtained when both T_{stim2} and I_{stim2} are large, causing an APD increase at low DIAs and a reduction at medium and large DIAs. This reduction of the dispersion of APD values has important implications for the frequency entrainment response of the MBR model.

The regular pacing technique adopted in the present study, by teasing out existing periodic patterns of responses at a given BCL, makes the bifurcation map a source of long term information about the space-clamped MBR model behaviour. Various bifurcation scenarios have been described for different versions of the BR and MBR

models in previous studies (Vinet et al., 1990; Rudy et al., 1990; Lewis and Guevara, 1990; Jalife et al., 1991). In these studies, T_{stim} values ranged from 1 to 100 ms while I_{stim} ranged from I_{thR} to $1.5I_{thR}$. Our present simulations results (using T_{stim} up to 45 ms and I_{stim} up to $5.25I_{thR}$) confirm the previous observations of various authors concerning three major bifurcation types as follows:

1) Period doubling occurs at low and medium I_{stim} when T_{stim} is short, and at medium I_{stim} when T_{stim} is longer. A simple iterative difference equation model was used to show that period doubling occurs when dAPD/dDIA $>$ 1.

2) Period adding exists at both low and high I_{stim} for large T_{stim} in the MBR model, due to the important reduction of APD dispersion which eliminates the region of APD(DIA) where the slope is larger than 1. Period adding also occurs at low I_{stim} when Thr(DIA) is a monotonically increasing function of decreasing DIA, such that I_{stim} may be set a value below Thr(DIA).

3) The 1:1 $\rightarrow$ 2:2 $\rightarrow$ 1:1 $\rightarrow$ 1:0 or 1:1 $\rightarrow$ 1:0 bifurcation cascade cannot be predicted by the iterative difference equation model since the Thr(DIA) and APD(DIA) functions do not include the basic underlying phenomena associated with blocked responses.

A new observation arising from the present study is the occurrence of blocked responses which cause a resetting of the response when I_{stim} is quite large, that is under conditions where Thr(DIA) and APD(DIA) are importantly modified by the applied

stimulus. The resetting effect causes an interruption of the bifurcation cascade after period 2, such that the system then moves to 1:0 entrainment.

8.2 Frequency Entrainment of a Pair of Coupled Myocytes

8.2.1 The R-Coupled System

The two-cell system coupled through a fixed resistance (R-coupled system) makes it possible to investigate two major aspects of intercellular coupling, namely the reciprocal loading of the two cells and the modulation of the intercellular current flow (Ig) as R is varied. Since the two coupled myocytes have identical properties, the coupling current depends on the value of R and it modulates the activation delay of C2 relative to C1.

The simulation study was carried out with a short stimulus (duration of 1 ms) of about 1.25 times the resting threshold of C1 when coupled to C2 (Chapter V). In the light of our simulation results with the space-clamped membrane (see Section 8.1 above and Chapters II, III and IV), these stimulus parameters are unlikely to affect the Thr(DIA) and APD(DIA) function of C1 and the reported observations can be taken to reflect correctly the frequency entrainment characteristics of the system.

The results have shown, for R < 170 MΩ, that both C1 and C2 behave as a single unit, whereby the action potential of C1 acts as an effective stimulus for C2. Each cell then exhibits the same period doubling bifurcation structure (as illustrated for C1 in Fig.5.7.1). There is only a small delay in the firing of C2 and its effects on the behaviour of the two-cell system is negligible.

When R is increased, namely in the range of 170 < R < 355 MΩ, the firing rate of C2 decreases since some of the C1 impulses do not succeed in exciting C2. There is then a variable delay between the C1 and C2 upstrokes, which affects the potential difference across R and thus changes Ig. We have not investigated this particular characteristic of the system in detail. The net result, however, is a continued period doubling bifurcation for both C1 and C2. The specific features of the C1 and C2 activation ratio bifurcation maps differ somewhat when C2 exhibits blocked responses.

When R is larger than 355 MΩ, the delay in activation between C1 and C2 increased and is reflected by the augmentation of the duration of the coupling current (Ig). In this range of R, Ig is low in amplitude but large in duration and has a biphasic behaviour. During a blocked response in C2, Ig drains a large amount of current from C1, which in turn diminishes APD_1 dramatically.

In this range of R values, the APD(DIA) curves for C1 were flat, with a low and a high segment. The first segment existed at high DIAs when C2 fired, while the lower

one was a consequence of the blocked responses in C2 at low DIAs. This transformation of the APD(DIA) curves eliminated the possibility of using a simple iterative model to predict the bifurcation structure of the system for all values of R.

The bifurcation map constructed from the cascade of responses, in this range of R values, displayed period adding cascades. The appearance of large period values (i.e., period 8, 9, 10, 11, 12, 13) at lower R ($<$495 MΩ) diminishes with the increase of R. Large periods were replaced by period 1 at lower BCLs. Then, when R was increased above 495 MΩ, only period 1, 2, 3, 4 were observed as the BCL was decreased. At R = 519, the system exhibited a transition from 1 $\rightarrow$ 2 $\rightarrow$ 1. Period 1 became prominent for R $\geq$ 520 MΩ.

The increase of R from 355 MΩ to 519 MΩ diminished the activation ratio (AR) in C2 and promoted higher ARs in C1. During the period adding bifurcation, C2 exhibited ARs of the form of n:1, while C1 ARs had the pattern of n:n-q , where q is a decreasing function with the increase of R.

8.2.2 The Rj-Coupled System

The R-coupled system made it possible to investigate the two major aspects of intercellular coupling, namely the reciprocal loading of the cells and the modulation of

the current flow between the two cells by the junctional resistance. When the coupling resistance is constant (junctional resistance R), these phenomena depend only on the difference in activation latency between the two cells. On the other hand, when the coupling resistance depends on the rate of firing of the two cells (junctional resistance Rj), we are in the presence of a negative feedback mechanism whereby an increase in the rate of firing of either cell increases Rj and thus reduces the coupling current. This is a potent mechanism to limit the rate of firing of the follower cell (second cell, not directly stimulated) and to simplify the bifurcation structure of both cells. In addition, when Rj is increased the firing rate of the second cell is reduced and Rj is forced to decrease.

The global picture that emerges is as follows. The Rj mechanism operates via a negative feedback loop which adjust Rj according to the rate and pattern of firing of both C1 an C2. This negative feedback is very strong when both C1 and C2 exhibit 1:1 responses at intermediate to high pacing rates. Then Rj increases rapidly to a maximum during the transient phase. Depending on the location of this maximum on the R bifurcation map (for the pacing rate considered, Chapter V, Section 5.7), the system will tend to adopt a steady state behaviour which is locked on the immediately lower transition locus. Since the transition between 1:1 and 2:2 responses is the most accessible at slow and intermediate pacing rates, it has received most of our attention in the present study. The observed steady state oscillations in Rj, APD_1 and APD_2 values thus reflect the hunting behaviour of a negative feedback system around some equilibrium

state. The ensemble of possible equilibrium states corresponding to different Rb and BCL values that described C1 and C2 bifurcation maps is similar to that of Fig. 5.7.1.

8.2.3 The Rj Model

This work has served to clarify some aspects of the role of the gap junction resistance (Rj) during repetitive activity of pair of myocytes. The gap junction as a calcium-dependent channel has not been considered earlier. Even though the postulated role of $[Ca]_{in}$ in modulating the gap junction resistance dates back to the work of Engelmann in 1877, it was tested and documented by the work of Deleze (1965) and Lowenstein (1966). Until now, no mathematical model has been used to characterize this calcium dependency. The experiment of Noma and Tsuboi (1987) provided a direct relationship between Rj and $[Ca]_{in}$. Maurer and Weingart (1987) showed similar results in a different setting, using higher $[Ca]_{in}$. Although the results of Noma and Tsuboi are not identical to those of Maurer and Weingart, both experiments showed a very sensitive calcium-dependency of the gap junction resistance.

The other important factor affecting the gap junction resistance is the intracellular pH (pH_{in}). Many studies and experiments had shown that lowering pH_{in} provokes an increase in the gap junction resistance (Rose et al., 1978; Hoyt et al., 1990.; White et al., 1990; Israel et al., 1990). This controversy continued in recent years, with several articles suggesting different and more complex interactions between $[Ca]_{in}$, pH_{in} , and Rj.

White et al. (1990) measured Rj in isolated cell pairs with both cells kept intact. $[Ca]_{in}$ and pH_{in} were changed by extracellular interventions. The concentration of protons and Ca^{2+} ions were monitored with fluorescent dyes and ion-sensitive microelectrodes. Their results showed that a decrease of pCa_{in} from 6.83 to 6.288 was accompanied by an increase of Rj. The increase of Rj was eliminated if pCa_{in} was not decreased more than 6.62. Alternatively, decreasing pCa_{in} produced no augmentation in Rj if acidification was prevented. This finding suggested that both $[Ca]_{in}$ and pH_{in} (*synergistic* interaction) are necessary to produce electrical uncoupling. Thus the role of calcium, during low pH_{in}, could not be ruled out as the mechanism that mediated these changes in the gap junction resistance.

In 1990, Peracchia challenged the pH hypothesis and demonstrated that the increase in gap junction resistance with acidification in crayfish septate axons was closely related to the changes in intracellular calcium but not to those of hydrogen ion concentration. In recent experiments, Toyama et al. (1994) have investigated the modulation of the gap junction resistance by Ca-calmodulin. Their results were consistent with those of Noma and Tsuboi. The sum of these observations point to $[Ca]_{in}$ and pH_{in} as factors affecting Rj during repetitive activity. We expect Rj to change since both $[Ca]_{in}$ and pH_{in} have been shown to vary during an action potential. Even if the Rj model described in this work focused on the role of $[Ca]_{in}$ and ignored the influence of pH_{in}, it provides a first quantitative illustration of the modulation of Rj through repetitive firing.

In the MBR model, the $[Ca]_{in}$ formulation is not an accurate reflection of the calcium variations of cardiac tissue. The physiological pCa_{in} range in normal tissue does not exceed 7 and may not decrease below 6.2. The MBR formulation overevaluated the calcium variations. Moreover, there is no $[Ca]_{in}$ accumulation in the MBR model during repetitive activation. Thus, at the end of each action potential, pCa_{in} always return to its base level. More recent models, such as the phase II-LR model (Luo and Rudy, 1994), include moderate calcium accumulation and could be used in place of MBR model. In the phase II-LR model, a BCL change from 300 to 100 ms caused $[Ca]_{in}$ variations corresponding to a pCa_{in} of 6.2 to 6.6 (unpublished results). This calcium accumulation by itself is enough to change Rj and r_∞ values (Fig. 6.6.1). However, the Rj variations during each action potential (shown in Fig. 7.2.2) will be smaller than those described in the present study. We expect, therefore, that a mechanism of intracellular Ca^{2+} accumulation during repetitive activity will provide qualitatively similar results.

8.3 Conclusion

Computer modeling is a powerful tool to examine physiological hypotheses. In many instances only partial information is available and the model can serve to illustrate the possible behaviour of unobserved variables. In most cases, the experimental setup is complicated and it can be quite difficult to maintain stable conditions since the properties of the tissue vary with time.

The MBR model used in this work has the merit of being relatively simple and well understood. We used frequency entrainment protocols extensively since it is a powerful mean to characterize the medium term dynamical properties of the membrane model and the two-cell system. The approach adopted has made it possible to compare the frequency entrainment responses of the isolated cell to those of the two-cell system involving either a fixed resistance (R-coupled system) or a variable (Rj-coupled system) coupling resistance.

Our simulation results can be compared to the experimental observations of Tan and Joyner (1990) who studied a pair of cardiac cells coupled by an RC circuit. They showed that a fast repetitive response arose due to electrical loading of the first cell (by shortening the APD of that cell) and that it was periodically disturbed after each activation of the second cell, which removed the loading on the first cell. Our results with the R-coupled system are exactly similar. When the coupling resistance is controlled by the firing rate of the two cells (Rj-coupled system), however, the sustained repetitive firing of the first cell may remain unaffected even when the follower cell is active. It follows, therefore, that the negative feedback process of Rj changes ensures a tighter coupling of cardiac cells than would be possible with a fixed gap junction resistance.

BIBLIOGRAPHY

ALLESSIE M.A., BONKE F.I.M., SCHOPMAN F.J.G., (1977). "Circus Movement in Rabbit Atrial Muscle as a Mechanism of Tachycardia. III. The "Leading Circle" Concept: A New Model of Circus Movement in Cardiac Tissue without the Involvement of an Anatomical Obstacle". *Circ Res.* 41:9-18.

ALLESSIE M.A., BONKE F.I.M., SCHOPMAN F.J.G., (1973). "Circus Movement in Rabbit Atrial Muscle as a Mechanism of Tachycardia". *Circ Res.* 32:54-62.

ALLESSIE M.A., BONKE F.I.M., SCHOPMAN F.J.G., (1976). "Circus Movement in Rabbit Atrial Muscle as a Mechanism of Tachycardia. II. The Role of Nonuniform Recovery of Excitability in the Occurrence of Unidirectional Block, as Studied with Multiple Micro-Electrodes". *Circ Res.* 39:168-177.

BARR R.C., PLONSEY R. (1984). " Propagation of Excitation in Idealized Anisotropic two-dimensional Tissue". *Biophys J.* 45:1191-1202.

BASS B.G., (1975). "Restitution of the Action Potential in Cat Papillary Muscle". *Am. J. Physiol.* 228(6):1717-1724.

BEELER G.W., REUTER H. (1977). "Reconstruction of the Action Potential of Ventricular Myocardial Fibres". *J. Physiol.* Great Britain, 268:177-210.

BENNETT M.V.L. and SPRAY D.C., (1984). "Gap Junctions: Two Voltage-Dependent Gates in Series Allow Voltage Induced Steady State Cycling Around a Circular Reaction Scheme". (Abstract) *Biophys. J.* 45: 60a..

BENNETT M.V.L., BARRIO L.C., BARGIELLO T.A., SPRAY D.C., HERTZBERG E., SÁEZ J.C. (1991). "Gap Junctions: New Tools, New Answers, New Questions". *Neuron.* 6:305-320.

BERNSTEIN RC, FRAME LH (1990). "Ventricular Reentry Around a Fixed Barrier. Resetting with Advancement in an in Vitro Model". *Circulation.* 81:267-280.

BOYETT MR, JEWELL BR (1978). "A Study of the Factors Responsible for Rate-Dependent Shortening of the Action Potential in Mammalian Ventricular Muscle". *J. Physiol.* 285:359-380.

BOYETT MR, JEWELL BR (1980). "Analysis of the Effects of Change in Rate and Rhythm upon the Electrical Activity in the Heart". *Prog. Biophys. Mol. Biol.* 36:1-52.

BURT JM, SPRAY DC (1989). "Volatile Anesthetics Block Intercellular Communication Between Neonatal Rat Myocardial Cells". *Circ. Res.* 65:829-837.

BURT JM, MASSEY KD., MINNICH BN. (1991). "Uncoupling of Cardiac Cells by Fatty Acids: Structure-activity Relationships". *Am. J Physiol.* 29:C439-C448.

CHAY T.R., LEE Y.S. (1985). "Phase Resteing and Bifurcation in the Ventricular Myocardium. *Biophys. J.* 47:641-651.

CHIALVO D.R., MICHAELS D.C., JALIFE L (1990). "Supernormal Excitability as a Mechanism of Activation of Purkinje fibers". *Circ. Res.* 66: 525-545.

CLARK G.P.Y., (1987). "Approximate Confidence Limits for a Parameter Function in Nonlinear Regression". *Journal of the American Statistical Association.* 82: 221-230.

COLE W.C., PICONE J. B., SPERELAKIS N. (1988). "Gap Junction Uncoupling and Discontinuos Propagation in the Heart. A Comparison of Experimental Data with Computer Simulation". *Biophys. J.* 53:809-818.

DAHL G., ISENBERG G., (1980). " Decoupling of Heart Muscle Cells: Correlation with Increased Cytoplasmic Calcium Activity and with Changes of Nexus Ultrastructure". *J. Membrane Biol.* 53:63-75.

DAVIDENKO JM, PERTSOV AV, SALOMONSZ R, BAXTER W, JALIFE J (1992). "Stationary and drifting spiral waves of excitation in isolated cardiac muscle". *Nature.* 355:349-35.

DE BAKKER JMT, VAN CAPELLE FJL, JANSE MJ, WILDE AAM, CORONEL R, BECKER AE, DINGEMANS KP, VAN HEMEL NM, HAUER RNW (1988). "Reentry as a Cause of Ventricular Tachycardia in Patients with Chronic Ischemic Heart Disease: Electrophysiological and Anatomic Correlations". *Circulation.* 77:589-606.

DELEZE J. (1965). "Calcium Ions and the Healing-over of Heart Fibers". In Electrophysiology of the Heart. Edited by Taccardi B. and Marchetti G. Pergamon, New York. 147-148.

DELMAR M, IBARRA J, DAVIDENKO J, LORENTE P, JALIFE J (1991). "Dynamics of the Background Outward Current of Single Guinea Pig Ventricular Myocytes. Ionic Mechanisms of Hysteresis in Cardiac Cells". *Circ. Res.* 69(5):1316-1326.

DE MELLO WC (1982). "Cell-to-Cell Communication in Heart and other Tissues". *Prog. Biophys. Mol. Biol.*, Pergamon Press. 39:147- 182.

DE MELLO WC (1982). "Intercellular Communication in Cardiac Muscle". *Circ. Res.* 51(1):1-9.

DE MELLO WC (1989). "Cyclic Nucleotides, Ca and Cell junctions". Chapter 6, In: N. Sperelakis, W.C. Cole (Eds.), Cell interactions and gap junctions, CRC Press, Boca Raton, Florida, II: 85-94

DEWEY MM, BARR L (1964). "A Study of the Structure and Distribution of the Nexus". *J Cell Biol.* 23:553-585

DIAZ P.J., RUDY Y., PLONSEY R. (1983). "Intercalated Discs as a Cause for Discontinuous Propagation in Cardiac Muscle: a Theoretical Simulation". *Ann. Biomed. Eng.* 11:177-189.

DIFRANCESCO D., NOBLE D.(1985). "A Model of Cardiac Electrical Activity Incorporating Ionic Pumps and Concentrations Changes'. *Phil. Trans. R. Soc. Lond.* B307: 353-398,.

DROUHARD J-P, ROBERGE FA (1982). "The Simulation of Repolarization Events of the Cardiac Purkinje Fiber Action Potential". *IEEE Trans. Biomed. Eng., BME*-29(7):481-493.

DROUHARD J-P, ROBERGE F.A.(1987). "Revised Formulation of the Hodgkin- Huxley Representation of the Sodium Current in Cardiac Cells". *Comput. Biomed. Res.* Academic Press, Inc., 20:333-350.

EBIHARA L.E., JOHNSON E.A.(1980). "Fast Sodium Current in Cardiac Muscle. A Quantitative Description". *Biophys. J.* 32: 779-790.

ELHARRAR V, SURAWICZ B (1983). "Cycle Length Effect on Restitution of Action Potential Duration in Dog Cardiac Fibers". *Am. J. Physiol.* 244 (Heart Circ. Physiol. 13):H782-H792.

ENGELMANN T.W., (1877). "Vergleichende Untersuchungen zur Lehre von der Muskel- und Nervenelektricitat". *Pfluegers Arch.* 15:116-148.

FITZHUGH R (1955). "Mathematical Models of Threshold Phenomena in the Nerve Membrane". *Bull. Math. Biophys.* 17:257-278.

FRAME LH, PAGE RL, HOFFMAN BF (1986). "Atrial Reentry around an Anatomical Barrier with a Partially Refractory Excitable gap. A Canine Model of Atrial Flutter". *Circ Res.* 58:495-511.

FRAZIER DW, WOLF PD, WHARTON JM, TANG AS, SMITH WM, IDEKER RE (1989). "Stimulus-Induced Critical Point. Mechanism for Electrical Initiation of Reentry in Normal Canine Myocardium". *J Clin Invest.* 83:1039-1052.

GIAUME C., KORN, H.(1983). "Bidirectional Transmissions at the Rectifying Synapse: a Voltage-Dependent Process". *Science.* 220, 84.

GUCKENHEIMER J., HOLMES P.(1988). "Nonlinear Oscillation, Dynamical Systems and Bifurcation of Vectors Fields". Applied Mathematical Science Series, 42 New York: Springer-Verlag.

HARRIS A., SPRAY D.C., BENNET M.V.L.(1981). "Kinetic Properties of a Voltage-Dependent Junctional Conductance". *J. Gen. Physiol.* 77:95-117.

HAUSWIRTH O, NOBLE D, TSIEN RW (1968). "Adrenaline: Mechanism of Action on the Pacemaker Potential in Cardiac Purkinje Fibers". *Science*, 162:916-917.

HENRIQUEZ CS, PLONSEY R (1987). "Effect of Resistive Discontinuities on Waveshape and Velocity in a Single Cardiac Fibre". *Med. Biol. Eng. Comput.* 25:428-438.

HIRAMATSU Y., BUCHANAN J.W., KNISLEY S.B., GETTES L.S. (1989). "Rate-Dependent Effects of Hypoxia on Internal Longitudinal Resistance in Guines Pig Papillary Muscles". *Circ. Res.* 63:923-929.

HODGKIN AL, HUXLEY AF (1952d). "A Quantitative Description of Membrane Current and its Application to Conduction and Excitation in Nerve". *J. Physiol.* 117:500-544.

HOYT R.H., COHEN M.L., CORR P.B., and SAFFITZ J.E.(1990). "Alterations of Intracellular Junctions Induced by Hypoxia in Canine Myocardium". *Am. J. Physiol.* 258:H1439-H1448.

ISRAEL D.A, EDELL D.J.,MARK R.G.(1990). "Time Delays in Propagation of Cardiac Action Potential". *Am. J. Physiol.* 258:H1906-1990.

JACK J.J.B., NOBLE D., TSIEN R.W. (1975). "Electrical Current Flow in Excitable Cells", Oxford, Clarendon Press.

JASLOVE S. and BRINK P., (1986) "The Mechanism of Rectification at the Electrotonic Motor Giant Synapse of the Crayfish". *Nature.* 232, 63.

JOYNER RW, OVERHOLT ED, RAMZA B et al.(1984). "Propagation Through Electrically-Coupled Cells: Two Inhomogeneously-Coupled Cardiac Tissue Layers. *Am. J. Physiol.*, 247 (Heart Circ. Physiol. 16):H596-H609.

JOYNER RW, VEENSTRA R, RAWLING D, CHORRO A (1984) - "Propagation Through Electrically-Coupled Cells. Effects of a Resistive Barrier". *Biophys. J.* 45:1017-1025.

JOYNER RW, OVERHOLT ED. (1985). "Effects of Octanol on Canine Subendocardial Purkinje-ventricular Transmission". *Am. J. Physiol.* 249:H1228-H1231.

JOYNER RW, VAN CAPELLE FJL (1986)." Propagation Through Electrically Coupled Cells. How a Small SA Node Drives a Large Atrium". *Biophys. J.* 50:1157-1164.

KAMEYAMA M.(1983). " Electrical Coupling Between Ventricular Paired Cells Isolated from Guinea-Pig". *Heart. J. Physiol.* 336:345-357.

LEMIEUX D.R., ROBERGE F.A., SAVARD P. (1990). " Simulation of the Voltage Dependance of the Na, K Pump Applied to Cardic Cells". *J. Theor. Biol.* 150:73-91.

LEMIEUX DR, ROBERGE FA, JOLY D (1992). "Modeling the Dynamic Features of the Electrogenic Na,K Pump of Cardiac Cells". *J. Theor. Biol.* Academic Press, 154:335-358.

LEMIEUX DR, CHICOINE H., ROBERGE FA (1994). "Modeling a Non-inactivating Delayed Rectifier Cardiac Current Using Voltage Clamp Data". *J. Theor. Biol.* Academic Press, 169:363-373.

LEON L.J., ROBERGE F.A. (1990). "A New Cable Model Formulation Based on Green's Theorem" *Annals of Biomedical Eng.* 18:1-17.

LEWIS TJ, GUEVARA MR (1990). "Chaotic Dynamics in an Ionic Model of the Propagated Cardiac Action Potential". *J. Theor. Biol.*, Academic Press, 146:407-432.

LOEWENSTEIN WR (1966). "Permeability of Membrane Junctions". *Ann. N.Y. Acad. Sci.* 137:441-472.

LOEWENSTEIN WR (1982). "Cell-to-Cell Communication. Permeability, Formation, Genetics and Functions of the Cell-Cell Membrane Channel". Chapter 18, In: Andreoli, Hoffman, Fanestic (Eds.), Membrane Physiology, 335-345.

LOEWENSTEIN WR (1981). "Junctional Intercellular Communication: The Cell-to-Cell Membrane Channel". *Physiol. Rev.* 61(4):829-913.

LUO C.H., RUDY Y (1991). "A Model of the Ventricular Cardiac Action Potential: Depolaization, Repolaization, and their Intercation". *Circ. Res.* 68: 1501-1526.

LUO C.H., RUDY Y (1994). "A Dynamic Model of the Cardiac Ventricular Action Potential: II Afterdepolaization, Triggered Activity, and Potentiation". *Circ. Res.* 74: 1097-1111.

MARGIOTTA, J.F. and WALCOTT, B. (1983). "Conductance and Permeabilty of a Recitfying Electrical Synapse". *Nature.* 52: 305.

MATLAB (1992). "High Performance Numeric Computation and Visualization Software". The Mathworks Inc. Mass.

MAURER P., WEINGART R.(1987). " Cell Pairs Isolated From Adult Guinea Pig and Rat: Effects of $[Ca^{++}]_i$ on Nexal Membrane Resistance". *Pfluegers Arch.* 409:394-402.

METZGER P., WEINGART R.(1985). " Electric Current Flow in Cell Pairs Isolated From Adult Rat Hearts". *J. Physiol.* 366:177-195.

MOORE JW, RAMON F (1974). "On Numerical Integration of the Hodgkin and Huxley Equations for a Membrane Action Potential". *J. Theor. Biol.* 45:249-273.

NAGUMO J, ARIMOTO S, YOSHIZAWA S (1962). "An Active Pulse Transmission Line Simulating Nerve Axon". *Proc. IRE.* 2061-2070.

NOBLE D. (1987). "Experimental and Theoretical Work on Excitation and Excitation-Contraction Coupling in the Heart. In: Cardiac electrophysiology: Past, present and future. Part II, *Experientia.* 43 (11/12):1146-1150.

NOMA A., TSUBOI N. (1987). "Dependence of Junctional Conductance on Proton, Calcium and Magnesium Ions in Cardiac Paired Cells of Guinea-Pig". *J. Physiol.* 382:193-211.

NORDIN C. (1993). "Computer Model of Membrane Current and Intracellulart Ca^{2+} Flux in the Isolated Guinea Pig Ventricular Myocyte". *Am. J. Physiol.* 265 H2117-H2136.

PERACCHIA C. PERACCHIA L.L. (1981). "Histidine Protonation and Gap Junction Changes with Uncoupling". *Proc. Int. Biophys. Congr. 7th* Mexico City Mexico 154.

PERACCHIA C (1990). "Biophysics of Gap Junction Channels". Boca Raton, CRC Press.

PERACCHIA C (1990). "Increase in Gap Junction Resistance with Acidification in Crayfish Septate Axons Is closely Related to Changes in Intracellular Calcium But Not Hydrogen Ion Concentration". *J. Membrane Biol.* 113:75-92.

PLONSEY R., BARR R.C. (1988). "Bioelctricity, a Quantitative Approach". Plenum Press, New-York.

RAMON F., RIVERA A. (1987). "Gap Junction Channel Modulation. A Physiological Viewpoint. *Prog. Biophys.* 48:127 1987.

RASMUSSON R.L., CLARK J.W., GILES W.R., ROBINSON K., CLARK R.B., SHIBATA E.F., CAMPBELL D.L. (1990). "A Mathematical Model od Electrophysiological Activity in a Bullfrog Atrial Cell". *Am. J. Physiol.* 259: H370-H389.

ROBERGE F.A., VINET A. VICTORRI B. (1986)."Reconstruction of Propagated Electrical Activity Using Two-Dimensional Model of Anisotropic Heart Muscle". *Circ. Res.* 58 461-476.

ROOK M.B., JONGSMA H.J., GINNEKEN A.C. (1988). "Properties of Single Channels Between Isolatede Neonatal Rat Heart's Cells". *Am. J. Physiol.*,225, H770-H782.

ROSE B., LOWENSTEIN W.R. (1976) "Permeability of a Cell Junction and the Local Cytoplasmic Free Ionized Calcium Concentration: A Study with Aequorin". *J. Membrane Biol.*, 28:, 87-119.

ROSE B., RICK R. (1978)"Intracellular pH, Intracellular Free Ca, and Junctional Cell-cell Coupling. *J. Membrane Biol.* 44:377-415.

RÜDISÜLI A., WEINGART R. (1989). "Electrical Properties of Gap Junction Channels in Guinea-pig Ventricular Cell Pairs Revealed by Exposure to Heptanol. *Pflügers Arch.*415:12-21.

SJÖSTRAND FS, ANDERSSON E (1954). "Electron Microscopy of the Intercalated Disks of Cardiac Muscle Tissue". *Experientia.* 10:369.

SOMMER JR, SCHERER B (1985). "Geometry of Cell and Bundle Appositions in Cardiac Muscle: Light Microscopy". *Am J Physiol.* 248:H792-H803.

SOSINKY G.E., JÉSIOR J.C. CASPAR D.L.D. GOODENOUGH D.A. (1988). "Gap Junction Structures VIII. Membrane Cross-Sections. *Biophys. J.* 53:709-822.

SPACH MS, MILLER WT III, GESELOWITZ DB, BARR RC, KOOTSEY JM, JOHNSON EA (1981). "The Discontinuous Nature of Propagation in Normal Canine Cardiac Muscle. Evidence for Recurrent Discontinuities of Intracellular Resistance that Affect the Membrane Currents". *Circ Res.* 48:39-54.

SPACH MS, KOOTSEY JM (1983). "The Nature of Electrical Propagation in Cardiac Muscle". *Am J Physiol.* 244:H3-H22.

SPACH MS (1983). "The Discontinuous Nature of Electrical Propagation in Cardiac Muscle. Consideration of a Quantitative Model Incorporating the Membrane Ionic Properties and Structural Complexities". *Ann Biomed Eng.* 11:209-261.

SPRAY D.C., STERN J.H., and HARRIS A.L. (1982). "Gap Junctional Conductance: Comparison of Sensitivities to H and Ca Ions". *Proc. Natl. Acad. Sci.* 79:441-462.

TAN R.C, JOYNER R.W. (1990). "Electrotonic Influences on Action Potentials from Isolated Ventricular Cells". *Circ. Res.* 67:1071-1081.

TERARR DA., VICTORY JGG. (1988). "Influence of Halothane on Electrical Coupling in Cell Pairs Isolated from Guinea-pig Ventricle". *Br J. Pharmacol.* 94:509-514.

TOYAMA J., SUGIURA H., KAMIYA K., KODAMA I., TERASAWA M. HIDAKA H.(1994). "Ca^{2+}-Calmodulin Mediated Modulation of the Electrical Coupling of Ventricular Myocytes Isolated from Guinea Pig Heart". *J Mol. Cell Cradiol.* 26:1007-1015.

TURIN L. and WARNER A.E.(1977). "Carbon Dioxide Reversibly Abolishes Ionic Communication Between Cells of Early Embryo". *Nature.* 56: 270-285, 1977.

TURIN L. and WARNER A.E. (1980). "Intracellular pH in Early *Xenopus* Embryos: Its Effect on Current Flow between Blastomeres". *J. Physiol.* 300:489-501, 1980.

UNWIN P.N.T., ZAMPIGHI G. (1980). "Srtucture of the Junction between Communicating Cells". *Nature.* 283:545-549.

VICTORRI B, VINET A, ROBERGE FA, DROUHARD J-P (1985). "Numerical Integration in the Reconstruction of Cardiac Action Potentials Using Hodgkin-Huxley-Type Models". *Comput. Biomed. Res.* Academic Press, 18:10-23.

VINET A, ROBERGE FA (1990). "A Model Study of Stability and Oscillations in the Myocardial Cell Membrane". *J. Theor. Biol.*, Academic Press, 147:377-412.

VINET A, CHIALVO DR, MICHAELS DC, JALIFE J (1990). "Nonlinear Dynamics of Rate-Dependent Activation in Models of Single Cardiac Cells". *Circ. Res.* 67(6):1510-1524.

VINET A., ROBERGE F.A.(1994). "Excitability and Repolarization in an Ionic Model of the Cardiac Cell Membrane". *J. Theor. Biol.* 170:183-199.

VINET A., ROBERGE F.A.(1994). "Analysis of an Iterative Difference Equation Model of the Cardiac Cell Membrane." *J. Theor. Biol.*170:201-211.

WATANABE M. OTANI N.F GILMOUR R.F. (1995). "Biphasic Resitution of Action Potential Duration and Complex Dynamics in Ventricular Myocardium". *Circ. Res.* 76:915-921.

WEINGART R. and MAURER P.(1988). " Action Potential Transfer in Cell Pairs Isolated from Adult Rat and Guinea Pig Ventricules". *Circ. Res.* 63:73-81, 1988.

WEINGART R. (1977). "The Actions of Ouabain on Intercellular Coupling and Conduction Velocity in Mammalian Ventricular Muscle". *J. Physiol.* 264:341-365

WEINGART R (1986). "Electrical Properties of the Nexal Membrane Studied in Rat Ventricular Cell Pairs". *J. Physiol.* 370:267-284.

WEINGART R (1987). "Cell-to-Cell Communication in Salivary Gland". Chapter 9, In: W.C. De Mello (Ed.), Cell-to-cell communication, Plenum Publishing Corp., 269-297.

WEINGART R, MAURER P (1987). "Cell-to-cell Coupling Studied in Isolated Ventricular Cell Pairs". *Experientia*, Birkhauser Verlag, Basel, Switzerland, 43(10):1091-1094.

WHITE RE, HARTZELL HC (1988). "Effects of Intracellular Free Magnesium on Calcium Current in Isolated Cardiac Myocytes". *Science*. 239:778-780.

WHITE RL, DOELLER JE, VERSELIS VK, WITTENBERG BA (1990). "Gap Junctional Conductance between Pairs of Ventricular Myocytes Is Modulated Synergistically by H^+ and Ca^{++}". *J. Gen. Physiol.*, The Rockefeller University Press. 95:1061-1075.

WIT AL, CRANEFIELD PF. (1978). "Reentrant Excitation as a Cause of Cardiac Arrhythmias". *Am J Physiol*. 235:H1-H17.

ZAMPIGHI G., CORLESS J.M. ROBERTSON J.D. (1980). "On Gap Junction Structure". *J. Cell. Biol.* 86:190-198.

ZIMMERMAN A. L., ROSE B. (1983). "Analysis of Cell-to-cell Diffusion Kinetics: Changes in Junctional Permeability without Accompanying Changes in Selectivity". (Abstract) *Biophys. J.* 41:216a..

Appendix A

In the (MBR) model, the maximum channel conductances are, $g_{Na} = 15.0$, $g_{si} = 0.09$, $g_x = 0.8$, and $g_{Nac} = 0.003$ (mS/cm^2), while the gating variables m, h, d,f, and x, are described by their steady state value $y_{i\infty} = \alpha_i / \beta_i + \alpha_i$ and time constant $\tau_i = 1/ \beta_i + \alpha_i$. The expression describing α_i or β_i is as follows:

$$\alpha_i \text{ or } \beta_i = \frac{C_1 \exp^{(C_2(V+C_3)} + C_4(V+C_5)}{\exp^{(C_6(V+C_3)} + C_7}$$

and the values for C_i are given in the following Table.

1/(ms)	C1	C2	C3	C4	C5	C6	C7
α_m				-0.9	42.65	-0.22	-1
β_m	1.437	-0.085	39.75				
α_h	0.1	-0.193	79.650				
β_h	1.7	0	20.5	0	0	0.095	1
α_d	0.095	-0.01	-5.0	0	0	-0.072	1
β_d	0.07	-0.017	44.0	0	0	0.05	1
α_f	0.012	-0.08	28	0	0	0.15	1
β_f	0.0065	-0.02	30	0	0	-0.2	1
α_x	0.0005	0.083	50	0	0	0.057	1
β_x	0.0013	-0.06	20	0	0	-0.04	1

The two potassium outward currents I_x and I_{k1} are expressed as follow:

$Ix = i_x x$

where

$$i_x = \frac{0.8\exp^{0.04(V+77)} - 1}{\exp^{0.04(V+35)}}$$

and

$$I_{k1} = \frac{0.35(4\exp^{0.04(V+85)} - 1)}{\exp^{0.08(V+53)} + \exp^{0.04(V+53)}} + \frac{0.2(V+23)}{1 - \exp^{-0.04(V+23)}}$$

ÉCOLE POLYTECHNIQUE DE MONTRÉAL
3 9334 00171200 7